



U.S. Department
of Transportation
**Research and
Special Programs
Administration**

Interaction and Load Transfer Through Track Support Systems - Part 1

Office of
University Research

**FINAL REPORT
UNDER CONTRACT
DOT-OS-80013**

**JANUARY 1983
DOT/RSPA/DMA-50/83/11**

**This document is available
to the U.S. public through
the National Technical In-
formation Service, Spring-
field, VA 22161**

NOTICE

This document is disseminated under the sponsorship of the Department of Transportation in the interest of information exchange. The United States Government assumes no liability for its contents or use thereof.

1. Report No. DOT/RSPA/DMA-50/83/11		2. Government Accession No.		3. Recipient's Catalog No.	
4. Title and Subtitle Interaction and Load Transfer in Track Support Structures, Part 1: One-, Two- and Three-Dimensional Nonlinear Soil-Structure Interaction Finite Element Procedures and Verification				5. Report Date September 1982	
				6. Performing Organization Code University of Arizona, Tucson, AZ	
7. Author(s) C. S. Desai, H. J. Siriwardane and R. Janardhanam				8. Performing Organization Report No.	
9. Performing Organization Name and Address Department of Civil Engineering and Engineering Mechanics, University of Arizona Tucson, Arizona 85721				10. Work Unit No. (TRAIS)	
				11. Contract or Grant No. DOT-OS-80013	
12. Sponsoring Agency Name and Address U.S. Department of Transportation Research and Special Programs Administration Office of University Research Washington, D. C. 20590				13. Type of Report and Period Covered Final Report September 1981-September 1982	
				14. Sponsoring Agency Code DPB-50	
15. Supplementary Notes Technical Monitor: John Putukian U.S. Department of Transportation Transportation Systems Center, Cambridge, MA 02142					
16. Abstract <p>This final report is presented in two parts, and is in continuation of two previous reports prepared under this contract. Part 1 contains details of the development of finite element procedures for nonlinear analysis of track support structures. It provides the user options for using one-, two- or three-dimensional idealizations, and options for using various elasticity and plasticity based constitutive models. The numerical predictions are verified with respect to a number of closed-form solutions and field problems. The latter includes verifications for the field behavior of the UMTA Test Section, TTC, Pueblo, Colorado.</p> <p>Part 2 contains comprehensive testing of 'solids' such as wood, ballast, sub-ballast and subgrade soil and interfaces; these materials were collected from the UMTA Test Section. The solid media were tested by using truly triaxial or multiaxial testing devices, whereas the interfaces between wood and ballast, concrete and ballast and ballast and subballast were tested by using a new cyclic multi-degree-of-freedom shear device. The laboratory test results were used to derive appropriate constitutive models for use in the finite element procedures.</p> <p>The research results involve new and unique aspects such as general three-dimensional nonlinear procedures, three-dimensional testing of materials and cyclic testing of interfaces. They will be useful for design of track support structures, and for maintenance and safety analysis of existing tracks.</p>					
17. Key Words Track Support Structures, Nonlinear Analysis, Multi-dimensional Finite Elements, Truly Triaxial Testing, Cyclic Shear Testing, Constitutive Modelling, Verifications, Design, Maintenance			18. Distribution Statement Available to the Public through the National Technical Information Service Springfield, Virginia 22161.		
19. Security Classif. (of this report) Unclassified		20. Security Classif. (of this page) Unclassified		21. No. of Pages Part 1 336 Part 2 322	22. Price

METRIC CONVERSION FACTORS

Approximate Conversions to Metric Measures

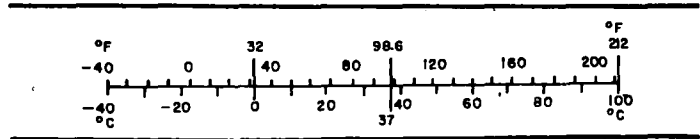
Symbol	When You Know	Multiply by	To Find	Symbol
LENGTH				
in	inches	2.5	centimeters	cm
ft	feet	30	centimeters	cm
yd	yards	0.9	meters	m
mi	miles	1.6	kilometers	km
AREA				
in ²	square inches	6.5	square centimeters	cm ²
ft ²	square feet	0.09	square meters	m ²
yd ²	square yards	0.8	square meters	m ²
mi ²	square miles	2.6	square kilometers	km ²
	acres	0.4	hectares	ha
MASS (weight)				
oz	ounces	28	grams	g
lb	pounds	0.45	kilograms	kg
	short tons (2000 lb)	0.9	tonnes	t
VOLUME				
tesp	teaspoons	5	milliliters	ml
Tbsp	tablespoons	15	milliliters	ml
fl oz	fluid ounces	30	milliliters	ml
c	cups	0.24	liters	l
pt	pints	0.47	liters	l
qt	quarts	0.95	liters	l
gal	gallons	3.8	liters	l
ft ³	cubic feet	0.03	cubic meters	m ³
yd ³	cubic yards	0.76	cubic meters	m ³
TEMPERATURE (exact)				
°F	Fahrenheit temperature	5/9 (after subtracting 32)	Celsius temperature	°C

* 1 in = 2.54 (exactly). For other exact conversions and more detailed tables, see NBS Misc. Publ. 286, Units of Weights and Measures, Price \$2.25, SD Catalog No. C13.10:286.



Approximate Conversions from Metric Measures

Symbol	When You Know	Multiply by	To Find	Symbol
LENGTH				
mm	millimeters	0.04	inches	in
cm	centimeters	0.4	inches	in
m	meters	3.3	feet	ft
m	meters	1.1	yards	yd
km	kilometers	0.6	miles	mi
AREA				
cm ²	square centimeters	0.16	square inches	in ²
m ²	square meters	1.2	square yards	yd ²
km ²	square kilometers	0.4	square miles	mi ²
ha	hectares (10,000 m ²)	2.5	acres	
MASS (weight)				
g	grams	0.035	ounces	oz
kg	kilograms	2.2	pounds	lb
t	tonnes (1000 kg)	1.1	short tons	
VOLUME				
ml	milliliters	0.03	fluid ounces	fl oz
l	liters	2.1	pints	pt
l	liters	1.06	quarts	qt
l	liters	0.26	gallons	gal
m ³	cubic meters	35	cubic feet	ft ³
m ³	cubic meters	1.3	cubic yards	yd ³
TEMPERATURE (exact)				
°C	Celsius temperature	9/5 (then add 32)	Fahrenheit temperature	°F



EXECUTIVE SUMMARY

Introduction

This report describes investigations towards development of general finite element procedures for nonlinear analysis of multi-component track support systems idealized as one-, two- or three-dimensional problems. It also considers perhaps the most significant aspects of any solution procedure; namely, the stress-strain or constitutive behavior of materials in the structure. Here attention is given to both testing and modelling of improved and appropriate models; the testing is carried out by using new and advanced testing devices for 'solids' (wood, ballast, subballast and subgrade soil) and interfaces between these materials.

Problem Studied

A numerical finite element procedure has been developed that can account for complex factors such as three-dimensional geometry, nonlinear behavior of materials, and interaction behavior at junctions or interfaces between various materials. In order to identify the interaction effects and relevant stress-strain behavior, a new cyclic multi-degree-of-freedom (CYMDOF) shear device has been developed and used. Truly triaxial (TT) or multiaxial testing devices with cubical specimens are used to characterize the behavior of ties, ballast, subballast and subgrade soil. The objective has been to develop a general procedure that permits evaluation of transfer of loads from moving vehicles through the track structure to the foundation.

Results Achieved

In addition to this report, two previous reports have been prepared. The topics covered in the two previous reports are: historical review of the problem; details of various components, their functions and role in the support structures; methods of determination of their properties; and available analytical and numerical procedures. These descriptions include advantages and limitations of the available methods, and identifies the need for a general model to account for various important and special factors that influence the track behavior and which are not included in previous works. Initial details of the numerical procedures developed, design and development of the CYMDOF device, and of laboratory testing and stress-strain modelling are also included in the previous reports.

Part 1 of this final report contains complete details of the one-, two- and three-dimensional finite element procedures and codes together with their verifications and applications. The latter involve comparison of predictions with a number of closed-form solutions, and observed results including field data from the UMTA Test Section, TTC, Pueblo, Colorado. The procedure includes development and use of four different constitutive models: linear elastic, nonlinear elastic (variable moduli), critical state and cap models; the latter allow for inelastic or plastic, hardening, stress path dependent and volume change behavior of the materials.

Part 2 of the report contains research accomplishment on the testing and modelling of the stress-strain behavior of materials by using the TT and CYMDOF devices. Comprehensive series of TT tests involving different initial confining pressures and a wide range of stress paths have been performed on wood (ties), ballast, subballast and subgrade (silty sand) collected from the UMTA Test Section. The CYMDOF device has been used to test interfaces between concrete and ballast, wood and ballast, and ballast-subballast under different normal loads and amplitudes of (repetitive) shear stress. These tests were conducted at the field density for the UMTA Test Section. Linear elastic, variable moduli, critical state and cap models have been developed for different materials depending upon the observed laboratory test behavior. These models were then used in the finite element codes for predicting the field behavior.

Utilization of Results

The research results will have significant potential in terms of both applications and further research. They can be used for stress-deformation analysis and design of track support structures for mass transport systems such as railroad tracks and for maintenance and safety analysis of existing tracks. Since the research has developed procedures for all the three-, one- two- and three-dimensional idealizations, they can provide options to the user depending upon his specific need. For instance, users interested in studying load-deflection behavior of the rail can use the one-dimensional option, while those interested in analyzing three-dimensional situations such as arbitrary geometry and loss or displacement of ties can use the three-dimensional option. Similarly, one can use simple linear elastic material model or advanced plasticity models.

The new CYMDOF device can permit study of behavior of interfaces as well as track materials under repetitive vertical and horizontal loads; the device will also be capable of testing under torsional and

rocking modes of deformation. The test results can permit evaluation of behavior under long repetitive loading useful for both design and maintenance and safety analysis. With some modifications, the device can allow repetitive and fatigue testing of interfaces and connections such as between tie-plate and tie and spikes in the track support structure. The device can also be used to study behavior of track materials with modifications such as cementing and impermeable membranes.

In the past, uniaxial or cylindrical triaxial tests have been used to characterize behavior of track materials. Perhaps for the first time, this study has considered detailed testing of track materials under fully three-dimensional state of stress. Hardly any previous works have considered the important question of the behavior of interfaces. Development and use of the new CYMDOF device is considered to open a new direction towards testing for behavior of interfaces.

The general numerical procedures and the test device constructed under this project are unique and new, and advances the state-of-the-art and knowledge related to mechanism of load transfer in track support structures.

Overall, the procedures and test device can provide improvements in design, maintenance and safety procedures. As a result, they can lead to savings in cost and enhancement of safety of track support structures.

It is expected that various governmental and private agencies and railroads involved in design and maintenance of track support structures can utilize the research results.

Conclusions

General and improved numerical procedures based on the finite element method developed under this project will allow evaluation of stresses, deformations and load transfer mechanism in track support structures. The new cyclic interface testing device will permit experimental determination of behavior of interfaces between various track components. The results will enhance the state-of-the-art and knowledge on analysis of track support structures, and can be applied for design, and maintenance and safety analysis of these structures.

PREFACE

The research investigations presented in this final report were supported by Contract No. DOT-OS-80013 through the Office of University Research, U. S. Department of Transportation, Washington, D. C. The report is presented in two parts. Part 1 contains details of development and application of nonlinear finite element procedures and provides options for using one-, two- and three-dimensional idealizations and a number of nonlinear elastic and elastic-plastic stress-strain or constitutive models. Testing and constitutive modelling of materials such as (wood) tie, ballast, subballast and subsoil, and interfaces between these materials are the subject of Part 2 of the report. Here development and use of new cyclic multi-degree-of-freedom shear device for interfaces and use of truly triaxial or multiaxial devices for the track materials are discussed. The investigations were conducted by C. S. Desai, H. J. Siriwardane and R. Janardhanam. The latter two were doctoral students and contributed investigations in Part 1 and Part 2, respectively; A. Muqtadir assisted in conducting the laboratory testing for ballast-subballast interface. C. S. Desai acted as the principal investigator for the project.

The research was initiated in 1978 at Virginia Polytechnic Institute and State University, Blacksburg, VA (Va. Tech.). Portions of the research investigations have been included in two previous reports: (1) Interaction and Load Transfer Through Track Guideway Systems, No. DOT/RSPA/DPB-50/80/13, Office of University Research, U. S. Department of Transportation, Washington, D. C., prepared in 1978 and published in 1980 and (2)

"Interaction and Load Transfer in Track Guideway Systems" prepared in June 1980 and is under publication. The previous two reports were prepared at Va. Tech. while this report was prepared at the University of Arizona, Tucson, AZ, as a continuation of the project, subcontracted through Va. Tech.

The project was monitored by J. Putukian, Transportation System Center (TSC), Cambridge, Mass.; previous monitors of the project were G. Butler, Urban Mass Transportation Administration (UMTA), Washington, D. C., and A. Sluz of TSC. G. Spons., UMTA Test Section at Transportation Test Center, Pueblo, Colorado, assisted in procuring various materials from the Test Section for testing in the laboratory, and Kaman Avidyne and Kaman Sciences, Inc. (E. Gadden, L. J. Mente, T. Stigliano) provided the report containing field observations at the UMTA Test Section at Pueblo, Colorado.

TABLE OF CONTENTS

	<u>Page</u>
EXECUTIVE SUMMARY	i
PREFACE	iv
Table of Contents	vi
List of Figures	xii
List of Tables	xxi
Chapter :	
1. INTRODUCTION	1
1.1 General Remarks	1
1.2 Literature Review	3
1.3 Aims of the Research	5
1.4 Scope of the Research	5
1.5 Summaries of Various Chapters	7
2. SOME FUNDAMENTALS OF SOLID MECHANICS	9
2.1 General Remarks	9
2.2.1 Stress Tensor	9
2.3 Invariants of Stress and Strain Tensors	10
2.4 Stress-Strain or Constitutive Relations	13
2.5 Elasticity	14
2.6 Plasticity	
2.6.1 Yield Criterion	16
2.6.2 Post Yield Behavior: Plastic Stress- Strain Relations	18
2.7 Generalized Plastic Stress-Strain Relations	18

	<u>Page</u>
3. FINITE ELEMENT METHOD: ONE-, TWO-, AND	
THREE-DIMENSIONAL IDEALIZATIONS	22
3.1 One-Dimensional Idealization: Beam-Column	
Elements	22
3.1.1 Element Stiffness Matrix	26
3.1.2 Element Load Vector	32
3.1.3 Computer Code for One-Dimensional	
Analysis	35
3.2 Two-Dimensional Idealization	36
3.2.1 Finite Element Formulation	36
3.2.2 Element Stiffness Matrix	43
3.2.3 Element Load Vector	45
3.2.4 Computer Code for Two-Dimensional	
Analysis	48
3.3 Three-Dimensional Idealization	49
3.3.1 Finite Element Formulation	49
3.3.2 Element Stiffness Matrix	58
3.3.3 Element Load Vector	59
3.3.4 Computer Code for Three-Dimensional	
Analysis	59
3.4 Resistance-Response Approach	61
4. ADVANCED CONSTITUTIVE LAWS USED IN SOIL-STRUCTURE	
INTERACTION ANALYSIS	63
4.1 General Remarks	63

	<u>Page</u>
4.2 Variable Moduli Models	64
4.2.1 Constant Poisson Ratio Model	66
4.2.2 Variable Moduli Model Based on Invariants of the Strain	67
4.2.3 Combined Stress-Strain Variable Moduli Model	68
4.3 Introduction to Advanced Plasticity Laws	73
4.3.1 Mohr-Coulomb Failure Criterion	74
4.4 Drucker-Prager Model	77
4.4.1 Derivation of the Incremental Constitutive Law	77
4.5 Critical State Model	86
4.5.1 Plastic Stress-Strain Behavior	87
4.6 Cap Model	91
4.7 Elasto-Plastic Constitutive Relationship for Hardening Models	98
4.7.1 Elasto-Plastic Constitutive Matrix for Critical State Model	102
4.7.2 Elasto-Plastic Constitutive Matrix for Hardening Cap, F_c	103
4.7.3 Elasto-Plastic Constitutive Matrix for Failure Envelope, F_f	103
5. COMPUTATIONAL ALGORITHMS	104
5.1 General	104

	<u>Page</u>
5.2 Stress Transfer Technique in One-Dimensional Analysis	108
5.3 Numerical Procedure for Beams on Nonlinear Foundations	112
5.3.1 Numerical Procedure for Unloading Conditions in Support Springs	115
5.4 Variable Moduli Model: Implementation in Two- and Three-Dimensional Analysis	117
5.5 Drucker-Prager Model: Implementation in Two- and Three-Dimensional Analysis	120
5.5.1 Subincrements of Strain	122
5.5.2 Procedure for Correcting Stresses	124
5.6 Critical State Model: Implementation in Two- and Three-Dimensional Analysis	128
5.6.1 Correction of Stresses Back to Critical State Line	130
5.6.2 Stress Computation During Hardening: Marching Scheme	134
5.6.3 Stress Computation During Hardening: Iterative Scheme	138
5.6.4 Stress Computation During Unloading	143
5.7 Cap Model: Implementation in Two- and Three-Dimensional Analysis	145
5.8 Convergence Criterion	146
5.9 Initial Conditions for Nonlinear Analysis	148

	<u>Page</u>
5.10 Solution Techniques	148
5.10.1 Equation Solver in One-Dimensional Finite Element Code	148
5.10.2 Equation Solver in Two-Dimensional Finite Element Code	149
5.10.3 Equation Solver in Three-Dimensional Finite Element Code	151
5.11 Efficient Implementation	151
6. INTERFACE MODELLING IN SOIL-STRUCTURE INTERACTION . .	153
6.1 Introduction	153
6.2 Review of Interface Models	157
6.3 Interface Element Used in Current Research . . .	162
7. CONSTITUTIVE MODELLING FOR NONLINEAR ANALYSIS	168
7.1 General	168
7.2 Test Results	169
7.3 Analysis of Data and Determination of Parameters	182
8. VERIFICATIONS OF ONE-, TWO-, AND THREE-DIMENSIONAL FORMULATIONS AND CODES	186
8.1 Beam-on-Elastic Foundation with One- Dimensional Code	186
8.2 Pure Beam Bending with Two-Dimensional Code . .	189
8.3 Variable Moduli Model: Two- and Three- Dimensional Analysis	189

	<u>Page</u>
8.4 Drucker-Prager Model: Two- and Three- Dimensional Analysis	193
8.5 Critical State Model: Two- and Three- Dimensional Analysis	197
8.6 Marching and Iterative Algorithms for Critical State Model	198
8.7 Footing Test with Critical State Model	202
8.8 Pure Bending with Three-Dimensional Analysis	205
8.9 Cap Model: Two- and Three-Dimensional Analysis	209
8.10 Interface Behavior	211
9. APPLICATIONS TO SOIL-STRUCTURE INTERACTION PROBLEMS	220
9.1 Analysis of a Footing-Soil System	220
9.2 Interaction in a Beam with a Nonlinear Foundation	252
9.3 Interaction in a Multicomponent System such as a Track-Support Structure	263
10. SUMMARY AND CONCLUSIONS	296
References	300
Appendix A	311
Appendix B	318
Appendix C	320
Appendix D	322
Appendix E	336

LIST OF FIGURES

		<u>Page</u>
Figure 3.1	One-Dimensional Idealization for Beam-Column Element	23
Figure 3.2	Interpolation Functions for Beam-Column Analysis	27
Figure 3.3	Transformation of Coordinates	30
Figure 3.4	Distributed Loads on Beam-Column Element	34
Figure 3.5	Two-Dimensional Isoparametric Elements	37
Figure 3.6	Distributed Surface Loads on Two-Dimensional Elements	46
Figure 3.7	Basic Hexahedral Finite Element	50
Figure 3.8	Node Numbers for 8 to 21 Variable Node Hexahedral Finite Element	52
Figure 3.9	Distributed Surface Loads on Three- Dimensional Elements	60
Figure 4.1	Typical Test Results for Geologic Media	69
Figure 4.2	Mohr-Coulomb Failure Criterion	75
Figure 4.3	Mohr-Coulomb and Drucker-Prager Yield Criteria on π -Plane	76
Figure 4.4	Drucker-Prager Criterion	78
Figure 4.5	Stress-Strain Matrix for Drucker-Prager Material Model	81
Figure 4.6	Hardening Behavior of Geologic Media	84
Figure 4.7	Void Ratio - $\ln p$ Relationship for the Critical State Model	88

	<u>Page</u>
Figure 4.8	State Boundary Surface 89
Figure 4.9	Yield Locus for Critical State Model in q-p Plane 92
Figure 4.10	Cap Model Proposed by DiMaggio and Sandler [24] 94
Figure 4.11	Failure and Hardening Surfaces in Cap Model . . . 97
Figure 5.1	Newton-Raphson Iterative Methods 106
Figure 5.2	Mixture of Incremental and Iterative Techniques 109
Figure 5.3	Stress Transfer Technique 111
Figure 5.4	Ramberg-Osgood Model 114
Figure 5.5	Iterative Procedure Used in Analysis of Beams on Nonlinear Supports 116
Figure 5.6	Possible Loading-Unloading Paths for Variable Moduli Model 119
Figure 5.7	Computational Procedure for Variable-Moduli Model 121
Figure 5.8	Numerical Scheme for Correcting Stresses in Drucker-Prager Model 123
Figure 5.9	Possible Stress Increments in a Hardening Model 131
Figure 5.10	State of Stress Outside the Yield Surface 135
Figure 5.11	Possible Stress Paths From an Existing Plastic State 144

	<u>Page</u>
Figure 5.12	Computational Procedure for Contraction of the Cap Shaped Yield Surface 147
Figure 5.13	Storage Scheme Used in Skyline Solution Procedure 152
Figure 6.1	Schematic Model For Soil-Structure Interaction 155
Figure 6.2	Typical Soil-Structure Interaction Problems in Geomechanics 156
Figure 6.3	Interface Element with Zero Thickness 158
Figure 6.4	Interface Elements for Two- and Three- Dimensional Analysis 164
Figure 6.5	Load-Deformation Behavior at an Interface . . . 165
Figure 7.1	Commonly Used Stress Paths 170
Figure 7.2a	Stress-Strain Response Curve for Hydrostatic Compression Test 171
Figure 7.2b	Mean Pressure-Volumetric Strain Response for Hydrostatic Test 172
Figure 7.3a	Stress-Strain Response for Conventional Triaxial Compression Test 174
Figure 7.3b	Octahedral Shear Stress-Strain Response for Conventional Triaxial Compression Test 175
Figure 7.4	Stress-Strain Response for Simple Shear Test . . 176
Figure 7.5	Stress-Strain Response for Triaxial Compression Test 178

	<u>Page</u>	
Figure 7.6	Stress-Strain Response for Triaxial Extension Test	179
Figure 7.7	Stress-Strain Response for Reduced Triaxial Compression Test	180
Figure 7.8	Stress-Strain Response for Conventional Triaxial Extension Test	181
Figure 7.9	Void Ratio-Log p Curve from Hydrostatic Test . .	183
Figure 7.10	Failure Envelope for Pueblo Sand	184
Figure 8.1	Deformations of a Beam-on-Elastic Foundation . .	188
Figure 8.2	Plane Stress Idealization of Beam Bending . . .	190
Figure 8.3	Simulation of Triaxial Test Specimens	192
Figure 8.4	Verification of Variable Moduli Model Predictions	194
Figure 8.5	Plane Strain Behavior of a Drucker-Prager Material	196
Figure 8.6	Triaxial Test Behavior of Critical State Model	200
Figure 8.7	Comparison of Two Numerical Schemes for Hardening Models	201
Figure 8.8a	Finite Element Mesh for Strip Footing Analysis with Critical State Model	203
Figure 8.8b	Prediction of Footing Displacements with Critical State Model	206
Figure 8.9	Displacement Field from a Strip Footing Analysis	207

	<u>Page</u>
Figure 8.10	Three-Dimensional Analysis of Beam Bending . . . 208
Figure 8.11	Beam Bending Analysis with Three-Dimensional Program 210
Figure 8.12	Triaxial Test Behavior of Cap Model 212
Figure 8.13	Deformation Behavior at an Interface in Plane-Strain Conditions 213
Figure 8.14	Relative Displacements Across an Interface Element 215
Figure 8.15	Effect of Interface Normal Stiffness on the Deformation Behavior 216
Figure 8.16	Performance of the Three-Dimensional Interface Element 217
Figure 8.17	Effect of Poisson's Ratio on the Deformations at the Interface 219
Figure 9.1	Finite Element Mesh Used for Analysis of Footing Problem 222
Figure 9.2	Finer Finite Element Used in the Strip Footing Analysis 223
Figure 9.3	Comparison of Predicted Stress Distributions from Finer and Coarse Finite Element Meshes . . 225
Figure 9.4	Plane Strain Analysis Using a Three- Dimensional Procedure (Simulated Plane Strain) 226
Figure 9.5	Deformation Analysis of a Strip Footing with Variable Moduli Model 230

	<u>Page</u>
Figure 9.6	Deformation Analysis of a Strip Footing with Drucker-Prager Model 231
Figure 9.7	Behavior of a Strip Footing at Ultimate Conditions with a Drucker-Prager Model 233
Figure 9.8	Deformation Analysis of a Strip Footing with Critical State Model 235
Figure 9.9	Deformation Analysis of a Strip Footing with Cap Model 237
Figure 9.10	Effect of Stresses Normal to the Plane of Deformation on the Behavior of a Elasto- Plastic Material in Plane-Strain Condition . . . 239
Figure 9.11	Displacement Vector Field for a Strip Footing on a Linear Elastic Material 241
Figure 9.12	Comparison of Displacement Fields for Drucker-Prager and Critical State Models at Ultimate Conditions 242
Figure 9.13	Comparison of Displacement Fields for Drucker-Prager and Cap Models at Ultimate Conditions 243
Figure 9.14	Finite Element Mesh for Footing-Soil Interaction with a Lateral Load 245
Figure 9.15	Interaction Behavior of a Footing with Soil . . 246
Figure 9.16a	Vertical Load-Displacement Relationship for the Strip Footing 248

	<u>Page</u>
Figure 9.16b	Lateral Load-Displacement Relationship for the Strip Footing 249
Figure 9.17	Displacement Field for Footing-Soil Interaction with a Lateral Load 251
Figure 9.18a	Effect of Stress Transfer on Beam Deflections 253
Figure 9.18b	Effect of Stress Transfer on Distribution of Reactions 255
Figure 9.19a	Effect of Stress Transfer on Equilibrium Conditions 256
Figure 9.19b	Effect of Stress Transfer on Equilibrium Conditions 257
Figure 9.20a	Predicted Displacements of Beam-on-Nonlinear- Foundation Without Equilibrium Iterations . . . 259
Figure 9.20b	Distribution of Reactions from a Nonlinear Analysis Without Equilibrium Iterations 260
Figure 9.21a	Beam Deflections from a Nonlinear Analysis with Equilibrium Iterations 261
Figure 9.21b	Distribution of Reactions from a Nonlinear Analysis with Equilibrium Iterations 262
Figure 9.22	Finite Element Idealization of a Track Support Structure 264
Figure 9.23	Three-Dimensional Finite Element Mesh for Analysis of FAST Section 267

	<u>Page</u>
Figure 9.24	Effect of Longitudinal Boundary Distance on the Stress Distribution Below the Wheel Load . . . 268
Figure 9.25	Effect of Longitudinal Boundary Distance on the Displacements from a Three-Dimensional Analysis 269
Figure 9.26	Effect of Tie Stiffness on the Stress Distribution Below the Load at FAST Section . . . 271
Figure 9.27	Effect of Tie Stiffness on Displacement Distribution 272
Figure 9.28	Comparison of Two Loading Configurations 273
Figure 9.29	Finite Element Mesh for Analysis of FAST Section 275
Figure 9.30	Comparison of Plane Strain and Three- Dimensional Stress Distribution 276
Figure 9.31	Comparison of Plane Strain and Three- Dimensional Displacement Distribution 277
Figure 9.32	Instrumentation Locations at UMTA Test Station [78] 279
Figure 9.33	One-Dimensional Analysis of UMTA Test Section 284
Figure 9.34	Finite Element Mesh for Plane Strain Analysis of UMTA Test Section 285
Figure 9.35	Three-Dimensional Finite Element Mesh for UMTA Test Section Analysis 286

	<u>Page</u>
Figure 9.36	Stress Distribution at UMTA Section from a Linear Analysis 288
Figure 9.37	Stress-Distribution from a Nonlinear Three- Dimensional Analysis of UMTA Test Section . . . 289
Figure 9.38	Displacement Field for UMTA Test Section from a Two-Dimensional Analysis 291
Figure 9.39	Displacement Field from a Three-Dimensional Analysis of UMTA Section 292
Figure 9.40	Effect of Interface Elements on the Vertical Stress Distribution 294
Figure 9.41	Nonlinear Three-Dimensional Interaction Analysis of UMTA Section at Higher Loads 295
Figure D.1	Determination of RR Curves from Three- Dimensional Analysis 324
Figure D.2	Representation of Proposed Resistance- Response Procedure (RR) 326
Figure D.3	Three-Dimensional Finite Element Mesh for Determining Resistance-Response Curves 327
Figure D.4	Two Loading Cases for Resistance-Response Analysis 329
Figure D.5	Displacement Predictions from Resistance- Response Analysis 332
Figure E.1	Exploded View Showing One Face Assembly of Multiaxial Cubical Test Apparatus [80] 334

LIST OF TABLES

		<u>Page</u>
Table 3.1	Stiffness Matrix for the Beam-Column Element . .	29
Table 8.1	Comparison of Displacements	191
Table 8.2	Comparison of Marching and Iterative Schemes for Critical State Model	199
Table 9.1	Comparison of Coarse and Finer Meshes with Respect to Surface Displacements	224
Table 9.2	Comparison of Plane-Strain and Constrained Three-Dimensional Analysis	228
Table 9.3	Deflections at Point of Load Application at UMTA Test Section	290

Chapter 1

INTRODUCTION

1.1 General Remarks

Most of the solids behave in a nonlinear manner although within certain ranges of loading the behavior can be idealized as linear. Behavior of geologic media is usually highly nonlinear, and pose a difficult problem for the analyst.

The behavior of structures supported on nonlinear geologic media becomes increasingly complex in view of the interaction effects. The aim of this research is to understand the fundamental behavior of nonlinear interaction by using theories and fundamentals of solid mechanics.

Complete understanding of nonlinear phenomena is of great practical and theoretical importance. These nonlinear phenomena can be found in all areas of mechanics and mathematical physics: solid, structural and geomechanics, fluid dynamics, biomechanics, electromagnetic field theory, quantum mechanics etc. Some of the obstacles that cause "nonlinear barriers" in engineering mechanics may be removed by using idealized mathematical models and effective numerical and computational procedures; such models and improved computational algorithms are investigated in this study.

Nonlinear behavior in solid mechanics can occur due to three reasons:

- (1) Geometric nonlinearity,
- (2) Material nonlinearity,

and

(3) Boundary nonlinearities or nonlinearity due to interfaces.

The boundary nonlinearities can occur in many structural systems when there exist situations in which one deformable body comes in contact with the other. The contact of a given body with another is in essence how loads are transmitted from one to another body. Therefore, the character of this contact (interface) plays an important role in the problems involving various engineering media. Material nonlinearity in geologic media can be due to several factors. These include initial state of stress, stress path dependent response, changes in physical states defined by density, void ratio or water content, hardening behavior, and state of body with arbitrary geometry and loading. Material nonlinearity is usually quantified by using constitutive relationships.

Nonlinear Interaction in Geomechanics

Soil-structure interaction analysis has received the attention of many researchers during the last decade; a review is given in Chapter 6 of this dissertation. Problems in geomechanics can involve nonlinearities due to all the three types described in the foregoing section. However, in the present study nonlinearities due only to interaction and material behavior are considered. Although for some problems various one-, and two-dimensional idealizations may give adequate and economical solutions, almost all real problems are three-dimensional in nature. In view of the fact that many problems encountered in soil-structure interaction can often be idealized as one-,

two-, and three-dimensional, a generalized procedure should have provision for nonlinear analysis of all the three idealizations. This can cover a wide range of problems in geomechanics such as footings, laterally loaded piles, long retaining walls, dams, beams and plates on deformable foundations, track support structures and buried pipes. Realistic solution procedures for the foregoing problems require appropriate provision for physical state, initial conditions, nonhomogeneities and interaction effects. Most conventional methods of solution based on classical theories of elasticity and plasticity are not adequate for this purpose. Hence, it becomes necessary to use numerical techniques such as the finite element method. Constitutive laws which define the nonlinear behavior play a very important role in developing reliable and consistent numerical procedures. This dissertation gives comprehensive treatment to these aspects. Brief reviews of numerical methods and constitutive laws are given below.

1.2 Literature Review

Finite Element Method

Considerable research work has been done on the theoretical development and applications of finite element method to solve nonlinear problems in solid mechanics. Historical development of the finite element method can be found in several books [15,62,89].

Techniques for Nonlinear Analysis

Most of the nonlinear problems are solved by assuming a series of "piecewise linear" analyses. Basically there have been two techniques

used in the past for nonlinear analysis, namely, incremental and iterative [15,35,53,88,89].

In the incremental technique, the constitutive matrix is updated at each load increment. Among many iterative procedures for nonlinear analysis, Newton-Raphson techniques have been widely used with the finite element method. Initial stress method which can be considered to be a modified Newton-Raphson technique is often used for solving nonlinear problems in solid mechanics [56,93,94]. This method has been found to give satisfactory results when plastic deformations are not large compared to elastic components. However, for geologic media, the material behavior is highly nonlinear and plastic, and hence, the above technique may not yield satisfactory results; this factor is considered in the current research.

Constitutive Laws

Several refinements and advances have been made in the theory of finite elements, and the reliability of the method has been proved by several applications. However, the accuracy of a nonlinear analysis is dependent significantly on the constitutive characterization (modelling), and the computational algorithms used in implementing advanced constitutive laws for geologic media.

Several advanced constitutive models have been developed in the last few years, and details of these models are available in various references [12,17,21,24,66,68,87]. Use of these advanced plasticity models for certain problems in geomechanics have been reported in several references [1,6,8,20,64,77,91]. Here both incremental and

iterative techniques have been used. Application of beam-column idealization to certain geomechanics problems have been reported in reference [18].

1.3 Aims of the Research

The aim of this research is to study the fundamental behavior of nonlinear soil-structure interaction problems idealized as one-, two-, and three-dimensional. Here basic principles of solid mechanics and numerical techniques are utilized with proper attention to constitutive laws. Within the context of numerical techniques, consistent and detailed computational algorithms are developed to implement several constitutive relationships.

The interface behavior is studied by using a special interface element in conjunction with the finite element method.

The objectives and scope of this dissertation can be stated as follows.

1.4 Scope of the Research

- (1) To formulate and develop an incremental-iterative finite element procedure to handle interaction in beam-columns supported on nonlinear foundations.
- (2) To formulate and develop an incremental finite element procedure to handle interaction in two- and three-dimensional problems.
- (3) To develop improved and consistent computational algorithms for handling material nonlinearities in one-, two-, and three-dimensional analysis. Here, a rather novel scheme is

developed which is found to yield improved solutions in terms of convergence with the advanced plasticity models.

- (4) To develop efficient and versatile finite element computer codes for one-, two-, and three-dimensional idealizations.
- (5) To define and incorporate various conventional and recent constitutive laws in the three formulations. Considerable attention is given to determination of constitutive parameters from appropriate laboratory tests that permit simulation of important factors that influence the behavior of geologic media.
- (6) To compare and verify numerical predictions with available closed form solutions, laboratory observations, and field observations. Here, the procedures developed are applied to problems such as beams-on-deformable foundations, footing loads on half spaces, and multicomponent systems such as track support structures.
- (7) Since three-dimensional procedures are often expensive, preliminary investigations are included towards development of a rather novel formulation called Resistance-Response (R-R) approach. It is expected that such an approach, with additional research, can provide economical solutions by essentially using one- and two-dimensional idealizations with minimum use of the three-dimensional procedure.

1.5 Summaries of Various Chapters

Chapter 2 of this dissertation is devoted to describe some fundamentals of solid mechanics. In this chapter, a brief description is given of invariants of stress and strain tensors, theory of elasticity, and generalized stress-strain relationships based on plasticity. Chapter 3 describes the formulation of one-, two-, and three-dimensional finite element idealizations. Procedures for computation of stiffnesses and load vectors for each of the idealizations are given.

Chapter 4 covers the theoretical aspects of advanced constitutive laws used in this study. Here, variable moduli, Drucker-Prager, critical state and cap models are described. Details of computational algorithms used in this study are developed and described in Chapter 5. Details of numerical solution procedures and solution techniques are also given. In Chapter 6, a review of available interface elements is presented. Details of the interface element used for soil-structure interaction in this study is given here.

Chapter 7 presents the laboratory experimental data on the granular material (sand) tested in this study. Chapter 8 presents verifications of the three computer codes developed; here, rather simple or previously solved problems are analysed. Chapter 9 is then devoted to presenting some applications of the procedures developed. Here, three soil-structure interaction problems are analysed, namely, a strip footing, a beam on a deformable foundation, and load transfer in track support structures. Deformation behavior of the strip footing is first presented. Then the study of the interaction in beam-foundation system is

presented. The last part of the chapter covers the analysis of track support structure; these results are compared with field measurements.

Finally, in Chapter 10, a summary of the work in the present study is given, and ideas on further research are recommended. Appendix D contains a description of the resistance-response approach.

CHAPTER 2

SOME FUNDAMENTALS OF SOLID MECHANICS

2.1. General Remarks

Often the trend in geomechanics has been to adopt and modify existing formulations developed for structural and continuum mechanics, notably those based on theories of classical elasticity and classical plasticity. It has been realized that the mechanical behavior of many materials encountered in geomechanics problems is much more complicated than that described by classical elasticity or plasticity theories. Hence, certain modifications to the classical theories are required. The purpose of this chapter is to describe the fundamentals of elasticity and plasticity, which will be used in deriving advanced plasticity models described in Chapter 4.

2.2. Basic Definitions

Basic definitions of the stress tensor, σ_{ij} , strain tensor, ϵ_{ij} , deviatoric stress tensor, S_{ij} , and deviatoric strain tensor, E_{ij} , can be found in references [33,34], and will not be repeated here.

2.2.1. Sign Convention

There are different sign conventions used in conjunction with solid, structural and geomechanics. In certain applications compressive normal stresses have been taken as positive while tensile normal stresses have been assumed as positive quantities in some other applications [34, 73]. Although the sign convention used does not influence the mechanics of deformation, it is important in interpreting information with a physical insight. In the current research compressive normal stresses are assumed to be positive.

2.3. Invariants of Stress and Strain Tensors

As will be seen in a forthcoming chapter, the mechanical behavior of geologic materials will not depend on the frame of reference, if an assumption is made regarding isotropy. Under these conditions, it is advantageous to describe the stress and strain tensors in certain forms of frame independent quantities. Fortunately, there exist three such quantities related to stress and strain, known as invariants. These quantities will be described in the following section.

There are two ways to define the invariants of stress or strain tensor. It is possible to define them with respect to the characteristic equations related to the determinant of the stress or strain tensor. On the other hand, it is also possible to define invariants which can be expressed directly by using the stress or strain tensor itself. In the applications to problems in mechanics, it is desirable to use the later definition as it has a fundamental meaning. This can be expressed as follows:

$$J_1 = \sigma_{ii} \quad (2.1a)$$

$$J_2 = \frac{1}{2} \sigma_{ij} \sigma_{ji} \quad (2.1b)$$

$$J_3 = \frac{1}{3} \sigma_{ik} \sigma_{kj} \sigma_{ji} \quad (2.1c)$$

where J_1 , J_2 and J_3 are the first, second and third invariants of the stress tensor, respectively. Similarly, the invariants of the strain tensor can be defined as

$$I_1 = \epsilon_{ii} \quad (2.2a)$$

$$I_2 = \frac{1}{2} \epsilon_{ij} \epsilon_{ji} \quad (2.2b)$$

$$I_3 = \frac{1}{3} \epsilon_{ik} \epsilon_{kj} \epsilon_{ji} \quad (2.2c)$$

Similar to the stress and strain tensors, there exist invariants of the deviatoric quantities as well. They are defined as,

$$J_{1D} = 0.0 \quad (2.3a)$$

$$J_{2D} = \frac{1}{2} S_{ij} S_{ij} \quad (2.3b)$$

$$\text{and } J_{3D} = \frac{1}{3} S_{ik} S_{kj} S_{ji} \quad (2.3c)$$

where J_{2D} and J_{3D} are the second and third invariants of the deviatoric stress tensor, respectively. The quantity J_{2D} is widely used in constitutive characterization, and it is directly related to the octahedral shear stress. This can be expressed as

$$J_{2D} = \frac{1}{6} [(\sigma_{11}-\sigma_{22})^2 + (\sigma_{22}-\sigma_{33})^2 + (\sigma_{11}-\sigma_{33})^2] \\ + (\sigma_{12}^2 + \sigma_{23}^2 + \sigma_{13}^2) \quad (2.4)$$

Octahedral shear stress, τ_{oct} , then can be expressed as

$$\tau_{\text{oct}} = \sqrt{\frac{2}{3} J_{2D}} \quad (2.5)$$

The invariants of the deviatoric strain tensor are defined as

$$I_{1D} = 0.0 \quad (2.6a)$$

$$I_{2D} = \frac{1}{2} E_{ij} E_{ji} \quad (2.6b)$$

$$\text{and } I_{3D} = \frac{1}{3} E_{ik} E_{kj} E_{ji} \quad (2.6c)$$

where I_{2D} and I_{3D} are the second and the third invariants of the deviatoric strain tensor. The quantity, I_{2D} , can be expressed as

$$I_{2D} = \frac{1}{6} [(\epsilon_{11} - \epsilon_{22})^2 + (\epsilon_{22} - \epsilon_{33})^2 + (\epsilon_{11} - \epsilon_{33})^2] \\ + \gamma_{12}^2 + \gamma_{23}^2 + \gamma_{13}^2 \quad (2.7)$$

Octahedral shear strain, γ_{oct} , can be expressed as

$$\gamma_{\text{oct}} = \sqrt{\frac{2}{3}} I_{2D} \quad (2.8)$$

2.4. Stress-Strain or Constitutive Relations

The mechanical behavior can be explained by using certain principles and laws of nature: conservation of mass, energy, linear and angular momenta, the law of electromagnetic flux, and the idea of thermodynamic irreversibility. The subject of continuum mechanics is general enough that it can be applied to any 'continuous' media with any material properties. However, the response of a continuum can not be uniquely determined only with the field equations. Hence, the internal constitution of matter plays an important role in the subject of continuum mechanics. "Constitutive laws" represent a mathematical model which describes our ideas of the constitution of matter. Constitutive law has to satisfy certain axioms of continuum physics, and a description of this is given in reference [31]. The main advantage of establishing a mathematical model is to apply our ideas in solving complex events quantitatively. A solution to a boundary value problem in continuum mechanics requires constitutive equations in addition to the governing field equations and boundary conditions. Establishment of constitutive equations can be based on the experimental observations or from physical

theories of molecular behavior. However, the first approach can impart physical significance in engineering science, and hence has been adopted widely. In the following section, the stress-strain relationships in the classical theory of elasticity will be described.

2.5. Elasticity

An external load causes stresses and strains in a body. Upon removal of the external load, the body may or may not recover the initial state of stress and strain. If the body returns to its original configuration, then it is called to have deformed elastically.

Generalized Hooke's Law

The generalized Hooke's law is expressed as

$$\sigma_{ij} = C_{ijkl} \epsilon_{kl} \quad (2.9)$$

where C_{ijkl} is a fourth order tensor. This is known as the stress-strain tensor or the constitutive tensor for elastic body under consideration. For an isotropic, homogeneous elastic body, the stress-strain relationship can be written as [33, 34].

$$\sigma_{ij} = \lambda' \epsilon_{kk} \delta_{ij} + 2\mu' \epsilon_{ij} \quad (2.10)$$

where λ' and μ' are known as Lamé's constants. These constants can be expressed in terms of Young's modulus, E , and Poisson's ratio ν as

$$\lambda' = \frac{E\nu}{(1+\nu)(1-2\nu)} \quad (2.11a)$$

and

$$\mu' = \frac{E}{2(1+\nu)} \quad (2.11b)$$

Although the above relationships are written in tensor notation, it is easier to use them in engineering practice if they are written in matrix notation. The stress and strain tensors can be arranged into the form of vectors as follows:

$$\{\sigma\}^T = [\sigma_{11} \quad \sigma_{22} \quad \sigma_{33} \quad \sigma_{12} \quad \sigma_{23} \quad \sigma_{13}] \quad (2.12a)$$

and

$$\{\epsilon\}^T = [\epsilon_{11} \quad \epsilon_{22} \quad \epsilon_{33} \quad \epsilon_{12} \quad \epsilon_{23} \quad \epsilon_{13}] \quad (2.12b)$$

There, in matrix notation, Equation (2.9) can be written as

$$\{\sigma\} = [C]\{\epsilon\} \quad (2.13)$$

where, for an isotropic material [84]

$$[C] = \frac{E}{(1+\nu)(1-2\nu)} \begin{bmatrix} 1-\nu & \nu & \nu & 0 & 0 & 0 \\ & 1-\nu & \nu & 0 & 0 & 0 \\ & & 1-\nu & 0 & 0 & 0 \\ & & & \frac{1-2\nu}{2} & 0 & 0 \\ & & & & \frac{1-2\nu}{2} & 0 \\ & & & & & \frac{1-2\nu}{2} \end{bmatrix} \quad (2.14)$$

The elastic constitutive matrix can also be expressed in terms of the shear modulus, G , and the bulk modulus, K . This relationship is given and used in Chapter 4 under variable moduli models.

2.6. Plasticity

As described in the previous section, elastic materials undergo only recoverable deformations, that is, they return to their initial state when the load is removed. However, some materials retain a part of the deformation upon unloading. These types of materials are called inelastic or plastic. Because the reloading paths do not follow the original loading path, the strains will be dependent on the history of stress applications when plastic deformation occurs. That is, the plastic behavior is characterized by the history-dependent deformations. As a first approximation, time effects have been neglected in the theory of plasticity [25]. There are two major aspects that constitute the theory of plasticity:

- (1) Yield Criterion, and
- (2) Post Yield Behavior.

2.6.1. Yield Criteria

Yield criterion can be defined as the limit of elastic deformations defined by a combination of states of stress. For a one-dimensional state of stress, yield criterion can be easily visualized. However, under multiaxial states of stress, this becomes more complicated, and an idealized mathematical definition is often required. The yield criterion has to be established based on experimental observations of

the material. For an isotropic material, the yield criterion can be expressed in terms of the invariants of the stress tensor as follows:

$$F = F(J_1, J_2, J_3) \quad (2.15)$$

where J_1 , J_2 and J_3 are the invariants of the stress tensor. However, the influence of hydrostatic stress on the plastic deformations has been found to be negligible for many metals. This assumption leads to the fact that the yield criterion depends only on the state of the deviatoric stress. Therefore, the yield criterion in Equation (2.15) can be expressed in terms of invariants of the deviatoric stress tensor as

$$F(J_{2D}, J_{3D}) = 0 \quad (2.16)$$

Here J_{2D} and J_{3D} are the invariants of the deviatoric stress tensor.

A detailed description of some of the yield criteria used in metal plasticity is given in Reference [54]. These include maximum stress theory, maximum strain theory, Tresca yield criterion, Von Mises yield criterion, and the maximum strain energy theory. Under certain situations, Von Mises and Tresca yield criteria have been used in some geomechanics applications. Both their yield criteria are, however, independent of mean pressure, and can be applied only for frictionless materials. Therefore, certain modifications and extensions are required to model the frictional behavior of

materials encountered in geomechanics problems. Details of such advanced plasticity models are given in Chapter 4.

2.6.2. Post Yield Behavior: Plastic Stress-Strain Relations

In order to formulate the plastic behavior mathematically, certain idealizations of the stress strain behavior are required. Some of the commonly used idealizations are [42, 54]

- (1) Perfectly Elastic,
- (2) Rigid Perfectly Plastic,
- (3) Rigid, Linear Strain Hardening,
- (4) Elastic Perfectly Plastic,
- (5) Elastic, Linear Strain Hardening
- (6) Strain Softening

Based on these idealizations, different stress-strain relationships can be defined. A generalized approach for determination of plastic stress-strain relationships is given in the following section.

2.7. Generalized Plastic Stress-Strain Relations

A generalized approach has been suggested by Drucker [25, 26, 28] for determining plastic stress-strain relations for any yield criterion, and a description is given in this section.

A precise definition of work hardening has been given by Drucker [25] which lead to some postulates in this theory. For more general states of stresses and stress paths, the concept of work hardening can be expressed in terms of the work done by an additional set of stresses due to an external agency. The work referred is only the

work done by the added set of forces (stresses) on the displacements (strains) which result, and not the total work done by all the forces acting [25]. Work hardening means that for all such added stresses, the material will remain in stable equilibrium. Furthermore, it is governed by the following postulates [25]:

- (1) During the application of stresses, the work done by the external agency will be positive.
- (2) Over a cycle of application and removal of stresses, the work done by the external agency will be zero or positive.

In other words, work hardening implies that useful net energy cannot be extracted from the material and a set of external forces in such a cycle. A detailed explanation of this concept can be found in reference [25].

Furthermore, certain conditions should be satisfied in order to insure appropriate description of physical process involved in plastic deformations. There are four conditions formulated by Prager [65], and are given below.

- (a) condition of continuity
- (b) condition of uniqueness
- (c) condition of irreversibility
- (d) condition of consistency.

The implications of these four conditions together with other assumptions made [25, 26, 27, 28, 65], will lead to important restraints on the plastic stress-strain behavior. These bring

the fact that the incremental plastic strain vector is normal to the yield surface. This is called the normality rule in the theory of plasticity. The convexity of the yield surface can be shown to be a consequence of some of the above requirements.

The normality rule can be written as [25, 26, 28]

$$d\epsilon_{ij}^p = \lambda \frac{\partial F}{\partial \sigma_{ij}} \quad (2.17)$$

where λ is a positive scalar factor of proportionality. A basic assumption made in the development of stress-strain relations for elastic-plastic materials is that for each load increment the corresponding strain increment can be decomposed into elastic and plastic components. That is

$$d\epsilon_{ij} = d\epsilon_{ij}^e + d\epsilon_{ij}^p \quad (2.18)$$

Substituting elastic strain-stress relations in Equation (2.10), one can write,

$$d\epsilon_{ij} = \frac{dS_{ij}}{2G} + \frac{dJ_1}{9K} \delta_{ij} + \lambda \frac{\partial F}{\partial \sigma_{ij}} \quad (2.19)$$

The concepts described in the foregoing sections can provide a basis for some of the research advanced plasticity models, and in determination of their constitutive or stress-strain relationships. These and other concepts are used in Chapter 4 for deriving constitutive relationships based on Drucker-Prager, critical state and

cap models for complex geologic media for which the conventional plasticity models described in this chapter are usually not appropriate.

Chapter 3
FINITE ELEMENT METHOD: ONE-, TWO-, AND
THREE-DIMENSIONAL IDEALIZATIONS

In view of the fact that many problems encountered in soil-structure interaction can often be idealized as one-, two- and three-dimensional, the procedures developed herein includes provision for generalized nonlinear finite element analysis for all three idealizations. Such problems include laterally loaded piles, long retaining structures, footing, beams on deformable foundations, buried pipes, interaction in track-support structures, etc., which covers a wide range of applications in geomechanics. Details of the formulations of one-, two-, and three-dimensional idealizations are given in this chapter.

3.1 One-Dimensional Idealization: Beam-Column Elements

Problems of beam-bending and beam-column analysis can be idealized using one-dimensional finite elements. For the element considered here, Figure (3.1a), the displacements, u , v , w in x -, y -, and z -directions respectively, and rotation θ_y about y -axis are assumed as follows [11]

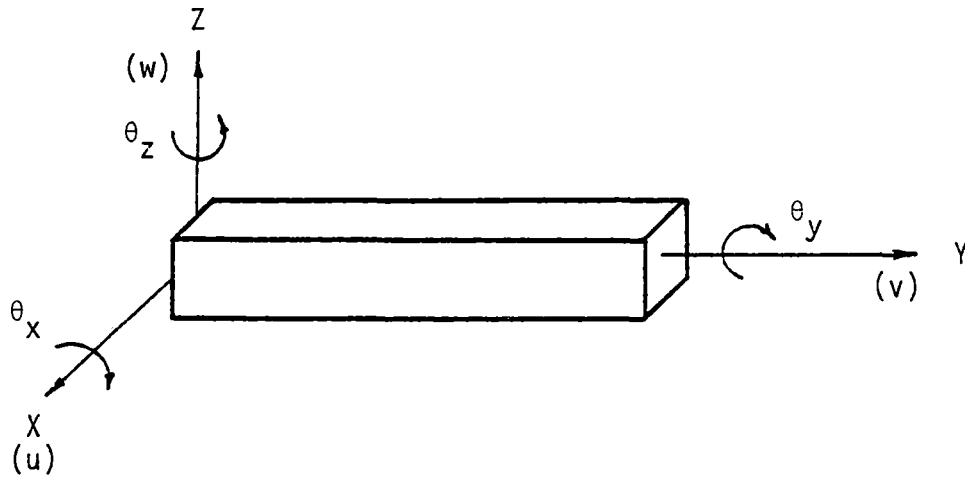
$$u = \alpha_1 + \alpha_2 y + \alpha_3 y^2 + \alpha_4 y^3 \quad (3.1a)$$

$$v = \alpha_5 + \alpha_6 y \quad (3.1b)$$

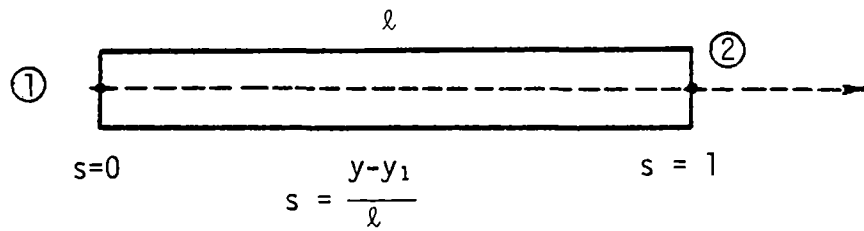
$$w = \alpha_7 + \alpha_8 y + \alpha_9 y^2 + \alpha_{10} y^3 \quad (3.1c)$$

$$\theta_y = \alpha_{11} + \alpha_{12} y \quad (3.1d)$$

This can be written in the matrix notation as follows:



(a) Coordinate Axes for Beam-Column Element



(b) Local Coordinate System for Beam-Column Element

Figure 3.1 One-Dimensional Idealization for Beam-Column Element

$$\{u\} = [\Phi]\{\alpha\} \quad (3.1e)$$

where

$$[\Phi] = \begin{bmatrix} 1 & y & y^2 & y^3 & 0 & 0 & 0 & 0 & 0 & 0 & 0 & 0 \\ 0 & 0 & 0 & 0 & 1 & y & 0 & 0 & 0 & 0 & 0 & 0 \\ 0 & 0 & 0 & 0 & 0 & 0 & 1 & y & y^2 & y^3 & 0 & 0 \\ 0 & 0 & 0 & 0 & 0 & 0 & 0 & 0 & 0 & 0 & 1 & y \end{bmatrix}$$

$\{u\}$ = vector of unknowns u , v , w and θ_y , and

$$\{\alpha\}^T = [\alpha_1, \alpha_2, \dots, \alpha_{12}]$$

Although, the use of generalized coordinates, Equations (3.1) forms the basis for finding displacements at any point, its direct use can be difficult. Hence, interpolation functions which are related to generalized coordinates can be used for expressing unknown variables at any point in the element.

The displacements at any point in the element, Figure (3.1), can be expressed using the interpolation functions. That is,

$$\{u\} = [N]\{q\} \quad (3.2a)$$

where

$$\{q\}^T = [u_1, v_1, w_1, \theta_{x_1}, \theta_{y_1}, \theta_{z_1}, u_2, v_2, w_2, \theta_{x_2}, \theta_{y_2}, \theta_{z_2}],$$

$$\{u\}^T = [u, v, w, \theta_y],$$

and

$$[N]^T = \begin{bmatrix} N_1 & 0 & 0 & 0 \\ 0 & N_5 & 0 & 0 \\ 0 & 0 & N_1 & 0 \\ 0 & 0 & -N_2 & 0 \\ 0 & 0 & 0 & N_5 \\ N_2 & 0 & 0 & 0 \\ N_3 & 0 & 0 & 0 \\ 0 & N_6 & 0 & 0 \\ 0 & 0 & N_3 & 0 \\ 0 & 0 & -N_4 & 0 \\ 0 & 0 & 0 & N_6 \\ N_4 & 0 & 0 & 0 \end{bmatrix}$$

Here, the quantities θ_x and θ_y can be expressed as

$$\theta_x = -\frac{dw}{dy} \quad (3.3a)$$

and

$$\theta_z = -\frac{du}{dy} \quad (3.3b)$$

The interpolation functions are commonly expressed in terms of local coordinates. The quantities in Equation (3.2b) are expressed as,

$$N_1 = 1 - 3s^2 + 2s^3 \quad (3.4a)$$

$$N_2 = -6s(s-1)^2 \quad (3.4b)$$

$$N_3 = 3s^2 - 2s^3 \quad (3.4c)$$

$$N_4 = -6s^2(s-1) \quad (3.4d)$$

$$N_5 = (1-s) \quad (3.4e)$$

$$N_6 = s \quad (3.4f)$$

and

$$s = (y - y_1)/\ell \quad (3.4g)$$

where s = local coordinate, Figure (3.1b), y = global coordinate of any point, y_1 = global coordinate of node 1, and ℓ = length of the element. A detailed description of derivation of interpolation functions in terms of the cubic polynomial in Equation (3.1) is given by Desai [11]. The variation of the Hermitian interpolation functions N_1 to N_4 are given in Figure (3.2).

3.1.1 Element Stiffness Matrix

The element equilibrium equations can be derived by invoking the principle of stationary (minimum) potential energy which for the beam-column element is given below. The total potential energy can be expressed as the summation of internal strain energy and the potential of externally applied loads. The following potential energy functional is used to derive element equations [11,35,89]

$$\begin{aligned} \mathbb{R}_p = & \ell \int_0^1 \frac{1}{2} EI_{xx} (w'')^2 ds + \ell \int_0^1 \frac{1}{2} EI_{zz} (u'')^2 ds \\ & + \frac{\ell}{2} \int_0^1 GJ \theta_y'^2 ds + \frac{\ell}{2} \int_0^1 AE v'^2 ds - A\ell \int_0^1 (\bar{X}u + \bar{Y}v + \bar{Z}w) ds \\ & - \ell \int_0^1 (\bar{T}_x u + \bar{T}_y v + \bar{T}_z w) ds - \sum_{L=1}^M \bar{P}_{iL} u_i \end{aligned} \quad (3.5)$$

where ℓ = length of the element, E = Young's modulus, G = shear modulus, I_{xx} , I_{zz} = the moment of inertia of the beam in x and z directions,

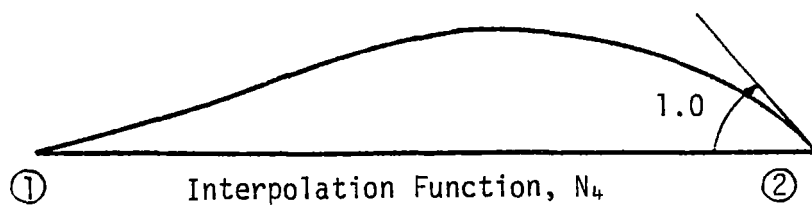
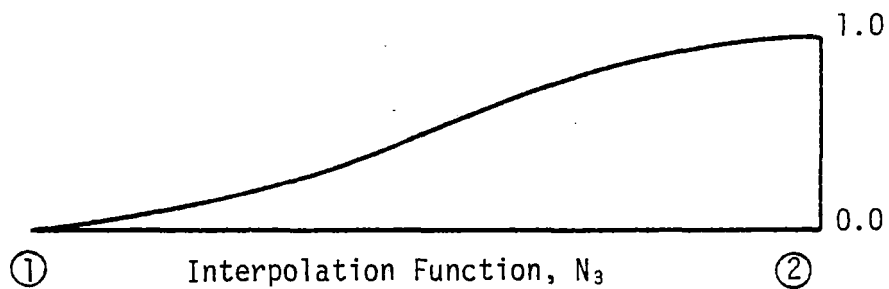
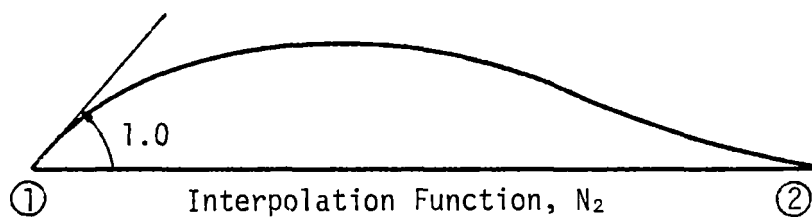
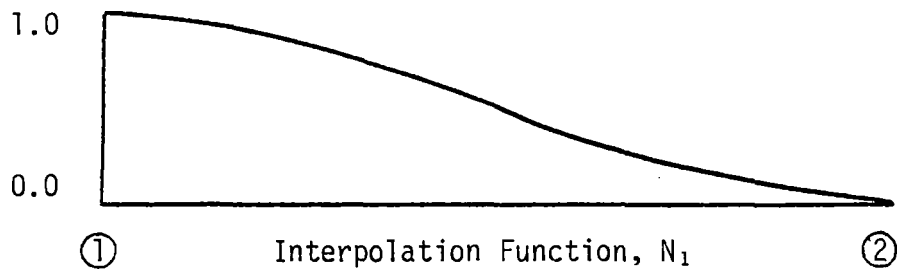


Figure 3.2 Interpolation Functions for Beam-Column Analysis

respectively, J = polar moment of inertia, \bar{X} , \bar{Y} , \bar{Z} = body forces, and \bar{T}_x , \bar{T}_y and \bar{T}_z = the surface traction forces in x , y , and z directions, respectively, $\bar{P}_{i\ell}$ = the concentrated force at node i , u_i = displacements at corresponding nodes ($= u, v, w$), and M = total number of degrees of freedom where \bar{P}_{iL} is applied. The overbar denotes a prescribed quantity, and the prime denotes the derivative with respect to y coordinate.

Substitution of u, v, w and their derivatives in Equation (3.5) for Π_p , and then finding the stationary value of Π_p leads to element equations as [11,35]

$$[k]\{q\} = \{Q\} \quad (3.6)$$

where $[k]$ is the element of stiffness matrix, and $\{Q\}$ is the element load vector. The stiffness matrix, $[k]$ is given in Table (3.1) with respect to the local coordinate or elemental coordinate system. This has to be transformed to global coordinate system before assembling it to the global stiffness. The transformation relationship from x_i ($i = 1, 2, 3$) to x'_i ($i = 1, 2, 3$), as shown in Figure (3.3), can be written as

$$x'_i = a_{ij}x_j \quad (3.7)$$

where a_{ij} is the coordinate transformation tensor. This can be expressed as,

$$a_{ij} \equiv \begin{pmatrix} \cos\theta'_{xx} & \cos\theta'_{xy} & \cos\theta'_{xz} \\ \cos\theta'_{yx} & \cos\theta'_{yy} & \cos\theta'_{yz} \\ \cos\theta'_{zx} & \cos\theta'_{zy} & \cos\theta'_{zz} \end{pmatrix} \quad (3.8)$$

Equation (3.7) can be written in the matrix notation as

Table 3.1

Stiffness Matrix for the Beam-Column Element

$\frac{12EI}{l^2} z$	0	0	0	0	$\frac{-6EI}{l^2} z$	$\frac{-12EI}{l^3} z$	0	0	0	0	$\frac{-6EI}{l^2} z$	u_1
0	$\frac{AE}{l}$	0	0	0	0	0	$\frac{-AE}{l}$	0	0	0	0	v_1
0	0	$\frac{12EI}{l^3} x$	$\frac{6EI}{l^2} x$	0	0	0	0	$\frac{-12EI}{l^3} x$	$\frac{6EI}{l^2} x$	0	0	w_1
0	0	$\frac{6EI}{l^2} x$	$\frac{4EI}{l} x$	0	0	0	0	$\frac{-6EI}{l^2} x$	$\frac{2EI}{l} x$	0	0	θ_{x1}
0	0	0	0	$\frac{GJ}{l}$	0	0	0	0	0	$\frac{-GJ}{l}$	0	θ_{y1}
$\frac{-6EI}{l^2} z$	0	0	0	0	$\frac{4EI}{l} z$	$\frac{6EI}{l^2} z$	0	0	0	0	$\frac{2EI}{l} z$	θ_{z1}
$\frac{-12EI}{l^3} z$	0	0	0	0	$\frac{6EI}{l^2} z$	$\frac{12EI}{l^3} z$	0	0	0	0	$\frac{6EI}{l^2} z$	u_2
0	$\frac{-AE}{l}$	0	0	0	0	0	$\frac{AE}{l}$	0	0	0	0	v_2
0	0	$\frac{-12EI}{l^3} x$	$\frac{-6EI}{l^2} x$	0	0	0	0	$\frac{12EI}{l^3} x$	$\frac{-6EI}{l^2} x$	0	0	w_2
0	0	$\frac{6EI}{l^2} x$	$\frac{2EI}{l} x$	0	0	0	0	$\frac{-6EI}{l^2} x$	$\frac{-4EI}{l} x$	0	0	θ_{x2}
0	0	0	0	$\frac{-GJ}{l}$	0	0	0	0	0	$\frac{GJ}{l}$	0	θ_{y2}
$\frac{-6EI}{l^2} z$	0	0	0	0	$\frac{2EI}{l} z$	$\frac{6EI}{l^2} z$	0	0	0	0	$\frac{4EI}{l} z$	θ_{z2}

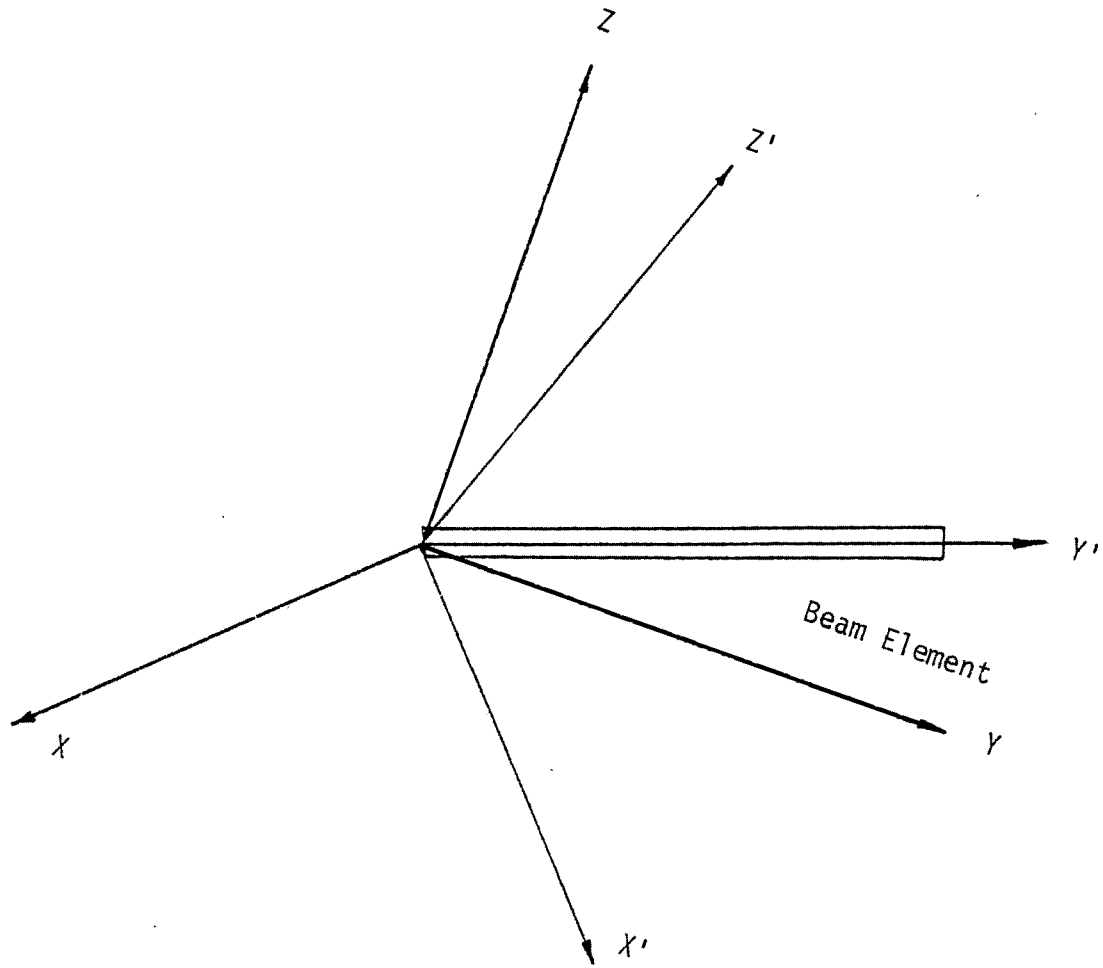


Figure 3.3 Transformation of Coordinates

$$\begin{Bmatrix} X' \\ Y' \\ Z' \end{Bmatrix} = [a] \begin{Bmatrix} X \\ Y \\ Z \end{Bmatrix} \quad (3.9)$$

Once the transformation matrix is known, the forces and moments can be transformed to the new coordinate system as [51]

$$\begin{Bmatrix} p'_x \\ p'_y \\ p'_z \\ m'_x \\ m'_y \\ m'_z \end{Bmatrix} = \begin{bmatrix} [a] & [0] \\ [0] & [a] \end{bmatrix} \begin{Bmatrix} p_x \\ p_y \\ p_z \\ m_x \\ m_y \\ m_z \end{Bmatrix} \quad (3.10)$$

where p_x , p_y and p_z are the nodal forces, and m_x , m_y , and m_z are the nodal moments in x , y , z directions, respectively, in local coordinates. Primed quantities on the left-hand side of Equation (3.10) denote forces and moments with respect to global coordinates. The stiffness matrix $[k]$ can be transformed in the following manner. The total stiffness matrix can be written as,

$$[k] = \begin{bmatrix} [\bar{k}_{11}] & [\bar{k}_{12}] \\ [\bar{k}_{21}] & [\bar{k}_{22}] \end{bmatrix} \quad (3.11)$$

(6 × 6) (6 × 6)
(6 × 6) (6 × 6)

where \bar{k}_{11} , \bar{k}_{12} , \bar{k}_{21} and \bar{k}_{22} are submatrices of the total local stiffness

matrix. These submatrices can be expressed as

$$\bar{k}_{ij} = \begin{bmatrix} \begin{bmatrix} \bar{k}_\alpha \\ (3 \times 3) \end{bmatrix} & \begin{bmatrix} \bar{k}_\beta \\ (3 \times 3) \end{bmatrix} \\ \begin{bmatrix} \bar{k}_\gamma \\ (3 \times 3) \end{bmatrix} & \begin{bmatrix} \bar{k}_\delta \\ (3 \times 3) \end{bmatrix} \end{bmatrix} \quad \text{for } i = 1, 2 \quad (3.12)$$

The transformed quantities of the submatrix \bar{k}_{ij} can be obtained as

$$[\bar{k}_{11}]' = \begin{bmatrix} \begin{bmatrix} [a] & [0] \\ (6 \times 6) \end{bmatrix} & \begin{bmatrix} \begin{bmatrix} \bar{k}_\alpha & \bar{k}_\beta \end{bmatrix} \\ \begin{bmatrix} \bar{k}_\gamma & \bar{k}_\delta \end{bmatrix} \end{bmatrix} & \begin{bmatrix} [a]^T & [0] \\ [0] & [a]^T \end{bmatrix} \end{bmatrix} \quad (4.13)$$

where $[\bar{k}_{11}]'$ is the transformed matrix referred in global coordinates. Similarly, $[\bar{k}_{12}]$, $[\bar{k}_{21}]$ and $[\bar{k}_{22}]$ can also be transformed to find the element stiffness in global coordinates as,

$$[k]' = \begin{bmatrix} \begin{bmatrix} [\bar{k}_{11}]' & [\bar{k}_{12}]' \\ [\bar{k}_{21}]' & [\bar{k}_{22}]' \end{bmatrix} \end{bmatrix} \quad (3.14)$$

3.1.2 Element Load Vector

External loads can either be point loads or distributed loads.

Global load vector due to point loads can be formed by adding them to

the correct location which corresponds to the degree of freedom of that node. Load vector due to surface traction can be evaluated as follows. Consider a general case where the surface traction varies linearly as shown in Figure (3.4). Surface traction at any point on the element can be expressed as [11],

$$p_x = (1 - s)p_{x_1} + sp_{x_2} \quad (3.15a)$$

$$p_y = (1 - s)p_{y_1} + sp_{y_2} \quad (3.15b)$$

$$p_z = (1 - s)p_{z_1} + sp_{z_2} \quad (3.15c)$$

where p_{i_1} and p_{i_2} are the nodal values of traction in "i" direction, at node 1 and node 2, respectively. The element load vector can be evaluated in global coordinates as

$$\{Q\} = \ell \int_0^1 \left[\begin{array}{cccc} [N_1] & [N_2] & [N_3] & [N_4] \end{array} \right]^T \left\{ \begin{array}{l} (1 - s)p_{x_1} + sp_{x_2} \\ (1 - s)p_{y_1} + sp_{y_2} \\ (1 - s)p_{z_1} + sp_{z_2} \end{array} \right\} ds \quad (3.16)$$

(12 × 3) (3 × 1)

where

$$[N_i] = \begin{bmatrix} N_i & & & \\ & N_i & & \\ & & N_i & \\ & & & N_i \end{bmatrix} \quad (i = 1, 4).$$

Substituting the expressions of N_1 , N_2 , N_3 and N_4 into Equation (3.16) and evaluating the integral, leads to the load vector as

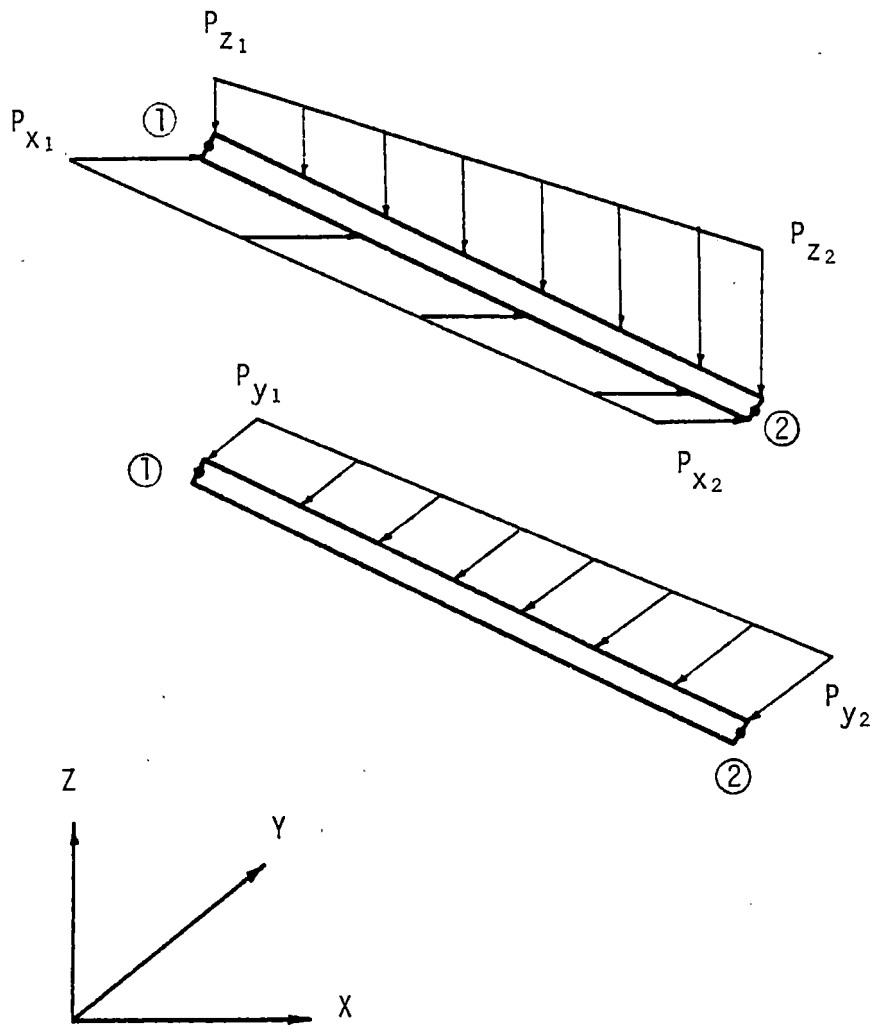


Figure 3.4 Distributed Loads on Beam-Column Element

$$\{Q\} = \frac{\ell}{20} \begin{Bmatrix} 7p_{x_1} + 3p_{x_2} \\ 7p_{y_1} + 3p_{y_2} \\ 7p_{z_1} + 3p_{z_2} \\ \frac{\ell}{3} (3p_{x_1} + 2p_{x_2}) \\ \frac{\ell}{3} (3p_{y_1} + 2p_{y_2}) \\ \frac{\ell}{3} (3p_{z_1} + 2p_{z_2}) \\ 3p_{x_1} + 7p_{x_2} \\ 3p_{y_1} + 7p_{y_2} \\ 3p_{z_1} + 7p_{z_2} \\ -\frac{\ell}{3} (2p_{x_1} + 3p_{x_2}) \\ -\frac{\ell}{3} (2p_{y_1} + 3p_{y_2}) \\ -\frac{\ell}{3} (2p_{z_1} + 3p_{z_2}) \end{Bmatrix}$$

3.1.3 Computer Code for One-Dimensional Analysis

A computer code is developed to compute the global stiffness and to modify it for given boundary conditions. This code has the capability of solving nonlinear problems using incremental and/or iterative techniques. It also has the capability of stress transfer procedures. Numerical procedures for nonlinear analysis are given in Chapter 5. This code uses a regular "Band Solution" technique. In order to make the program more efficient, most vectors and matrices are stored in a one-dimensional array using the technique of dynamic dimensioning. This makes it possible to change the program capacity with a change in only

one DIMENSION statement. Further details of this code and user's manual are given in reference [76].

3.2. Two-Dimensional Idealization

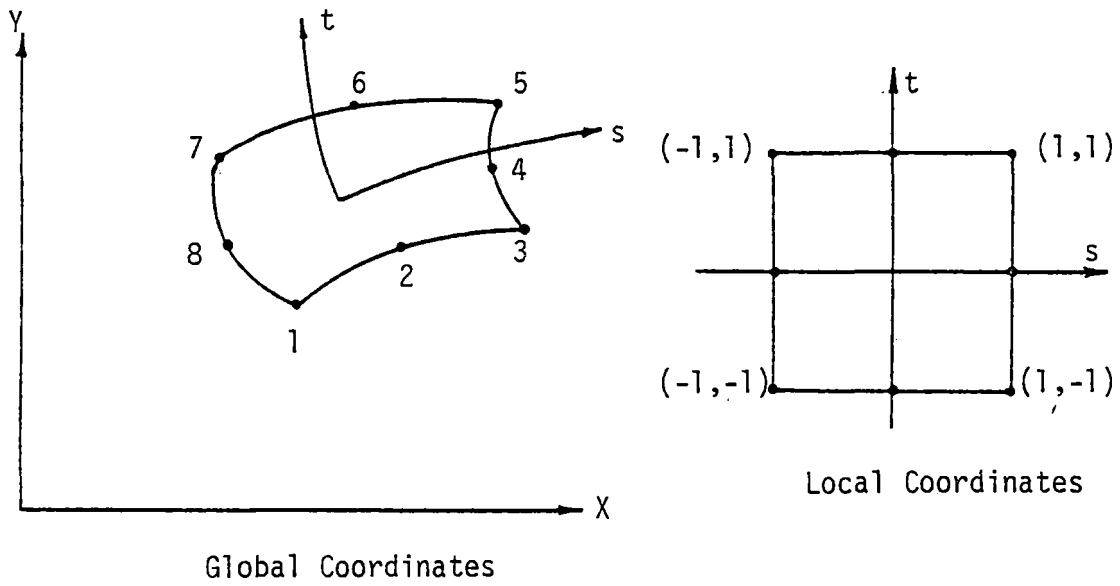
Many problems in engineering can be analyzed as two-dimensional under certain assumptions; there are plane stress, plane strain and axisymmetric idealizations. In plane idealizations, only the stresses and strains in one plane have to be considered. There is another class of problems where bodies of revolution are considered under axisymmetric loadings. These are called axisymmetric problems, and the mathematical problem is very similar to that of plane stress or plane strain. Triangular and quadrilateral elements are commonly used in the finite element analysis of two-dimensional bodies. Often in the past, a 4-node quadrilateral element composed of four constant strain triangles has been used. However, in general, the stiffness matrix of a four-node quadrilateral element can be developed by using the isoparametric concept [90]. In the current research, four-node and eight-node isoparametric quadrilateral elements are used.

3.2.1. Finite Element Formulation

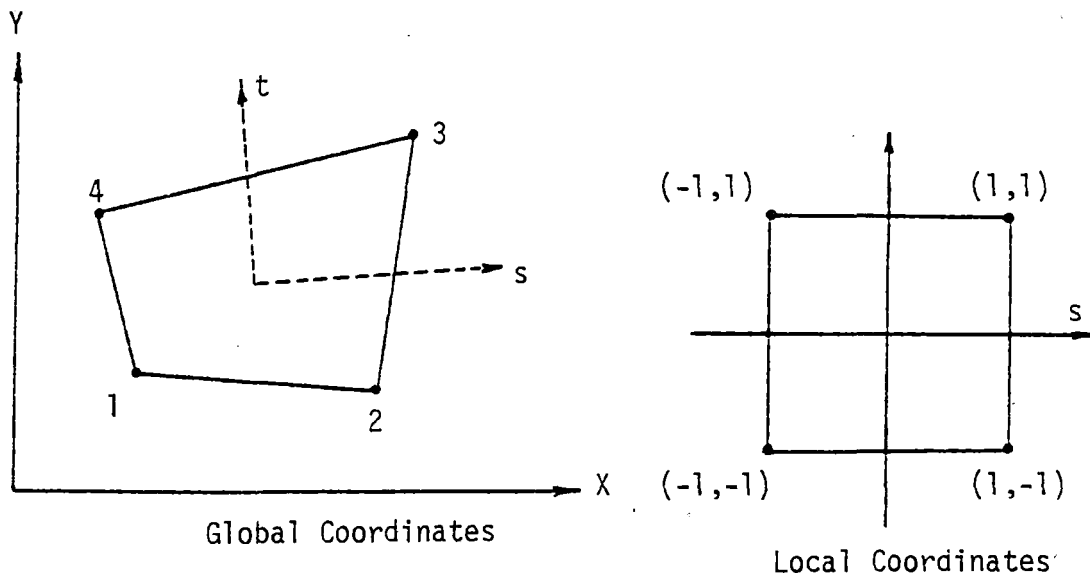
The computer code developed herein has capability of having either four-node or eight-node elements, Figure (3.5). The displacements u , v at a point in the x and y direction, respectively, can be expressed by using interpolation functions, and nodal displacements as follows:

$$u = N_1u_1 + N_2u_2 + N_3u_3 + \dots N_8u_8 \quad (3.18a)$$

$$v = N_1v_1 + N_2v_2 + N_3v_3 + \dots N_8v_8$$



(a) 8-Node Isoparametric Element



(b) 4-Node Isoparametric Element

Figure 3.5 Two-Dimensional Isoparametric Elements

where N_1, N_2, \dots, N_8 are interpolation functions in local coordinates, and u_i, v_i are the displacements of node "i" in the x and y directions, respectively. This can be written in the matrix form as follows:

$$\begin{Bmatrix} u \\ v \end{Bmatrix} = [N] \{q\} \quad (3.18b)$$

where

$$[N] = \begin{bmatrix} N_1 & 0 & N_2 & 0 & \dots & N_8 & 0 \\ 0 & N_1 & 0 & N_2 & \dots & 0 & N_8 \end{bmatrix}$$

and

$$\{q\}^T = [u_1 \ v_1 \ u_2 \ v_2 \ \dots \ u_8 \ v_8]$$

For the eight-node element, the interpolation functions can be written as

$$\begin{aligned}
N_1 &= \frac{1}{4} (1 - s)(1 - t)(-s - t - 1) \\
N_3 &= \frac{1}{4} (1 + s)(1 - t)(s - t - 1) \\
N_5 &= \frac{1}{4} (1 + s)(1 + t)(s + t - 1) \\
N_7 &= \frac{1}{4} (1 - s)(1 + t)(-s + t - 1) \\
N_2 &= \frac{1}{2} (1 - s^2)(1 - t) \\
N_4 &= \frac{1}{2} (1 - t^2)(1 + s) \\
N_6 &= \frac{1}{2} (1 - s^2)(1 + t) \\
N_8 &= \frac{1}{2} (1 - t^2)(1 - s)
\end{aligned} \tag{3.19a}$$

For the four-node element,

$$N_i = \frac{1}{4} (1 + ss_i)(1 + tt_i) \tag{3.19b}$$

where s and t correspond to the local coordinates which vary from -1 to $+1$, and the subscript "i" denotes the values at node i . Here, N_i is the interpolation function corresponding to node "i" as shown in Figure (3.5). In the isoparametric formulation, the coordinates at a point (x,y) can also be expressed using the same interpolation functions. That is, for the eight-node element,

$$x = \sum_{i=1}^8 N_i x_i \tag{3.20a}$$

$$y = \sum_{i=1}^8 N_i y_i \tag{3.20b}$$

Strain-Displacement Relationship

The strains ϵ_x , ϵ_y , and γ_{xy} can be written as

$$\begin{aligned}\epsilon_x &= \frac{\partial u}{\partial x} \\ \epsilon_y &= \frac{\partial v}{\partial y} \\ \gamma_{xy} &= \frac{\partial u}{\partial y} + \frac{\partial v}{\partial x}\end{aligned}\tag{3.21a}$$

For the axisymmetric idealization, the circumferential strain, ϵ_θ , can be expressed as

$$\epsilon_\theta = \frac{u}{x}\tag{3.21b}$$

The strain vector $\{\epsilon\}$ then contains

$$\{\epsilon\} = \begin{Bmatrix} \frac{\partial u}{\partial x} \\ \frac{\partial v}{\partial y} \\ \frac{\partial u}{\partial y} + \frac{\partial v}{\partial x} \\ \frac{u}{x} \end{Bmatrix}\tag{3.21c}$$

Substituting the expressions in Equation (3.18) into Equation (3.21c) the following relationship is obtained.

$$\begin{Bmatrix} \epsilon_x \\ \epsilon_y \\ \gamma_{xy} \\ \epsilon_\theta \end{Bmatrix} = \begin{bmatrix} \frac{\partial N_1}{\partial x} & 0 & \frac{\partial N_2}{\partial x} & 0 & \dots & \frac{\partial N_8}{\partial x} & 0 \\ 0 & \frac{\partial N_1}{\partial y} & 0 & \frac{\partial N_2}{\partial y} & \dots & 0 & \frac{\partial N_8}{\partial y} \\ \frac{\partial N_1}{\partial y} & \frac{\partial N_1}{\partial x} & \frac{\partial N_2}{\partial y} & \frac{\partial N_2}{\partial x} & \dots & \dots & \dots \\ \frac{N_1}{x} & 0 & \frac{N_2}{x} & 0 & \dots & \dots & \frac{N_8}{x} \end{bmatrix} \begin{Bmatrix} u_1 \\ v_1 \\ u_2 \\ v_2 \\ \vdots \\ \vdots \\ u_8 \\ v_8 \end{Bmatrix}\tag{3.22a}$$

or

$$\{\epsilon\} = [B]\{q\} \quad (3.22b)$$

Here, the matrix $[B]$ is called the strain-displacement transformation matrix. In order to evaluate the global derivatives of the interpolation (shape) functions, it is required to find a transformation from local to global coordinates. Using the chain rule of differentiation

$$\frac{\partial}{\partial s} = \frac{\partial}{\partial x} \frac{\partial x}{\partial s} + \frac{\partial}{\partial y} \frac{\partial y}{\partial s} \quad (3.23a)$$

$$\frac{\partial}{\partial t} = \frac{\partial}{\partial x} \frac{\partial x}{\partial t} + \frac{\partial}{\partial y} \frac{\partial y}{\partial t}$$

or in vector form,

$$\begin{Bmatrix} \frac{\partial}{\partial s} \\ \frac{\partial}{\partial t} \end{Bmatrix} = \begin{bmatrix} \frac{\partial x}{\partial s} & \frac{\partial y}{\partial s} \\ \frac{\partial x}{\partial t} & \frac{\partial y}{\partial t} \end{bmatrix} \begin{Bmatrix} \frac{\partial}{\partial x} \\ \frac{\partial}{\partial y} \end{Bmatrix} \quad (3.23b)$$

This can also be written as

$$\begin{Bmatrix} \frac{\partial}{\partial s} \\ \frac{\partial}{\partial t} \end{Bmatrix} = [J] \begin{Bmatrix} \frac{\partial}{\partial x} \\ \frac{\partial}{\partial y} \end{Bmatrix} \quad (3.23c)$$

where $[J]$ is known as the Jacobian matrix. This can be expressed in terms of nodal coordinates as,

$$[J] = \begin{bmatrix} \frac{\partial}{\partial s} \sum N_i x_i & \frac{\partial}{\partial s} \sum N_i y_i \\ \frac{\partial}{\partial t} \sum N_i x_i & \frac{\partial}{\partial t} \sum N_i y_i \end{bmatrix} \quad (3.24a)$$

$$= \begin{bmatrix} \frac{\partial N_1}{\partial s} & \frac{\partial N_2}{\partial s} & \dots & \dots & \dots & \dots & \dots & \frac{\partial N_8}{\partial s} \\ \frac{\partial N_1}{\partial t} & \frac{\partial N_2}{\partial t} & \dots & \dots & \dots & \dots & \dots & \frac{\partial N_8}{\partial t} \end{bmatrix} \begin{Bmatrix} x_1 & y_1 \\ x_2 & y_2 \\ x_3 & y_3 \\ \dots & \dots \\ \dots & \dots \\ \dots & \dots \\ \dots & \dots \\ x_8 & y_8 \end{Bmatrix} \quad (3.24b)$$

In order to evaluate [B] matrix in Equation (3.22), the global derivatives of the interpolation functions have to be known, and they can be evaluated using the Jacobian matrix. That is, for example,

$$\begin{Bmatrix} \frac{\partial N_1}{\partial x} \\ \frac{\partial N_1}{\partial y} \end{Bmatrix} = [J]^{-1} \begin{Bmatrix} \frac{\partial N_1}{\partial s} \\ \frac{\partial N_1}{\partial t} \end{Bmatrix} \quad (3.25)$$

where $[J]^{-1}$ is the inverse of the Jacobian matrix.

Constitutive Relationship

As will be shown in the subsequent section, the constitutive relationship is required to derive potential energy, and the stiffness of the element under consideration. For the class of problems in solid

mechanics that is considered in this study, constitutive relationship means only a relationship between stress and strain quantities. This is written as

$$\begin{Bmatrix} \sigma_x \\ \sigma_y \\ \tau_{xy} \\ \sigma_\theta \end{Bmatrix} = \begin{bmatrix} C_{11} & C_{12} & C_{13} & C_{14} \\ C_{21} & C_{22} & C_{23} & C_{24} \\ C_{31} & C_{32} & C_{33} & C_{34} \\ C_{41} & C_{42} & C_{43} & C_{44} \end{bmatrix} \begin{Bmatrix} \epsilon_x \\ \epsilon_y \\ \gamma_{xy} \\ \epsilon_\theta \end{Bmatrix} \quad (3.26a)$$

or

$$\{\sigma\} = [C]\{\epsilon\} \quad (3.26b)$$

Here $\{\sigma\}$ is the vector of stress components, and $[C]$ is the constitutive matrix. The fourth column and the fourth row of $[C]$ matrix, are meaningful only for the axisymmetric idealization. The constitutive matrix $[C]$ will take different forms depending on the stress-strain model used. Details of constitutive matrix, $[C]$, for different models are given in Chapter 4.

3.2.2. Element Stiffness Matrix

Element stiffness can be determined using the well known principle of minimum potential energy. According to this principle, the displacement fields that satisfy internal compatibility and kinematic boundary conditions as well as equations of equilibrium, make the potential energy a stationary value. For stable equilibrium, the potential energy has to be a minimum. Potential energy of a body can be expressed as the sum of internal energy (strain energy), and the potential of body forces and surface tractions. The following potential energy functional is used

for the derivation of element stiffness matrix:

$$\begin{aligned} \Pi_p = & \iiint_V U(u,v,w)dv - \iiint_V (\bar{X}u + \bar{Y}v + \bar{Z}w)dv \\ & - \iint_{S_1} (\bar{T}_x u + \bar{T}_y v + \bar{T}_z w)ds \end{aligned} \quad (3.27)$$

where S_1 is that portion of the surface of the body on which surface tractions are prescribed. $U(u,v,w)$ denotes the strain energy density. The last two integrals in Equation (3.27) represent the work done (hence the potential lost) by body forces, \bar{X} , \bar{Y} , \bar{Z} , and surface tractions, \bar{T}_x , \bar{T}_y , \bar{T}_z . The overbar denotes specified quantities. The quantities u , v , w are the displacements in x , y , and z directions, respectively. The functional in Equation (3.27) can be written in terms of nodal displacements, and initial stress conditions as follows:

$$\begin{aligned} \Pi_p = & \frac{1}{2} \iiint_V (\{q\}^T [B]^T [C] [B] \{q\} + 2\{q\}^T [B]^T \{\sigma_0\})dv \\ & - 2 \iiint_V \{q\}^T [N]^T \{\bar{X}\}dv - \iint_{S_1} \{q\}^T [N]^T \{\bar{T}\}ds \end{aligned} \quad (3.28)$$

Here, $[B]$ is the strain-displacement relationship, $\{q\}$ is the displacement vector, $[C]$ is the constitutive relationship, $\{\sigma_0\}$ is the vector of initial stress, and $[N]$ is the matrix of interpolation functions.

Now the element equilibrium equations can be found by minimizing the potential energy functional Π_p . The element equilibrium equations take the following form:

$$[k]\{q\} = \{Q\} \quad (3.29a)$$

where $[k]$ is the element stiffness matrix, and $\{Q\}$ is the element load vector. These can be expressed as

$$[k] = \iiint_V [B]^T [C] [B] dv \quad (3.29b)$$

and

$$\{Q\} = \iiint_V [N]^T \{\bar{X}\} dv + \iint_{S_1} [N]^T \{\bar{T}\} ds - \iiint_V [B]^T \{\sigma_0\} dv \quad (3.29c)$$

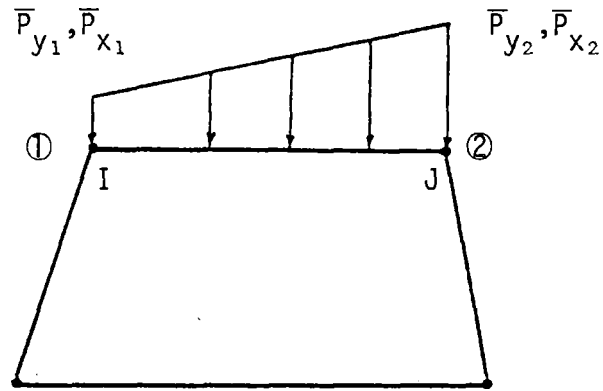
Having established the matrices $[B]$, and $[C]$, the integral in Equation (3.29b) can be evaluated using numerical integration techniques. Here, the Gaussian quadrature is used to evaluate the integrals. Hence, the integral in Equation (3.29b) becomes

$$\iiint_V [B]^T [C] [B] dv = \int_{-1}^{+1} \int_{-1}^{+1} \int_{-1}^{+1} [B]^T [C] [B] \det[J] dr ds dt \quad (3.30)$$

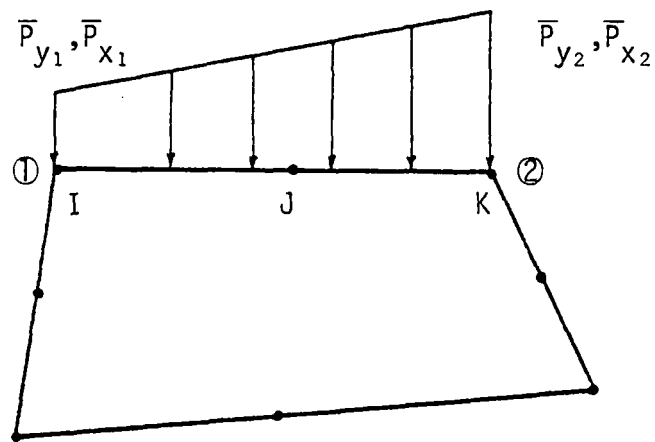
where r , s , t represent the local coordinates. Details of numerical integration procedures can be found in references [15, 89]. In this research program, two- and three-point integration schemes are used.

3.2.3. Element Load Vector

In this section, the load vector due to uniformly distributed surface loads are evaluated. The computer code developed herein has the capability of having 4-node elements or 8-node elements, and hence load vector for both elements are given below. Consider a uniformly distributed load as shown in Figure (3.6). The load vector due to surface loads is



(a) Surface Loading on a 4-Node Element



(b) Surface Loading on a 8-Node Element

Figure 3.6 Distributed Surface Loads on Two-Dimensional Elements

$$\{Q\} = \int_S [N]^T \{p\} ds \quad (3.31a)$$

$$= \int_S [N]^T \begin{bmatrix} \frac{1}{2}(1-s) & \frac{1}{2}(1+s) & 0 & 0 \\ 0 & 0 & \frac{1}{2}(1-s) & \frac{1}{2}(1+s) \end{bmatrix} \begin{Bmatrix} \bar{p}_{1x} \\ \bar{p}_{2y} \\ \bar{p}_{2x} \\ \bar{p}_{1y} \end{Bmatrix} \quad (3.31b)$$

where $\{p\}$ is the vector of surface tractions. For the 4-node element the load vector, due to the loading shown in Figure (3.6), takes the following form:

$$\{Q\} = \begin{Bmatrix} \frac{\ell}{6} (2\bar{p}_{x_1} + \bar{p}_{x_2}) \\ \frac{\ell}{6} (\bar{p}_{x_1} + 2\bar{p}_{x_2}) \\ \frac{\ell}{6} (2\bar{p}_{y_1} + \bar{p}_{y_2}) \\ \frac{\ell}{6} (\bar{p}_{y_1} + 2\bar{p}_{y_2}) \end{Bmatrix} \quad (3.32)$$

For the 8-node element, the load vector due to uniformly distributed surface traction, Figure (3.6), reduces to the following form:

$$\{Q\} = \begin{Bmatrix} \frac{\ell}{6} \bar{p}_{x_1} \\ \frac{\ell}{6} \bar{p}_{x_2} \\ \frac{\ell}{3} (\bar{p}_{x_1} + \bar{p}_{x_2}) \\ \frac{\ell}{6} \bar{p}_{y_1} \\ \frac{\ell}{6} \bar{p}_{y_2} \\ \frac{\ell}{3} (\bar{p}_{y_1} + \bar{p}_{y_2}) \end{Bmatrix} \quad (3.33)$$

3.2.4. Computer Code for Two-Dimensional Analysis

A computer code is developed to compute global stiffness, global load vector and to modify it for given boundary conditions. This code can handle both 4-node and 8-node isoparametric elements. Interface element described in Chapter 6 is also implemented. This code can solve nonlinear (material) problems using incremental and/or iterative techniques by using the original Newton-Raphson scheme. Variety of constitutive models such as Variable Moduli, Drucker-Prager, critical state and cap models are implemented. Numerical procedures for nonlinear analysis are given in Chapter 5. The equilibrium equations are solved by using Frontal Solution Technique [44]. Here, a few subroutines such as for data input/output, equation solver, Jacobian and shape functions, and linear stiffness which are fairly standard in finite element computations have been based on previous work [43,50] with some improvements and modifications; major emphasis in this study has been on formulations, computational algorithms and computational techniques for

nonlinear analysis. In order to make the program more efficient, most vectors and matrices are stored as one-dimensional arrays by using the technique of dynamic dimensioning. This makes it possible to change the program capacity with a change in only one DIMENSION statement. Further details of this code and the user's guide are given in reference [76].

3.3. Three-Dimensional Idealization

Almost all real problems are three-dimensional by nature, although for some problems various two-dimensional idealizations give adequate and economical solutions. Here, a finite element procedure is developed for nonlinear analysis of three-dimensional problems in a truly three-dimensional sense. Several types of three-dimensional elements have been developed, and details can be found in references [15,89]. A variable-node element which can have any number of nodes between 8 and 21, has been employed. Different types of elements can be formed by degenerating the basic element [4].

3.3.1. Finite Element Formulation

A hexahedral finite element, Figure (3.7), is used as the basic element. With the displacement formulation, the components, u_i , $i = 1, 2, 3$ (u , v , and w , respectively) at any point in the element can be expressed in terms of the components of displacement at the nodes using interpolation functions. This relationship can be written as,

$$u_i = \sum_{p=1}^m N_p u_{pi} \quad (3.34)$$

where N_p denotes the interpolation function at node p , u_{pi} denotes the displacement at node p in the direction "i", and m is the total number

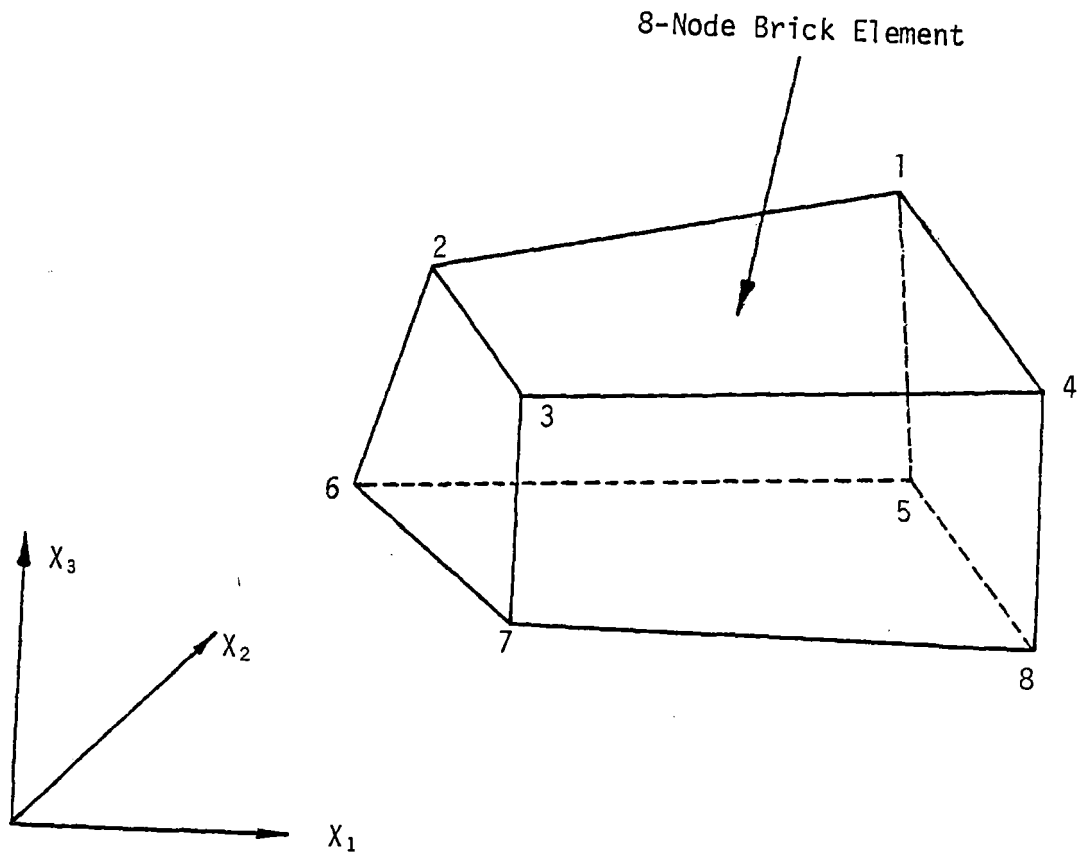


Figure 3.7 Basic Hexahedral Finite Element

of nodes in the element. The shape functions for each node in the 21-node element, Figure (3.8), are given below [4].

$$\begin{aligned}
 N_1 &= g_1 - (g_9 + g_{12} + g_{17})/2 - g_{21}/8 \\
 N_2 &= g_2 - (g_9 + g_{10} + g_{18})/2 - g_{21}/8 \\
 N_3 &= g_3 - (g_{10} + g_{11} + g_{19})/2 - g_{21}/8 \\
 N_4 &= g_4 - (g_{11} + g_{12} + g_{20})/2 - g_{21}/8 \\
 N_5 &= g_5 - (g_{13} + g_{16} + g_{17})/2 - g_{21}/8 \\
 N_6 &= g_6 - (g_{13} + g_{14} + g_{18})/2 - g_{21}/8 \\
 N_7 &= g_7 - (g_{14} + g_{15} + g_{19})/2 - g_{21}/8 \\
 N_8 &= g_8 - (g_{15} + g_{16} + g_{20})/2 - g_{21}/8
 \end{aligned} \tag{3.35a}$$

and

$$N_j = g_j - g_{21}/4, \quad j = 9, 10, \dots, 21 \tag{3.35b}$$

$$N_{21} = g_{21} \tag{3.35c}$$

where

$$g_i = G(r, r_i) \cdot G(s, s_i) \cdot G(t, t_i) \tag{3.36a}$$

and

$$g_{21} = (1 - r^2)(1 - s^2)(1 - t^2) \tag{3.36b}$$

Here, r, s, t represent the local coordinates, and subscripts represent the corresponding node number. The value of $G(\beta, \beta_i)$ is given as [4],

$$G(\beta, \beta_i) = \frac{1}{2} (1 + \beta\beta_i) \quad \text{for} \quad \beta_i = \pm 1 \tag{3.37a}$$

or

$$G(\beta, \beta_i) = 1 - \beta^2 \quad \text{for} \quad \beta_i = 0 \tag{3.37b}$$

The value of g_i is zero if node "i" is not included in the element.

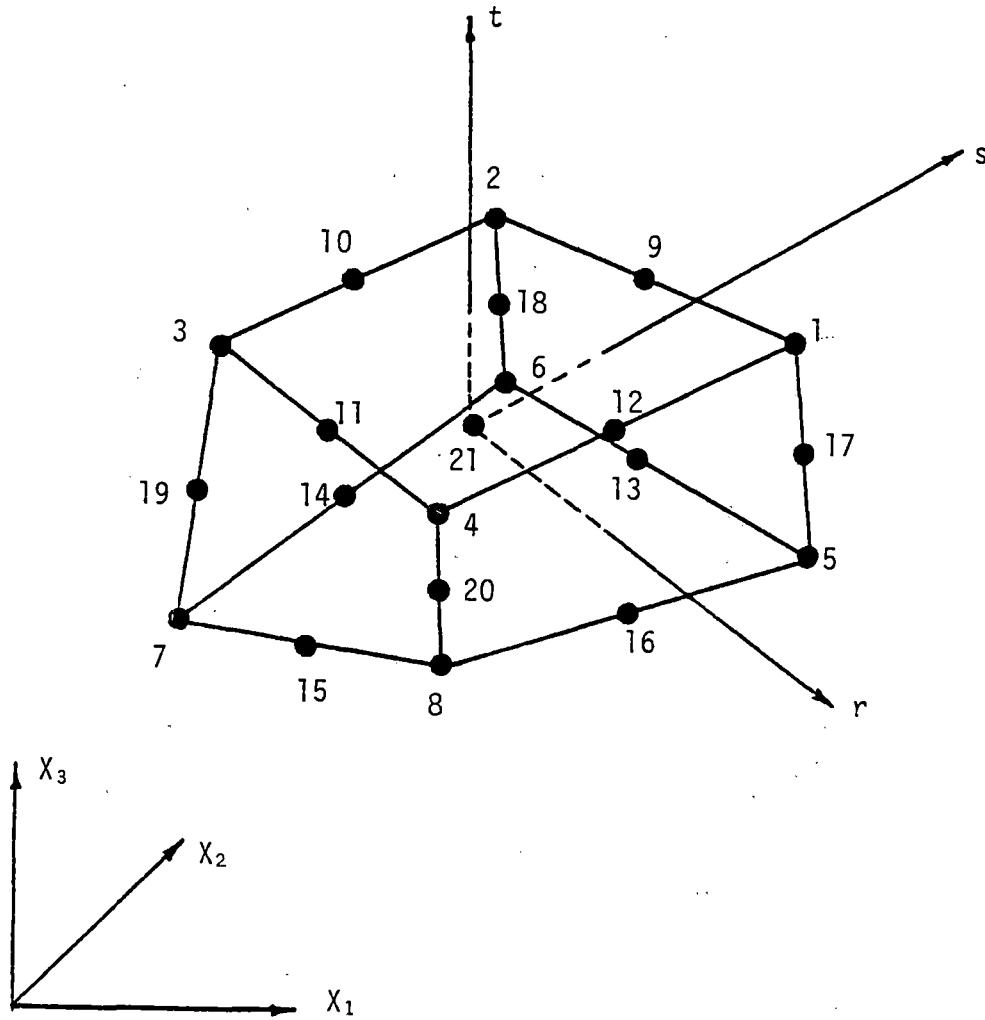


Figure 3.8 Node Numbers for 8 to 21 Variable
Node Hexahedral Finite Element

$$\begin{aligned}
N_1 &= g_1 - (g_9 + g_{12} + g_{17})/2 - g_{21}/8 \\
N_2 &= g_2 - (g_9 + g_{10} + g_{18})/2 - g_{21}/8 \\
N_3 &= g_3 - (g_{10} + g_{11} + g_{19})/2 - g_{21}/8 \\
N_4 &= g_4 - (g_{11} + g_{12} + g_{20})/2 - g_{21}/8 \\
N_5 &= g_5 - (g_{13} + g_{16} + g_{17})/2 - g_{21}/8 \\
N_6 &= g_6 - (g_{13} + g_{14} + g_{18})/2 - g_{21}/8 \\
N_7 &= g_7 - (g_{14} + g_{15} + g_{19})/2 - g_{21}/8 \\
N_8 &= g_8 - (g_{15} + g_{16} + g_{20})/2 - g_{21}/8
\end{aligned} \tag{3.35a}$$

and

$$N_j = g_j - g_{21}/4, \quad j = 9, 10, \dots, 21 \tag{3.35b}$$

$$N_{21} = g_{21} \tag{3.35c}$$

where

$$g_i = G(r, r_i) \cdot G(s, s_i) \cdot G(t, t_i) \tag{3.36a}$$

and

$$g_{21} = (1 - r^2)(1 - s^2)(1 - t^2) \tag{3.36b}$$

Here, r, s, t represent the local coordinates, and subscripts represent the corresponding node number. The value of $G(\beta, \beta_i)$ is given as [4],

$$G(\beta, \beta_i) = \frac{1}{2} (1 + \beta\beta_i) \quad \text{for} \quad \beta_i = \pm 1 \tag{3.37a}$$

or

$$G(\beta, \beta_i) = 1 - \beta^2 \quad \text{for} \quad \beta_i = 0 \tag{3.37b}$$

The value of g_i is zero if node "i" is not included in the element.

Equation (3.34) can be written in the matrix form as

$$\{u\} = [N]\{q\}$$

where $\{u\}^T = [u_1, u_2, u_3]$ or $\{u, v, w\}$,

$$[N] = \begin{bmatrix} N_1 & 0 & 0 & N_2 & 0 & 0 & \dots & N_m & 0 & 0 \\ 0 & N_1 & 0 & 0 & N_2 & 0 & \dots & 0 & N_m & 0 \\ 0 & 0 & N_1 & 0 & 0 & N_2 & \dots & 0 & 0 & N_m \end{bmatrix}$$

(3 × 3m)

and

$$\{q\}^T = [u_{11}, u_{12}, u_{13}, u_{21}, u_{22}, u_{23}, \dots, u_{m1}, u_{m2}, u_{m3}]$$

(1 × 3m)

Strain-Displacement Relationship

Once the displacement quantities are defined, the next step is to determine the strains in the element. The strains at a point in the element can be written as

$$\begin{Bmatrix} \epsilon_{11} \\ \epsilon_{22} \\ \epsilon_{33} \\ \gamma_{12} \\ \gamma_{23} \\ \gamma_{13} \end{Bmatrix} = \begin{Bmatrix} u_{1,1} \\ u_{2,2} \\ u_{3,3} \\ u_{1,2} + u_{2,1} \\ u_{2,3} + u_{3,2} \\ u_{1,3} + u_{3,1} \end{Bmatrix} \quad (3.39)$$

where $u_{i,j}$ denotes $\frac{\partial u_i}{\partial x_j}$ for $i = 1, 2, 3$ and $j = 1, 2, 3$. The quantities in Equation (3.39) can be written in terms of the nodal displacements as

$$\begin{aligned}
\frac{\partial u_1}{\partial x_i} &= \left[\frac{\partial N_1}{\partial x_i} \quad 0 \quad 0 \quad \frac{\partial N_2}{\partial x_i} \quad 0 \quad 0 \quad \dots \quad \frac{\partial N_m}{\partial x_i} \quad 0 \quad 0 \right] \{q\} \\
\frac{\partial u_2}{\partial x_i} &= \left[0 \quad \frac{\partial N_1}{\partial x_i} \quad 0 \quad 0 \quad \frac{\partial N_2}{\partial x_i} \quad 0 \quad \dots \quad 0 \quad \frac{\partial N_m}{\partial x_i} \quad 0 \right] \{q\} \quad (3.40) \\
\frac{\partial u_3}{\partial x_i} &= \left[0 \quad 0 \quad \frac{\partial N_1}{\partial x_i} \quad 0 \quad 0 \quad \frac{\partial N_2}{\partial x_i} \quad \dots \quad 0 \quad 0 \quad \frac{\partial N_m}{\partial x_i} \right] \{q\}
\end{aligned}$$

Here, m is the number of nodes in the element. Substituting Equation (3.40) into Equation (3.39), it is possible to express the strain vector in terms of nodal displacements as,

$$\{\epsilon\} = [B]\{q\} \quad (3.41a)$$

where $[B]$ is the strain-displacement relationship. By partitioning matrix $[B]$, Equation (3.41a) can be expressed as

$$\{\epsilon\} = \left[[B]_1 \quad [B]_2 \quad \dots \quad [B]_m \right] \{q\} \quad (3.41b)$$

where m is the number of nodes in the element. Here,

$$[B]_i = \begin{bmatrix} \frac{\partial N_i}{\partial x_1} & 0 & 0 \\ 0 & \frac{\partial N_i}{\partial x_2} & 0 \\ 0 & 0 & \frac{\partial N_i}{\partial x_3} \\ \frac{\partial N_i}{\partial x_2} & \frac{\partial N_i}{\partial x_1} & 0 \\ 0 & \frac{\partial N_i}{\partial x_3} & \frac{\partial N_i}{\partial x_2} \\ \frac{\partial N_i}{\partial x_3} & 0 & \frac{\partial N_i}{\partial x_1} \end{bmatrix} \quad (3.42)$$

In order to evaluate the global derivatives of the shape functions, it is required to establish a transformation relationship from global to local coordinates. This can be done by using the Jacobian matrix [15.89]. By using the chain rule of differentiation

$$\frac{\partial}{\partial r} = \frac{\partial}{\partial x_1} \left(\frac{\partial x_1}{\partial r} \right) + \frac{\partial}{\partial x_2} \left(\frac{\partial x_2}{\partial r} \right) + \frac{\partial}{\partial x_3} \left(\frac{\partial x_3}{\partial r} \right)$$

$$\frac{\partial}{\partial s} = \frac{\partial}{\partial x_1} \left(\frac{\partial x_1}{\partial s} \right) + \frac{\partial}{\partial x_2} \left(\frac{\partial x_2}{\partial s} \right) + \frac{\partial}{\partial x_3} \left(\frac{\partial x_3}{\partial s} \right) \quad (3.43a)$$

$$\frac{\partial}{\partial t} = \frac{\partial}{\partial x_1} \left(\frac{\partial x_1}{\partial t} \right) + \frac{\partial}{\partial x_2} \left(\frac{\partial x_2}{\partial t} \right) + \frac{\partial}{\partial x_3} \left(\frac{\partial x_3}{\partial t} \right)$$

or in the matrix form,

$$\begin{Bmatrix} \frac{\partial}{\partial r} \\ \frac{\partial}{\partial s} \\ \frac{\partial}{\partial t} \end{Bmatrix} = \begin{bmatrix} \frac{\partial x_1}{\partial r} & \frac{\partial x_2}{\partial r} & \frac{\partial x_3}{\partial r} \\ \frac{\partial x_1}{\partial s} & \frac{\partial x_2}{\partial s} & \frac{\partial x_3}{\partial s} \\ \frac{\partial x_1}{\partial t} & \frac{\partial x_2}{\partial t} & \frac{\partial x_3}{\partial t} \end{bmatrix} \begin{Bmatrix} \frac{\partial}{\partial x_1} \\ \frac{\partial}{\partial x_2} \\ \frac{\partial}{\partial x_3} \end{Bmatrix} \quad (3.43b)$$

This can be written as

$$\begin{Bmatrix} \frac{\partial}{\partial r} \\ \frac{\partial}{\partial s} \\ \frac{\partial}{\partial t} \end{Bmatrix} = [J] \begin{Bmatrix} \frac{\partial}{\partial x_1} \\ \frac{\partial}{\partial x_2} \\ \frac{\partial}{\partial x_3} \end{Bmatrix} \quad (3.44)$$

where $[J]$ is the Jacobian matrix. The Jacobian matrix can be expressed in terms of nodal coordinates as,

$$[J] = \begin{bmatrix} \frac{\partial N_1}{\partial r} & \frac{\partial N_2}{\partial r} & \cdots & \frac{\partial N_m}{\partial r} & x_{11} & x_{21} & x_{31} \\ \frac{\partial N_1}{\partial s} & \frac{\partial N_2}{\partial s} & \cdots & \frac{\partial N_m}{\partial s} & x_{12} & x_{22} & x_{32} \\ \frac{\partial N_1}{\partial t} & \frac{\partial N_2}{\partial t} & \cdots & \frac{\partial N_m}{\partial t} & \cdots & \cdots & \cdots \\ & & & & \cdots & \cdots & \cdots \\ & & & & x_{1m} & x_{2m} & x_{3m} \end{bmatrix} \quad (3.45)$$

where x_{im} is the x_i -coordinate of node m , and it does not mean a tensor quantity. In order to evaluate the $[B]$ matrix in Equation (3.42) the global derivatives of interpolation functions have to be known, and can be evaluated using the Jacobian matrix, Equation (3.45). The global derivatives can be expressed using Equation (3.44) as

$$\begin{Bmatrix} \frac{\partial}{\partial x_1} \\ \frac{\partial}{\partial x_2} \\ \frac{\partial}{\partial x_3} \end{Bmatrix} = [J]^{-1} \begin{Bmatrix} \frac{\partial}{\partial r} \\ \frac{\partial}{\partial s} \\ \frac{\partial}{\partial t} \end{Bmatrix} \quad (3.46)$$

where $[J]^{-1}$ is the inverse of Jacobian matrix.

Constitutive Relationship

The constitutive relationship can be written in a general form as

$$d\sigma_{ij} = C_{ijkl}^{ep} d\epsilon_{kl} \quad (3.47)$$

where $d\sigma_{ij}$, $d\epsilon_{kl}$ are the incremental stress and incremental strain tensors, respectively, and C_{ijkl}^{ep} is the constitutive matrix which refers to elastic or elasto-plastic behavior. The simplified form of the constitutive matrix for an isotropic linear elastic material is given in Equation (2.14). The major emphasis in this dissertation is the non-linear behavior which is characterized by the constitutive relationships. A detailed description of the constitutive relationships based on variety of constitutive models is given in the next chapter. The task of development of a numerical procedure with nonlinear analysis is complete only when a (sophisticated) constitutive relationship is properly incorporated in the solutions procedure. Aspects of the computational algorithms used in this dissertation are given in Chapter 5.

3.3.2. Element Stiffness Matrix

Element stiffness can be determined by using the principle of minimum potential energy as described previously in Section 3.2.2. The stiffness matrix, $[k]$, and the load vector, $\{Q\}$, can be evaluated from Equations (3.29b) and (3.29c). Once the matrices such as $[B]$ and $[C]$ are established, evaluation of stiffness and load vector reduces to performing integrations involved in the above equations. Here, the integrals are evaluated by using numerical integration schemes based on Gaussian quadrature. A two-point integration scheme is used for the

8-node elements while a three-point scheme is used for elements with more than 8 nodes.

3.3.3 Element Load Vector

In this section, only point loads and uniformly distributed loads are considered. Point loads can be directly added to the global load vector of the assemblage. However, distributed loads need to be converted to equivalent nodal loads before adding them to the global load vector. The nodal load vector due to a distributed load can be evaluated by integrating Equation (3.31). For uniformly distributed loads on 4- and 8-node surfaces, the equivalent nodal loads, are shown in Figure (3.9).

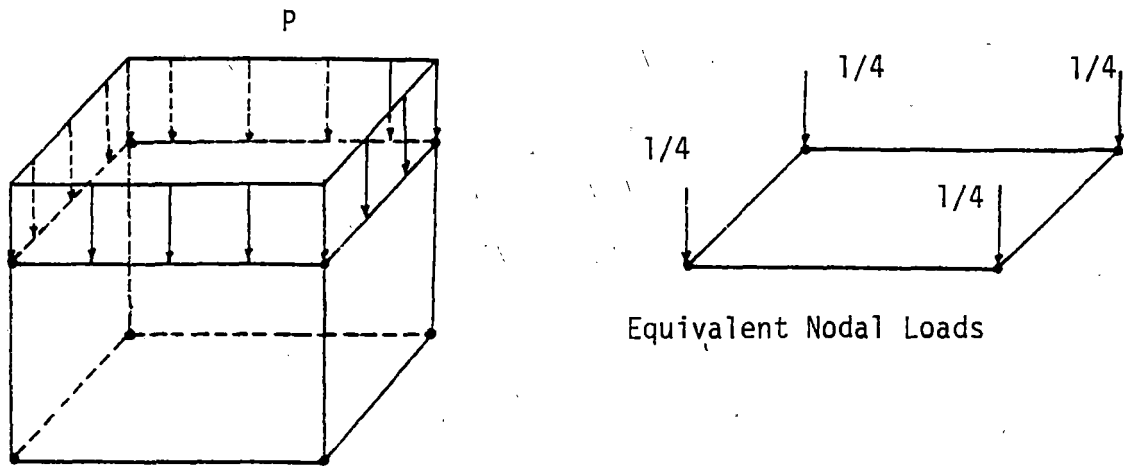
Load vector due to body forces can be computed by integrating the first term in Equation (3.29c). That is, load vector due to body forces can be evaluated as,

$$\{Q\} = \iiint_V [N]^T \{\bar{X}\} dV \quad (3.48)$$

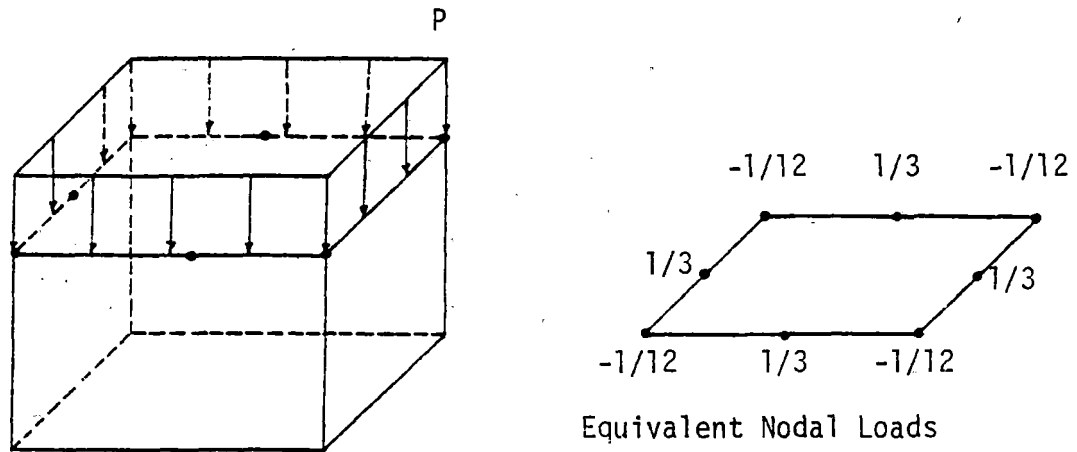
This is done by using a numerical integration technique similar to that used in stiffness computation.

3.3.4. Computer Code for Three-Dimensional Analysis

A computer code is developed for nonlinear three-dimensional analysis of soil-structure interaction. This code can handle 8 to 21 variable node solid elements. Interface element described in Chapter 6 is also implemented to study interaction effects. This code can solve nonlinear (material) problems using incremental and iterative



(a) Uniform Surface Loading on a 4-Node Surface



(b) Uniform Surface Loading on a 8-Node Surface

Figure 3.9 Distributed Surface Loads on Three-Dimensional Elements

techniques. The numerical procedure is based on the original Newton-Raphson scheme. The nonlinear constitutive models implemented in the program are:

Variable Moduli Model
Drucker-Prager Model
and Critical State Model
Cap Model.

Numerical algorithms used in the nonlinear analysis are described in Chapter 5. Here, the skyline technique [3,5] is used in the solution of equilibrium equations. In contrast to previously developed three-dimensional formulations [3,5], the procedure and code developed here includes a number of important and significant factors such as a variety of constitutive models (variable moduli, Drucker-Prager, Critical State, Cap) and a three-dimensional interface element with linear and nonlinear capabilities. Furthermore, even the Drucker-Prager model in ADINA, and NONSAP is limited to two-dimensional analysis.

In order to make the program more efficient, most vectors and matrices are stored as one-dimensional arrays by using the technique of dynamic dimensioning. This makes it possible to change the program capacity with a change in only one DIMENSION statement. Further details of this computer code are available in a separate report [76].

3.4 Resistance-Response Approach

Since three-dimensional procedures are often expensive, preliminary investigations are performed towards a rather new formulation called

Resistance-Response approach [19,22,23] by combining one-, two-, and three-dimensional procedures. Details of the preliminary work is given in Appendix D.

CHAPTER 4

ADVANCED CONSTITUTIVE LAWS USED IN SOIL-STRUCTURE INTERACTION ANALYSIS

4.1. General Remarks

In Chapter 2, the fundamentals of classical elasticity and plasticity were described. The assumptions made in those theories allow consideration of only highly idealized materials. Despite this, the classical models have been widely used for certain types of structural materials such as steel, aluminum and concrete. However, for materials such as soils and rocks, the above models have been found to be inadequate. In classical linear elasticity, the stress-strain relationship is assumed to be linear. In nonlinear elasticity, the material is assumed to return to its original state upon unloading, although the stress-strain relationship is nonlinear. These assumptions are usually not valid for geologic materials because their behavior is very often nonlinear and inelastic or plastic.

In many classical plasticity models the yielding or plastic flow behavior was assumed to be independent of the first invariant of the stress tensor, that is, mean pressure. These type of materials are called non-frictional materials. Behavior of most geologic media can be quite different and their strength is dependent on the hydrostatic stress. Under fully or partially drained conditions, the

strength of the geologic materials such as soils increase with mean pressure and exhibit frictional characteristics. Of course, there are exceptions such as undrained behavior of saturated clays which can be similar to that of metals. In this chapter, some of the advanced constitutive laws that accounts for frictional and plastic behavior are discussed. Then, the constitutive relations are derived in the incremental form which can be readily implemented in a numerical procedure such as the finite element technique used in this study. Computational algorithms for implementation of these models are described in Chapter 5. Determination of constitutive parameters and details of laboratory experimental results for a granular material are included in Chapter 4.

Theoretical considerations and development of advanced plasticity models considered herein are reviewed in a few books [17, 21]. Details of theory and derivations of constitutive relationships for some of the models for two- and three-dimensional analysis are presented here.

4.2. Variable Moduli Models

In most of the elasto-plastic models, it is generally assumed that the behavior below the yield surface is linear elastic. However, in the recent years more reliable laboratory test data on geologic materials became available concurrently with the advances in experimental mechanics. Evidently, some modifications were

required in the existing elasto-plastic models such as Drucker-Prager model, described later in this chapter, in order to match observed experimental data. It has been observed that the material behavior even before reaching the yield criterion is nonlinear. Furthermore, it has also been realized that the behavior in the "elastic" region is different under loading and unloading. These realizations led to the development of more advanced constitutive laws based on the principles of theory of plasticity described in Chapter 2.

The use of different elastic properties such as bulk and shear moduli under loading and unloading conditions could reproduce the hysteretic nature of response quite independent of the yield criterion used. In fact, all the piecewise linear models used in the past are based on this concept. As such, no explicit yield criterion is used in variable parameter models. In the 'variable moduli' models [58, 60] the bulk modulus and shear modulus are assumed to be dependent on the states of stress and strain tensors. It is evident from experimental observations that the stress-strain relationships of many geologic materials are not unique; they are not only dependent on the state of stress but also on the stress path. Therefore, the variable moduli materials are mathematically expressed in incremental forms. That is,

$$\dot{s}_{ij} = 2G\dot{\epsilon}_{ij} \quad (4.1)$$

and
$$\dot{p} = 3K\dot{\epsilon}_v \quad (4.2)$$

where S_{ij} and E_{ij} are the deviatoric stress and strain tensors, respectively, and p and ε_v are the mean pressure and volumetric strain, respectively; the overdot denotes incremental quantities. In general, different functions for G and K are used under loading and unloading-reloading conditions. Depending on the functional forms assumed for G and K , a family of variable moduli models can be developed [58], which have often been used in the investigations of ground shock effects in hysteretic media [59]. There have been three major models developed for these purposes. They are

- (a) Constant Poisson Ratio Model
- (b) A model in which K and G are functions of the invariants of the strain tensor, and
- (c) A model in which K is a function of invariants of the strain tensor, and G is a function of invariants of the stress tensor.

4.2.1. Constant Poisson Ratio Model

In this model the ratio of the bulk modulus to shear modulus is assumed to remain constant. That is,

$$\frac{K}{G} = \frac{2(1+\nu)}{3(1-2\nu)} = \text{constant} \quad (4.3)$$

However, the values of K and G will be variables. They can be functions of mean pressure or volumetric strain or both. Closed-form solutions for relationships of stress and strain can be obtained for special cases such as uniaxial strain and triaxial stress states. These are given in reference [58]. It has been

found that this model is satisfactory for only the uniaxial states of strain, and its behavior in the triaxial conditions contradicts the experimental observations. Therefore, this model may not be suitable under general states of stresses.

4.2.2. Variable Moduli Model Based on the Invariants of the Strain Tensor

In this model, bulk and shear moduli are assumed to be functions of the first invariant of the strain tensor, I_1 , and second invariant of the deviatoric strain tensor, $\sqrt{I_{2D}}$. They are expressed as [58]

$$K = K_0 + K_1 I_1 + K_2 I_1^2 \quad (4.4)$$

$$G = G_0 + G_1 \sqrt{I_{2D}} + G_2 I_1 \quad (4.5)$$

Where K_0 , G_0 are the initial bulk and shear moduli respectively, and K_1 , K_2 , G_1 , G_2 are the material parameters.

The quantity $\sqrt{I_{2D}}$ has been used instead of I_{2D} mainly because it has the same order as I_1 . As could be seen in Equations (4.4) and (4.5), the bulk modulus and shear modulus reduce to K_0 and G_0 under zero strain conditions. Using the above relations, the general incremental stress-strain relationship can be written as,

$$d\epsilon_{ij} = \frac{dS_{ij}}{2[G_0 + G_1 \sqrt{I_{2D}} + G_2 I_1]} + \frac{dp\delta_{ij}}{3[K_0 + K_1 I_1 + K_2 I_1^2]} \quad (4.6)$$

This expression can be integrated to obtain stress-strain relationship under any stress path configuration. One major limitation

of this model is that the problem of unloading has not been given attention. Furthermore, in many existing finite element procedures, stresses are stored rather than strains, and hence the implementation of this model in an existing program can require additional difficulties.

4.2.3. Combined Stress-Strain Variable Moduli Model

In this model, the bulk modulus, K , is expressed in terms of the first invariant of the strain tensor, and the shear modulus, G , is expressed in terms of the first invariant of the stress tensor and the second invariant of the deviatoric stress tensor. That is

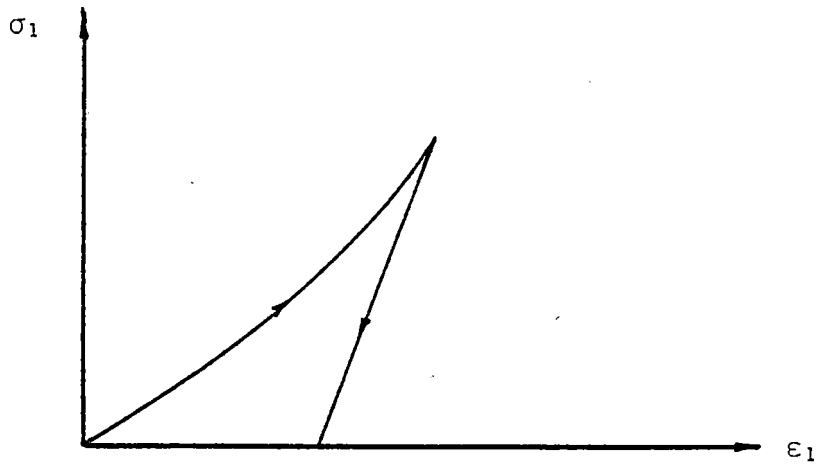
$$K = K_0 + K_1 I_1 + K_2 I_1^2 \quad (4.7)$$

$$G = G_0 + \gamma_1 \left(\frac{J_1}{3}\right) + \gamma_2 \sqrt{J_{2D}} \quad (4.8)$$

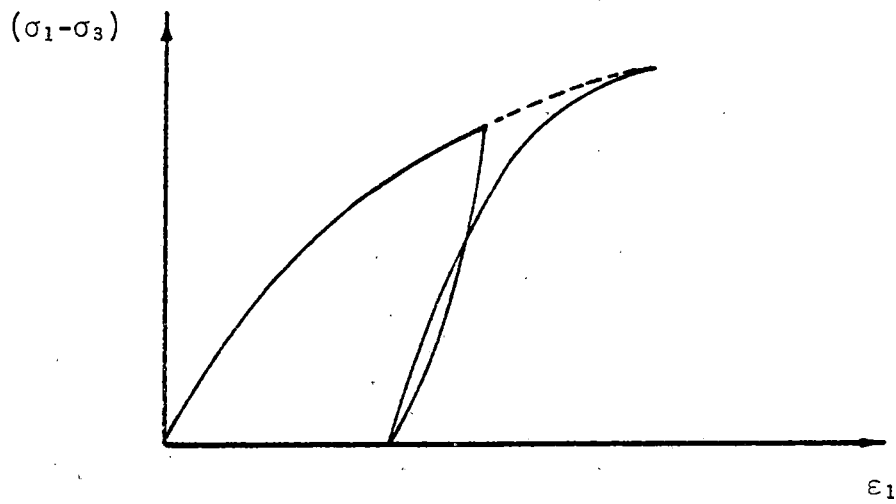
Here, K_0 , G_0 are initial values of bulk and shear moduli, respectively, and K_1 , K_2 , γ_1 , γ_2 are other material parameters required in this model.

It is evident from experimental observations that the behavior of geologic media under loading and unloading can be quite different. Typical experimental results on uniaxial compression test and triaxial compression tests are shown in Figure (4.1).

By integrating the incremental form of the general stress-strain relationship, it is possible to obtain a solution for stress as an exact function of strain for uniaxial and triaxial conditions. Details



(a) Uniaxial (Compression) Test



(b) Conventional Triaxial Compression Test

Figure 4.1 Typical Test Results for Geologic Media

of these derivations can be found in Reference [60], and only the final relationship is given here.

$$\begin{aligned} \epsilon_1 = & \frac{1}{\gamma_1 + \sqrt{3}\gamma_2} \ln \left[\frac{3G_0 + \sigma_3(2\gamma_1 - \sqrt{3}\gamma_2) + \sigma_1(\gamma_1 + \sqrt{3}\gamma_2)}{3(G_0 + \gamma_1\sigma_3)} \right] \\ & + \frac{1}{3} \sigma_3^{\sigma_1} \int \left(\frac{d\sigma_1}{3K} \right) \end{aligned} \quad (4.9a)$$

$$\text{or } \epsilon_1 = \frac{1}{\gamma_1 + \sqrt{3}\gamma_2} \ln \left[\frac{G}{G_{\text{initial}}} \right] + \frac{1}{3} \sigma_1^{\sigma_3} \int \left(\frac{d\sigma_1}{3K} \right) \quad (4.9b)$$

It is an experimental observation that the shear modulus, G , decreases with increasing deviatoric stress. For shear modulus to decrease with $\sqrt{J_{2D}}$, certain conditions should be satisfied by the material parameters. That is,

$$\gamma_1 + \sqrt{3}\gamma_2 < 0 \quad (4.10)$$

Furthermore, γ_1 has to be a positive quantity while γ_2 has to be a negative quantity. It is reasonable to assume that the shear modulus reaches a value of zero at failure. Hence, under triaxial conditions, the maximum stress difference, $(\sigma_1 - \sigma_3)_{\text{max}}$ has the following value [60],

$$(\sigma_1 - \sigma_3)_{\text{max}} = - \left[\frac{3(G_0 + \gamma_1\sigma_3)}{\gamma_1 + \sqrt{3}\gamma_2} \right] \quad (4.11)$$

It is known that the material behavior under loading is quite different from unloading conditions, Figure (4.1). Under uniaxial state of stress, loading and unloading can be easily visualized as

the configuration is only one-dimensional. However, under three-dimensional states of stresses unloading and reloading cannot be easily seen as in the case of uniaxial conditions. In order to account for inelastic behavior in load-unload cycles, different relationships for G and K have to be assumed under unloading conditions. It may be reasonable to assume that the response under unloading and reloading up to the maximum past state of stress is essentially elastic. However, it may be possible to separate unloading and reloading by assuming different parameters for above cases; this of course will increase the number of parameters required to describe the behavior. Furthermore, shear behavior can be quite different from bulk behavior under reloading. Therefore, it is possible to express the unloading-reloading behavior as

Unloading-Reloading

$$G = G_{un} \quad (4.12a)$$

$$K = K_{un} \quad (4.12b)$$

Loading

$$G = G_{ld} \quad (4.12c)$$

$$K = K_{ld} \quad (4.12d)$$

where G_{un} and K_{un} are unloading values of shear and bulk moduli, respectively, and G_{ld} and K_{ld} are reloading values of shear and bulk moduli, respectively.

Under a fully three-dimensional state of stress, it is possible that the material is loading in shear, that is, $\sqrt{\dot{J}_{2D}} > 0$, while unloading in pressure, $\dot{J}_1 < 0$. Behavior under unloading and reloading is quite complicated and further research work has to be done for a better understanding. In this research, however, it is assumed that unloading and re-loading can be described by same elastic properties. Unloading under shear is detected by a decrease in $\sqrt{J_{2D}}$, and unloading in bulk behavior is detected by a decrease in mean pressure, $J_1/3$. That is

$$G = G_{un} \quad \text{when } \sqrt{J_{2D}} < \sqrt{(J_{2D})_{max}} \quad (4.13a)$$

$$K = K_{un} \quad \text{when } J_1 < (J_1)_{max} \quad (4.13b)$$

where $\sqrt{(J_{2D})_{max}}$ and $(J_1)_{max}$ are the maximum past values. One major difference between variable moduli models and plasticity models, is the way unloading is defined. In plasticity models, unloading is defined by a yield criterion which represent both deviatoric and hydrostatic states of stresses. However, in variable moduli models, behavior under deviatoric and hydrostatic states of stresses are decomposed and described independently.

Since the moduli, G and K , vary continuously with the states of stress in variable moduli models, solution of boundary value problems have to be done using incremental procedures. The incremental stress-strain relationship is written below in terms of G and K so that it could be implemented in a numerical procedure such as the finite element technique.

$$d\sigma_{ij} = K \cdot d\epsilon_{kk} \delta_{ij} + 2G(d\epsilon_{ij} - \frac{d\epsilon_{kk}}{3} \delta_{ij}) \quad (4.14)$$

Under plane strain and axisymmetric idealizations, the incremental stress-strain relationship takes the following form:

$$\begin{Bmatrix} d\sigma_{11} \\ d\sigma_{22} \\ d\sigma_{12} \\ d\sigma_{33} \end{Bmatrix} = \begin{bmatrix} K + \frac{4G}{3} & K - \frac{2G}{3} & 0 & K - \frac{2G}{3} \\ K - \frac{2G}{3} & K + \frac{4G}{3} & 0 & K - \frac{2G}{3} \\ 0 & 0 & 2G & 0 \\ K - \frac{2G}{3} & K - \frac{2G}{3} & 0 & K + \frac{4G}{3} \end{bmatrix} \begin{Bmatrix} d\epsilon_{11} \\ d\epsilon_{22} \\ d\epsilon_{12} \\ d\epsilon_{33} \end{Bmatrix} \quad (4.15)$$

Here the fourth row and column are meaningful only for axisymmetric idealizations; for the plane strain conditions, constitutive matrix has the dimensions of (3x3).

4.3. Introduction to Advanced Plasticity Laws

As described in Chapter 2, in classical plasticity, the yielding or plastic flow behavior was assumed to be independent of the first invariant of the stress tensor. These types of materials are called non-frictional materials. This assumption can be valid for materials such as metals which are considered to be frictionless. However, most geologic materials do not obey this type of behavior.

The strength of most geologic media is dependent on the hydrostatic stress. Under fully or partially drained conditions, the strength of the soil increases with mean pressure and exhibits

frictional characteristics. There are certain exceptions. For instance, the undrained behavior of a saturated clay is similar to that of metals.

In this section, frictional materials, and their stress-strain behavior based on the postulates described in Chapter 2 are discussed.

4.3.1. Mohr-Coulomb Failure Criterion

According to the Mohr-Coulomb criterion, the shear strength increases with increasing normal stress on the failure plane:

$$\tau = C + \sigma \tan \phi \quad (4.16)$$

where τ is the shear stress on the failure plane, C is the cohesion of the material, σ is the normal effective stress on the failure surface, and ϕ is the angle of internal friction. This failure criterion is shown graphically in Figure (4.2). The concept of Mohr circle can be used to express this criterion in terms of principal stresses. This criterion represents an irregular hexagonal pyramid in three-dimensional stress space. The projection of this surface on the π -plane is shown in Figure (4.3).

Mohr-Coulomb criterion ignores the effects of intermediate principal stress. A generalization of this criterion, and the corresponding constitutive law is derived in the next section.

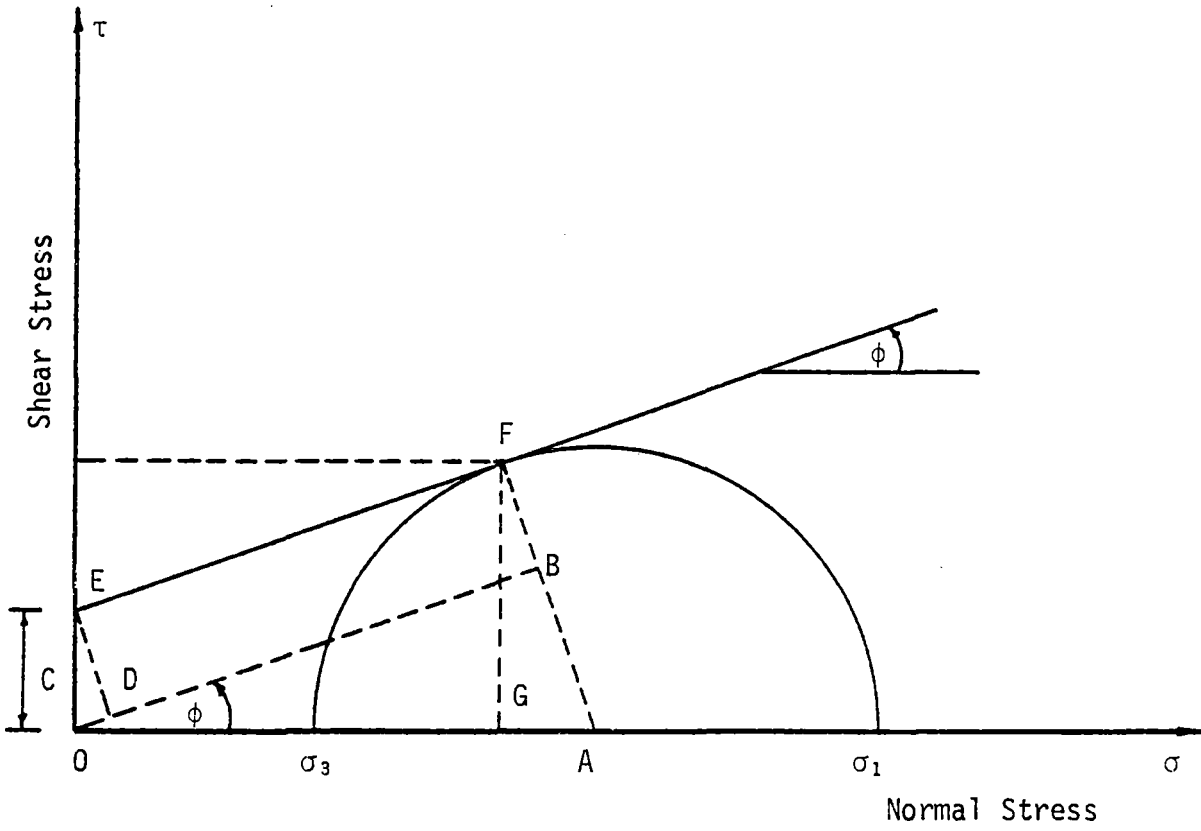


Figure 4.2 Mohr-Coulomb Failure Criterion

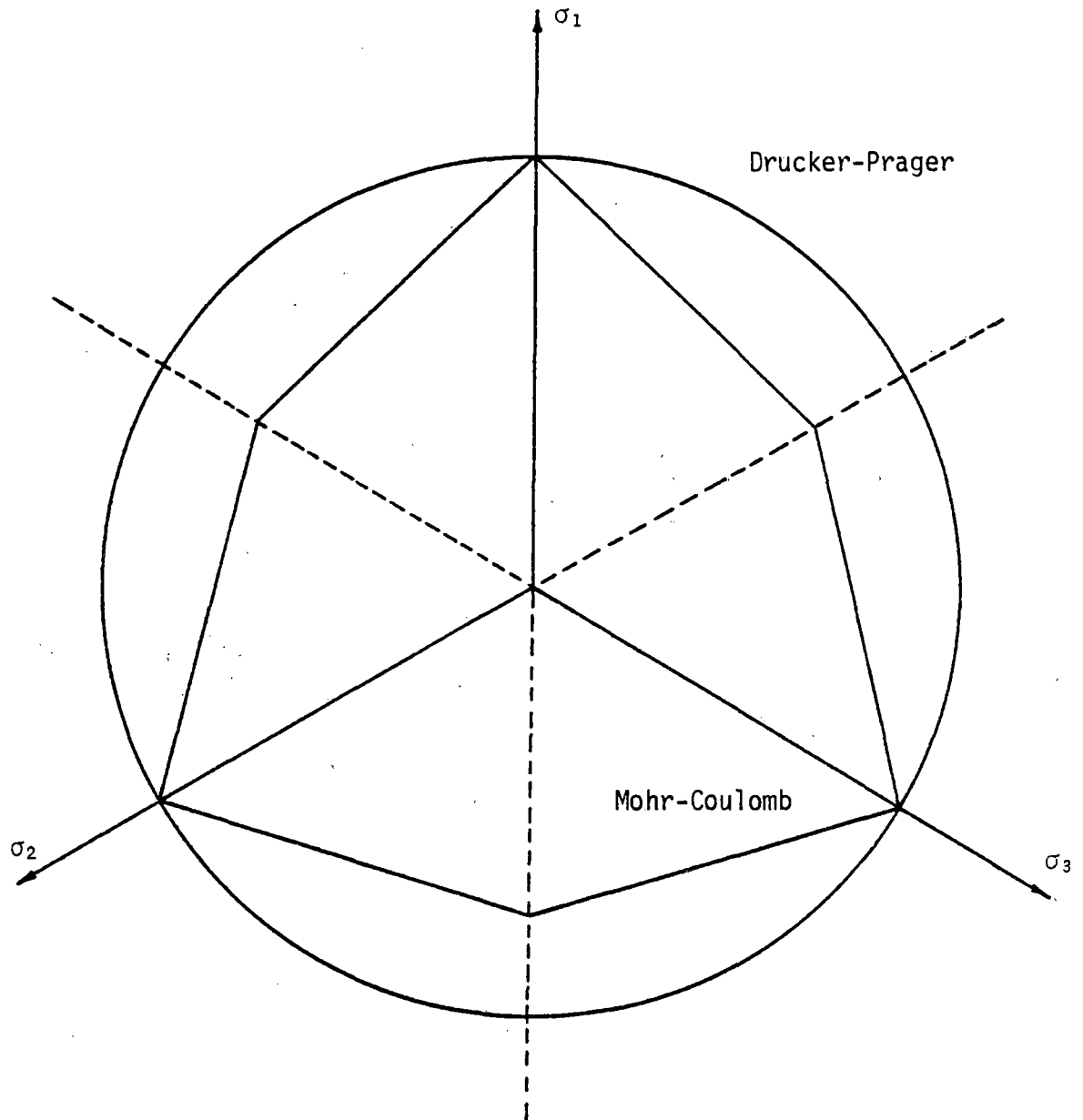


Figure 4.3 Mohr-Coulomb and Drucker-Prager
Yield Criteria on π -Plane

4.4. Drucker-Prager Model

A generalization to account for the effects of all principal stresses was suggested by Drucker and Prager [30] by using the invariants of the stress tensor. This generalized criterion can be written as

$$f = \sqrt{J_{2D}} - \alpha J_1 - k \quad (4.17)$$

where α and k are positive material parameters, J_1 is the first invariant of the stress tensor, and J_{2D} is the second invariant of the deviatoric stress tensor. Equation (4.17) represents a straight line on J_1 vs $\sqrt{J_{2D}}$ plot, Figure (4.4). In the three-dimensional stress space, this criterion represents a right circular cone. The projection on the π -plane is a circle as shown in Figure (4.3).

The stress-strain relationships based on this criterion can be derived using the yield function given by Equation (4.17), and the flow rule given by Equation (2.17). These relationships will be derived using tensor notation. Then the incremental stress-strain relationships will be written in the matrix form which can be implemented in numerical solution procedures such as the finite element technique.

4.4.1. Derivation of the Incremental Constitutive Law

Basic steps in deriving the incremental law for the Drucker-Prager model are given below. The failure criterion for this model is given in Equation (4.17). When the state of stress or

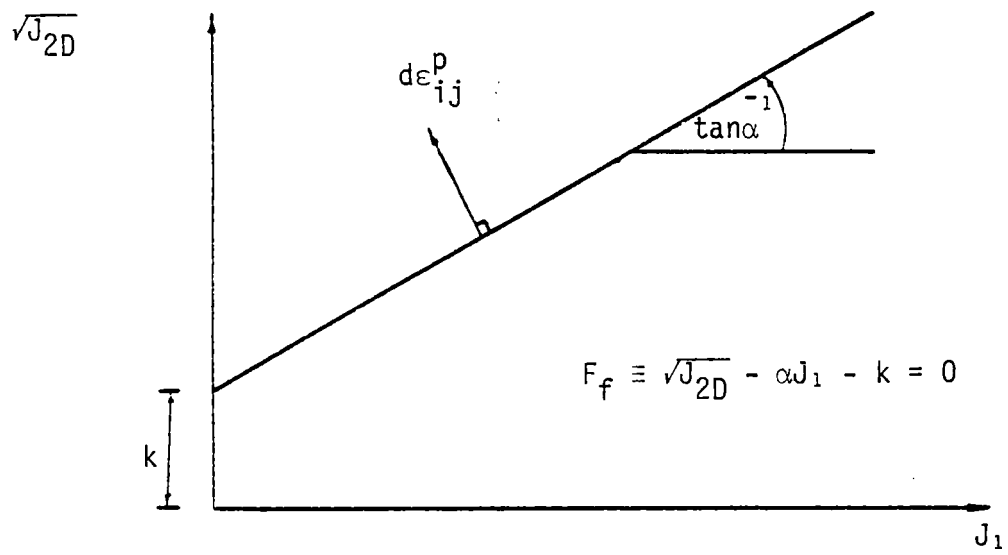


Figure 4.4 Drucker-Prager Criterion

stress point lies on the yield surface, Equation (4.17) is always satisfied, and hence the variation of f will be zero. That is,

$$df = 0 \quad (4.18a)$$

$$\text{or} \quad df = \frac{\partial f}{\partial \sigma_{ij}} d\sigma_{ij} = 0 \quad (4.18b)$$

Substitution of Equation (4.17) into Equation (4.18b) leads to

$$df = \left(\frac{S_{ij}}{2\sqrt{J_{2D}}} - \alpha \delta_{ij} \right) d\sigma_{ij} = 0 \quad (4.19)$$

where S_{ij} is the deviatoric stress tensor. Assuming that the total strain can be decomposed into elastic and plastic components, it is possible to write,

$$d\varepsilon_{ij}^e = d\varepsilon_{ij} - d\varepsilon_{ij}^p \quad (4.20)$$

Here, the superscripts 'e', and 'p' denote elastic and plastic components, respectively. However, the incremental plastic strains can be expressed by using the flow rule given in Equation (2.17).

That is,

$$d\varepsilon_{ij}^e = d\varepsilon_{ij} - \lambda \frac{\partial f}{\partial \sigma_{ij}} \quad (4.21)$$

Therefore,

$$d\varepsilon_{ij}^e = d\varepsilon_{ij} - \lambda \left(\frac{S_{ij}}{2\sqrt{J_{2D}}} - \alpha \delta_{ij} \right) \quad (4.22)$$

Now, the incremental stress can be expressed as

$$d\sigma_{ij} = Kd\epsilon_{mm}^e \delta_{ij} + 2G(d\epsilon_{ij}^e - \frac{d\epsilon_{mm}^e}{3} \delta_{ij}) \quad (4.23)$$

The value of λ can be obtained by substituting Equations (4.22) and (4.23) into Equation (4.19). The value of λ is then substituted in Equation (4.22) to obtain the incremental stress-strain relationship. Further details of the derivation are given in Appendix A.

The incremental stress-strain relationship for Drucker-Prager model has been previously obtained and used by Reyes and Deere [67], and Christian [6] for plane-strain idealizations. They have used an approach based on plastic work to derive the stress-strain relationship. In the current research, this is derived directly as described in Equations (4.18) through (4.23) by using tensor manipulations. The incremental form of the constitutive relationship derived in Appendix A can be written as,

$$d\sigma_{ij} = 2Gd\epsilon_{ij} - 2G[A(\sigma_{mn} \delta_{ij} + \sigma_{ij} \delta_{mn}) + B\delta_{mn} \delta_{ij} + C\sigma_{mn} \sigma_{ij}]d\epsilon_{mn} \quad (4.24)$$

The quantities A, B and C are defined in Appendix A, and will not be repeated here.

In the matrix notation, the three-dimensional stress-strain relationship for the Drucker-Prager material can be written as shown in Figure (4.5). Here, the symmetry of this matrix may not be clear at the first glance. However, it can be easily shown that

$$T_a \sigma_{bb} + R_a = T_b \sigma_{aa} + R_b \quad (4.25)$$

$$\begin{Bmatrix} \Delta\sigma_{11} \\ \Delta\sigma_{22} \\ \Delta\sigma_{33} \\ \Delta\sigma_{12} \\ \Delta\sigma_{23} \\ \Delta\sigma_{13} \end{Bmatrix} = 2G \begin{bmatrix} (1-T_1\sigma_{11}-R_1) & -(T_1\sigma_{22}+R_1) & -(T_1\sigma_{33}+R_1) & -(T_1\sigma_{12}) & -(T_1\sigma_{23}) & -(T_1\sigma_{13}) \\ -(T_2\sigma_{11}+R_2) & (1-T_2\sigma_{22}-R_2) & -(T_2\sigma_{33}+R_2) & -(T_2\sigma_{12}) & -(T_2\sigma_{23}) & -(T_2\sigma_{13}) \\ -(T_3\sigma_{11}+R_3) & -(T_3\sigma_{22}+R_3) & (1-T_3\sigma_{33}-R_3) & -(T_3\sigma_{12}) & -(T_3\sigma_{23}) & -(T_3\sigma_{13}) \\ -T_1\sigma_{12} & -T_2\sigma_{12} & -T_3\sigma_{12} & (1/2-C\sigma_{12}^2) & -C\sigma_{12}\sigma_{23} & -C\sigma_{12}\sigma_{13} \\ -T_1\sigma_{23} & -T_2\sigma_{23} & -T_3\sigma_{23} & -C\sigma_{12}\sigma_{23} & (1/2-C\sigma_{23}^2) & -C\sigma_{12}\sigma_{23} \\ -T_1\sigma_{13} & -T_2\sigma_{13} & -T_3\sigma_{13} & -C\sigma_{12}\sigma_{13} & -C\sigma_{13}\sigma_{23} & (1/2-C\sigma_{13}^2) \end{bmatrix} \begin{Bmatrix} \Delta\epsilon_{11} \\ \Delta\epsilon_{22} \\ \Delta\epsilon_{33} \\ \Delta\gamma_{12} \\ \Delta\gamma_{23} \\ \Delta\gamma_{13} \end{Bmatrix}$$

Where $T_a = A + C\sigma_{aa}$; Here repeated subscript does not mean summation

and $R_a = A\sigma_{aa} + B$; Here repeated subscript does not mean summation.

Figure 4.5. Stress-Strain Matrix for Drucker-Prager Material Model

Here, the repeated subscript does not mean summation. When the current state of stress is known, this matrix can be easily computed. Under the plane strain/axisymmetric idealizations, the incremental stress-strain matrix can be obtained by deleting appropriate rows and columns of the three-dimensional relationship shown in Figure (4.5).

Limitations of Drucker-Prager Model

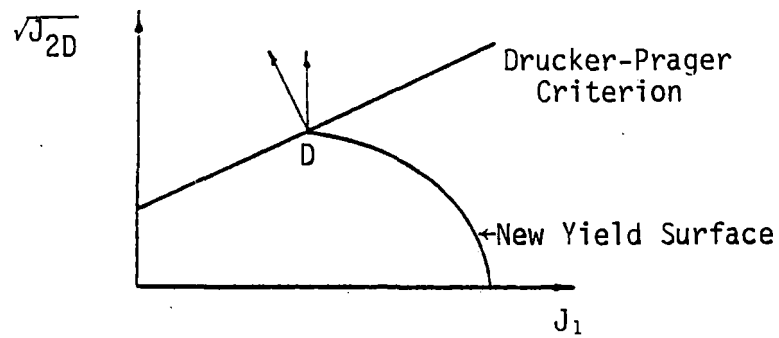
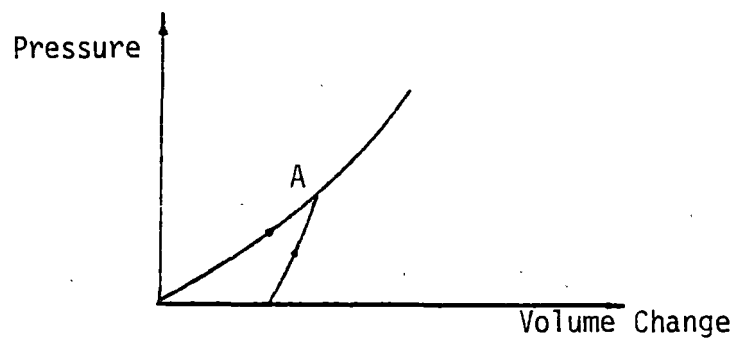
As shown in Figure (4.4) the incremental plastic strain vector has a negative volumetric component, which indicates volume increase or dialation at failure. However, experimental data on normally consolidated clays and loose sands indicates only compressive deformations or decrease in volume during shear, which is in conflict with predictions from the Drucker-Prager model. This discrepancy may be due to several reasons. It is possible that the normality rule may not be valid. On the other hand Drucker-Prager law may not be applicable to these materials.

Some problems can be solved without using the normality rule for the Drucker-Prager criterion. Here the stresses satisfy the yield criterion while the strain states are forced to satisfy certain conditions such as no volume changes. The major difficulty in discarding normality is that it implies that the material is unstable according to Drucker's postulates [25]. The limitations of Drucker-Prager model has also been described by Christian [6,17].

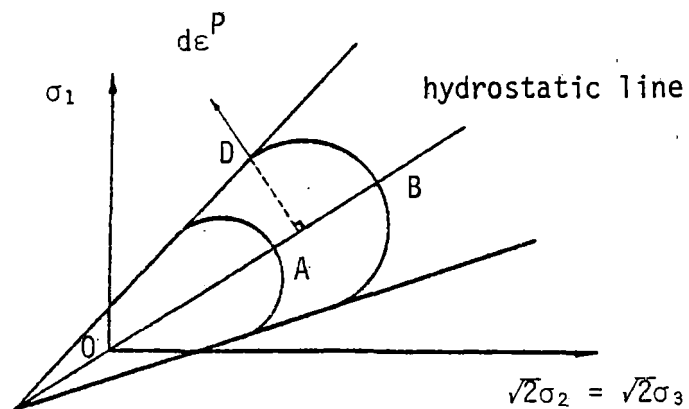
Hardening Behavior

The abandoning of normality may not be desirable as it is a very important rule in plasticity. It has also been observed that geologic media, especially soils, undergo plastic volumetric deformations even when the hydrostatic stress (J_1) is changed. This phenomenon cannot be explained with the Drucker-Prager model. In order to account for this phenomenon, the yield surface should intersect J_1 axis as shown in Figure (4.6a). This idea was first presented by Drucker, Gibson and Hankel [29] with respect to the behavior of a soil specimen in conventional triaxial test. A soil specimen which is subjected to a hydrostatic state of stress as shown by point A, when unloaded, deforms elastically. Until the stress state reaches point A upon reloading, Figure (4.6b), the material continues to deform elastically. Furthermore, the behavior under hydrostatic state of stress involves work hardening and not perfect plasticity. For work hardening materials when the stress point moves outside the yield surface, a new yield surface is established.

According to the concept described above, the yield surface should pass through A as shown in Figure (4.6c). Furthermore, the yield surface should be convex as discussed in Chapter II. For simplicity, Drucker, Gibson and Hankel [29] assumed that the hardening yield surface can be approximated by a circular arc at the open end, Figure (4.6c). With this idea of a new yield surface, it is possible to explain the observed behavior of (geologic) media under hydrostatic conditions, and at failure without abandoning

(a) Yield Surface Intersecting J_1 Axis

(b) Behavior Under Hydrostatic Loading and Unloading



(c) Hardening Caps

Figure 4.6 Hardening Behavior of Geologic Media

the normality rule. The new yield surface intersects the Drucker-Prager failure surface at an angle, Figure (4.6a). It is possible to explain the observed volumetric behavior of geologic media, if we assume that the incremental plastic strain vector is normal to the hardening yield surface at the point of intersection, D. When the hydrostatic stress is increased to bring the sample to point B as shown in Figure (4.6c); the yield curve must also expand to point B. Hence, there will be a family of yield curves corresponding to points on the hydrostatic axes. In other words, as the material work hardens, the yield surface expands to a new position. However, when the state of stress reaches a point on the yield surface which is locally parallel to the hydrostatic axis, the plastic volumetric changes will be zero, and hence no further hardening will take place. This leads to the fact that incremental plastic strain vector at point D as shown in Figure (4.6c) is normal to curved yield surface as well as the hydrostatic axis.

Drucker-Prager failure criterion plots as a right circular cone in the three-dimensional stress space, and the idea of the circular yield surface is similar to placing a dome at the open end of the cone. Although the idea of having a cap was first conceived with circular yield surfaces, the actual yield surface may not be circular. This received the attention of several researchers, and as a result several cap models have been developed recently. Cap models are described in the subsequent sections of this chapter.

4.5. Critical State Model

Introduction

Historical development of critical state model can be found in several publications of the soil mechanics group at Cambridge University [68, 69, 73]. Some of the important parameters used in the development of critical state concept are defined below.

The experimental work for this model has been carried out with a conventional triaxial apparatus by Roscoe and his co-workers [68, 69, 73], and hence, the quantities are defined with respect to this configuration. For the axisymmetric triaxial conditions, $\sigma_2 = \sigma_3$, and hence the quantities p , q , dv and $d\varepsilon$ are defined as follows.

$$p = \frac{\sigma_1 + 2\sigma_3}{3} = \frac{J_1}{3} \quad (4.26a)$$

$$q = \sigma_1 - \sigma_3 = \sqrt{3J_2D} \quad (4.26b)$$

$$dv = d\varepsilon_1 + 2d\varepsilon_3 \quad (4.26c)$$

$$d\varepsilon = \frac{2}{3} (d\varepsilon_1 - d\varepsilon_3) \quad (4.26d)$$

where p is the mean pressure, q is related to shear stress, dv is the incremental volumetric strain, and $d\varepsilon$ is the incremental shear strains. Here, σ_1 and σ_3 are the major and minor quantities of effective stresses.

Critical State Line

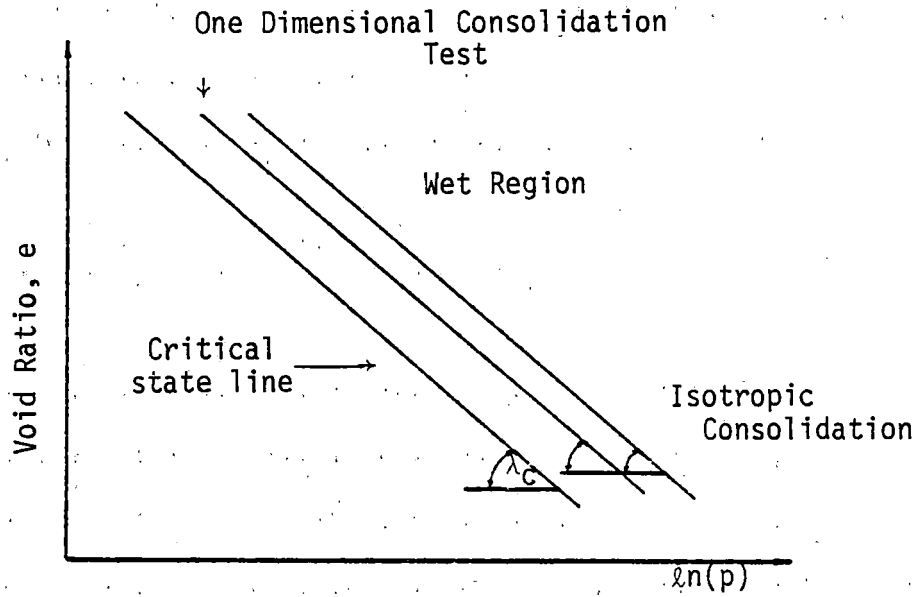
When a saturated soil sample is sheared, it passes through progressive states of yielding before reaching a state of collapse. That is, the stress path passes through several yield surfaces (hardening caps) causing plastic deformations. The yielding continues to occur until the material reaches a critical state, after which the void ratio remains constant during subsequent deformations. That is, the material will pass through a state in which the arrangements of the particles is such that no volume change takes place during shearing. This can be considered as the ultimate state of the material. The ultimate states have been observed to fall on a straight line on q - p space, irrelevant of how the material is brought to this state. This is called the critical state line [69].

The critical state line, and the isotropic pressure-volume line on e - $\log p$ plot have been observed to be parallel, as shown in Figure (4.7a). The slope of this line on the q - p plot is denoted by 'M', and it is a material parameter. This shows that the failure takes place when the material reaches a critical state.

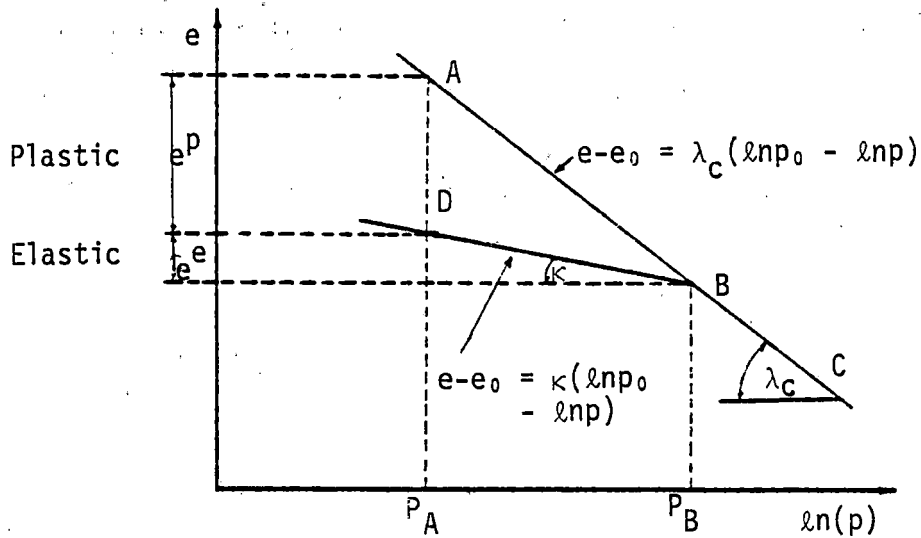
A three-dimensional view of the possible stress states in the p - q - e space are shown in Figure (4.8). It is interesting to note that e - $\log p$ relationship from any proportional loading stress path is parallel to the critical state line, Figure (4.7a).

4.5.1. Plastic Stress-Strain Behavior

Isotropic loading of a soil is shown in Figure (4.7b) on the e - $\log p$ plot. If the material is normally consolidated at



(a) Void Ratio - $\ln p$ Relationships



(b) Isotropic Loading-Unloading Behavior

Figure 4.7 Void Ratio - $\ln p$ Relationship for the Critical State Model

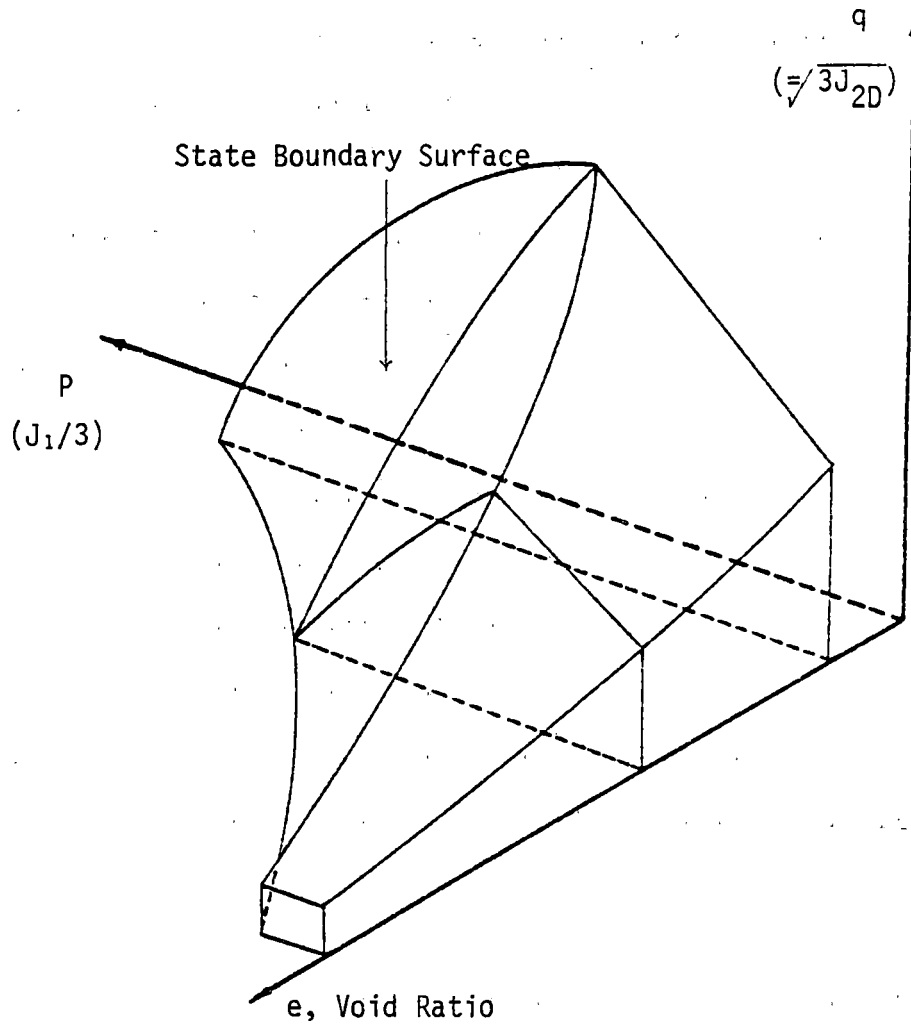


Figure 4.8 State Boundary Surface

A, the isotropic loading will follow the path AB. When the sample is unloaded to the mean pressure, P_A , the unloading path does not follow the loading path AB because of the elastic-plastic nature. Instead, the material follows path BD upon unloading. When the material is reloaded from pressure, P_A to P_B , the material follows the same path as unloading, that is, DB. Since the unloading and reloading follows the same path, this shows elastic behavior. As shown in Figure (4.7b) the slope of the loading path is denoted by λ_c , and the slope of unloading-reloading path is denoted by κ . The vertical distance AD shows the plastic component, and DE shows the elastic component of the change in volume, respectively. Therefore, the plastic volumetric strains, dv^P , can be evaluated as [73]

$$dv^P = \frac{(\lambda_c - \kappa)}{1 + e_0} \frac{dp_0}{p_0} \quad (4.27)$$

where p_0 is the hardening parameter, e_0 is the void ratio, and the superscript 'p' denotes plastic changes. In the stress-strain theory based on the critical state concept, it is assumed that there is no recoverable energy associated with shear distortions, i.e., $d\epsilon^e = 0$; the superscript 'e' denotes elastic components. Therefore, at all times,

$$d\epsilon = d\epsilon^P \quad (4.28)$$

According to the normality condition discussed in Chapter 2, the incremental plastic strain vector is normal to the yield surface

at any point. With reference to Figure (4.9), this can be expressed as

$$\frac{d\varepsilon^p}{dv^p} = - \frac{dp}{dq} \quad (4.29)$$

The ratio of shear and volumetric plastic strains can be found in terms of p and q by assuming a dissipated energy function as described in Reference [68]. Hence, Equation (4.29) can be integrated to obtain the yield function. For the modified cam clay model [68], the yield function has been obtained as,

$$F \equiv q^2 - M^2 p_0 p - M^2 p^2 = 0 \quad (4.30)$$

4.6. Cap Model

In the previous section, a model which is known as critical state model was described. The underlying foundation of the critical state model is the idea of using a yield surface to control the hydrostatic behavior as proposed by Drucker et al [29]. Since this second yield surface acted as a cap to the domain included by first yield surface, the models based on this idea are called "cap models". In this study, however, the word 'cap model' is loosely used to refer to the model proposed by Dimagio and Sandler [24]. In the critical state model, the yield criterion is expressed in terms of 'q' and 'p' which are based on the conventional triaxial configuration. Therefore, a generalization is required in order to implement the critical state model in a truly three dimensional situation. One of the limitations of the critical state model is that, it cannot

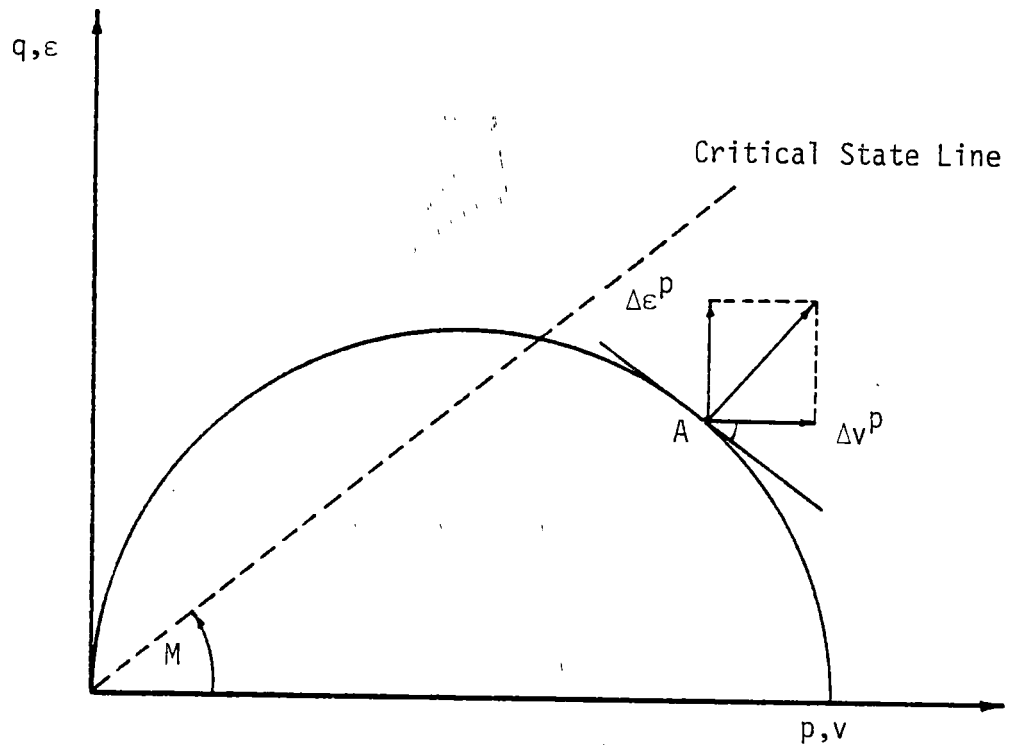
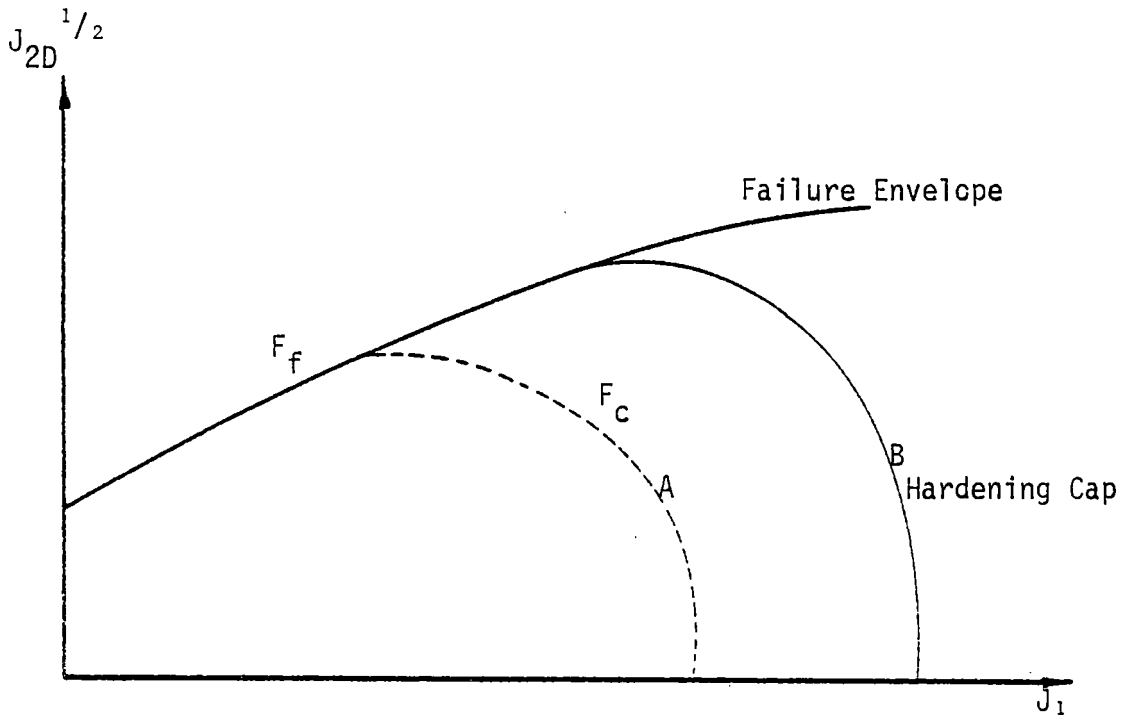


Figure 4.9 Yield Locus for Critical State Model
in q - p Plane

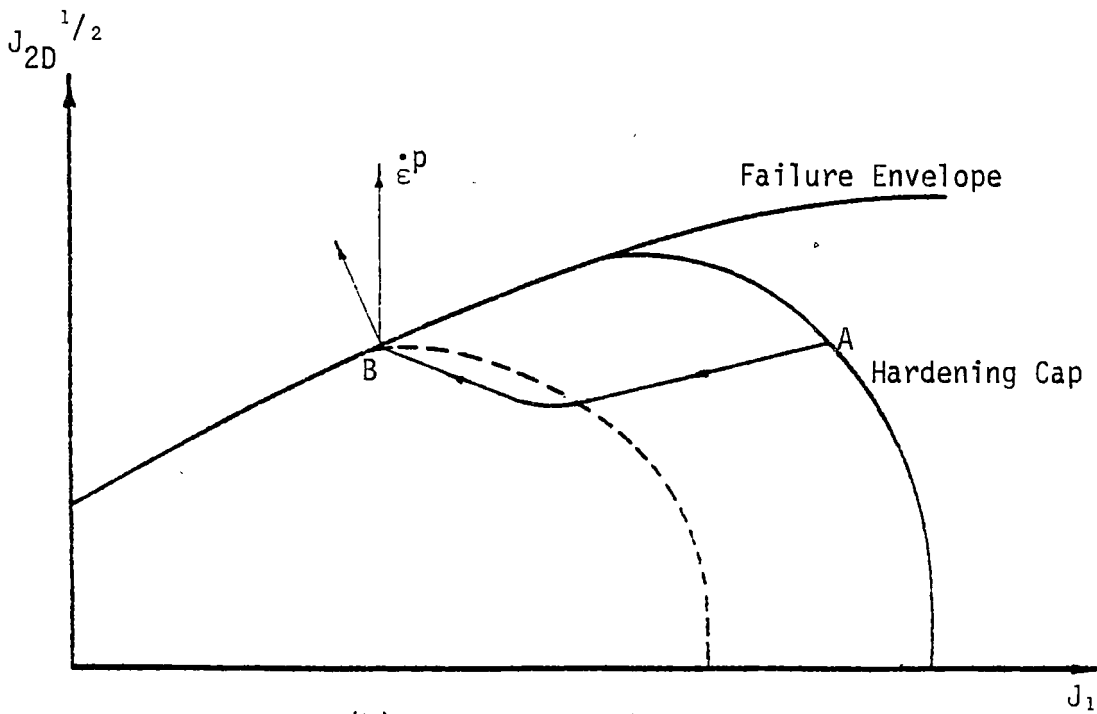
predict the behavior of geologic materials under very high pressures. Under very high pressures, the strength has been observed to be similar to a frictionless material while the critical state model include only the frictional behavior. Other limitation is that, it can be applied only for cohesionless materials.

Attempts have been made to use Drucker-Prager model with a non-associative flow rule in order to control the predicted plastic dilatation behavior. However, this violates the stability postulates, and hence its use may have certain mathematical difficulties with regard to uniqueness [24, 71].

A model based on classical plasticity and work hardening concepts have been proposed by Dimagio and Sandler [24], which overcomes many of the limitations discussed in the foregoing sections. This model has a yield surface which combines ideal plasticity and strain hardening as shown in Figure (4.10a). An associated flow rule is used to describe the plastic deformations. This model satisfies the continuity, stability and uniqueness requirements. As shown in Figure (4.10a) the yield surface is composed of a modified Drucker-Prager surface, and a cap surface. Here, the Drucker-Prager surface is assumed to be fixed in position while the cap could expand or contract depending upon plastic volumetric deformations. Actually the modified Drucker-Prager surface demarcates the ultimate conditions in which the material could exist. That is, any state of stress outside this surface cannot exist. Since this describes the ultimate or failure limit, it is referred to in this



(a) Expanding Yield Cap



(b) Contracting Yield Cap

Figure 4.10 Cap Model Proposed by DiMaggio and Sandler [24]

thesis as the "failure surface" which also acts as a part of the yield surface. Mathematically this can be expressed as

$$F_f (J_1, \sqrt{J_{2D}}) = 0 \quad (4.31)$$

where F_f is the failure criterion. Here, the subscript 'f' denotes failure states.

In this model, the strain hardening cap could expand or contract as the plastic volumetric strain increases or decreases, respectively. This is expressed as

$$F_c (J_1, \sqrt{J_{2D}}, \epsilon_V^p) = 0 \quad (4.32)$$

Unlike in the critical state model, strain hardening can be reversed in this model since the movement of the cap is governed by the plastic volumetric strain. Contraction of the cap can happen, only if the stress point (point A) which is on a cap moves to the failure line (point B) through the elastic region as shown in Figure (4.10b). At point B, the incremental plastic strain vector has a negative volumetric component if the normality rule is assumed. This causes plastic dilatation which causes the contraction of the cap towards point B. When the cap reaches point B, the stress point becomes a corner, and the incremental plastic strain vector rotates in clockwise direction controlling the amount of dilatancy [24, 71].

The ideally plastic portion of the yield surface is approximated by the following function [24, 71]:

$$F_f(J_1, \sqrt{J_{2D}}) = \sqrt{J_{2D}} - [\alpha - \gamma \exp(-\beta J_1)] = 0 \quad (4.33a)$$

where α , γ and β are material parameters. This can be generalized by adding another term in Equation (4.33a) so that the failure envelope changes from one Drucker-Prager criterion to another Drucker-Prager criterion at high pressures. In the original version of the cap model, failure envelope was similar to a von Mises criterion under very high pressures. The generalization can be expressed as

$$F_f(J_1, \sqrt{J_{2D}}) = \sqrt{J_{2D}} - [\alpha + \theta J_1 - \gamma \exp(-\beta J_1)] \quad (4.33b)$$

It is interesting to note that Equation (4.33b) reduces to Equation (4.33a) when $\theta = 0.0$. Here, θ is an additional material parameter.

The cap portion of the yield surface is assumed to be elliptic, as shown in Figure (4.11). The equation of the ellipse can be written as

$$F_c(J_1, \sqrt{J_{2D}}, \epsilon_V^p) = \left[\frac{(J_1 - L(\epsilon_V^p))}{(X(\epsilon_V^p) - L(\epsilon_V^p))} \right]^2 + \left[\frac{\sqrt{J_{2D}}}{\alpha + \theta J_1 - \gamma \exp(-\beta L(\epsilon_V^p))} \right]^2 - 1 = 0 \quad (4.34)$$

where the quantities $X(\epsilon_V^p)$ and $L(\epsilon_V^p)$ refer to geometric properties of the elliptic yield cap as shown in Figure (4.11). It is assumed that the ratio of major to minor axes remains the same for all ellipses; this ratio is denoted by 'R'. Hence,

$$X(\epsilon_V^p) = L(\epsilon_V^p) + R[\alpha + \theta J_1 - \gamma \exp\{-\beta L(\epsilon_V^p)\}] \quad (4.35)$$

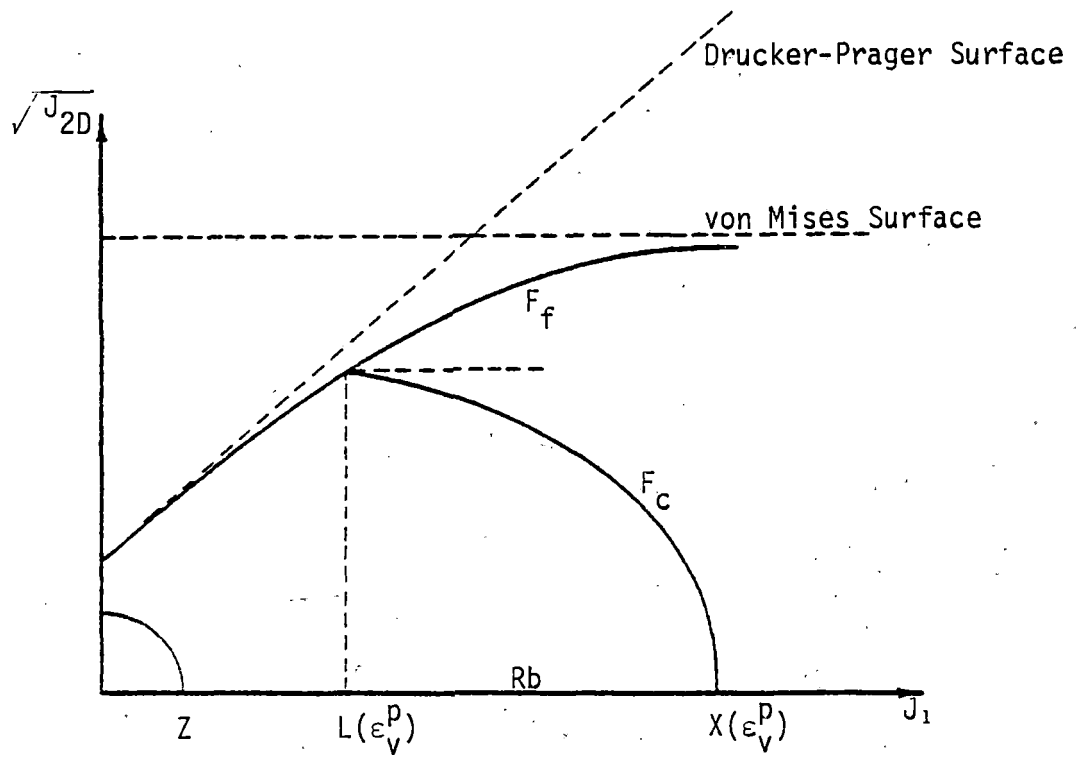


Figure 4.11 Failure and Hardening Surfaces in Cap Model

Equation (4.35) can also be expressed as,

$$F_c = \sqrt{J_{2D} - \frac{1}{R} [\{RF_f(L)\}^2 - (J_1 - L)^2]}^{1/2} \quad (4.36a)$$

or

$$F_c = R^2 J_{2D} - (X-L)^2 + (J_1 - L)^2 \quad (4.36b)$$

In order to relate X or L with the plastic volumetric strain, ϵ_V^P , it is required to analyse the hydrostatic behavior of the material. This has been expressed in the following manner.

$$\epsilon_V^P = W[1 - \exp(-DX)] \quad (4.37)$$

where D and W are material parameters. The inverse relation can be expressed as

$$X = -\frac{1}{D} \ln\left[1 - \frac{\epsilon_V^P}{W}\right] \quad (4.38)$$

For a given value of ϵ_V^P , X can be found from Equation (4.38). The corresponding value of L can be found by solving Equation (4.35) using a trial and error method.

4.7. Elasto-Plastic Constitutive Relationship for Hardening Models

Yield criterion for a hardening type material can be generally expressed as,

$$F = F(\sigma_{ij}, I_1^P) \quad (4.39)$$

where σ_{ij} is the stress tensor, and I_1^P is the first invariant of the plastic strain tensor or simply the plastic volumetric strain. In a cap type material model, there are two distinct surfaces on which

plastic deformations can take place; cap surface and the failure surface. In this thesis they are denoted as F_c and F_f , respectively. In the following section a general procedure for deriving elasto-plastic constitutive tensor is given. Subsequently, this is specialized and simplified for critical state and cap models. The flow rule for plastic flow can be written as, Equation (2.17),

$$\begin{aligned} d\varepsilon_{ij}^p &= \lambda \frac{\partial Q}{\partial \sigma_{ij}} \\ &= \lambda A_{ij} \end{aligned} \quad (4.40)$$

where Q is the plastic potential, and λ is a non-negative constant which varies throughout loading, and A_{ij} is equal to $\frac{\partial Q}{\partial \sigma_{ij}}$. During plastic flow, the state of stress will always satisfy Equation (4.39) and therefore,

$$dF = 0 \quad (4.41a)$$

That is,

$$\frac{\partial F}{\partial \sigma_{ij}} d\sigma_{ij} + \frac{\partial F}{\partial I_1^p} dI_1^p = 0 \quad (4.41b)$$

This can be written as

$$B_{ij} d\sigma_{ij} + \frac{\partial F}{\partial I_1^p} dI_1^p = 0 \quad (4.41c)$$

where $B_{ij} = \frac{\partial F}{\partial \sigma_{ij}}$, which is the gradient of the yield surface. The incremental stress tensor can be related to the elastic portion of

incremental strain tensor, by using the elastic constitutive tensor as,

$$d\sigma_{ij} = C_{ijkl} d\epsilon_{kl}^e \quad (4.42)$$

Here the superscript, 'e', denotes the elastic quantities. As described in Chapter 2, it is assumed that the total increments of strain can be decomposed to elastic and plastic components as

$$d\epsilon_{ij} = d\epsilon_{ij}^e + d\epsilon_{ij}^p \quad (4.43)$$

Here, the superscripts 'e' and 'p' denote elastic and plastic components, respectively. Equation (4.43) can be substituted into Equation (4.42) to obtain

$$d\sigma_{ij} = C_{ijkl} (d\epsilon_{kl} - d\epsilon_{kl}^p) \quad (4.44)$$

substituting Equation (4.40) into Equation (4.44), the following relationship could be obtained.

$$d\sigma_{ij} = C_{ijkl} (d\epsilon_{kl} - \lambda A_{kl}) \quad (4.45)$$

By contracting the indices in Equation (4.40),

$$d\epsilon_{ii}^p = dI_1^p = \lambda A_{ii} \quad (4.46)$$

Substitution of Equation (4.45) and (4.46) in Equation (3.48c), leads to

$$B_{ij} C_{ijkl} (d\epsilon_{kl} - \lambda A_{kl}) + \frac{\partial F}{\partial I_1^p} \lambda A_{ii} = 0 \quad (4.47a)$$

Collection of terms leads to

$$(B_{ij}C_{ijkl}A_{kl} - \frac{\partial F}{\partial I_1^p} A_{ii}) \lambda = B_{ij}C_{ijkl}d\epsilon_{kl} \quad (4.47b)$$

which gives

$$\lambda = \frac{B_{ij}C_{ijkl}d\epsilon_{kl}}{(B_{ij}C_{ijkl}A_{kl} - \frac{\partial F}{\partial I_1^p} A_{ii})} \quad (4.48)$$

By using the value of λ in Equation (4.45), stress-strain relationship can be obtained as

$$d\sigma_{ij} = [C_{ijrs} - \frac{C_{ijkl}A_{kl}B_{mn}C_{mnr s}}{B_{mn}C_{mnr s}A_{rs} - \frac{\partial F}{\partial I_1^p} A_{ii}}] d\epsilon_{rs} \quad (4.49)$$

For associated plasticity, $Q = F$, and hence $A_{ij} = B_{ij}$. Hence the elasto-plastic constitutive relationship can be written as

$$d\sigma_{ij} = [C_{ijrs} - \frac{C_{ijkl}A_{kl}A_{mn}C_{mnr s}}{A_{mn}C_{mnr s}A_{rs} - \frac{\partial F}{\partial I_1^p} A_{ii}}] d\epsilon_{rs} \quad (4.50a)$$

$$\text{or} \quad d\sigma_{ij} = C_{ijrs}^{ep} d\epsilon_{rs} \quad (4.50b)$$

where C_{ijrs}^{ep} is the elasto-plastic constitutive tensor which is symmetric.

4.7.1. Elasto-Plastic Constitutive Matrix for Critical State Model

A detailed derivation of the constitutive relationship can be found in Appendix B, and only a brief description is given here. The quantity A_{ij} in Equation (4.40) can be evaluated as follows

$$A_{ij} = \frac{\partial F_c}{\partial \sigma_{ij}} = \frac{\partial F_c}{\partial q} \frac{\partial q}{\partial \sigma_{ij}} + \frac{\partial F_c}{\partial p} \frac{\partial p}{\partial \sigma_{ij}} \quad (4.51)$$

In classical critical state soil mechanics literature, the quantities q and p are expressed with respect to cylindrical tri-axial device. However, for applications in plane strain, axisymmetric and three-dimensional stress analysis, it is required to define the quantities with respect to a general state of stress. These are given in Appendix B. Since A_{ij} is symmetric, it is easier to express its components in a vectorial form as follows:

$$\{A\}^T = [A_{11}, A_{22}, A_{33}, A_{12}, A_{13}, A_{23}] \quad (4.52)$$

Other unknown quantity in Equation (4.50), $\frac{\partial F_c}{\partial I_1^p}$ can be evaluated as follows:

$$\frac{\partial F_c}{\partial I_1^p} = \frac{\partial F_c}{\partial p_0} \frac{\partial p_0}{\partial I_1^p} \quad (4.53)$$

Substitution of Equation (4.27) into Equation (4.53) leads to

$$\frac{\partial F_c}{\partial I_1^p} = \frac{\partial F_c}{\partial p_0} \frac{p_0(1+e_0)}{(\lambda_c - \kappa)} \quad (4.54)$$

The elasto-plastic constitutive tensor, Equation (4.50) can be expressed in the matrix form as,

$$[C^{ep}] = [C^e] - \left[\frac{[C^e]\{A\}\{A\}^T[C^e]}{\{A\}^T[C^e]\{A\} - \frac{\partial F_c}{\partial I_1^p} (A_{11} + A_{22} + A_{33})} \right] \quad (4.55)$$

The constitutive relationship for plane strain, and axisymmetric idealizations can be obtained by deleting appropriate rows and columns of the above matrix.

4.7.2. Elasto-Plastic Constitutive matrix for Hardening Cap, F_c

The quantity A_{ij} in Equation (4.40) and $\partial F_c / \partial I_1^p$ in Equation (4.50) for the hardening cap is derived in Appendix C. The elasto plastic constitutive matrix for the cap can be evaluated by substituting quantities from Appendix C in Equation (4.50).

4.7.3. Elasto-Plastic Constitutive Matrix for Failure Envelope, F_f

Since $F_f(J_1, \sqrt{J_{2D}})$ does not depend on ϵ_V^p ,

$$\frac{\partial F_f}{\partial \epsilon_V^p} = 0 \quad (4.56)$$

By using Equations (4.33b) and (4.40),

$$A_{ij} = \frac{S_{ij}}{2\sqrt{J_{2D}}} - (\theta + \gamma\beta e^{-\beta J_1}) \delta_{ij} \quad (4.57)$$

Hence, $[C^{ep}]$ on the failure envelope can be computed by using Equations (4.57) and (4.55) in a similar manner as described in the previous section.

Chapter 5

COMPUTATIONAL ALGORITHMS

5.1. General

The computational procedures used in the nonlinear analysis are described in this chapter. Within the scope of this study three finite element programs based on one-, two- and three-dimensional idealizations have been developed; they can be used for stress-deformation analysis of many problems in solid mechanics, and are specifically designed for soil-structure interactions.

In the one-dimensional analysis (Beam-Column), the nonlinearity is included only in the support springs, while in the two- and three-dimensional analysis material nonlinearity is fully incorporated.

There are two important aspects of numerical analysis of nonlinear problems in solid mechanics. One is the numerical procedure used to satisfy the equilibrium conditions. This has to be accompanied with appropriate and consistent convergence criteria. The other important aspect is the computational procedure used for evaluation of correct stresses and strains. Although, these are listed as two aspects, they are very closely related.

Most nonlinear problems are analysed as a series of "piecewise linear" problems by using incremental techniques; here, the constitutive matrix is updated at each load increment. Since the characteristics of deformations change with the states of stress and strain, the increment size can play an important role in a nonlinear analysis. There are two widely accepted computational schemes which are used in conjunction with

finite element solutions; namely incremental and iterative techniques [15,89]. In the iterative technique, the number of iterations required to reach convergence can be quite large for highly nonlinear field problems. It has often resulted in poor convergency [89].

In the incremental technique, the increment size can be made suitably small to achieve convergence. Furthermore, the load-deformation history can be traced by using incremental procedure since the displacements at each load increment are computed. However, this may require a larger number of increments in highly nonlinear problems.

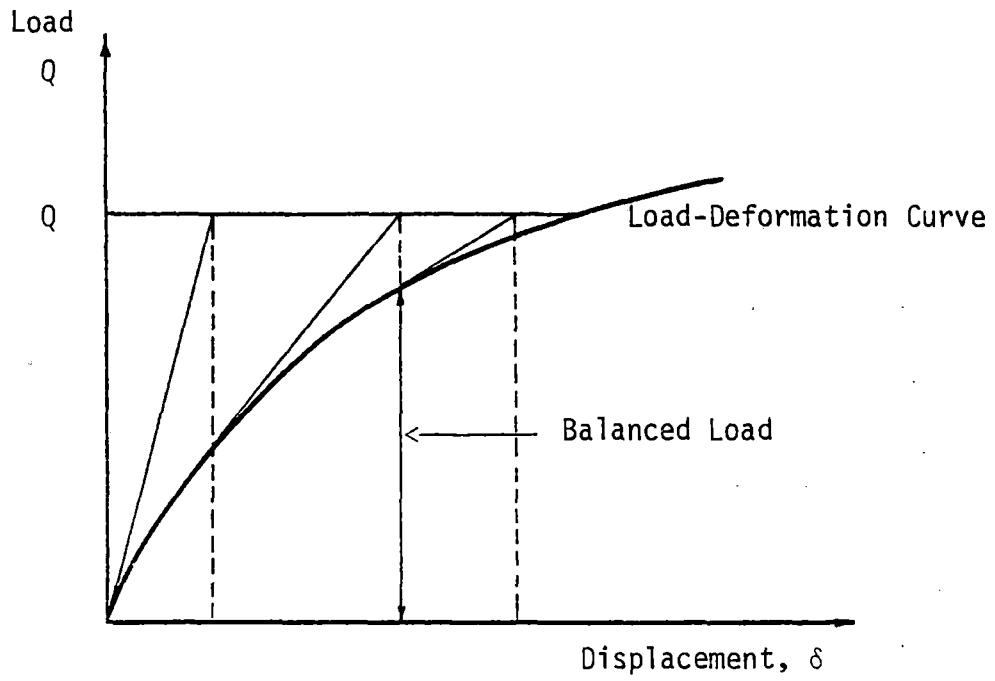
For highly nonlinear problems, where plastic deformations occur from very small load levels incremental technique alone may not be sufficient to satisfy the equilibrium conditions. Therefore, it is required to use a combination of incremental and iterative methods for such problems. Details of these methods are available in references [15,89]. Numerical procedure used herein is given below.

Computational Procedure

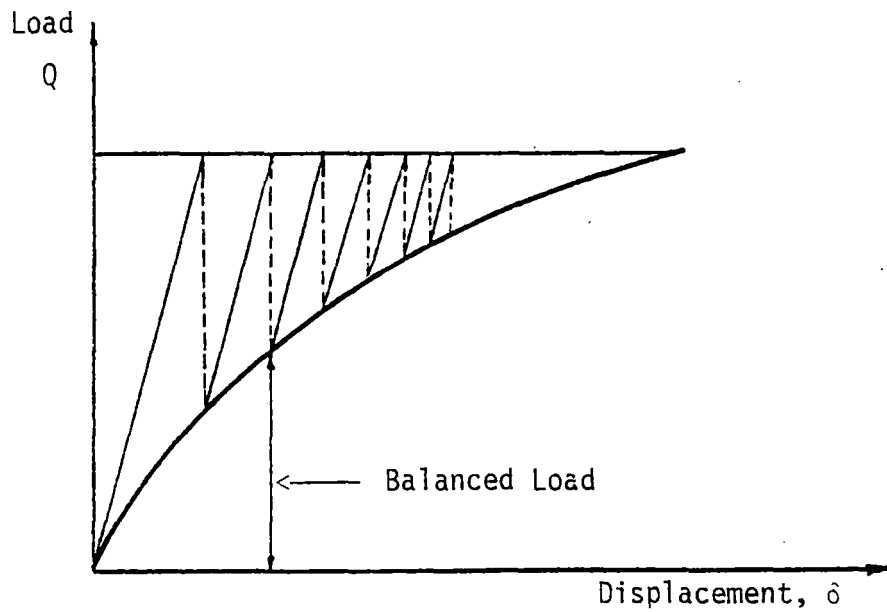
It is evident from the literature that there have been basically two computational procedures to handle nonlinear problems. These are namely the Newton-Raphson approach, and the modified Newton-Raphson approach. Graphical representation of these two methods are shown in Figure (5.1) with respect to a load-displacement relationship. The problem under consideration is written mathematically as

$$[k] \{\Delta q\} = \{\Delta Q\} \quad (5.1)$$

where $[k]$ is the tangent stiffness matrix, $\{q\}$ and $\{Q\}$ are displacement



(a) Original Newton-Raphson Method



(b) Modified Newton-Raphson Method

Figure 5.1 Newton-Raphson Iterative Methods

and load vectors, respectively. In the original Newton-Raphson method, the tangent stiffness is used every time Equation (5.1) is solved. However, this can be quite expensive computationally since formulation and solution of the system of equations have to be performed at each iteration stage. To overcome this difficulty, the modified Newton-Raphson method, Figure (5.1b), has been used. Here, the initial stiffness is used throughout the analysis. However, for highly nonlinear problems, modified Newton-Raphson method can require a larger number of iterations to reach convergence.

For nonlinear constitutive problems in solid mechanics, Zienkiewicz et. al., [94] have proposed a technique known as "Initial Stress Method". In this, they have given a physical interpretation to certain quantities, and have identified the error as an unbalanced load vector. Initial stress method can be interpreted as the modified Newton-Raphson method with the elastic stiffness kept constant throughout the analysis. In this scheme, the balanced load vector can be expressed as

$$\{Q\}_{Bal} = \iiint_V [B]^T \{\sigma\} dV \quad (5.2)$$

where $[B]$ is the strain-displacement matrix and σ is the current stress. With the physical interpretation given in initial stress method, convergence implies a state of static equilibrium. Because of the nonlinear constitutive models used in the current research, satisfaction of equilibrium equations can be quite difficult with the modified Newton-Raphson (initial stress) method unless a larger number of iterations is used. On the other hand, use of larger load increments with larger number of iterations for problems studied herein have been found to give erratic

results with the hardening type constitutive models. Use of small load increments, and the initial stress technique with constant elastic stiffness could give satisfactory results. However, this could be fairly expensive since the number of increments can be high for a nonlinear problem. Still, when the plastic deformations are much higher than elastic deformation, this technique could be unsatisfactory.

Mixed Incremental and Iterative Procedure

In the current research, a mixed procedure which combines incremental and iterative techniques is used, Figure (5.2); a similar procedure has been used by Phan [64].

The original Newton-Raphson method is used in one-, two-, and three-dimensional finite element programs developed within the scope of this study. In both the analysis of a beam-column on a nonlinear soil support, and the nonlinear analysis of two- and three-dimensional bodies with Variable Moduli models, the iterations are performed by using Newton-Raphson method; here midpoint Runge-Kutta scheme is used at intermediate steps within a load increment. This point will be discussed subsequently in this chapter.

5.2. Stress Transfer Technique in One-Dimensional Analysis

Some of the boundary value problems which can be analysed by using the one-dimensional idealization include beams on a continuous foundation such as a rail, axially and laterally loaded piles, and long retaining structures. This idealization can also be used to analyse the behavior of one-dimensional bodies which are supported by finite number of supports. In these problems, the continuous support is

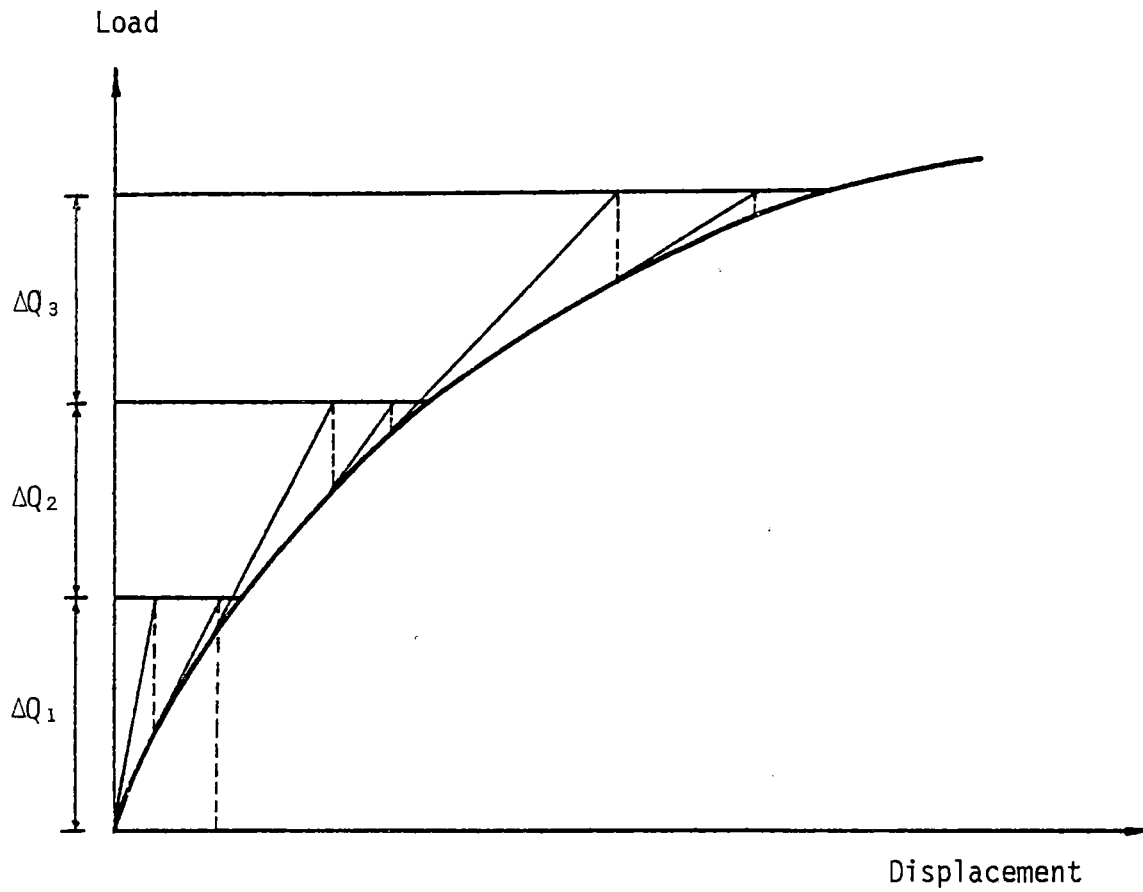


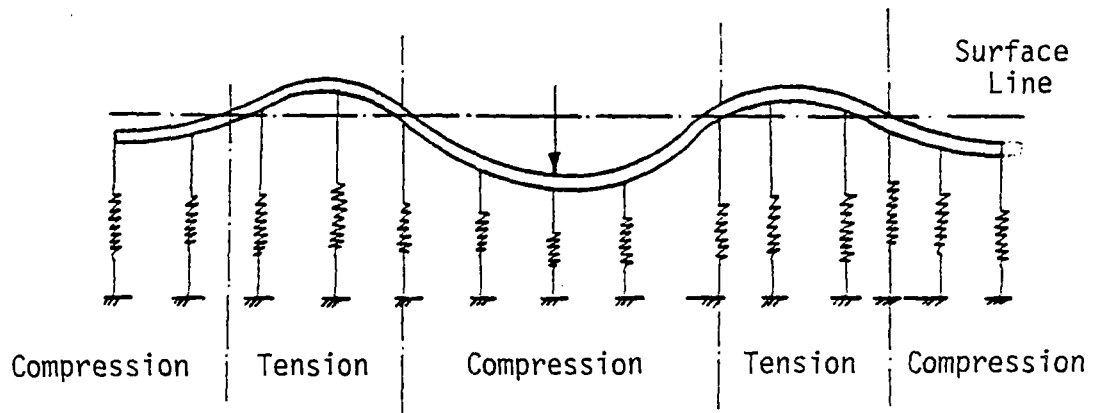
Figure 5.2 Mixture of Incremental and Iterative Techniques

replaced by a finite number of linear or nonlinear springs. The net effects of continuous supports are simulated by using springs.

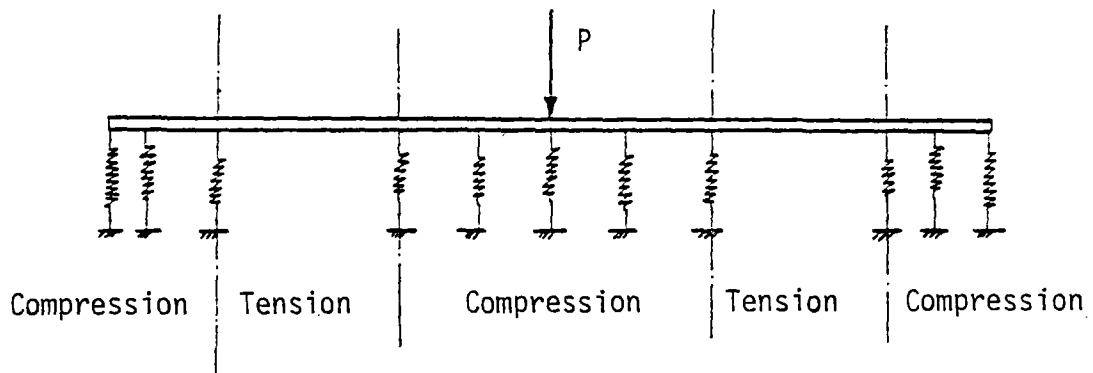
There is a basic difference between a beam on a deformable foundation, and a laterally loaded pile although both can be idealized as one-dimensional. The difference is that the beam on the surface can separate from the supporting soil into the open air while at least one side of the pile is always in contact with the soil. When there is a separation at the junction, the support conditions can be quite different. This requires the use of a stress transfer technique in modelling the separation of structural elements from the supports. One dimensional idealization of a beam on a continuous foundation is shown in Figure (5.3a). As can be seen in this figure, certain portions of the beam can deform so as to separate from the surface.

The classical Winkler-Zimmerman theory for beams on elastic foundation, neglects the above mentioned aspect. Furthermore, for nonlinear supports, a general nonlinear theory does not exist at this time. The numerical procedure developed herein is capable of accounting for above mentioned factors.

Since the soil usually can not carry tensile loads, an iterative procedure is needed to remove tensile stress conditions. This scheme is called "stress transfer iterations (cycles)". In the context of computational procedure, this has a complete different meaning than iterations (for equilibrium conditions) used in nonlinear analysis. The stress transfer technique can be used for both linear and nonlinear support conditions. The computational procedure used in stress transfer technique is outlined below.



(a) Deformation of a Beam-on-Continuous Foundation



(b) Re-Analysis After One Stress Transfer

Figure 5.3 Stress Transfer Technique

- (1) Perform a trial analysis at 'i'th step assuming complete supports and obtain the incremental displacement vector, Δq^i .
- (2) Compute the incremental support reactions simply by multiplying the current spring stiffness with corresponding incremental displacement, that is, $\Delta R^i = K^{i-1} \Delta q^i$.
- (3) Check to see if the total reaction is in tension. If so, separation occurs at that node. Identify all the nodes where separation occurs, and assign tensile stiffness for corresponding nodes.
- (4) Resolve the problem at 'i'th step. This completes one iteration (cycle) for stress transfer.

After the first stress transfer iteration, it may happen that some other regions can go into tension, and some tensile portions can come back to compression. For this situation a second stress transfer iteration (ISFER=2), can be used. The computer program developed herein has the capability of performing any number of stress transfer iterations within each increment used. Numerical results obtained by using this program are given in Chapters 8 and 9.

5.3. Numerical Procedure for Beams on Nonlinear Foundations

General Remarks

In most real situations, the response of soil to external loads can be nonlinear. This nonlinearity can be due to several reasons described in Chapter 1. In the one-dimensional idealization, the continuous supports can be replaced by a finite number of springs which

may have nonlinear characteristics. It is known that the principle of superposition is not valid for nonlinear behavior, and the response at one point, in general, can be quite dependent on other loads acting on the medium. However, for certain cases, when the loads are far apart, it may be possible to assume that the response at one location is independent from other loadings. Furthermore, there can be real situations where beams are resting on discrete nonlinear supports. The procedure used in the nonlinear analysis is described below.

Nonlinear Analysis

In this study, the nonlinearity of the support springs is represented by using Ramberg-Osgood model which is described in reference [17]. A graphical representation of this model is shown in Figure (5.4). Here, the tangent spring stiffness, K_t , at any state is expressed as

$$K_t = \frac{K_{ti} - K_{tf}}{\left[1 + \left[\frac{(K_{ti} - K_{tf})u}{P_u}\right]^m\right]^{(m+1)/m}} + K_{tf} \quad (5.3)$$

where K_{ti} is the initial stiffness, K_{tf} is the final stiffness, P_u is the ultimate load on the spring, u is the deflection, and m is an exponent which characterizes the shape of the load-deformation curve.

The nonlinear analysis is performed using a prescribed number of sequences, increments, and iterations. Here, the sequences mean different sets of loadings. Each loading set can be divided into a number of increments, and any number of iterations per each step (increment) can be performed. Stress transfer cycles can be performed within loading iterations. Steps used in the nonlinear analysis are given below when

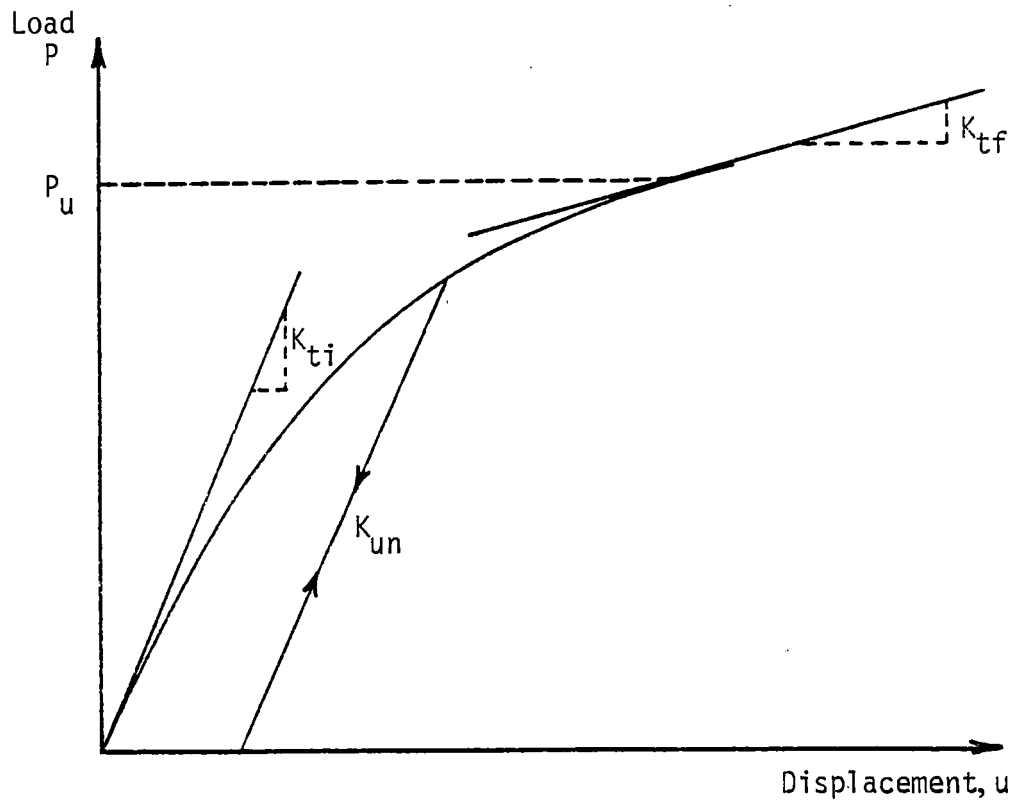


Figure 5.4 Ramberg-Osgood Model

moving from 'i'th step to 'i+1'th step.

- (1) Compute K_i based on q_i at the 'i'th step. Then perform the analysis for load, $\Delta Q = Q_{i+1} - Q_i$, and determine the incremental displacement vector.
- (2) Compute the spring constants corresponding to average value of $q_i^{(n-1)}$ and $q_i^{(n)}$. Here $q_i^{(n)}$ denotes the displacements computed in the 'n'th iteration. Skip this step if no iterations are to be performed.
- (3) Compute reactions based on $q_i^{(n)}$ and spring constants computed in step (2). Find the unbalanced load fraction by comparing the external loads and reactions, that is

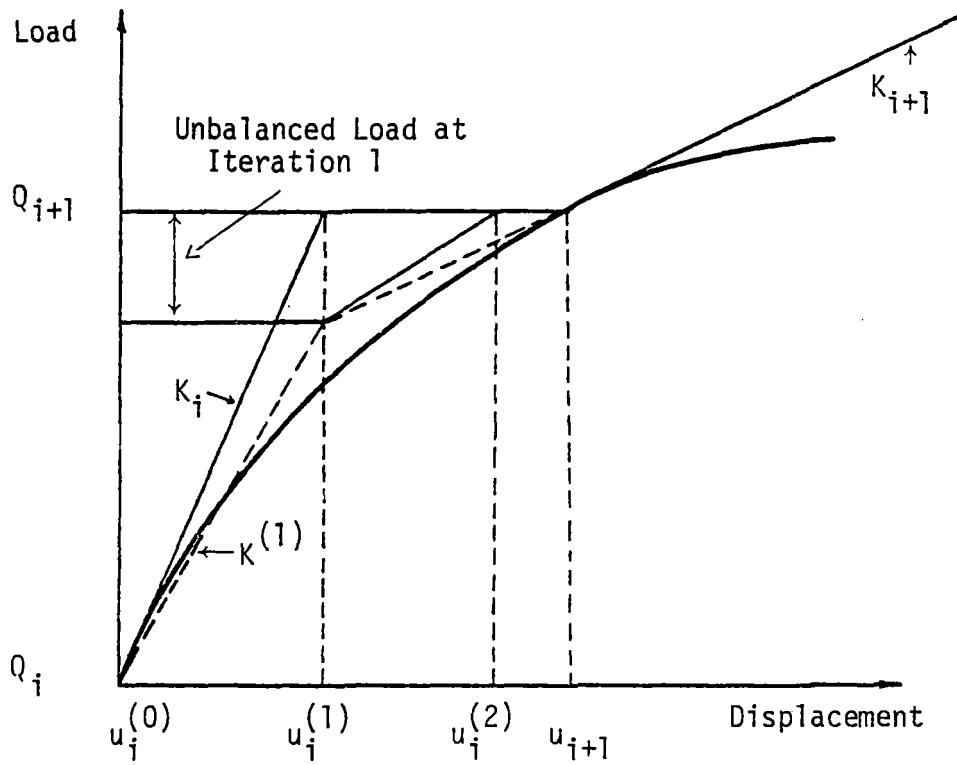
$$\text{Unbalanced load} = Q - \sum_1^m R_i.$$

- (4) Compute the spring constants at $q_i^{(n)}$, and solve the problem for unbalanced load vector. This will give new displacements $q_i^{(n+1)}$ which can be used for (n+1)th iteration.
- (5) When acceptable equilibrium is reached $q_i^{(n)}$ becomes q_{i+1} . For the next increment, use the spring constants based on $q_i^{(n)}$, after 'n'th iteration. A graphical representation of the above procedure is shown in Figure (5.5).

When no iterations are to be performed, this becomes purely an incremental procedure. In this case, the spring stiffness is updated at each step and the procedure becomes straight forward.

5.3.1. Numerical Procedure for Unloading Conditions in Support Springs

As described in Chapter 4, many solids behave differently under loading and unloading conditions; this is usually characterized through



$$K^{(1)} = K \text{ at } \frac{1}{2} (u_i + u_i^{(1)})$$

Figure 5.5 Iterative Procedure Used in Analysis of Beams
on Nonlinear Supports

constitutive behavior. The spring supports used in this analysis simulate approximately the effective resistance from the semi-infinite solid. Therefore, the deformation characteristics of the springs can be different for loading and unloading. The unloading criterion used in this analysis is the maximum compressive displacement of each spring. Since the springs are placed on the negative sides of the coordinate axes, compressive displacements have negative signs. Modelling of unloading behavior can be quite important for sequential loading conditions. Here, the maximum compressive displacements of each spring is updated and stored for comparison purposes. At any step of load increment, a trial solution is performed, and displacements of each spring is checked with the maximum past value. If the current displacement of any spring is less than its maximum past value, it is considered to be undergoing unloading or reloading. Unloading-reloading properties are assigned to those springs, and the analysis is repeated. In this analysis, the unloading-reloading stiffness is taken as the initial value at zero displacements, Figure (5.4). However, any other value can be used to model the unloading behavior.

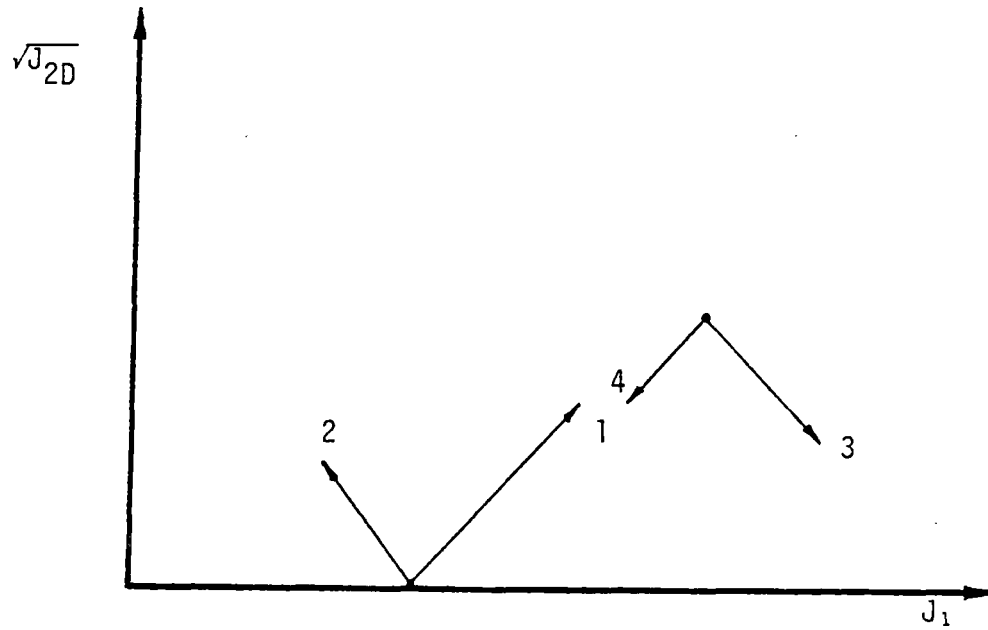
5.4. Variable Moduli Model: Implementation in Two- and Three-Dimensional Analysis

Details of the variable moduli model used in the present research are given in Chapter 4. As could be seen in Equation (4.7), the variable moduli model gives the variation of shear and bulk moduli with the stress and strain states. Furthermore, these quantities can be dependent on whether the material is in a loading or an unloading state;

the criterion for unloading are given in Chapter 4. The computational procedure used here is capable of accounting for loading, unloading and reloading in shear or bulk behavior. Some possible stress paths are shown in Figure (5.6).

At the beginning of a load increment, the values of bulk modulus, K , and the shear modulus, G , are computed based on the current state and the history. The constitutive matrix, Equation (4.14), is then formed and a complete finite element analysis is carried out to determine the incremental displacement vector. Then, the incremental stresses are computed based on the current constitutive relationship. After adding the incremental quantities to the previous state of stress, the criterion for unloading and reloading in bulk and shear behavior are checked at each integration point. Depending upon the above check, unloading constitutive parameters are assigned to the corresponding integration points for subsequent analysis. If it is found that all integration points of at least one element has changed its state from loading to unloading or vice versa, then the analysis is re-performed with appropriate constitutive parameters. Once the incremental stresses are computed, the equilibrium iterations are performed as described below.

In view of the nonlinearity, the constitutive relationship changes within the increment itself. Therefore, a new constitutive relationship $[C_{ave}]$ is established based on the average stresses during the increment. This new relationship $[C_{ave}]$ is used to compute a stress vector assuming that the computed strains are correct. At this stage stresses are updated, and the unbalanced load vector is computed. This pro-



1. Loading in Both Bulk and Shear Behavior
2. Loading in Shear; Unloading in Bulk Behavior
3. Unloading in Shear; Loading in Bulk Behavior
4. Unloading in Both Shear and Bulk Behavior

Figure 5.6 Possible Loading-Unloading Paths for Variable Moduli Model

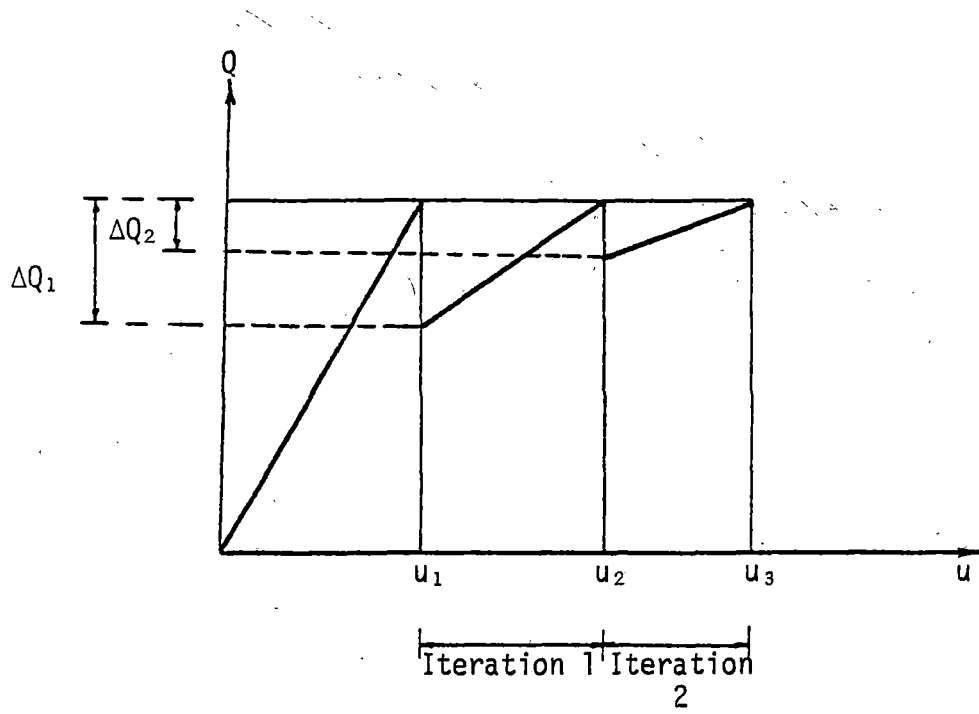
cedure is repeated in subsequent iterations until convergence is reached. A graphical representation of this procedure is given in Figure (5.7). The convergence criterion used in the current research is described subsequently in this chapter.

Steps used in the nonlinear analysis are listed below with reference to Figure (5.7).

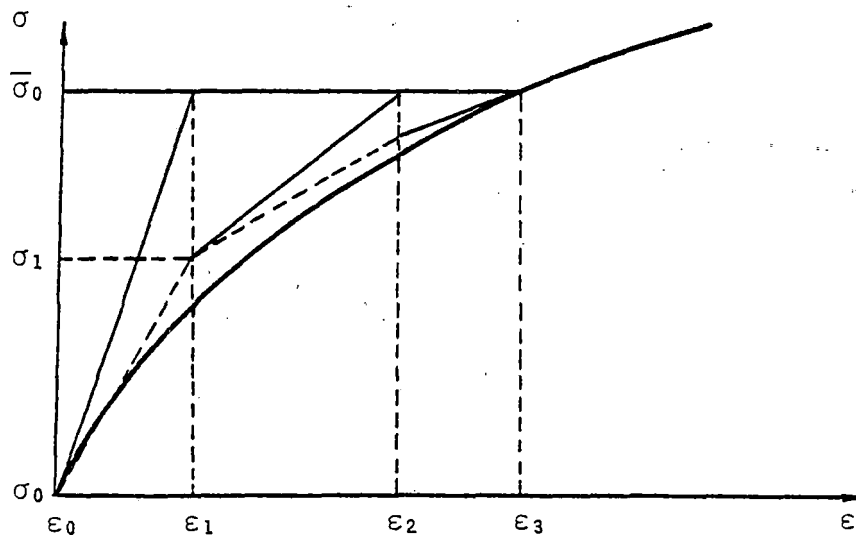
- (1) Apply external load Q and perform the analysis with properties based on σ_0 . Compute $\bar{\sigma}_0$, Figure (5.7b).
- (2) Compute $\sigma_a^{(0)} = (\sigma_0 + \bar{\sigma}_0) \times \theta$, $\theta = 0.5$ at midpoint. Hence compute elastic properties based on $\sigma_a^{(0)}$. The superscript '0' denotes zeroth iteration, and the subscript 'a' denotes average values.
- (3) Calculate new stresses $\{\sigma_1\} = [C_a^{(0)}] [B] \{q\}$. Hence compute balanced load $\{Q_1\} = \int [B]^T \{\sigma_1\} dV$. Therefore, unbalanced load $\{\Delta Q_1\} = \{Q\} - \{Q_1\}_{bal}$.
- (4) Compute elastic properties based on σ_1 . Perform a new analysis with ΔQ_1 as the load vector. Repeat the above procedure until equilibrium is satisfied.

5.5. Drucker-Prager Model: Implementation in Two- and Three-Dimensional Analysis

In this model, the material behaves elastically until the state of stress reaches yield criterion. Hence, for an incremental strain, $\{\Delta \epsilon\}$, the incremental stress, $\{\Delta \sigma\}$, can be computed using elastic constitutive relationship if the final state of stress lies within the yield surface. That is,



(a) Load-Displacement Curve within an Increment



(b) Stress-Strain Curve within an Increment

Figure 5.7 Computational Procedure for Variable-Moduli Model

$$F(\{\sigma_0\} + \{\Delta\sigma\}) < 0 \quad (5.4)$$

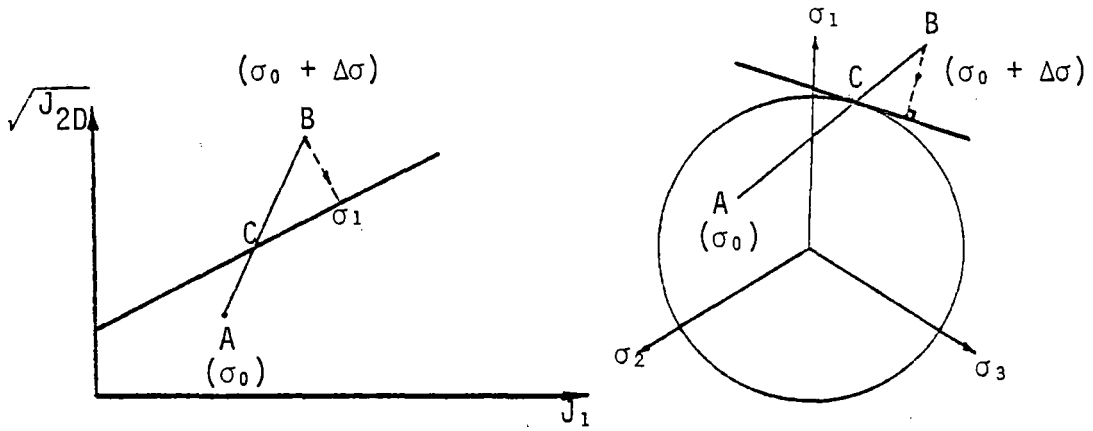
where $\{\sigma_0\}$ is the state of stress prior to the increment. However, for certain strain increments, the state of stress can go outside of the yield surface; that is, $F(\sigma) > 0$. This situation is shown in Figure (5.8a). For this case, the material behaves elastically until it reaches point C in Figure (5.8a), and then deforms elasto-plastically. Here, it is assumed that yielding initiates at point C which is the intersection of stress vector with the yield surface. For this situation, the incremental stress can be computed as follows [70]:

$$\{\Delta\sigma\} = S[C^e] \{\Delta\epsilon\} + (1-S) [C^{ep}] \{\Delta\epsilon\} = \{\Delta\sigma_1\} + \{\Delta\sigma_2\} \quad (5.5)$$

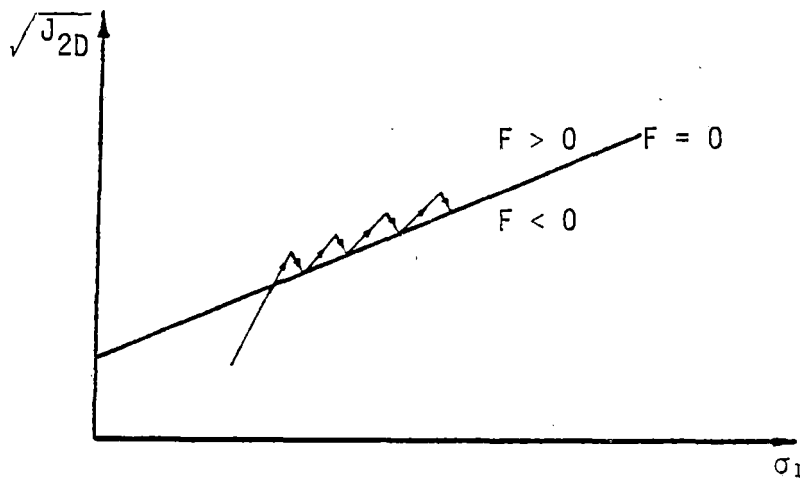
where S is the fraction of strain increment that is required to initiate yielding, $[C^e]$ and $[C^{ep}]$ are elastic and elasto-plastic constitutive matrices, respectively. Once the fraction S is determined, computation of $\{\Delta\sigma_1\}$ in Equation (5.5) is straight forward.

5.5.1 Subincrements of Strain

However, computation of $\{\Delta\sigma_2\}$ requires an integration of Equation (5.5) since $[C^{ep}]$ changes with the stress level. This can be done by dividing $(1-S) \{\Delta\epsilon\}$ into a number of smaller steps which are called as 'subincrements' in this study. However, computed stresses at each subincrement may be inaccurate depending upon the direction of strain increment. That is, the computed stresses may lie outside the yield surface. In such situations, stresses can be brought back to the yield surface by some other means.



(a) Stress Point Outside the Yield Surface



(b) Marching Scheme for Stress Return

Figure 5.8 Numerical Scheme for Correcting Stresses in Drucker-Prager Model

Previous Work

There are several computational schemes to correct the drifting tendency that is described above. Davidson and Chen [9] arbitrarily corrected the stresses at constant hydrostatic stress (J_1) for plane strain problems using Drucker-Prager criterion. For two-dimensional stress analysis, Nayak and Zienkiewicz [56] used a scheme which brought the stresses back to the yield surface along the normal to the yield surface. Christian et. al., [7] have investigated three schemes for correcting stress states which violate the yield criterion; they have employed Mohr-Coulomb criterion in plane strain idealizations. In the first scheme they used, average stress was kept constant, while the second involved bringing stresses along the normal to Mohr-Coulomb envelope, and the third involved correcting stresses at constant vertical stress, σ_v . They have concluded that for bearing capacity problems, the results were very sensitive to the manner in which the stresses were brought back to the yield surface.

5.5.2 Procedure for Correcting Stresses

In the current research, the stresses are brought back along the normal to the yield surface. Here, the stresses calculated at each subincrement, Figure (5.8b), by using the forward marching scheme with updated constitutive matrix is taken as the first approximation. When the stresses are outside the yield surface, $dF > 0$; let this value be F_1 . A change in yield function can be expressed as

$$dF = \frac{\partial F}{\partial \sigma_{ij}} d\sigma_{ij} \quad (5.6)$$

It is mentioned in Chapter 4, that $\frac{\partial F}{\partial \sigma_{ij}}$ is the gradient of the yield surface. In vector form, Equation (5.6) can be written as

$$dF = \left\{ \frac{\partial F}{\partial \sigma} \right\}^T \{d\sigma\} \quad (5.7)$$

since the stress calculated at the first approximation is outside the yield surface, it can be substituted in Equation (5.7) to get

$$0 - F_1 = -F_1 = \left\{ \frac{\partial F}{\partial \sigma} \right\}^T \{d\sigma\} \quad (5.8)$$

when the change of stress $\{d\sigma\}$ is such that it is normal to the yield surface, Equation (5.8) can be written as

$$-F_1 = \left\{ \frac{\partial F}{\partial \sigma} \right\} r \left\{ \frac{\partial F}{\partial \sigma} \right\} \quad (5.9)$$

Hence,

$$r = \frac{-F_1}{\left(\left\{ \frac{\partial F}{\partial \sigma} \right\}^T \left\{ \frac{\partial F}{\partial \sigma} \right\} \right)} \quad (5.10)$$

and

$$\{d\sigma\} = \frac{-F_1 \left\{ \frac{\partial F}{\partial \sigma} \right\}}{\left(\left\{ \frac{\partial F}{\partial \sigma} \right\}^T \left\{ \frac{\partial F}{\partial \sigma} \right\} \right)} \quad (5.11)$$

The above procedure can be used to move a point which is on the yield surface ($F = 0$) to an outside location ($F = F_1$). Since the quantity $\{\partial F/\partial \sigma\}$ is calculated based on the stresses outside the yield surface, it may not be exactly normal to the yield surface. Therefore, when $\{d\sigma\}$ in Equation (5.11) is computed based on the stresses at the first approximation, it may not bring the stress point exactly on to the yield surface. Hence, the second approximation gives

$$\{\sigma\}_2 = \{\sigma\}_1 + \{d\sigma\} \quad (5.12)$$

Now, Equation (5.11) can be evaluated based on $\{\sigma\}_2$ to lead to the third approximation for $\{\sigma\}$. This procedure can be repeated until satisfactory convergence is reached. This procedure has been found to bring the stress point rapidly to the yield surface. A comparison of the results based on this procedure and the previous work is given in Chapter 8 under verifications. By making the subincrement size of strains smaller, this procedure can bring the stress point back to the yield surface even in the first iteration; this however, depends on the number of subincrements.

Evaluation of S

The quantity 'S' in Equation (5.5) can be computed by using simple geometry. Since, the fractional stress $S\{\Delta\sigma\}$ brings the stress point on to the yield surface, the yield criterion has to be satisfied. That is

$$F(\{\sigma_0\} + S\{\Delta\sigma\}) = 0 \quad (5.13a)$$

This leads to a quadratic equation in S as given below.

$$AS^2 + 2BS + C = 0 \quad (5.13b)$$

where

$$A = (\dot{\sigma}_x - \dot{p})^2 + (\dot{\sigma}_y - \dot{p})^2 + (\dot{\sigma}_z - \dot{p})^2 + 2(\dot{\tau}_{xy}^2 + \dot{\tau}_{yz}^2 + \dot{\tau}_{zx}^2) \\ - 2\alpha^2(\dot{\sigma}_x + \dot{\sigma}_y + \dot{\sigma}_z)^2$$

$$\begin{aligned}
B = & (\sigma_x - p)(\dot{\sigma}_x - \dot{p}) + (\sigma_y - p)(\dot{\sigma}_y - \dot{p}) + (\sigma_z - p)(\dot{\sigma}_z - \dot{p}) \\
& + 2(\tau_{xy}\dot{\tau}_{xy} + \tau_{yz}\dot{\tau}_{yz} + \tau_{zx}\dot{\tau}_{zx}) \\
& - 2\alpha^2(\sigma_x + \sigma_y + \sigma_z)(\dot{\sigma}_x + \dot{\sigma}_y + \dot{\sigma}_z) - 2\alpha k(\dot{\sigma}_x + \dot{\sigma}_y + \dot{\sigma}_z)
\end{aligned}$$

and

$$\begin{aligned}
C = & (\sigma_x - p)^2 + (\sigma_y - p)^2 + (\sigma_z - p)^2 + 2(\tau_{xy}^2 + \tau_{yz}^2 + \tau_{zx}^2) \\
& - 2\alpha^2(\sigma_x + \sigma_y + \sigma_z)^2 - 2k^2 - 4\alpha k(\sigma_x + \sigma_y + \sigma_z)
\end{aligned}$$

Here, the overdot denotes the incremental quantities, p is the mean pressure, and other quantities have the same meaning as defined in previous chapters. Equation (5.13b) can be solved for the value of S .

In view of the nonlinearities involved in elasto-plastic behavior, this analysis is carried out incrementally by using the original Newton-Raphson method described previously in this chapter. At the beginning of any load increment, stiffnesses are formulated based on the current constitutive relationships. Equilibrium equations are then solved to get the incremental nodal displacements, and hence the incremental strains at each integration point. Computed strains are assumed to be correct, and the corresponding 'correct' stresses are computed by dividing the incremental strains into subincrements as described in the foregoing section. These stresses and displacements are then updated, and the unbalanced load vector is computed. Subsequent iterations are performed in a similar manner to reach an acceptable level of convergence. After the specified number of iterations are performed, next increment of loading is applied. For this increment, the load vector is taken as the vector sum of external incremental load, and whatever the

unbalanced load at the previous step. Numerical results obtained by using the above scheme in two- and three-dimensional analysis are given in Chapters 8 and 9.

5.6. Critical State Model: Implementation in Two- and Three-Dimensional Analysis

In this model, there are two yield surfaces, namely the failure or the critical state line, and the expanding yield cap. Theoretical details of this model are given in Chapter 4. The material behaves elastically when the state of stress lies within the yield surface. When the state of stress goes outside the current yield cap (surface), the material undergoes elasto-plastic deformations. In this process the material hardens until the state of stress falls on a new yield or hardening cap.

There are not many applications of the critical state model in conjunction with finite element analysis, and most of these applications were restricted to two-dimensional plane strain idealizations.

Previous Work

A plane strain finite element analysis of a footing problem has been reported by Simpson [75] by using the critical state model. Here, constant strain triangular elements were employed. The elasto-plastic constitutive matrix, $[C^{ep}]$, was used for computing incremental strains, $d\epsilon$, and incremental stresses, $d\sigma$, for each load increment. Then the stresses and strains were updated before going to the next increment. However, success of this method depends on increment size of the load.

An axisymmetric triaxial specimen, and a plane strain footing problem were analysed by Zienkiewicz and Naylor [57,91] by using the critical state model in conjunction with finite element procedure. They have used the 'initial stress' approach in the analysis. However, no mention was made regarding a convergence criterion required to satisfy the equilibrium condition. This type of analysis may require a larger number of iterations in view of the nonlinearity described by the critical state model. The initial stress method may not be appropriate when the plastic deformations are much higher than elastic deformations. This is evident from the fact, that the applications have been limited to study the load-deformation behavior at lower loads that are not close to the failure.

Phan [64] has reported the use of this model in a three-dimensional analysis.

Present Study

In the current research, a constitutive relationship based on modified cam clay theory [68] has been implemented in two- and three-dimensional finite element procedures. Here, attention has been given to computational algorithms. A procedure based on original Newton-Raphson method is used herein. All possible stress paths to model loading-unloading are considered. Since there are two yield surfaces in this model, F_f is used to denote the failure or critical state line while F_c is used to denote the hardening cap.

For an incremental strain $\{d\varepsilon\}$, corresponding incremental stress can be computed by using elastic constitutive relationship if the final state of stress lies within the yield surface. In the critical state model, however, the elastic properties are functions of the current state, and hence the behavior is nonlinear elastic within the yield surface. Therefore, an incremental procedure has to be used even in the elastic region to compute stress increments when strain increments are known. If the final state of stress lies within the yield surfaces and failure, following conditions will be satisfied:

$$F_c(\{\sigma_0\} + \{\Delta\sigma\}) < 0 \quad (5.14a)$$

and

$$F_f(\{\sigma_0\} + \{\Delta\sigma\}) < 0 \quad (5.14b)$$

where $\{\sigma_0\}$ is the state of stress prior to the increment. However, for certain strain increments, the state of stress can violate one or both of the conditions given in Equation (5.14). In the following section, these two possibilities are considered separately.

5.6.1. Correction of Stresses Back to the Critical State Line

In this section, the possibility of violation of Equation (5.14b) is considered. The incremental stress computed by using elastic constitutive matrix can violate the critical state condition in several ways as shown in Figure (5.9). State of stress at the beginning of the increment is shown by point A in Figure (5.9). After the current increment, the point can move to B, C, D or E as shown in this figure. If the stress point has followed path AE, then the material is still in the elastic

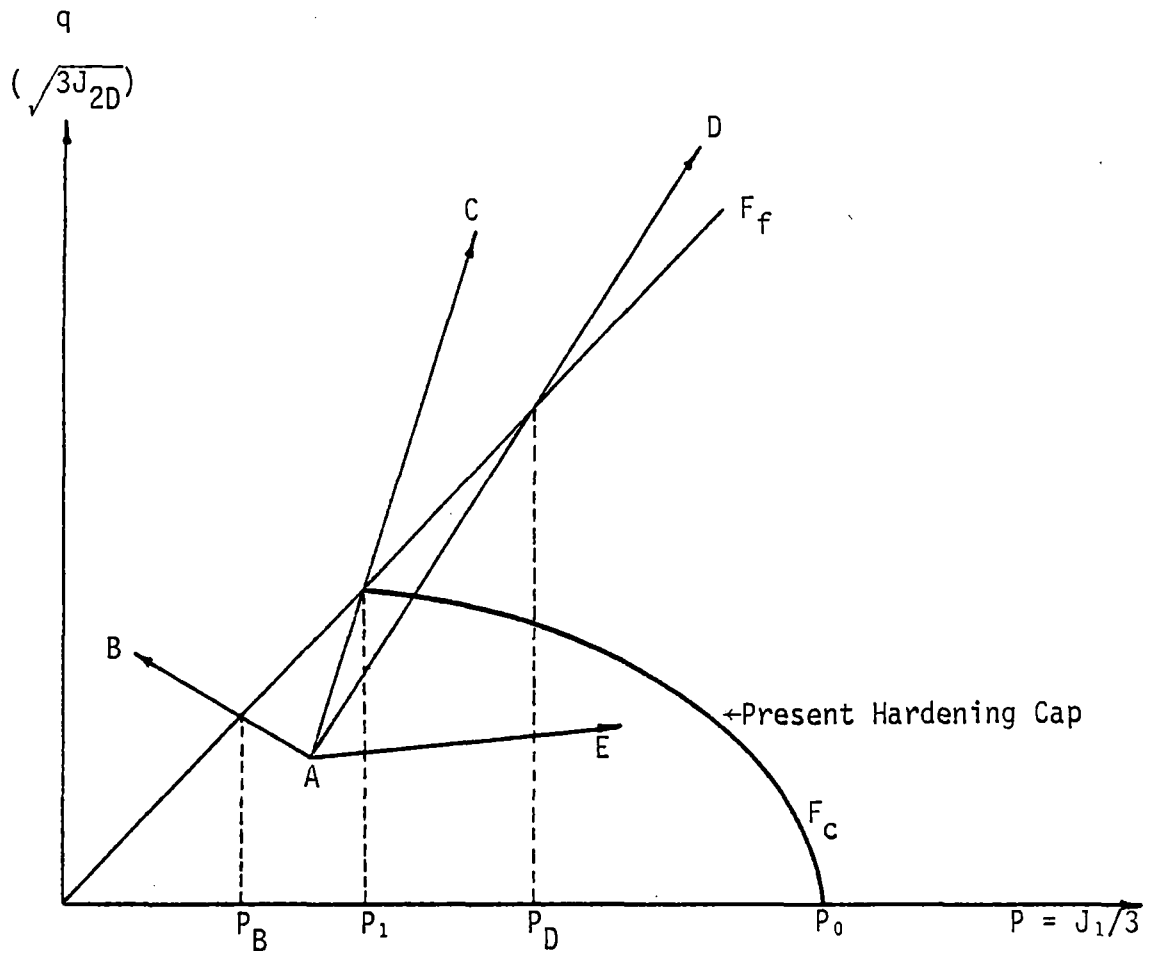


Figure 5.9 Possible Stress Increments in a Hardening Model

region. Therefore, the computed stresses are correct, and the next increment of load can be analysed. However, if the stress point goes to B, C, or D, then the material has entered an unstable area, and hence the computed stresses have to be corrected. The stress paths shown by AB, AC and AD intersect the critical state line at different locations. Stress path AB intersects the critical state line directly from the elastic region. Stress path AC intersects both the critical state line and the present yield cap simultaneously while the path AD intersects the critical state line after going through some hardening.

For the stress paths AC and AD, there is a 'corner' at the intersection with the critical state line; that is, two yield surfaces intersect. In a previous section on the Drucker-Prager model, it is mentioned that the material undergoes plastic deformation while moving on the yield surface. However, in this model, the deformation behavior at critical state is quite different than that of the Drucker-Prager model although the yield surfaces look alike. At the critical state, it is assumed that the material undergoes large shear deformations at constant hydrostatic stress, and hence the material cannot sustain any more loads. Therefore, it is necessary to find the fraction of incremental strain which will bring the stress point right to the critical state. After that the material does not carry any more stresses, and hence there can be an unbalanced load fraction. This is redistributed to the surrounding elements by using an iterative method.

The fraction of the strain increment can be easily found by using the procedure followed in the Drucker-Prager model. For this

purpose, in fact, the critical state line can be considered as a special case of the Drucker-Prager criterion. Critical state line can be expressed as

$$\sqrt{J_{2D}} = \frac{M}{3\sqrt{3}} J_1 \quad (5.15)$$

Comparison of Drucker-Prager model, Equation (4.17), with Equation (5.15) shows that the Drucker-Prager criterion reduces to critical state line if $\alpha = M/3\sqrt{3}$ and $k = 0$. Therefore, Equation (5.13) can be used to compute the fraction S , Equation (5.5) for this model too. Once the point of intersection is determined, it is required to check whether the material has followed a path similar to AB or AD. Any stress path between AB and AC has the same mathematical meaning for this purpose, and hence the procedure followed in this research is described with respect to path AB. If the value at P_B , Figure (5.9), is less than or equal to P_1 which corresponds to the intersection of the current yield cap with critical state line, then the stress path goes to critical state directly through the elastic region. However, if the value of P_B is greater than P_1 (such as P_D), then material undergoes yielding through a successive series of hardening caps before reaching the critical state. For such a situation, the computation of stress is different, and will be described in a subsequent section. The foregoing criterion is checked at each integration point of the finite element discretization. For subsequent analysis a low elastic modulus is assigned for integration points which are at the critical state. The foregoing procedure describes how the stresses are corrected when the stress point goes outside the critical state line. The corrected incremental stress corresponding to

a given incremental strain is the fraction that brings the stress point right on to the critical state.

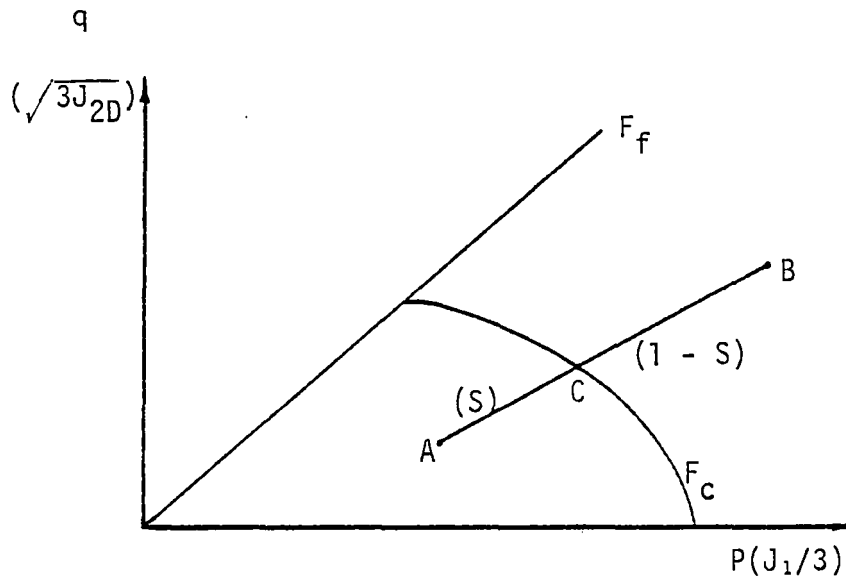
5.6.2. Stress Computation During Hardening: Marching Scheme

In this section, the possibility of violation of Equation (5.14a) is considered. The incremental stress computed by using elastic constitutive matrix can move the stress point outside the current yield surface as shown in Figure (5.10). Until the state of stress reaches the current yield surface, the material deforms elastically. Subsequently, it undergoes elasto-plastic deformation. The incremental stress can be calculated by using Equation (5.5).

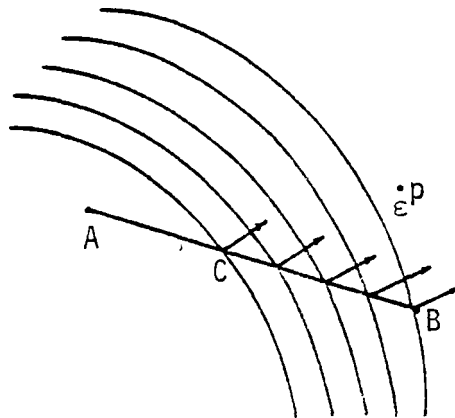
First step in this procedure is to check whether the incremental stress just computed by using elastic properties moves outside the current hardening surface. That is,

$$F_C(\{\sigma_0\} + \{\Delta\sigma\}) > 0 \quad (5.16)$$

If $F_C < 0$, then the material is still in the elastic region, and hence no correction is needed for incremental stresses. When $F_C = 0$, a correction is not needed. However, for subsequent analysis, elasto-plastic constitutive relations are assigned at those integration points. For the case given by Equation (5.16), there is a transition from elastic to elasto-plastic behavior. It is assumed that the material starts yielding at the stress corresponding to point C, Figure (5.10a), which is the intersection of stress vector AB and the current yield surface. The fraction 'S' of the strain increment required to initiate yielding can be computed from geometric considerations, and is given later in this section. The correct incremental stress which corresponds to a



(a) State of Stress Outside the Current Yield Cap



(b) Expanding Yield Caps for Subincrements of Strain

Figure 5.10 State of Stress Outside the Yield Surface

given incremental strain has to be computed separately for elastic and elasto-plastic behavior. That is

$$\{\Delta\sigma\} = \{\Delta\sigma\}^e + \{\Delta\sigma\}^{ep} \quad (5.17)$$

where the superscripts 'e' and 'ep' denote quantities that correspond to elastic and elasto-plastic behavior, respectively. Here,

$$\{\Delta\sigma\}^e = S[C^e] \{\Delta\varepsilon\} = [C^e] \{\Delta\varepsilon\}^e \quad (5.18a)$$

and

$$\{\Delta\sigma\}^{ep} = (1-S) [C^{ep}] \{\Delta\varepsilon\} = [C^{ep}] \{\Delta\varepsilon\}^{ep} \quad (5.18b)$$

Computation of $\{\Delta\sigma\}^e$ in Equation (5.18a) becomes straight forward once the fraction S is determined. However, in order to evaluate $\{\Delta\sigma\}^{ep}$, it is required to divide $\{\Delta\varepsilon\}^{ep}$ into subincrements. A marching scheme (forward integration) can then be used to compute $\{\Delta\sigma\}^{ep}$. It is important to note that for each subincrement, the yield surface expands as shown in Figure (5.10b). Hence, hardening parameters, P_0 , and void ratio e_0 , Equation (4.27) in Chapter 4 are updated together with the stress increment at each subincrement of strain.

During the forward marching scheme along subincrements, there is a possibility that a state of stress can reach critical state. This possibility is shown by path AB in Figure (5.9). Hence, the state of stress after each subincrement is checked for the violation of Equation (5.14b). If after a subincrement of strain the state of stress goes outside the critical state line, a correction is made to scale the stresses back to critical state line as described in the previous section.

The corrected stress increment $\{\Delta\sigma\}^{ep}$ is the accumulated quantity over the subincrements. If the critical state is reached at an inter-

mediate subincrement, the accumulated quantity at the critical state is taken as the correct stress increment $\{\Delta\sigma\}^{ep}$ in Equation (5.18b). Hence, the stress increment corresponding to the given strain increment can be computed using Equation (5.17).

The fraction 'S' in Equation (5.18) can be computed by using geometric considerations. The equation of the yield surface is derived in Chapter 4 as

$$F_c = q^2 - M^2 p p_0 + M^2 p^2 \quad (5.19)$$

In terms of the invariants defined in Chapter 2, this can be written as

$$F_c = 27J_{2D} - M^2 J_1 J_{01} + M^2 J_1^2 \quad (5.20)$$

where J_{01} is the first invariant of stress tensor corresponding to P_0 in Equation (5.19), which is the hardening parameter. The form of the yield surface expressed in Equation (5.20) is quite useful in three-dimensional analysis.

Evaluation of S

The fraction S of the stress increment required to initiate yielding can be computed from geometric considerations. This fraction of the stress increment when added to the current stresses, brings the state of stress on to the yield surface, and hence,

$$F_c(\{\dot{\sigma}_0\} + S \{\dot{\Delta}\sigma\}) = 0 \quad (5.21a)$$

This leads to a quadratic equation in S as given below. Here the overdot denotes incremental quantities.

$$AS^2 + BS + C = 0 \quad (5.21b)$$

where

$$A = 27 \dot{J}_{2D} + M^2 J_1^2$$

$$B = 54 a - M^2 J_{01} \dot{J}_1 + 2M^2 J_1 \dot{J}_1$$

$$C = 27 J_{2D} - M^2 J_1 J_{01} + M^2 J_1^2$$

$$a = \frac{1}{6} [(\sigma_{11} - \sigma_{22})(\dot{\sigma}_{11} - \dot{\sigma}_{22}) + (\sigma_{22} - \sigma_{33})(\dot{\sigma}_{22} - \dot{\sigma}_{33}) \\ + (\sigma_{11} - \sigma_{33})(\dot{\sigma}_{11} - \dot{\sigma}_{33})] + \sigma_{12} \dot{\sigma}_{12} + \sigma_{23} \dot{\sigma}_{23} + \sigma_{13} \dot{\sigma}_{13}$$

and

$$\dot{J}_{2D} = \frac{1}{6} [(\dot{\sigma}_{11} - \dot{\sigma}_{22})^2 + (\dot{\sigma}_{22} - \dot{\sigma}_{33})^2 + (\dot{\sigma}_{11} - \dot{\sigma}_{33})^2] + \dot{\sigma}_{12}^2 \\ + \dot{\sigma}_{23}^2 + \dot{\sigma}_{13}^2$$

5.6.3. Stress Computation During Hardening: Iterative Scheme

In this section, an alternative procedure is described for stress computation during hardening behavior. The algorithm developed herein for the critical state model is based on the work of Sandler and Rubin [72] for the cap model. The input quantities required in this procedure are the current stresses, current hardening parameter, P_0 , and the incremental strains. The output quantities are the correct stresses and the new hardening parameter.

All the possible stress paths described in the previous section are considered in this iterative scheme too. The first step in this procedure is to compute trial stresses based on elastic properties. Based on the trial stresses, quantities such as J_1^E and J_{2D}^E can be

computed; here the superscript 'E' denotes elastic trial quantities. Trial stresses can go outside the critical state line, or yield surface or it can go into the tensile zone. Here, the tensile strength can be any value although in the current research it is taken as zero. If J_1^E goes beyond the tensile strength, the stresses are made equal to the tensile strength, and the tensile constitutive properties are assigned at that integration point for subsequent analysis. If the state of stress goes to the critical state directly from the elastic region, then the procedure described in the previous section is used to correct the stresses. In the case of expanding yield surface, the following iterative procedure is used.

Underlying mathematical basis is given below prior to describing the iterative scheme. The equation of the yield surface, Equation (4.30), can be arranged as

$$F_c = \sqrt{J_{2D}} - F_c(J_1, J_{10}) = 0 \quad (5.22)$$

where J_{10} is the first invariant of stress corresponding to P_0 in Equation (4.30). Using the flow rule described in Chapter 2, the incremental plastic strains can be written as

$$d\epsilon_{ij}^P = \lambda \left(\frac{S_{ij}}{2\sqrt{J_{2D}}} - g \delta_{ij} \right) \quad (5.23)$$

where

$$g = \frac{\partial F_c}{\partial J_1}$$

Using Equation (5.23), the proportionality constant λ can be expressed as

$$\lambda = - \frac{d\epsilon_V^P}{3g} \quad (5.24)$$

Hence, the deviatoric portion of the incremental plastic strain tensor can be expressed as

$$de_{ij}^P = d\epsilon_{ij}^P - \frac{1}{3} d\epsilon_{kk}^P \delta_{ij} \quad (5.25a)$$

Substitution of Equations (5.23) and (5.24) into Equation (5.25a) lead to

$$de_{ij}^P = - \frac{d\epsilon_v^P S_{ij}}{6g\sqrt{J_{2D}}} \quad (5.25b)$$

If the quantities de_{ij}^P and $d\epsilon_{kk}^P$ are known, then the correct states of stresses can be expressed as

$$S_{ij} = S_{ij}^E - 2Gde_{ij}^P \quad (5.26a)$$

$$J_1 = J_1^E - 3Kd\epsilon_v^P \quad (5.26b)$$

Substituting Equation (5.25b) into Equation (5.26a), the following relationship can be obtained.

$$S_{ij} \left(1 - \frac{Gd\epsilon_v^P}{3g\sqrt{J_{2D}}} \right) = S_{ij}^E \quad (5.27)$$

By squaring Equation (5.27), it is possible to write

$$\sqrt{J_{2D}} \left(1 - \frac{Gd\epsilon_v^P}{3g\sqrt{J_{2D}}} \right) = \sqrt{J_{2D}}^E \quad (5.28)$$

Using Equations (5.27) and (5.28), the deviatoric stress tensor can be expressed as

$$S_{ij} = \frac{\sqrt{J_{2D}}}{\sqrt{J_{2D}}^E} S_{ij}^E \quad (5.29)$$

Now it is clear that if the value of $d\epsilon_V^P$ was known, the correct values of J_1 and $\sqrt{J_{2D}}$ can be computed by using Equations (5.26b) and (5.29). There is an important requirement that the values of $d\epsilon_V^P$, J_1 and $\sqrt{J_{2D}}$ have to satisfy. The value of $d\epsilon_V^P$ has to be consistent with the new hardening parameter which will place J_1 and $\sqrt{J_{2D}}$ on a new yield surface. In the current research, a value of J_{01} is assumed, tested and refined to satisfy the above requirement by using an iterative procedure. New value of J_{01} is denoted by \bar{J}_{01} with an overbar.

Yield surface based on the critical state concept can also be expressed as

$$\sqrt{J_{2D}} - \frac{1}{\sqrt{27}} (M^2 J_1 \bar{J}_{01} - M^2 J_1^2)^{1/2} = 0.0 \quad (5.30)$$

By comparing Equations (5.22) and (5.30),

$$F_C = \frac{1}{\sqrt{27}} (M^2 J_1 \bar{J}_{01} - M^2 J_1^2)^{1/2} \quad (5.31)$$

Hence, the gradient of F_C with respect to J_1 can be expressed as

$$g = \frac{M^2 (\bar{J}_{01} - 2J_1)}{54 F_C} \quad (5.32)$$

The plastic volumetric strain corresponding to the new hardening parameter \bar{J}_{01} can be expressed as

$$d\epsilon_V^P = \frac{dJ_{01}}{J_{01}} (\lambda_C - \kappa) \quad (5.33)$$

The iterative scheme used herein is given below.

Step 1: Assume dJ_{01} and compute \bar{J}_{01} as $\bar{J}_{01} = J_{01} + dJ_{01}$

Step 2: Compute $d\epsilon_V^P$ from Equation (5.33). Hence compute J_1 using Equation (5.26b)

Step 3: Compute g from Equation (5.32). Also, compute $\sqrt{J_{2D}}$ by using Equation (5.30).

Step 4: This value of $\sqrt{J_{2D}}$, if correct, will be equal to that is given in Equation (5.28). This is done by defining a factor as ψ as follows:

$$\psi = \frac{\sqrt{J_{2D}}^E - a}{\sqrt{J_{2D}}^E + a} \quad (5.34)$$

where

$$a = \sqrt{J_{2D}} - G \frac{d\varepsilon^P}{3g}$$

If the value of Q is less than a specified smaller value, the value of $\sqrt{J_{2D}}$ and J_1 are assumed to be correct.

Otherwise, a new value of dJ_{01} is assumed and procedure is repeated.

A criterion was used in selecting a value for dJ_{01} . Initial value was selected as J_{01}/N where N is the maximum number of iterations. For each iteration the value of dJ_{01} is increased by J_{01}/N until convergence is reached. For certain assumed values of dJ_{01} , it may be possible that the quantity $(M^2 J_1 \bar{J}_{01} - M^2 J_1^2)$ is negative. This will lead to an imaginary value for $\sqrt{J_{2D}}$ in Equation (5.30). In this event, next iteration is performed with a higher value for dJ_{01} .

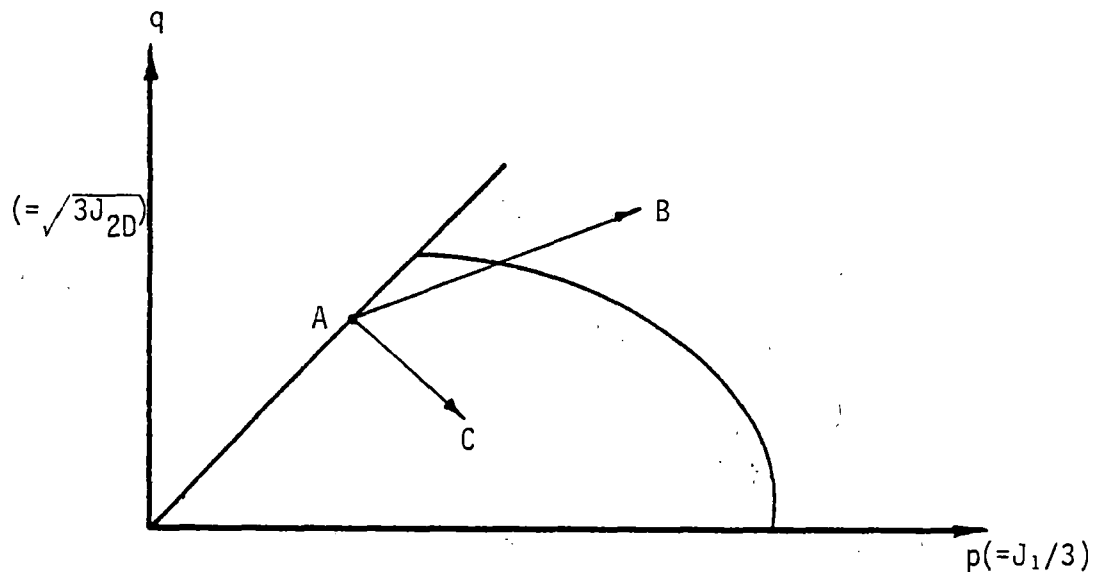
Although, the iterative scheme is an alternative to the marching scheme described in the previous section, its relative merit will depend on how fast the convergence and its performance in the solution of boundary value problems. A comparison of these two schemes is given in Chapter 8, Verifications. In the current research, however, the

marching scheme is used since further research is needed to verify the merits of iterative technique proposed in the forgoing section as an alternative.

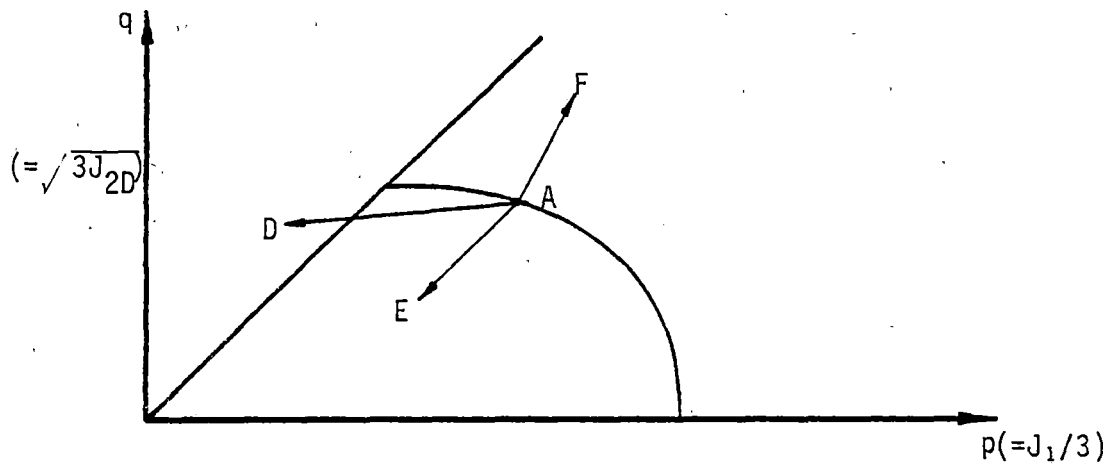
5.6.4. Stress Computation During Unloading

In the foregoing section, computational procedures for correcting stresses during yielding were described. Subsequent to yielding or reaching a critical state, it is possible that the state of stress can go into the elastic region. This type of behavior is called "unloading" in this section. Some of the possible paths for unloading are shown in Figure (5.11). Unloading can be detected when the stresses have been computed. If unloading is detected, however, the computed stress increments, called as trial stress increments, are assumed to be correct, and the unloading constitutive parameters are assigned at those integration points for subsequent analysis. In view of the above assumption, there may be a slight error in the stresses since unloading properties were not used within this increment. However, in subsequent equilibrium iterations, this error gets corrected.

Instead of the above procedure, it is possible to correct the stresses immediately after detecting unloading conditions. Unloading stiffness is usually much greater than the elasto-plastic stiffness, and hence incremental strains computed by this procedure can be smaller than true values. The best scheme will be to re-solve the particular step which can be quite expensive. Since the transition to unloading occurs only at few integration points, the procedure used herein is adequate.



(a) Possible Stress Paths After Reaching Failure



(b) Possible Stress Paths After Reaching a Yield Surface

Figure 5.11 Possible Stress Paths From an Existing Plastic State

5.7. Cap Model: Implementation in Two- and Three-Dimensional Analysis

Details of the mathematical aspects of the cap model are given in Chapter 4, and only the computational algorithms used in implementing this model are given here. This model has been used often in ground motion predictions due to ground shock effects [2]. Computationally, cap model is similar to the critical state model except for the differences in functional forms for the yield caps and failure envelopes. Therefore, computational procedures described for critical state model are applicable here too, and will not be repeated. However, there are few differences in certain aspects of this model, and only those differences are described here.

From the point of view of computational algorithms, there is one conceptual difference between these two models regarding the motion of cap at failure or critical state. In the critical state model, the position of the cap is a function of the maximum past pressure, P_0 , Figure (4.7a) and Equation (4.30), while in the cap model the position of the cap is determined from the plastic volumetric strain, Figure (4.11) and Equation (4.34). After reaching the critical state line, there will not be any volumetric plastic deformations and hence the hardening parameters will not change at the critical state. However, in the cap model the incremental plastic strain vector is normal to the failure envelop, and hence, there will be plastic volumetric deformations. As in the Drucker-Prager model, Figure (4.4), these plastic strains tend to reduce the compressive plastic volumetric strains.

Since the movement of the cap is controlled by the increase or decrease of the plastic volumetric strains, the cap can expand or contract in this model [24,71]. This situation is shown in Figure (5.12) where the state of stress moves from A to B. Cap can expand when the state of stress moves from A to C as shown in this figure. The incremental plastic strain is normal to the failure envelop at point B, and it has a negative component in the J_1 -direction. Hence, the plastic volumetric strains get reduced, causing a contraction of the cap. This situation will continue until point B becomes a corner between failure surface and yield cap. This aspect is taken into account in the implementation of the cap model. A detailed algorithm for cap model is given in reference [72] for two-dimensional analysis, and used here for plane-strain and axi-symmetric idealizations. This procedure is modified and implemented in three-dimensional computer code developed in this research.

5.8. Convergence Criterion

Convergence criterion used for equilibrium can be based either on a norm of the incremental displacements or a norm of the residual forces. In the current research, norm of the displacement changes is used as the convergence criterion, and is defined as,

$$||\{\Delta q_i\}||_N = (\{\Delta q_i\}^T \{\Delta q_i\})^{1/2} \quad (5.35a)$$

Here, the subscript 'N' denotes the iteration number. In the current research, convergence is assumed at 'N'th iteration if $||\Delta q_i||_N$ is less than 10.0 percent of $||\Delta q_i||$ corresponding to zeroth iteration. That is,

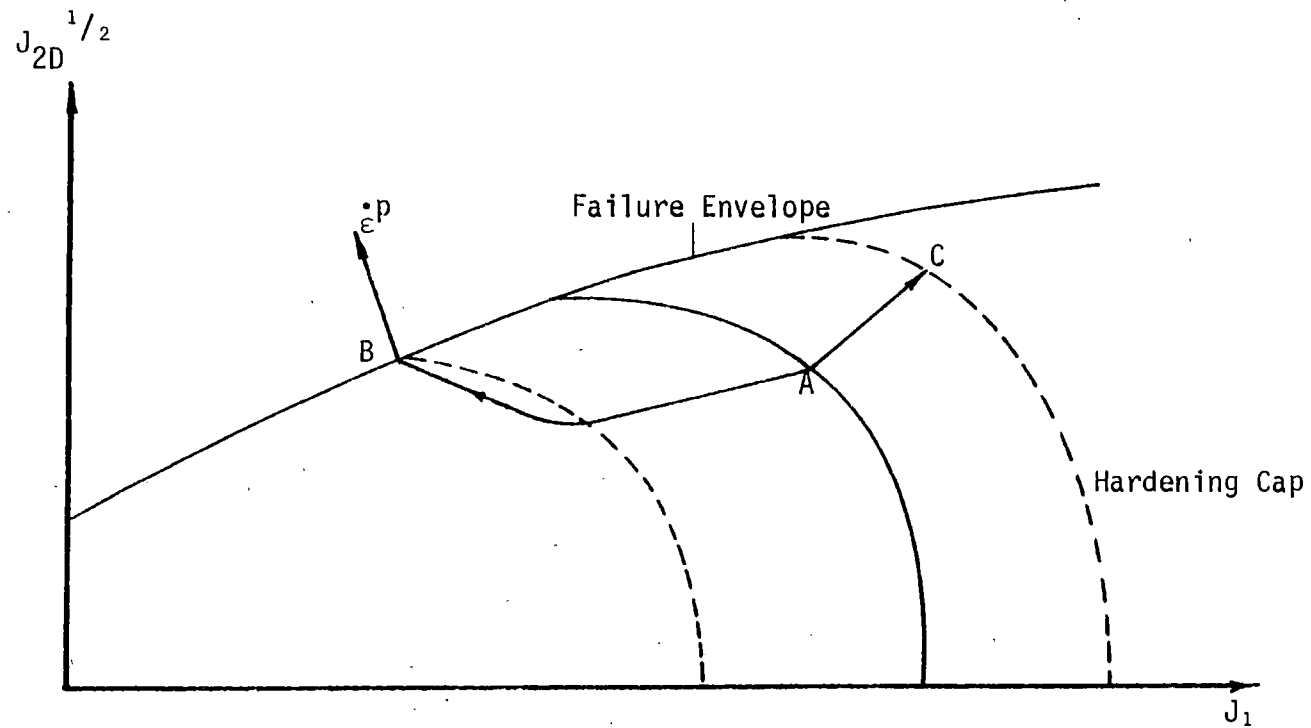


Figure 5.12 Computational Procedure for Contraction of the Cap Shaped Yield Surface

$$\frac{\|\Delta q_j\|^N}{\|\Delta q_j\|_0} \leq 0.10 \quad (5.35b)$$

5.9 Initial Conditions For Nonlinear Analysis

Since the constitutive relations are stress dependent, initial state of stress plays an important role in the nonlinear analysis. In the two- and three-dimensional procedures developed herein, initial stresses can be either specified by the user or can be computed by using the program(s). Corresponding hardening parameters are computed on the basis of initial stresses, and used in the subsequent incremental analysis.

5.10 Solution Techniques

Finite element analysis of a problem at each load increment/iteration finally reduces to solving a set of simultaneous equations. In the current research, the global stiffness matrix is symmetric, and hence only the upper or lower half of the coefficients need to be stored. There are several methods for solving a linear set of equations: Gauss, Jordon, and Cholesky elimination procedures. A detailed description of these methods is available in reference [32]. In the current research, the linear equations are solved by using the Gaussian elimination technique. In the current research, three different procedures, namely, Band solution technique, Frontal solution technique, and Skyline solution technique are employed.

5.10.1. Equation Solver in One-Dimensional Finite Element Code

A band-solution (BANSOL) technique is used in the one-dimensional

finite element procedure developed herein. Band solution technique is commonly used in many finite element computer programs. Details of this can be found in references [15,89].

5.10.2. Equation Solver in Two-Dimensional Finite Element Code

In the two-dimensional idealization, Frontal solution technique developed by Irons [44] is used as the equation solver. Frontal solution technique is one of the techniques for solving equations specially in the context of finite element method. This solution procedure is similar to Gaussian elimination, but it takes advantage of some mathematical properties of the global stiffness coefficients. The underlying idea of this technique is given below.

In general, a set of simultaneous equations can be written as,

$$[k_{ij}] \{q_j\} = \{Q_i\} \quad (5.36)$$

where $[k]$ represents coefficient matrix, $\{q\}$ is the vector of unknown (displacements) $\{Q\}$ is the load vector. After elimination of variable number 'p', the modified coefficient can be written as

$$k_{ij}^* = k_{ij} - \left(\frac{k_{ip} k_{pi}}{k_{pp}} \right) \quad (5.37a)$$

and

$$Q_i^* = Q_i - \frac{k_{ip} Q_p}{k_{pp}} \quad (5.37b)$$

Here k_{pp} does not represent any tensor summation; it represents the coefficient of 'p'th degree of freedom. If certain changes are made to coefficients k_{ij} without changing corresponding row and column of variable 'p', it can be observed that exactly same changes are reflected

in modified coefficients k_{ij}^* too. Therefore, when there are no changes in the column and row of 'p'th variable, the modified coefficients k_{ij}^* will not be affected even if the changes are made after the reduction (or elimination) of that variable. In fact, this is general enough that any equation number 'S', can be eliminated without causing any difference as long as coefficients of the row 'S' and column 'S' do not change subsequently. This property of a set of simultaneous equations has been used in the development of Frontal solution technique.

In the context of finite element method, there is a specific meaning to any coefficient of the stiffness matrix with respect to the corresponding degree-of-freedom. For instance, k_{pp} of the stiffness matrix $[K]$ means the stiffness coefficient of the 'p'th degree-of-freedom. During the assembly process of element stiffness to form the global stiffness, contributions to a certain degree-of-freedom from each element get accumulated. However, if there are no more additions to a certain degree-of-freedom, then there will not be any changes in the row or column of that degree-of-freedom in the global stiffness matrix. Therefore, this variable can be eliminated even though assembly may not be complete. In the Frontal solution technique, any degree-of-freedom is eliminated from simultaneous equations when it appears for the last time in the assembly process. The equation corresponding to this degree-of-freedom, can then be stored in back-up storage (tape, disk, etc.) thereby creating space in the incore storage. A subroutine available in reference [43] is adopted in the current research.

5.10.3. Equation Solver Used in Three-Dimensional Analysis

Unlike one- and two-dimensional analysis, the matrices involved in three-dimensional analysis are much larger in size. Furthermore, numbering of nodal points to obtain a minimum bandwidth in a complicated three-dimensional problem is a difficult task. In the solution of large system of equations, use of backup storage is computationally inefficient, and hence incore solutions are preferable. In order to make use of available incore storage of the computing machine efficiently, a compacted storage scheme called "Skyline technique" has been developed by Bathe et al., [3,5] for storing the global stiffness matrix. In this technique, only the coefficients below the "skyline" are stored as shown in Figure (5.13). Zero coefficients within the skyline may become nonzero elements during Gauss elimination process. Detailed description of this technique is available in references [3,4,5]. In the three-dimensional program developed in the current research, solution routine based on the skyline technique is adopted.

5.11. Efficient Implementation

In order to make the programs more efficient, most vectors and matrices are stored as one-dimensional arrays using the technique of dynamic dimensioning. This is done for the one-, two- and three-dimensional finite element codes developed herein. This not only makes the computations more efficient, but also makes it possible to change the program capacity with a change in only one DIMENSION statement. Required pointers to identify locations in the one dimensional array are set-up in a Subroutine, and stored in a COMMON Block.

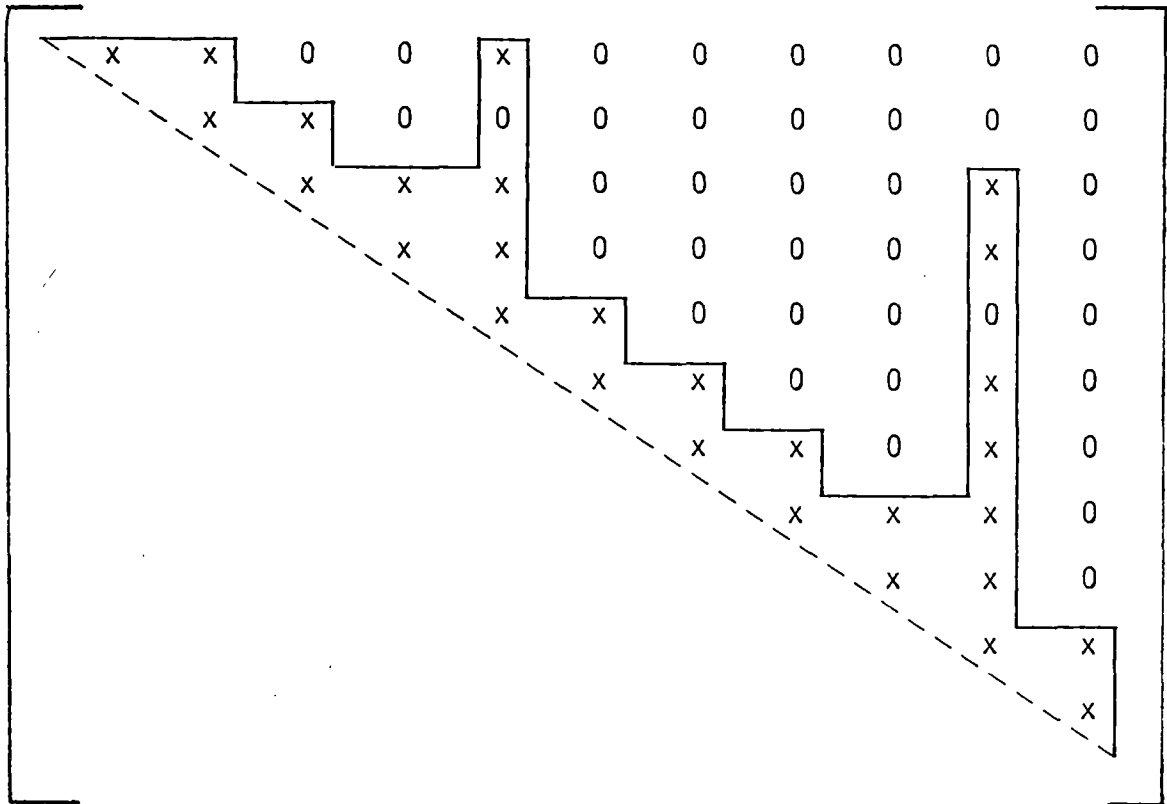


Figure 5.13 Storage Scheme Used in Skyline Solution Procedure

Chapter 6

INTERFACE MODELLING IN SOIL-STRUCTURE INTERACTION

6.1. Introduction

In almost all solid mechanics problems there exist situations of interaction between two or more deformable bodies that come in contact with each other. In geomechanics, there are many problems in which interaction between dissimilar media exist, e.g., soil-structure interaction. In fact, the interaction between the bodies govern the mechanism of load transfer to the supporting foundation. Therefore, the characteristics of the contacts play an important role on the behavior of the system. However, contact problems in solid mechanics are difficult to handle in view of conceptual and mathematical difficulties. Furthermore, these problems are nonlinear since the contact surfaces between the bodies and the boundary conditions at the contact are not known in advance.

Some of the classical contact problems such as Hertzian, and Sigrani types [48] that have been solved are restricted for bodies with elastic properties and simple geometry. An important class of contact problems in solid mechanics have been analyzed by Kikuchi and Oden [48] by using variational inequalities; this reference presents a very good review of the history of contact problems. In most of the real problems encountered in geomechanics, material behavior is highly nonlinear, and the geometry is complicated. Therefore, application of mathematical theories developed in classical contact problems can become extremely difficult. However, the problem of soil-structure interaction can be

handled in a somewhat different way by using numerical procedures such as the finite element method.

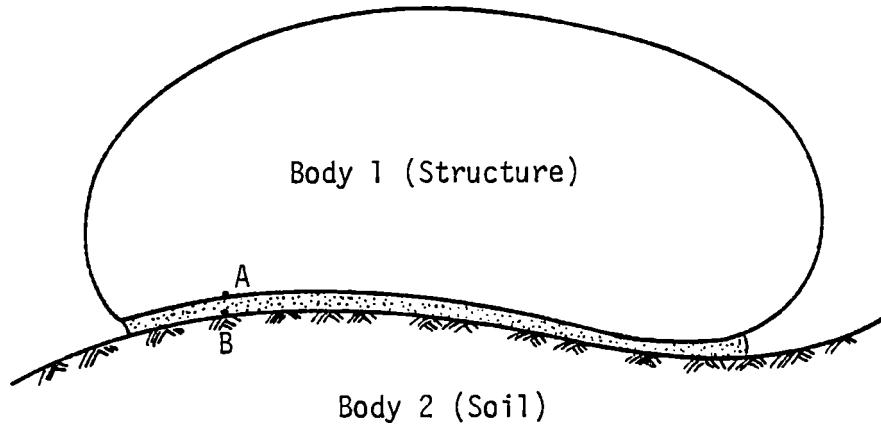
In the application of the finite element method to problems in solid mechanics, it is assumed that the body under consideration is continuous. This can happen only when there is perfect bonding between dissimilar materials during the loading history.

There are many problems in structural and geomechanics where perfect bonding between dissimilar media is not maintained throughout the loading. In these cases, the interface behavior between the dissimilar media plays an important role. Some examples of this type include the interaction between the reinforcement (steel) and the surrounding concrete, retaining walls, and piles in geologic media.

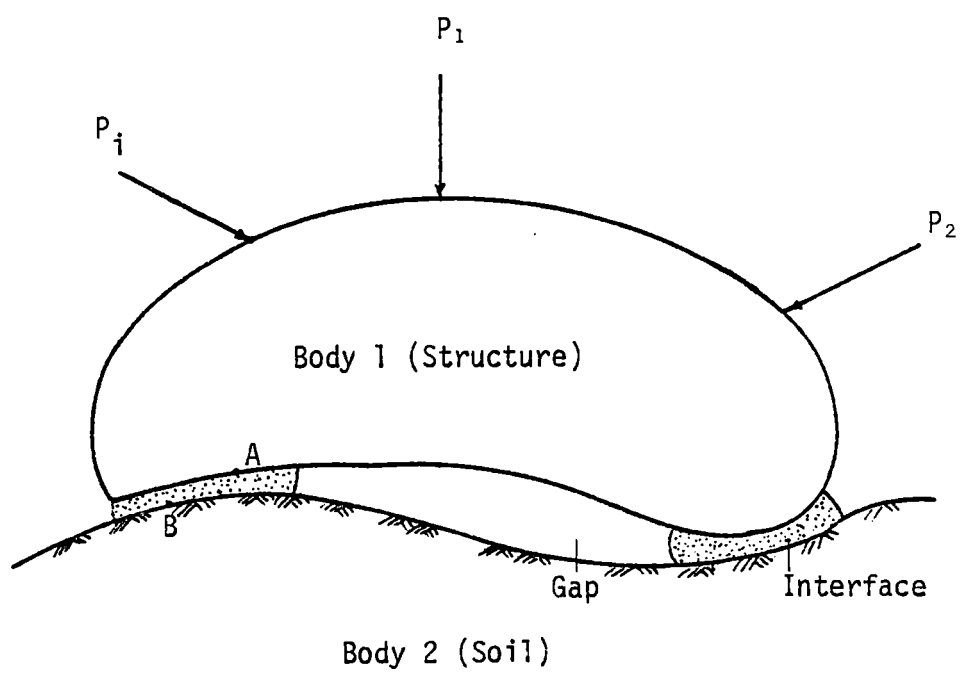
Statement of Problem

A schematic model describing soil-structure interaction is shown in Figure (6.1). During the loading history, a point in the structure can deform differently than the adjacent point in soil causing relative slip. Furthermore, certain portions of the interface can open up causing gaps, or existing gaps can close up during deformations. This interaction behavior is the fundamental mechanism how loads are transferred from structure to soil and vice versa. Hence, these modes of deformation play an important role in development of a model for soil-structure interaction.

Two typical problems, a laterally loaded pile and a beam on a deformable foundation are shown in Figure (6.2) in order to show the interaction behavior. Figure (6.2a) shows the possibility of opening

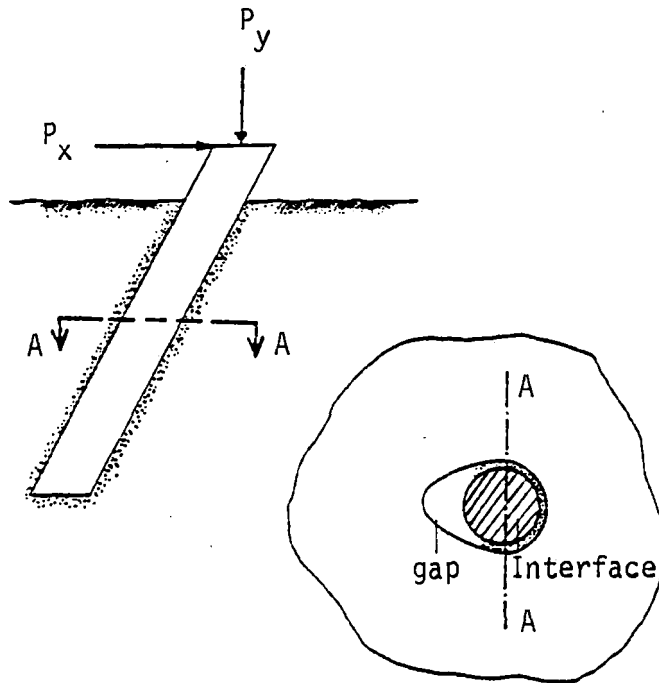


(a) Soil-Structure System Before Deformations

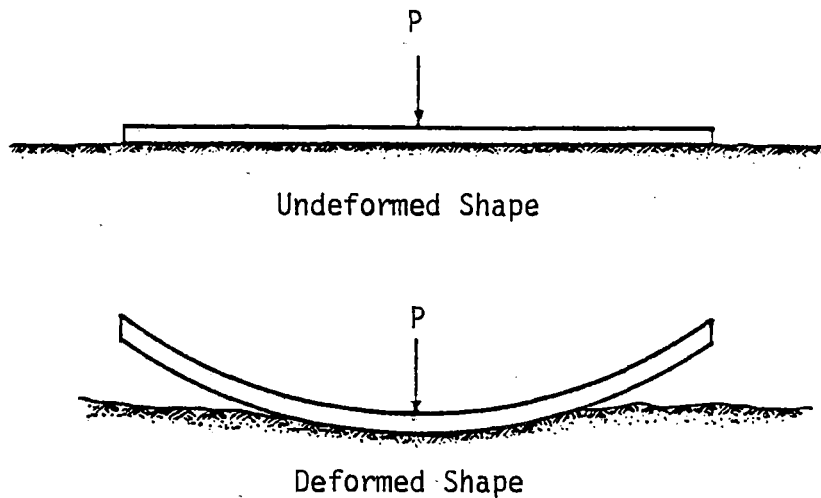


(b) Soil-Structure System After Deformations

Figure 6.1 Schematic Model For Soil-Structure Interaction



(a) Interaction in a Laterally Loaded Pile



(b) Beam-on-Deformable Foundation

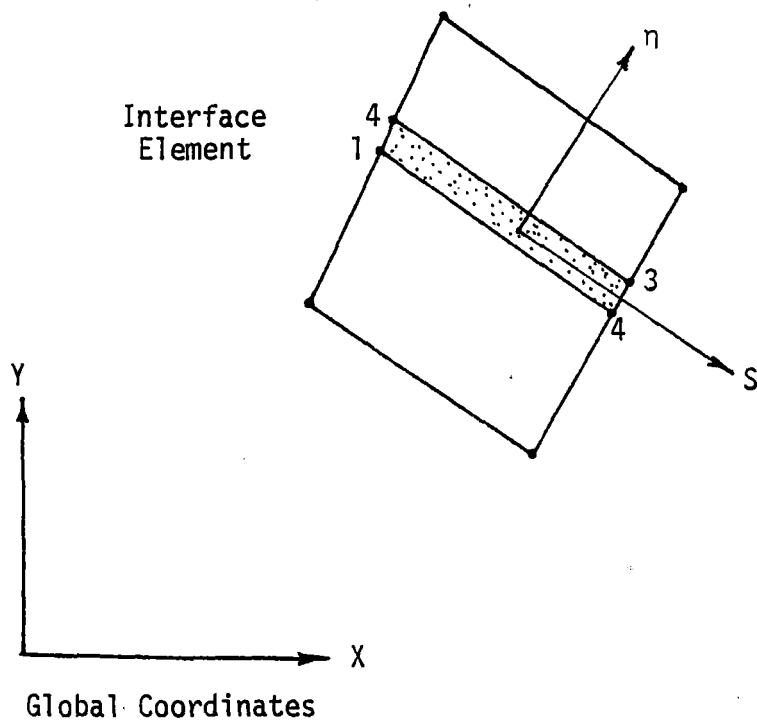
Figure 6.2 Typical Soil-Structure Interaction Problems
in Geomechanics

up a gap during deformations. This is a truly three-dimensional problem. The deformation behavior of the structure-foundation system depends on the characteristics of the interfaces. Figure (6.2b) shows a one-dimensional problem, which is a beam on a deformable foundation. During deformations the beam can move above the surface level causing gaps; this can significantly change how the beam interacts with the foundation. There can be several interaction problems which can be idealized as two-dimensional, such as strip footings, dams, retaining walls, track support structures, underground tunnels, and so on. Hence, a generalized procedure for interaction analysis must consider applications in all three idealizations. This study addresses the procedures for interaction analysis in one-, two- and three-dimensional problems, Chapters 3, 4, and 5.

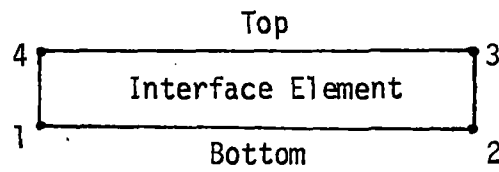
6.2. Review of Interface Models

In the finite element procedures, interaction behavior is often modelled by using a special element which can account for relative movements between dissimilar media. Interface elements used in the past can be classified in two categories. These are, compatible interface elements and equilibrium interface elements.

The idea of a compatible interface element was first introduced by Goodman et al. [38] in modelling the rock joint behavior; this can be treated as a generalization of the model used by Ngo et al. [61] for joints and cracks in concrete. In the two-dimensional analysis of rock masses, they used a line interface or joint element which permitted relative displacements between adjacent elements, Figure (6.3). Since



(a) Interface Element



(b) Top and Bottom Surfaces of Interface

Figure 6.3 Interface Element with Zero Thickness

the element is assumed to have zero thickness, the node pairs (1, 4) and (2, 3) have the same initial coordinates. The energy stored in this element is assumed to be due to the relative displacements between top and bottom surfaces. Relative displacements are defined as

$$u_i^r = u_i^T - u_i^B \quad (6.1)$$

Here, u_i^r is the relative displacement, and u_i^T and u_i^B are the displacements of two points (which had same coordinates originally) on the top and the bottom surfaces of the interface element, respectively. The constitutive behavior of the element is characterized by the material property matrix which expresses the joint stiffness per unit length in the normal and tangential directions. This can be written as

$$k_j = \begin{bmatrix} k_s & 0 \\ 0 & k_n \end{bmatrix} \quad (6.2)$$

where k_s is the shearing stiffness, and k_n is the normal stiffness of the interface element. These parameters have to be determined experimentally. The potential energy of this element was expressed as [38]

$$\Pi_p = \frac{1}{2} \int_{-L/2}^{L/2} \{q_r\}^T [k] \{q_r\} dx \quad (6.3)$$

where $\{q_r\}$ is the relative displacement vector, and L is the length of the element. Element stiffness based on the above potential energy functional has been derived in reference [38]. Some applications of this interface element are reported in references [10,37,50]. In three-dimensional analysis, the interface element based on the above

concept has a two-dimensional configuration since the thickness is assumed to be zero. Extension of this element to three-dimensional analysis has been reported by Desai and Appel [16], Mahtab and Goodman [52], and Phan [64].

There are some limitations of Goodman's interface element in modelling soil-structure interaction. With this interface, a block of solid elements can penetrate into the adjacent elements violating the kinematic considerations. Furthermore, opening and closing of gaps cannot be modelled. Zienkiewicz et al. [92] proposed an interface element assuming uniform strain in the thickness direction. Here, the interface stiffness was derived based on the nodal displacement vector. This element may give rise to ill-conditioning when gaps occur at the interface. Furthermore, it can produce erratic results due to the ill-conditioning which can generate very large off-diagonal coefficients or very small diagonal terms in the stiffness matrix for certain cases.

Ghaboussi et al. [36] have proposed and used a somewhat different interface element which uses relative displacements as the degree-of-freedom; however, conceptually it is similar to the Goodman approach. Derivation of stiffness for plane strain and axisymmetric conditions are given in reference [36]. Wilson [85] has illustrated the numerical problems which may develop when absolute displacements are used as independent degree-of-freedom. He has suggested a slightly different interface element as given in reference [36]. Review of various applications of interface elements is presented in references [10,37].

Modes of Deformation

There are three basic modes of deformations at an interface: Non-slip, slip, separation and closing. All the interface elements described above fall into one category, that is compatible type, and separation mode cannot be handled by using this type of element. An interface element based on equilibrium considerations has been proposed and used by Katona et al. [46]. This model seems to be capable of handling separation modes at the interfaces. However, its implementation in a finite element procedure can be more difficult. It also requires several iterations for checking the proper mode of interaction, and to obtain equilibrium conditions, and question of appropriate interface constitutive parameters still remains.

Hermann [40] has proposed an algorithm for implementation of an interface element for two-dimensional configurations. It can consider no-slip, slip and separation modes. In this model the idea of "bond spring" has been used to model the interaction behavior. Here, relative slippage or separation does not occur until attainable bond stress has been fully mobilized. However, there can be relative displacements prior to bond failure depending upon the bond spring stiffness. For very large spring stiffness values, the relative movement can be very small. When the maximum bond stress, τ_{max} , is reached, slippage is resisted by the stress applied as loads at the interface surface. Implementation of this model seems to be difficult in view of the complexity, in establishing the modes of deformation.

Recently Pande et al. [63] used an 8-node quadratic interface element for two-dimensional analysis based on the isoparametric element concept. They have studied the problems of numerical ill-conditioning due to use of very thin elements, that is, large aspect ratios. Furthermore, they have investigated relative merits of conventional isoparametric elements and isoparametric parabolic elements based on commonly used approach of relative displacements. They have concluded that the differences in the results obtained from these two elements were insignificant up to a large aspect ratio of the element, i.e., 50,000.

6.3. Interface Element Used in Current Research

The concept of using a "thin" regular element to simulate an interface has been a topic of discussion [13,49] in the geomechanics program at Virginia Tech. Since all existing interface elements allow for "large" relative displacements while retaining continuity, it may be appropriate to consider and investigate a thin regular element to simulate the junction or interface. The interface element used herein is based on the previous concept, and is in some respects similar to the proposal of Pande and Sharma [63]. In their work, interface element was taken as a very thin isoparametric element, and its constitutive matrix was similar to a solid element with different properties. For higher-order elements, mid-side nodes along the thickness have been retained in order to obtain a linear strain variation. In the current research, the interface constitutive relationship is modified to account for slip behavior by introducing an independent shear modulus. This idea is also extended for a three-dimensional interface element.

The thickness of the interface element is arbitrarily taken as a very small value. As the interface element is based on the isoparametric element concept, its nodal connectivity can be similar to any other solid element. However, the thickness and the constitutive properties are different from solid elements. Interface elements available in two- and three-dimensional computer codes developed herein are shown in Figure (6.4). The suggested constitutive relationship for the two-dimensional interface element is given below.

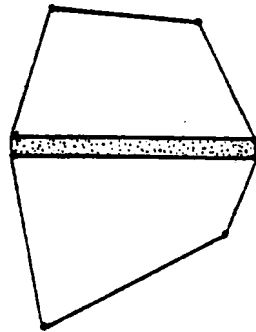
$$[C^{int}] = \begin{bmatrix} \frac{E(1-\nu)}{(1+\nu)(1-2\nu)} & \frac{E\nu}{(1+\nu)(1-2\nu)} & 0 \\ \text{sym} & \frac{E(1-\nu)}{(1+\nu)(1-2\nu)} & 0 \\ & & G_{int} \end{bmatrix} \quad (6.4)$$

where G_{int} is the shear modulus for the interface element. This value may not be consistent with the relationships with E and ν given in Chapter 2. Value of G_{int} has to be determined from laboratory experiments.

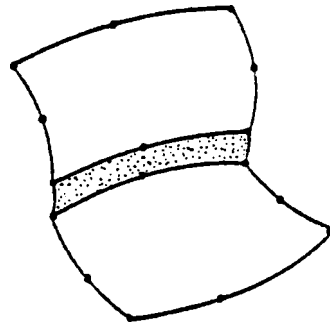
Procedure for evaluating G_{int} is shown in Figure (6.5). The shear behavior between two dissimilar materials can be simulated in the laboratory by a direct shear tests. A linear relationship between the shear force, P_s , and lateral displacement, u , is assumed as shown in Figure (6.5a). The change in the right angle, Figure (6.5b), during shear can be expressed as

$$\theta \approx \Delta u/t \quad (6.5)$$

where t is the assumed thickness for the interface element. Hence

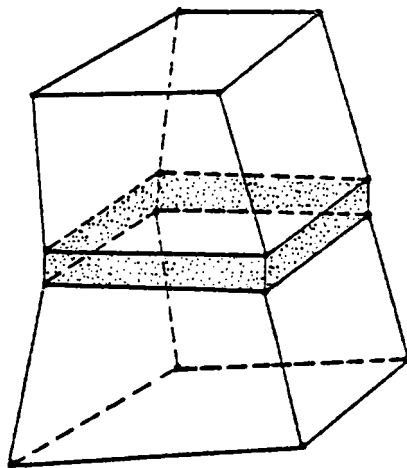


4-Node Interface Element

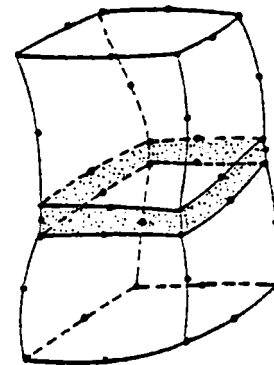


8-Node Interface Element

(a) Interface Elements in Two-Dimensional Analysis



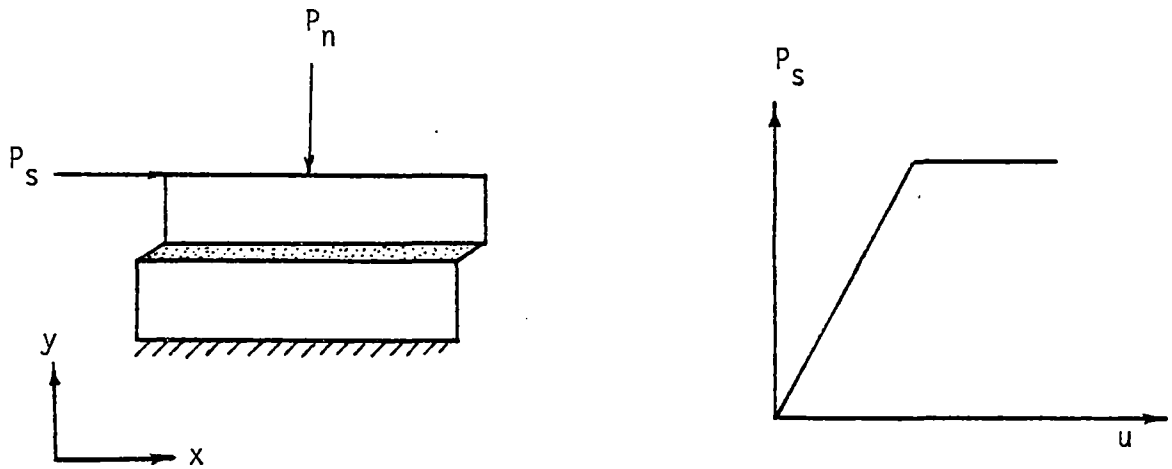
8-Node Interface Element



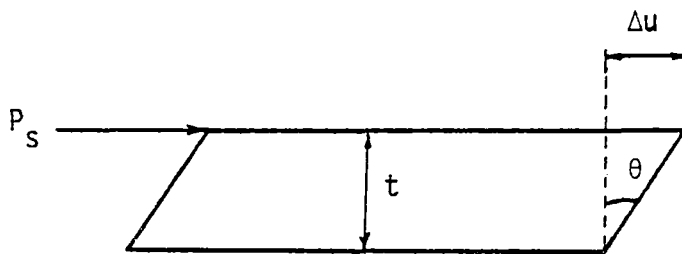
20-Node Interface Element

(b) Interface Elements in Three-Dimensional Analysis

Figure 6.4 Interface Elements for Two- and Three-Dimensional Analysis



(a) Shear Test at the Interface



(b) Deformations at the Interface

Figure 6.5 Load-Deformation Behavior at an Interface

$$G_{int} = \frac{P_s/A}{\Delta u/t} = \frac{P_s \cdot t}{A \cdot \Delta u} \quad (6.6)$$

where A is the area of the interface. This idea is extended to the three-dimensional analysis, and the constitutive matrix for the interface element is taken as

$$[C_{int}] = \begin{bmatrix} C_1 & C_2 & C_2 & 0 & 0 & 0 \\ C_2 & C_1 & C_2 & 0 & 0 & 0 \\ C_2 & C_2 & C_1 & 0 & 0 & 0 \\ 0 & 0 & 0 & G_{int} & 0 & 0 \\ 0 & 0 & 0 & 0 & G_{int} & 0 \\ 0 & 0 & 0 & 0 & 0 & G_{int} \end{bmatrix} \quad (6.7)$$

where

$$C_1 = \frac{E(1 - \nu)}{(1 + \nu)(1 - 2\nu)}$$

$$C_2 = \frac{E\nu}{(1 + \nu)(1 - 2\nu)}$$

and G_{int} is the shear modulus determined experimentally for the interface element since values of E and ν do not have much influence on the slip behavior at the interface, these can be taken as average properties of the adjacent solid elements. This idea is consistent with the assumption that the normal stiffness of an interface should be dependent upon the characteristics of the adjoining elements [14].

Success of the above elements in soil-structure interaction analysis has to be determined from future research. Further modifications may be required to improve its capabilities, and in determining

parameters for the normal mode of deformation. Like in many previously used interface elements, modelling of separation mode may be difficult at the current stage. However, possibilities exist for improvements since tensile condition can be checked at each integration point in the current element. One definite advantage is the ease with which it can be implemented in any existing finite element procedure. Some applications of these interface elements are given in Chapters 8 and 9.

Chapter 7

CONSTITUTIVE MODELLING FOR NONLINEAR ANALYSIS

7.1. General

Details of advanced constitutive models used in this study are described in Chapter 4, and computational algorithms used in implementing these models are described in Chapter 5. It has been realized that, constitutive modelling is an important ingredient of a nonlinear analysis. A sophisticated nonlinear analysis can be meaningless unless the material nonlinearity is properly modelled. The constitutive characterization has to be done by conducting appropriate laboratory experiments on the materials. Hence, the purpose of this chapter is to describe procedure for constitutive modelling with respect to some laboratory experimental work conducted in this study.

The material used in the study is a granular material (sand) obtained from an UMTA test section at the Transportation Test Center, Pueblo, Colorado. Physical properties and compaction characteristics of this material has been reported in references [45,23]. A part of the details of a comprehensive series of laboratory tests for the sand, and derivation of constitutive model are included in this chapter. A general description and philosophy of determination of constitutive parameters is available in reference [21].

Laboratory tests with the truly triaxial device for constitutive models of other materials such as wood, ballast and subballast, and laboratory tests with the dynamic multi-degree-of-freedom shear device

for interfaces between different components in UMTA test section have been described in reference [45].

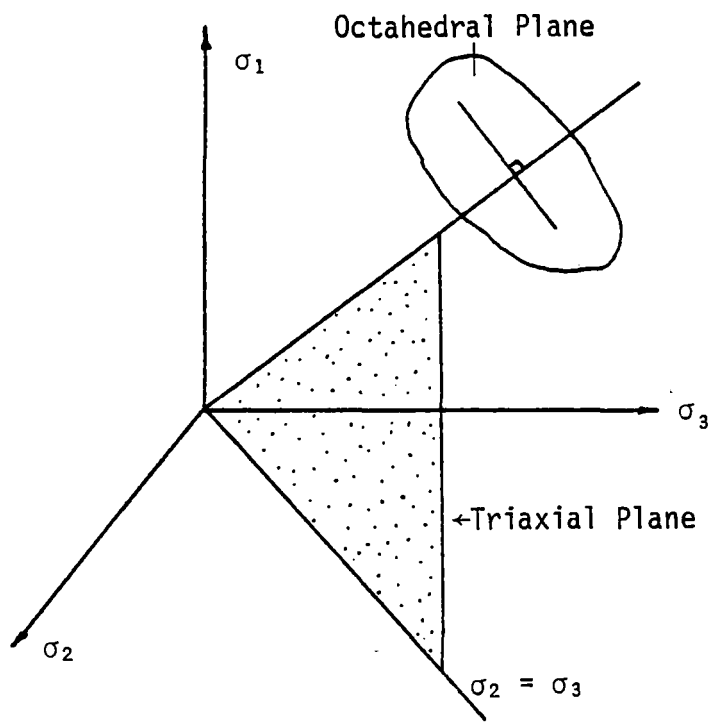
Test Details of Sand

All the tests reported herein were conducted by using a truly triaxial or multiaxial device [79,80]. This device is shown in Appendix E. A water content of 9.0% was used based on the results reported in reference [45]. Since at low degrees of saturation the development of excess pore pressure is prevented, all tests conducted herein are classified as fully drained. The density of test samples varied from 1.86 gm/cm^3 to 2.08 gm/cm^3 with an average value of 1.99 gm/cm^3 .

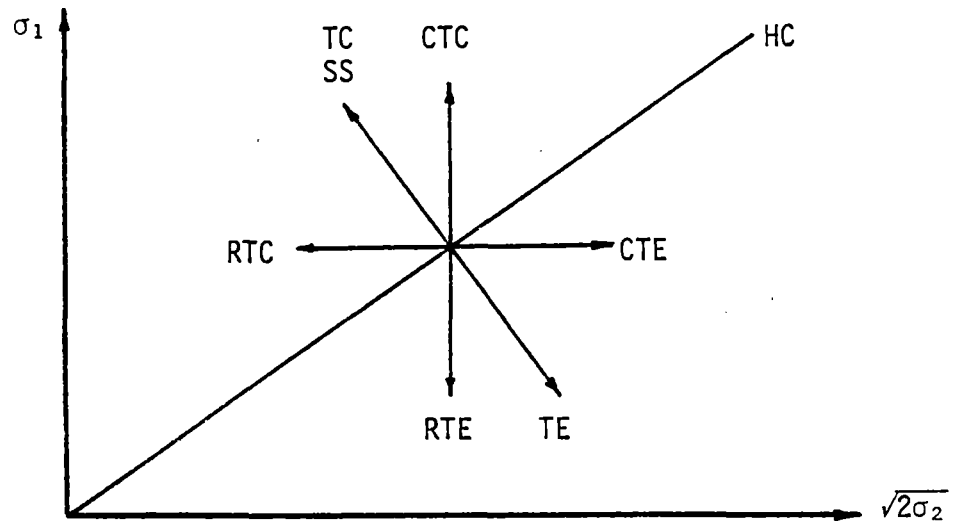
The samples were prepared in three layers by tamping. The procedure for sample preparation was similar to that used by Mould [55]. Various stress paths and their abbreviations used in the testing program are shown in Figure (7.1). These include Hydrostatic or Isotropic Compression (HC), Conventional Triaxial Compression (CTC), Conventional Triaxial Extension (CTE), Reduced Triaxial Compression (RTC), Reduced Triaxial Extension (RTE), Triaxial Compression (TC), Triaxial Extension (TE), and Simple Shear (SS) stress paths.

7.2. Test Results

The experimental observations on the behavior of the sand are described in this section. Figures (7.2a, b) present hydrostatic compression curves for the sand used in this study. The initial density of the material was 1.86 gm/cm^3 . The normal strains in z-direction, ϵ_z , is lower than the normal strains in other two directions. This may be due to the fact that the sample was compacted in the z-direction.



(a) Principal Stress Space



(b) Projections of Stress Paths on Triaxial Plane

Figure 7.1 Commonly Used Stress Paths

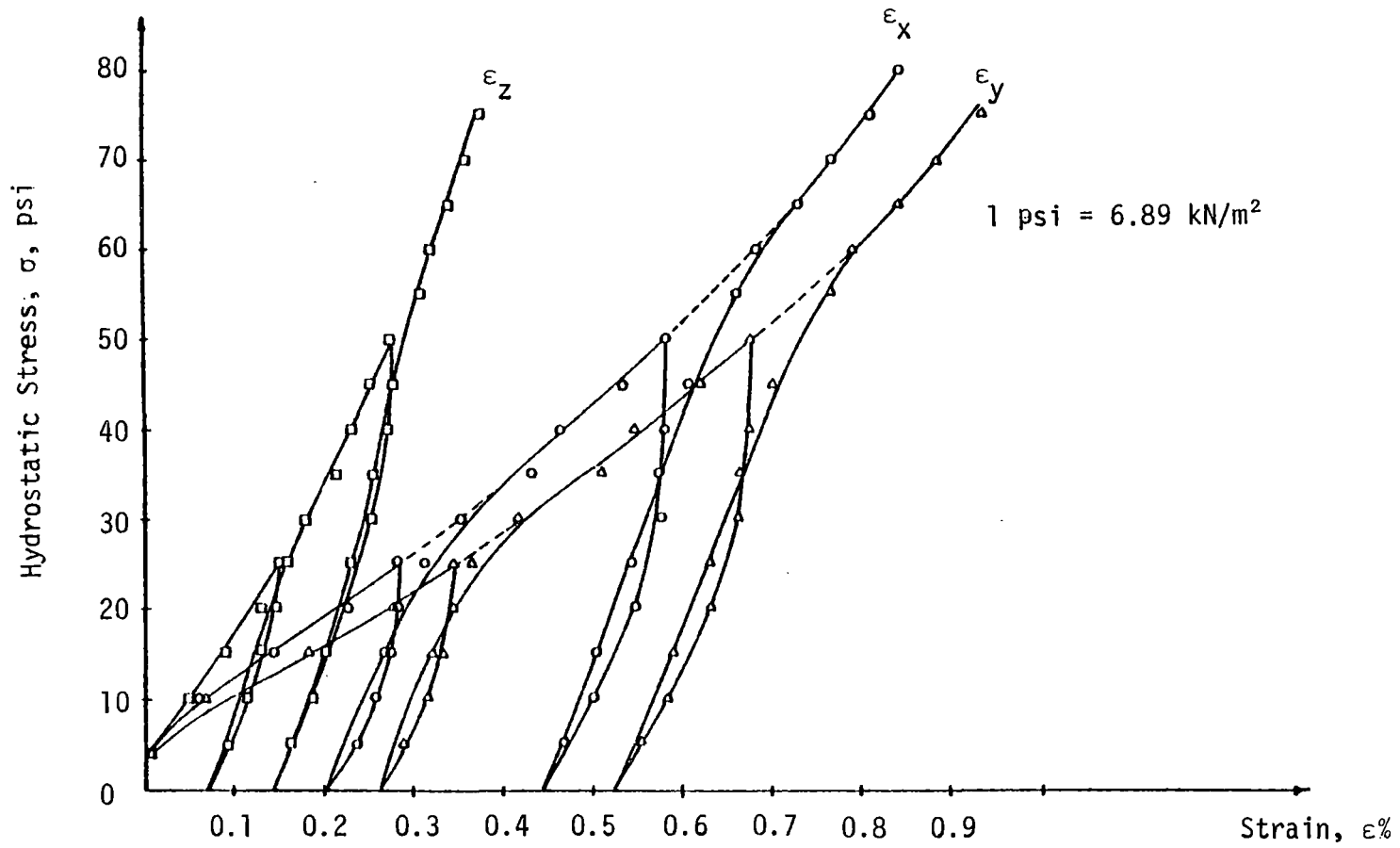


Figure 7.2a Stress-Strain Response Curve for Hydrostatic Compression Test

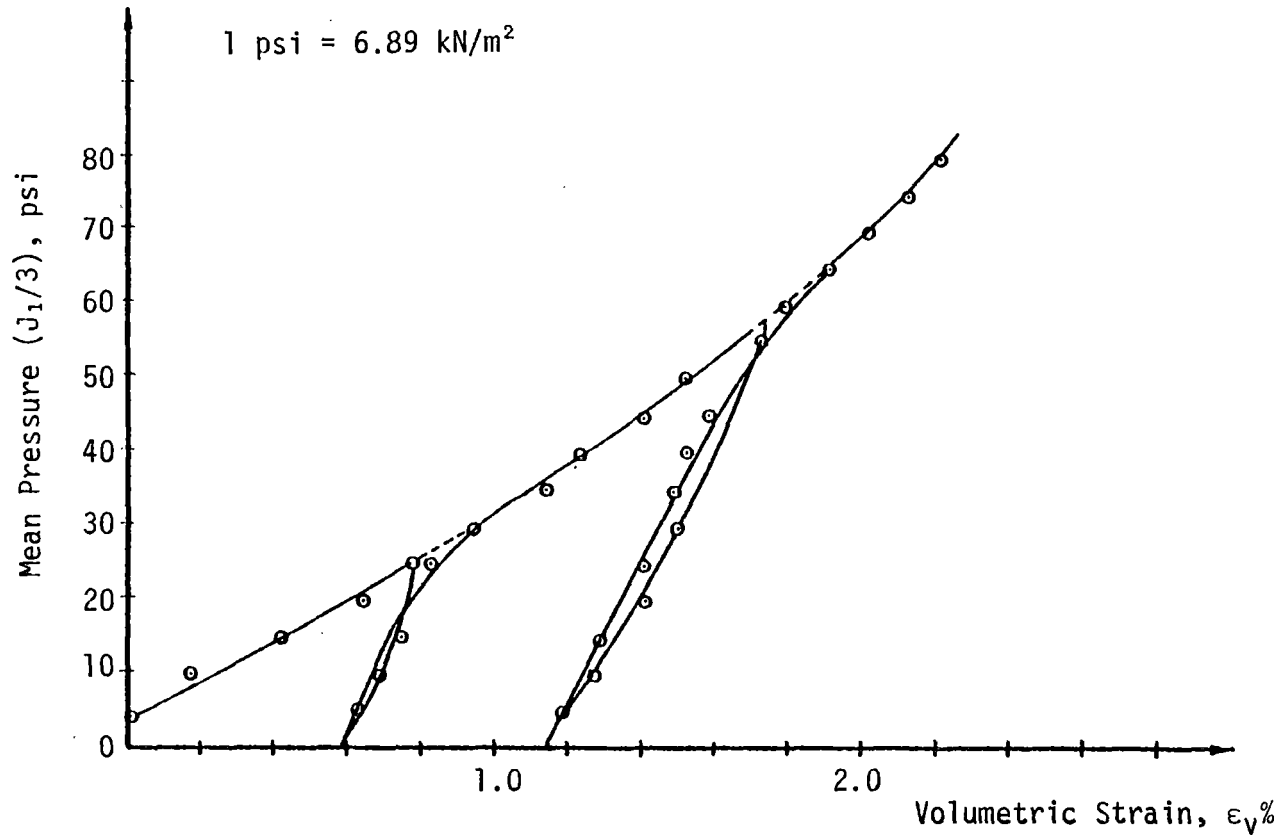


Figure 7.2b Mean Pressure-Volumetric Strain Response for Hydrostatic Test

The mean pressure-volumetric relationship obtained from the hydrostatic test is shown in Figure (7.2b). The loading curve tends to bend upwards as the mean pressure increases, and this shows evidence of hardening behavior.

In the Conventional Triaxial Compression (CTC) test, σ_1 was increased while keeping σ_2 and σ_3 constant. The sample was initially loaded to a hydrostatic (isotropic) pressure of 20.0 psi (138.0 kN/m²), and then a CTC stress path was followed. Figure (7.3a) shows the observed relationship between Octahedral shear stress and the normal strains. Octahedral shear stress (τ_{oct}) versus Octahedral shear strain (γ_{oct}) relationship is shown in Figure (7.3b). The shear modulus can be determined by considering the unloading-reloading behavior shown in this figure. The initial density of the sample was 1.89 gm/cm³. The ultimate strength for this test reached at about 9.0% strain.

The Simple Shear (SS) test was conducted by increasing σ_1 and decreasing σ_3 by the same amount from an initial hydrostatic state of stress while σ_2 was held constant. This stress path is in a Octahedral plane. The sample was initially loaded to a hydrostatic stress of 20 psi (138 kN/m²). Figure (7.4) shows the observed relationships between Octahedral shear stress and the normal strains. The normal strain in the y-direction, ϵ_y , is only about 1.0% even at ultimate states. The normal strain, ϵ_z , at the ultimate conditions is about 7.0% while ϵ_x is about 6.0%. The difference between loading and unloading-reloading behavior is clearly seen in this test too.

Triaxial Compression (TC) test was conducted by increasing σ_1 , and decreasing both σ_2 and σ_3 by equal amounts such that the total mean

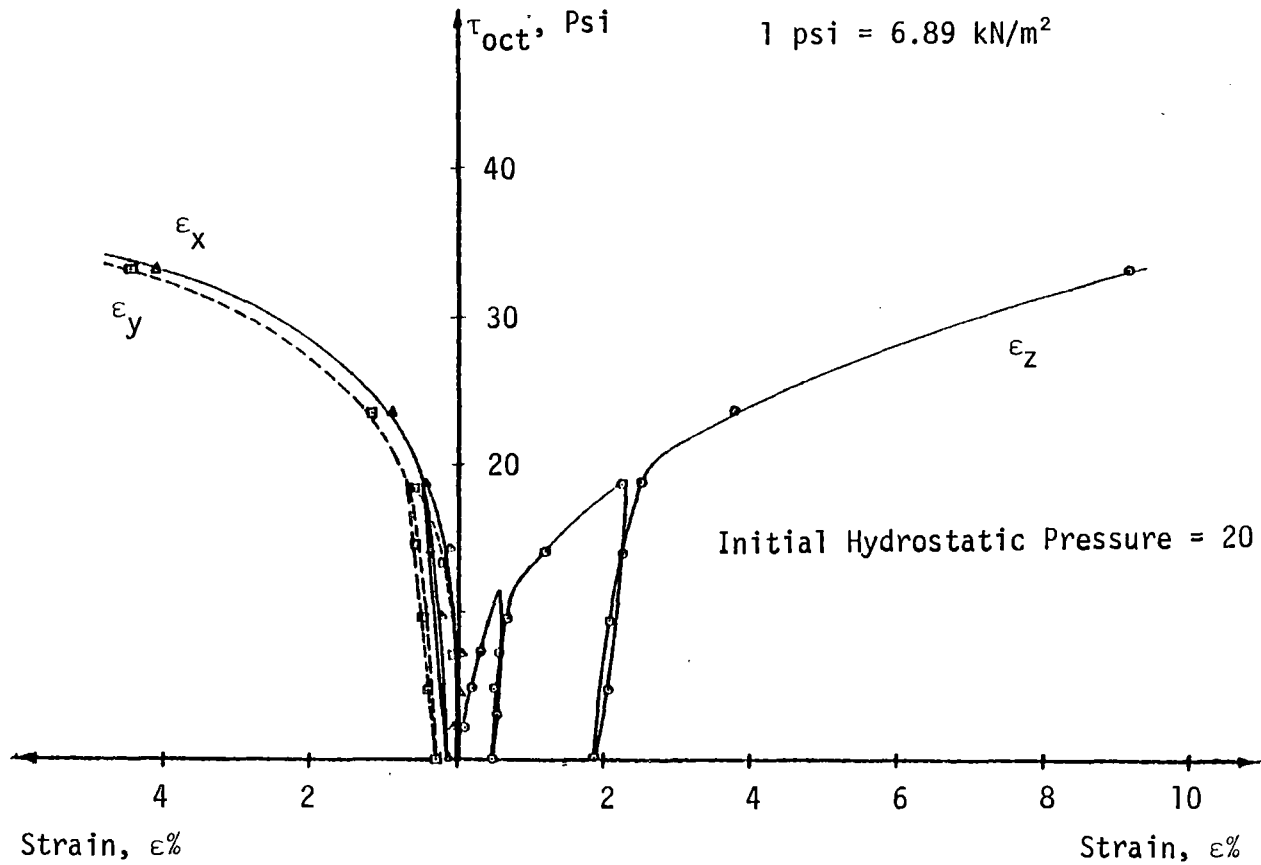


Figure 7.3a Stress-Strain Response for Conventional Triaxial Compression Test

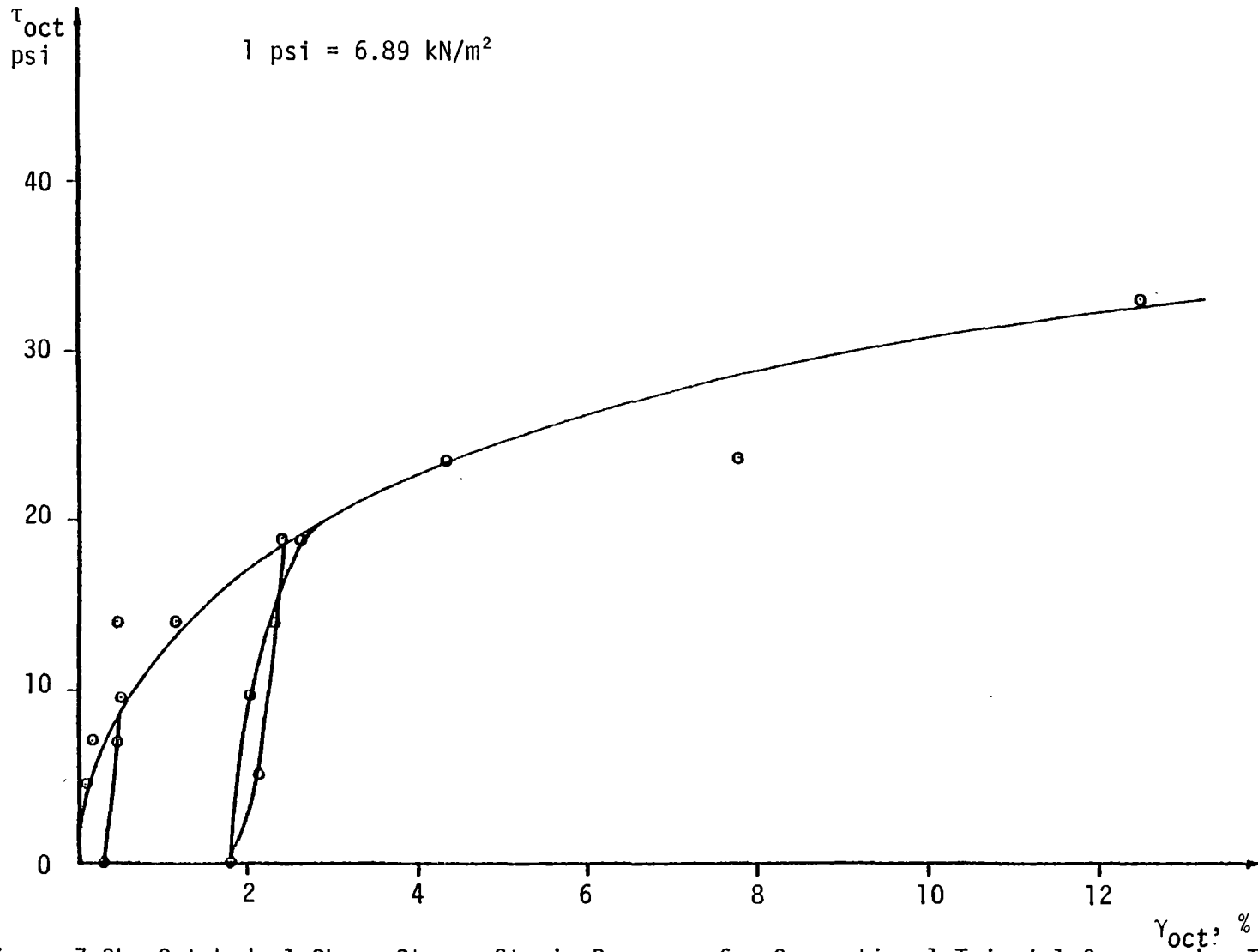


Figure 7.3b Octahedral Shear Stress-Strain Response for Conventional Triaxial Compression Test

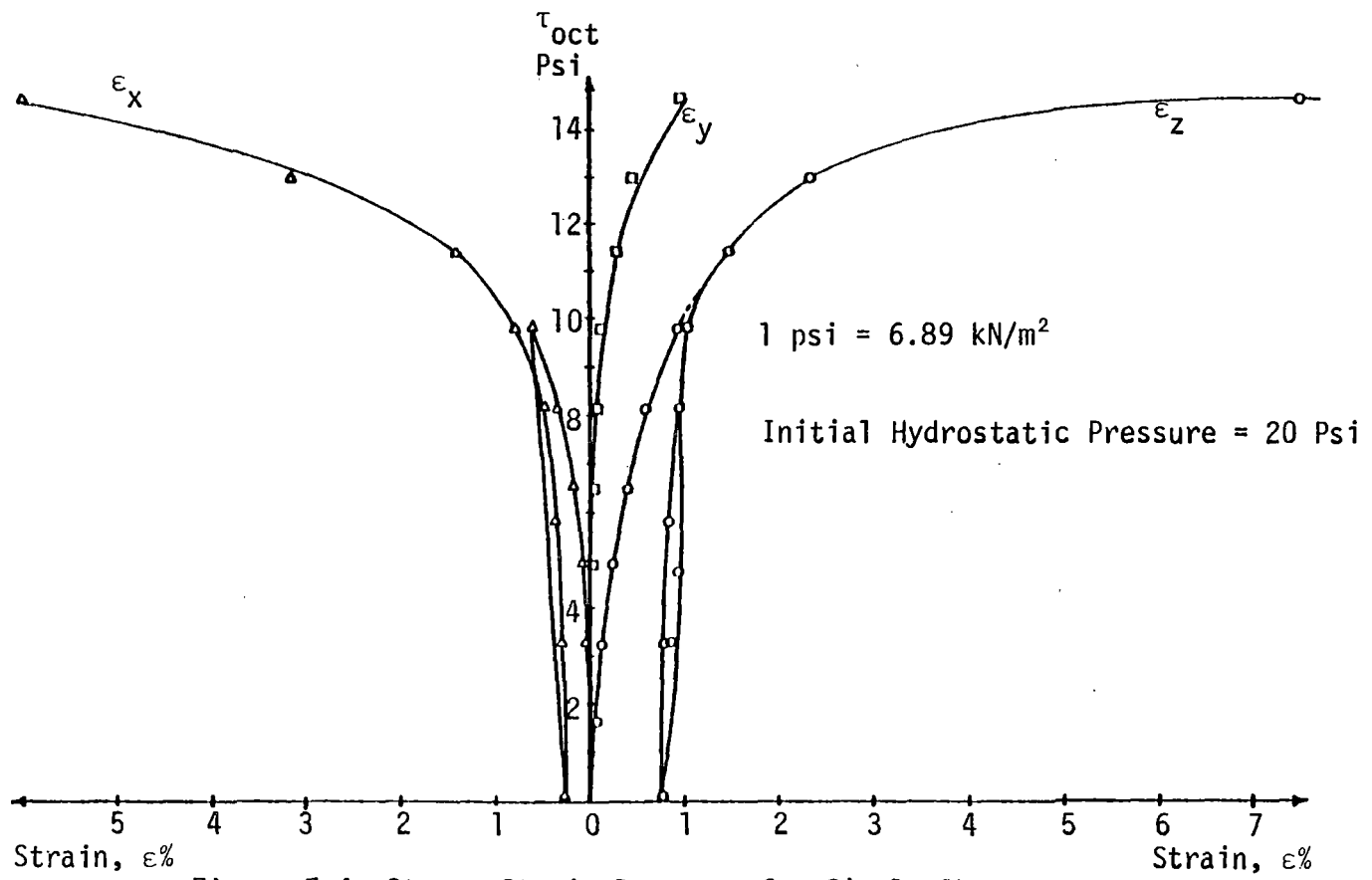


Figure 7.4 Stress-Strain Response for Simple Shear Test

pressure, $J_1/3$, remained constant. This stress path is in an Octahedral plane.

The sample was initially loaded to a hydrostatic (isotropic) pressure of 25.0 psi (172.5 kN/m²). The initial density of the sample was 2.03 gm/cm³. Figure (7.5) shows the observed relationships between Octahedral shear stress and normal strains. The normal strain, ϵ_z , at the ultimate conditions is about 8.0%.

The Triaxial Extension (TE) was conducted by decreasing σ_1 , and increasing both σ_2 and σ_3 by equal amounts such that the total mean pressure, $J_1/3$, remained constant; as a result this stress path also lies on an Octahedral plane. The sample was initially loaded to a hydrostatic stress of 20 psi (138.0 kN/m²). The initial density was 2.04 gm/cm³.

Figure (7.6) shows the observed relationships between Octahedral shear stress and normal strains from a TE test. The normal strains ϵ_x and ϵ_y at ultimate conditions is about 6.0%.

In Reduced Triaxial Compression (RTC) test σ_1 was held constant while σ_2 and σ_3 were reduced in equal amounts. Hence, the value of J_1 decreased along this stress path. Figure (7.7) shows the observed relationship between Octahedral shear stress and normal strains from a RTC test. The initial density of the sample was 2.01 gm/cm³. Sample was initially loaded to a hydrostatic (isotropic) pressure of 20.0 psi (138.0 kN/m²). This produced a well-defined ultimate state at a relatively small strains for the sand.

In Conventional Triaxial Extension (CTE) test, σ_1 and σ_2 were increased in equal amounts while keeping σ_3 constant. Figure (7.8)

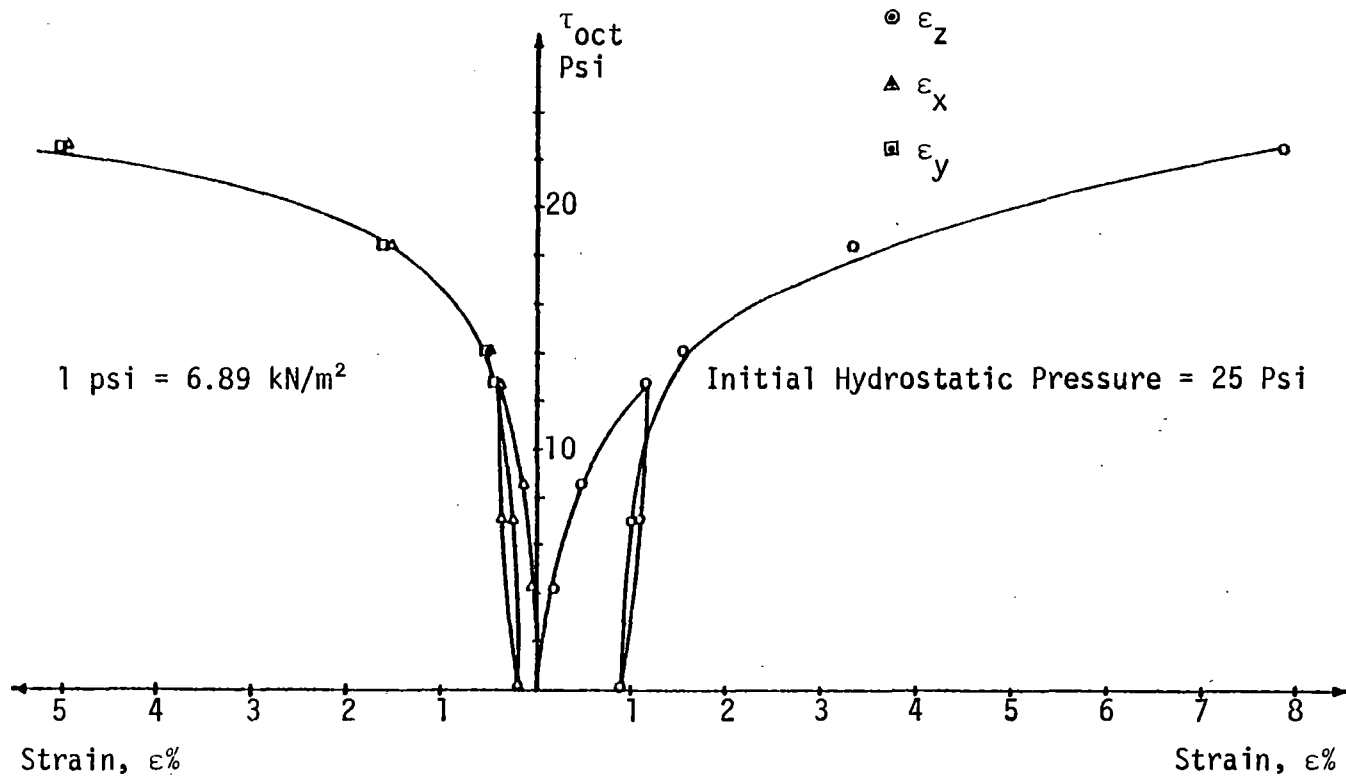


Figure 7.5 Stress-Strain Response for Triaxial Compression Test

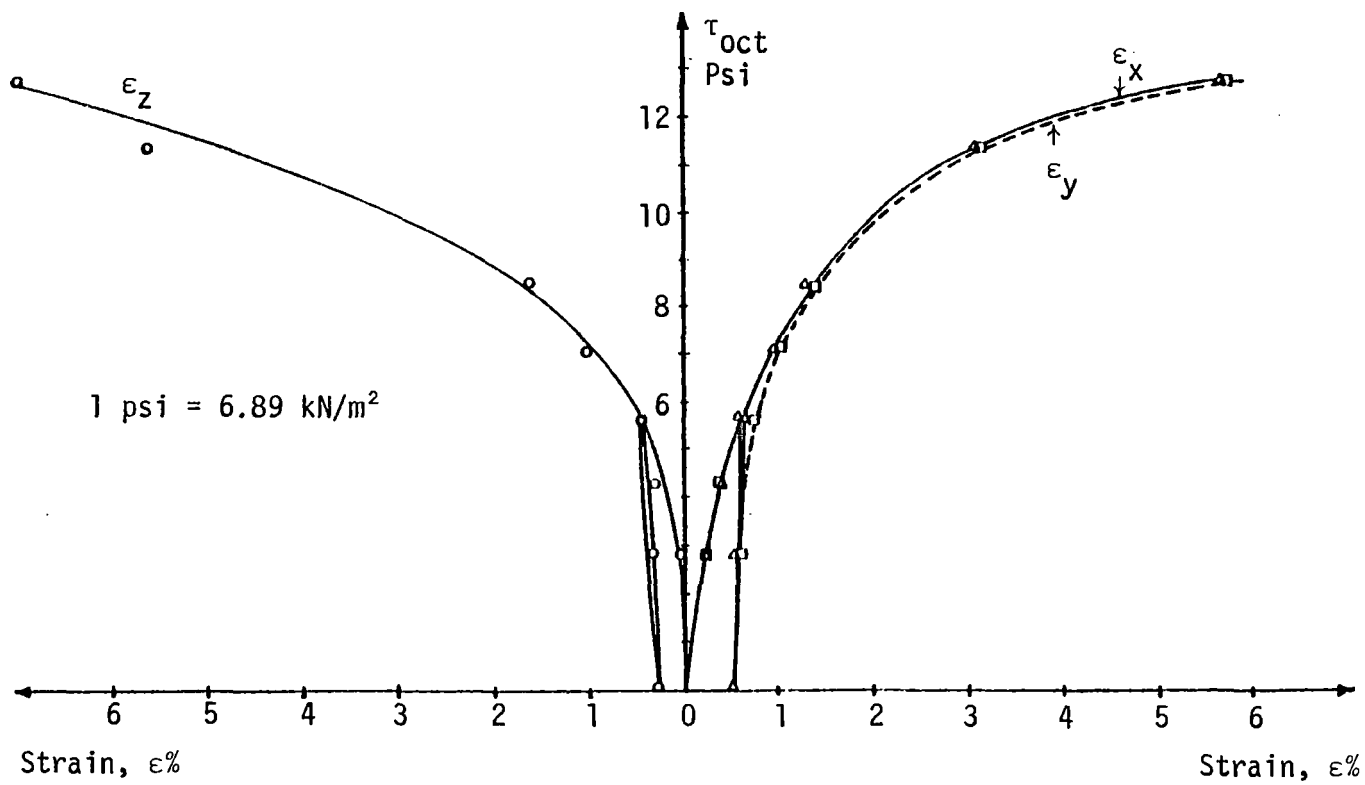


Figure 7.6 Stress-Strain Response for Triaxial Extension Test

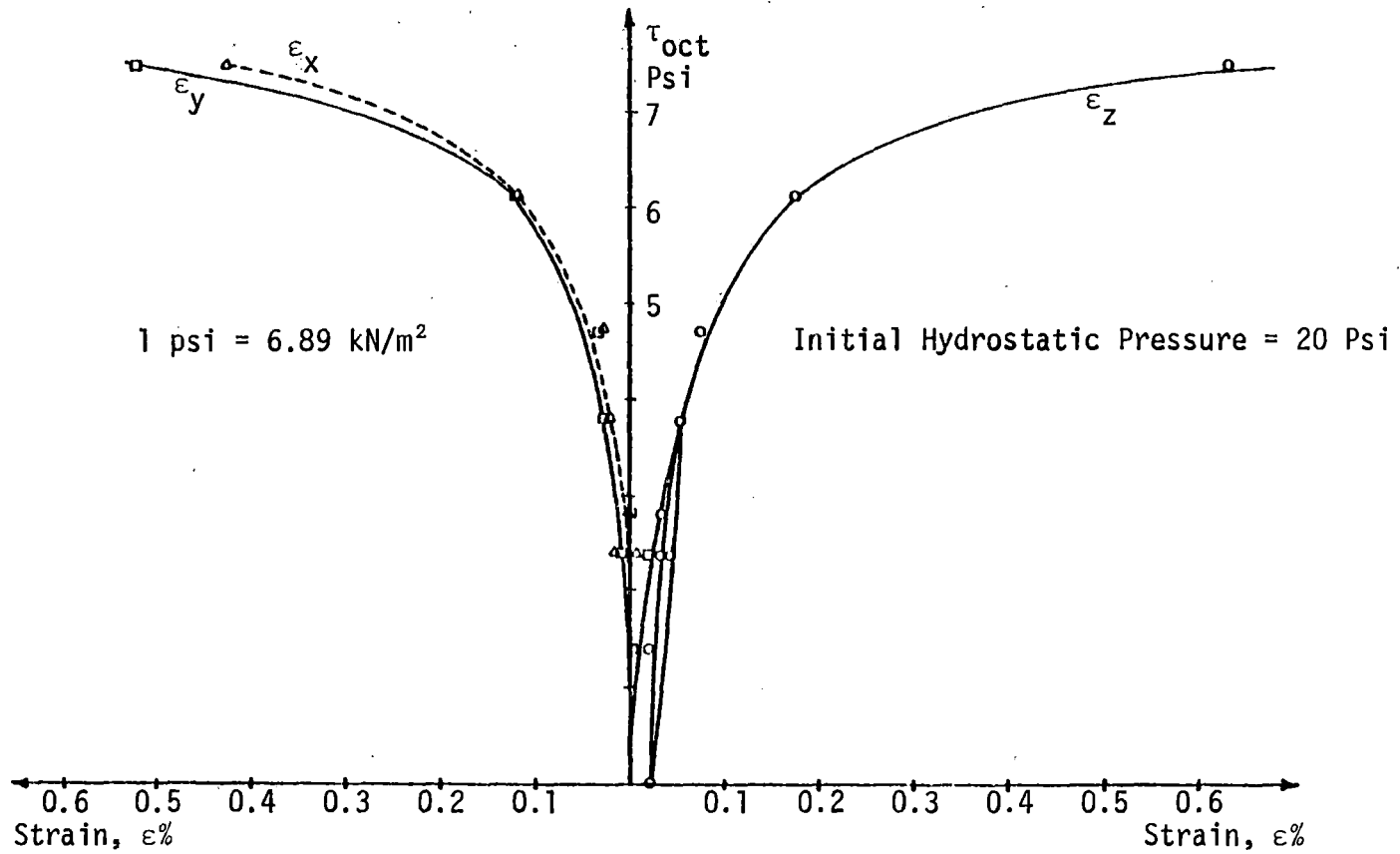


Figure 7.7 Stress-Strain Response for Reduced Triaxial Compression Test

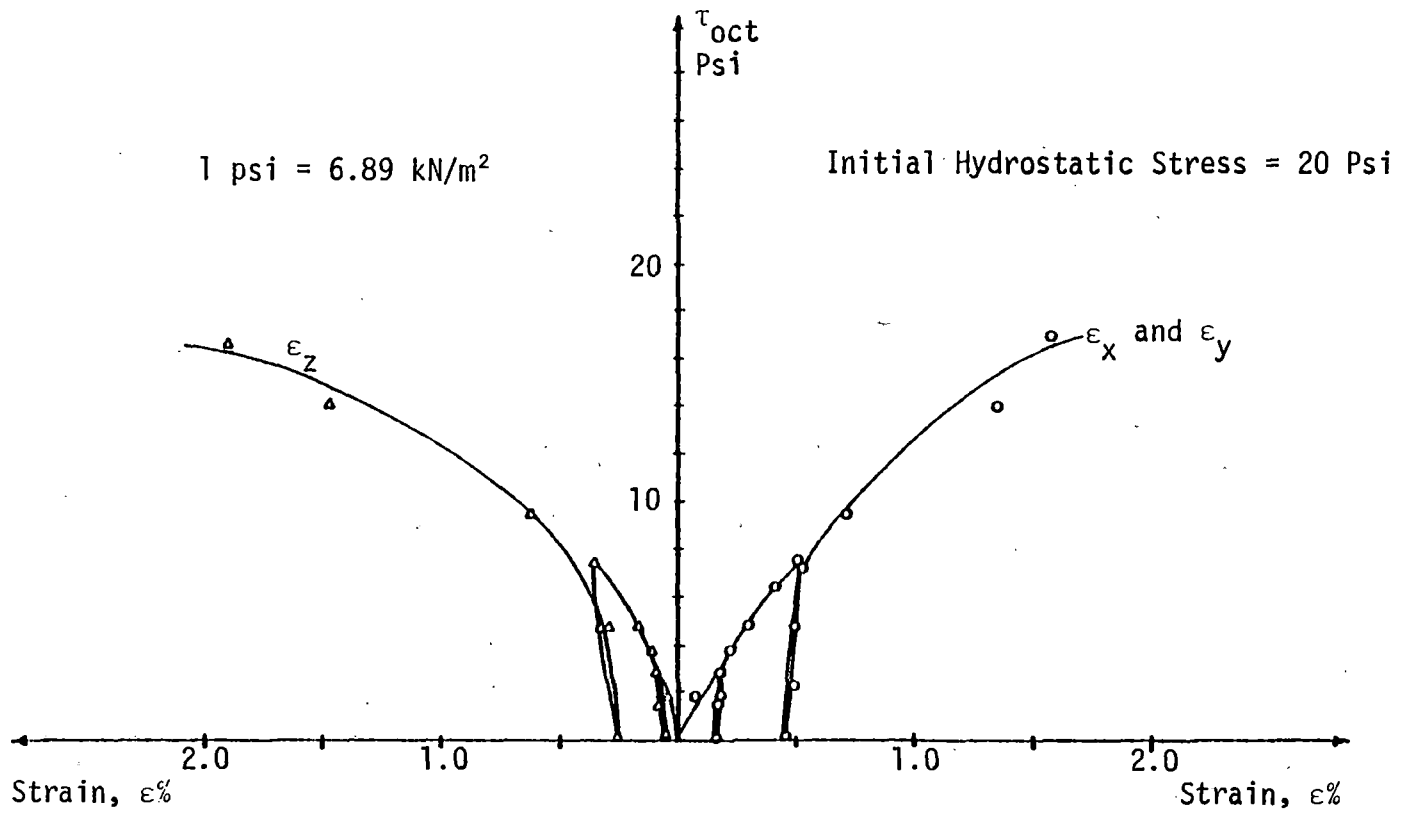


Figure 7.8 Stress-Strain Response for Conventional Triaxial Extension Test

shows the observed variation of τ_{oct} with the normal strains in a CTE test. The initial density of the sample was 2.02 gm/cm^3 , and the initial hydrostatic pressure was 20.0 psi (138.0 kN/m^2). An ultimate state was reached at a relatively small strain of about 2.0%.

7.3. Analysis of Data and Determination of Parameters

This section describes the constitutive parameters for the sand determined from the foregoing laboratory tests. Here, the sand is modelled by using the critical state concept described earlier in Chapter 4. The void ratio, $e - \log p$ relationship obtained from hydrostatic test data, Figure (7.2), is shown in Figure (7.9). From this figure, the values of λ_c and κ can be determined.

In the previous section, only typical experimental data on this sand is included. Some experimental data on the same sand is available in reference [45]. The critical state parameter, M , can be determined by plotting ultimate states observed in individual tests as shown in Figure (7.10). The elastic properties for the material can be obtained by considering unloading-reloading behavior of the sand.

The Constitutive parameters for the sand are stated below.

$$E = 12,000 \text{ psi} \text{ (} 82800.0 \text{ kN/m}^2 \text{)}$$

$$\nu = 0.28$$

$$M = 1.24$$

$$\lambda_c = 0.014$$

$$\kappa = 0.0024$$

$$e_0 = 0.270$$

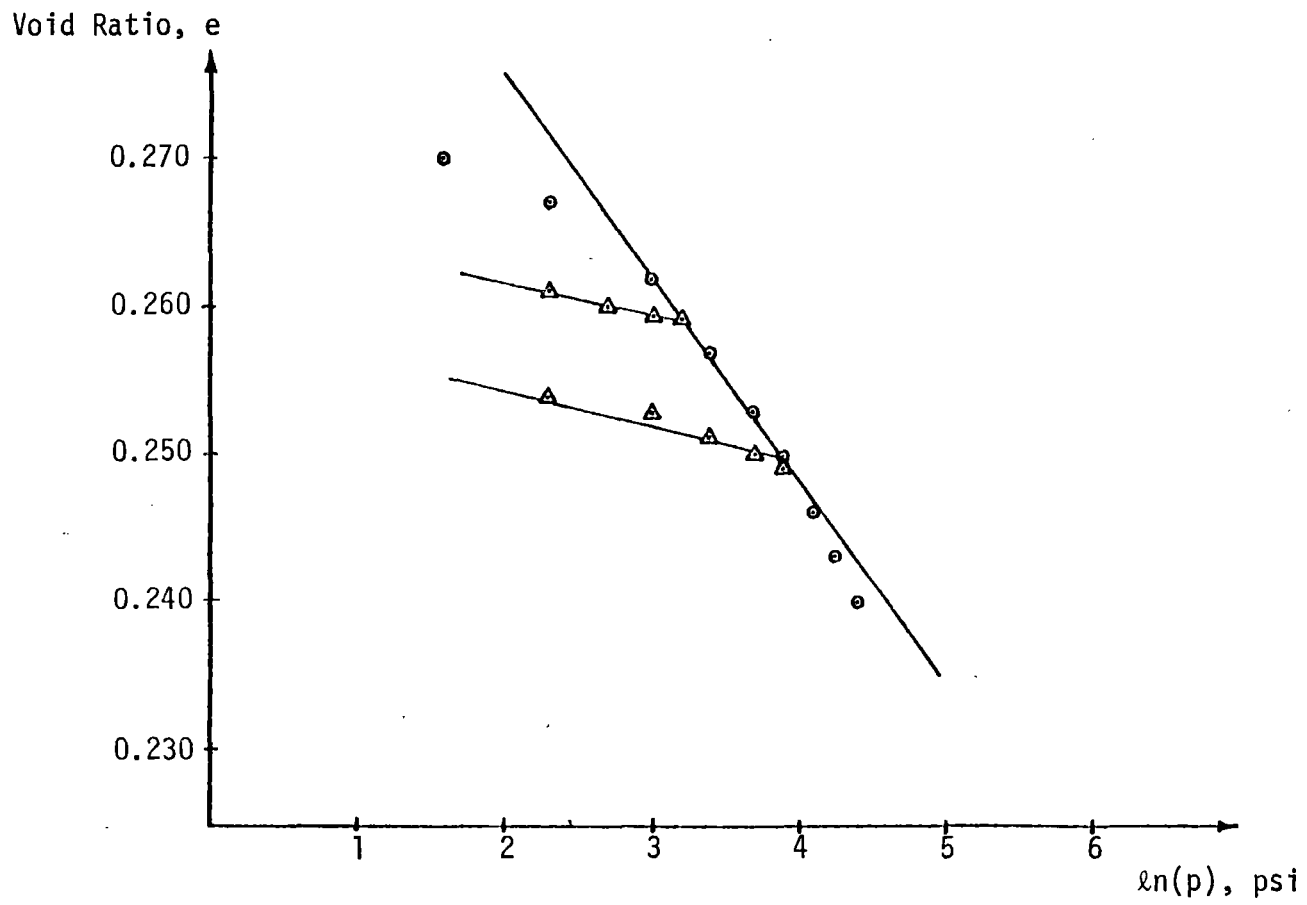


Figure 7.9 Void Ratio-Log p Curve from Hydrostatic Test

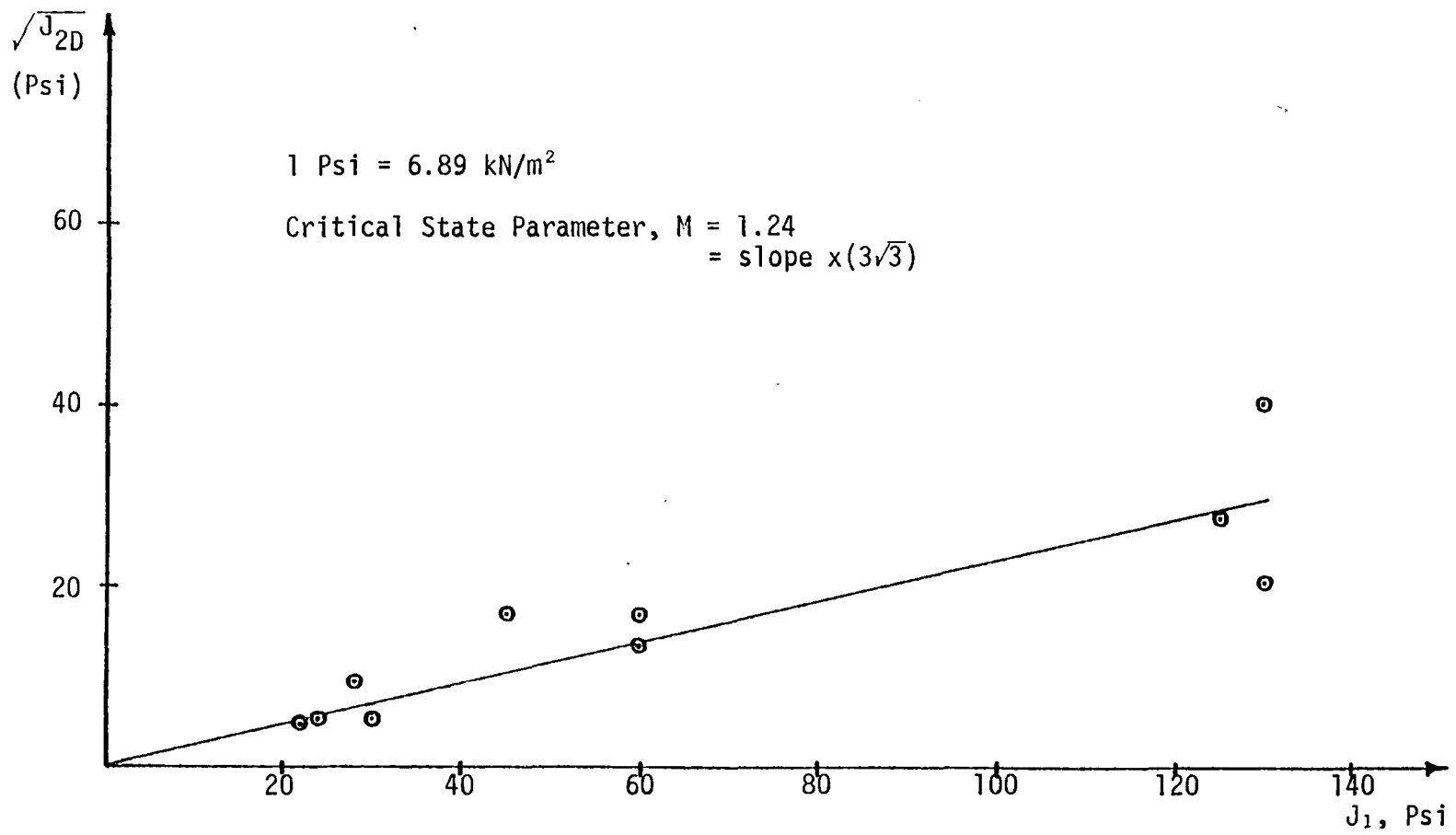


Figure 7.10 Failure Envelope for Pueblo Sand

These properties can be used with the critical state model in characterizing the sand under consideration, as expressed in Equations (4.27 and 4.30).

Chapter 8

VERIFICATIONS OF ONE-, TWO-, AND THREE-DIMENSIONAL FORMULATIONS AND CODES

Theoretical formulations of one-, two- and three-dimensional finite element idealizations, details of constitutive relationships, computational algorithms for nonlinear analysis and solution techniques are discussed in Chapters 3, 4, 5 and 6, respectively. Three finite element computer codes are developed for the above three idealizations which can handle general nonlinear geomechanics problems including soil-structure interaction. In order to verify the accuracy of the computer codes, several problems are solved, and results are compared with previous applications or closed-form solutions wherever applicable. Certain plane strain problems are solved using both the two-dimensional and three-dimensional codes. Plane strain conditions are simulated in three-dimensional code by constraining nodal displacements normal to the plane. These results are given in Chapter 9. These computer codes have several capabilities, and these are described in a separate report [76].

The structures of the three programs are designed in such a manner that modifications or additions to any aspect can easily be implemented. In fact, the subroutine names, variable names, etc., have been kept, as much as possible the same in all the three codes.

8.1. Beam-on-Elastic Foundation with One-Dimensional Code

Problem of a beam-on-elastic foundation is solved by using the one-dimensional code, described in Chapter 3. This problem can also

be solved in a closed-form manner by using the theory of beams-on-elastic foundations [41].

The following properties are used for the example problem shown in Figure (8.1).

Cross sectional area of the beam = 13.35 in² (86.12 cm²)

Second moment of area, I = 94.9 in⁴ (3950. cm⁴)

E = 30 × 10⁶ psi (20.67 × 10⁷ kN/m²)

ν = 0.35

Subgrade reaction, k_s = 2,000 lb/in² (13.78 × 10³ kN/m²)

It is assumed that the continuous foundation can be replaced by a series of elastic supports. The spacing of the elastic supports is taken as 20 inches (50 cm), Figure (8.1). The infinite beam is described by using 25 elements with a length of 500 in (1250 cm). The end boundaries are assumed to be fixed at approximately half the wavelength [41] of the deflection curve, away from the point load; the wavelength is defined as equal to π/λ where λ is the characteristic length of the beam.

Finite element results, Figure (8.1), compare very well with the closed-form solution given in reference [41]. The approximation achieved by replacing a continuous elastic support by separate ones gives good results. However, there is a limitation on the support spacing, a, [41], which should satisfy the following requirement:

$$a < \frac{\pi}{4} \sqrt[3]{\frac{\pi EI}{C}} \quad (7.1)$$

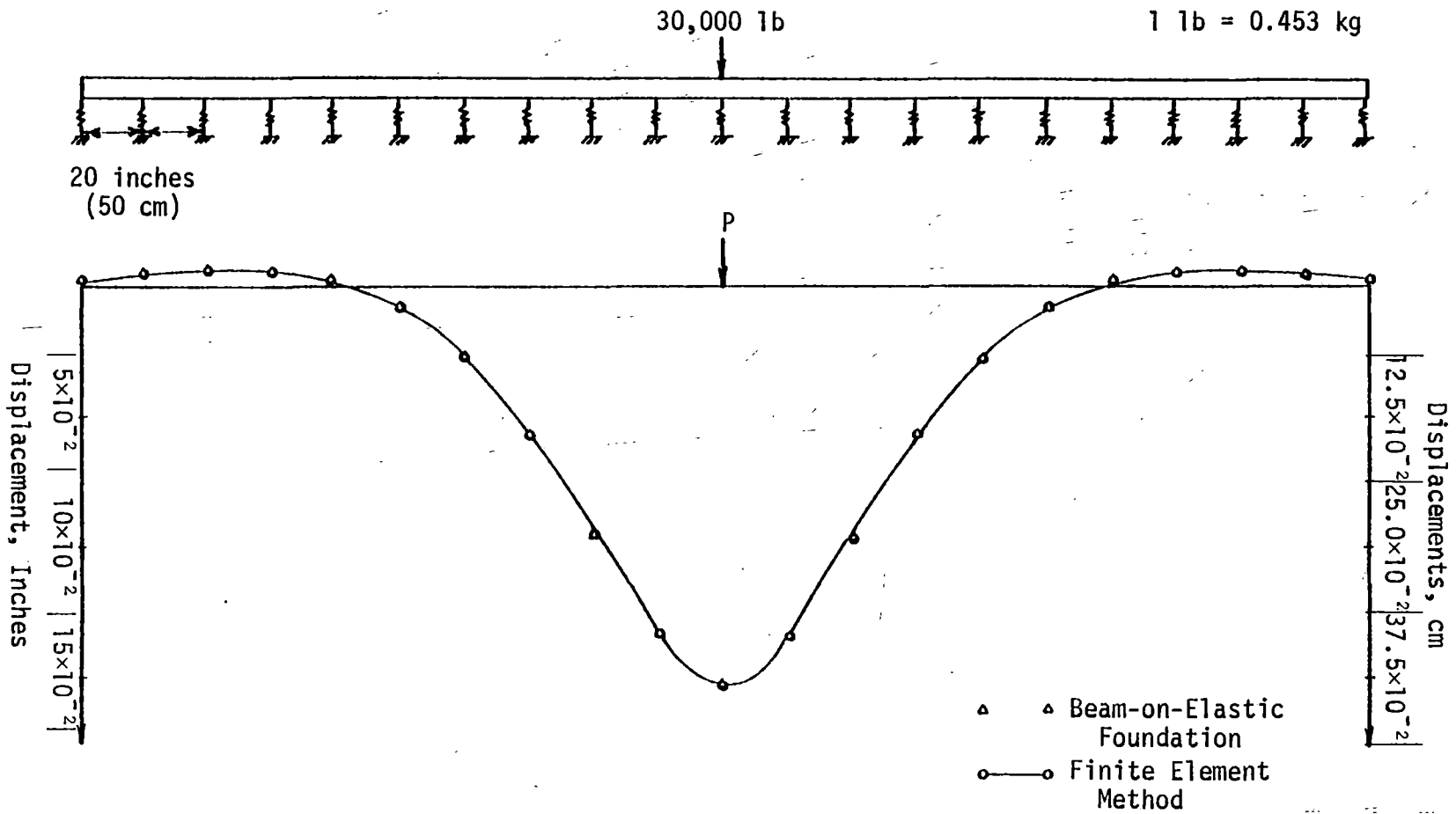


Figure 8.1 Deformations of a Beam-on-Elastic Foundation

where C is the stiffness of the support, and EI indicates the flexural rigidity of the beam.

8.2. Pure Beam Bending Problem with Two-Dimensional Code

The problem of pure bending, Figure (8.2), has been modelled assuming plane stress conditions. Since the problem is symmetric, and antisymmetric in y - and x -axes, respectively, only one fourth of the beam is discretized. This problem has been solved by Desai and Abel [15] by using quadrilateral finite elements composed of four constant strain triangles. Material properties used in the analysis are

$$E = 30 \times 10^6 \text{ psi } (20.69 \times 10^6 \text{ N/cm}^2)$$

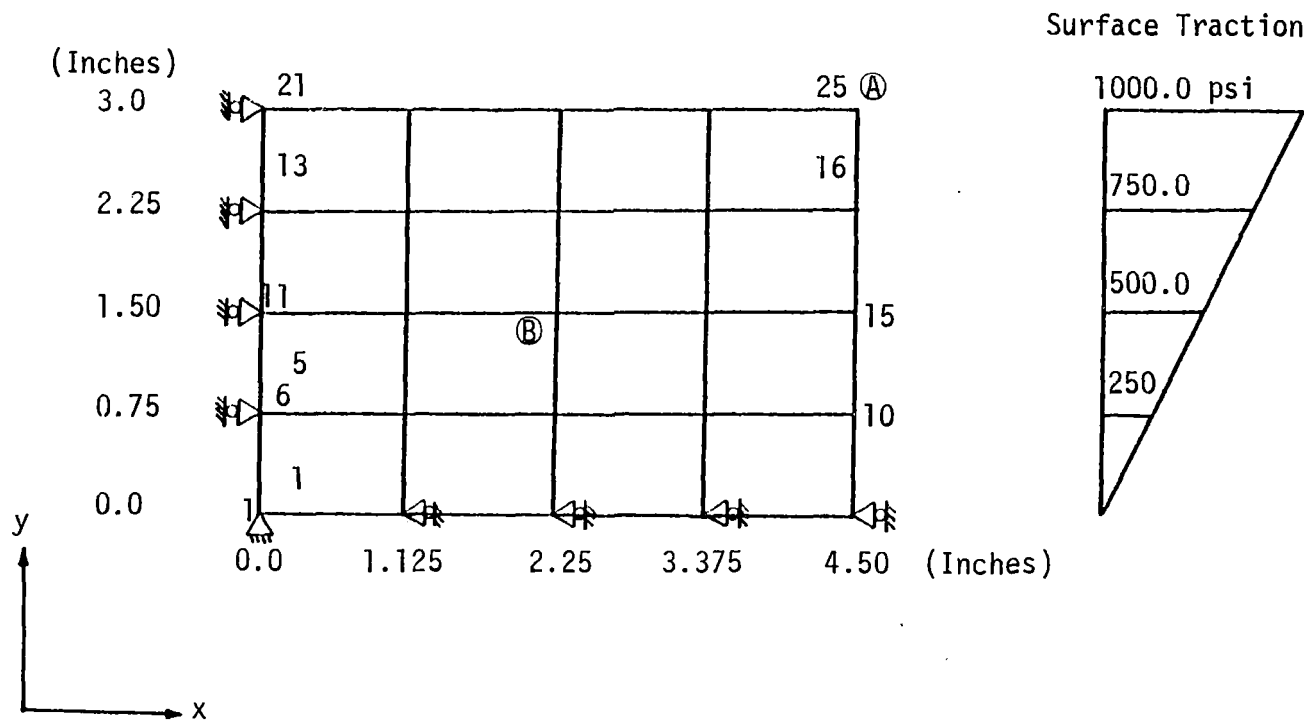
$$\nu = 0.3$$

$$\text{Thickness} = 1.0 \text{ inch } (2.54 \text{ cm})$$

The coordinates and the surface loadings are shown in Figure (8.2). Table 8.1 gives a comparison between the results of the present analysis by using 8-node elements, and those obtained by Desai and Abel [15]. The correlation between the results of the present analysis and the closed-form solution is considered to be highly satisfactory. It also indicates that the 8-node quadrilateral yields improved accuracy compared to that by the 4-node quadrilateral.

8.3. Variable Moduli Model: Two-, and Three-Dimensional Analysis

Behavior of a conventional triaxial specimen is analyzed by using variable moduli model, Equation (4.7), in two- and three-dimensional idealizations. A case of cylindrical (axisymmetric) specimen, Figure (8.3a), is analyzed by using the two-dimensional code, while a truly



1 Inch = 2.54 cm

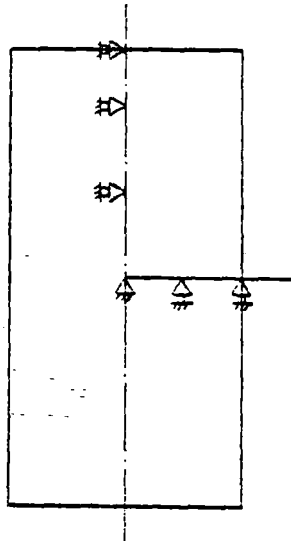
1 psi = 6.89 kN/m²

Figure 8.2 Plane Stress Idealization of Beam Bending

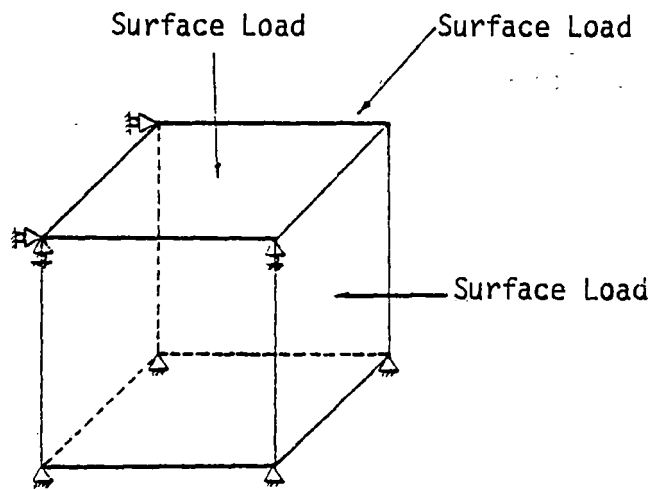
Table 8.1
Comparison of Displacements

	Displacement at Point A (inches)	
	$u(\times 10^{-4})$	$v(\times 10^{-4})$
Exact	1.5000	-1.2750
Desai & Abel: 4-node (25 nodes, 16 elements)	1.4552	-1.2399
Present code: 8-node (65 nodes, 16 elements)	1.5001	-1.2749

	Displacement at Point B (inches)	
	$u(\times 10^{-4})$	$v(\times 10^{-4})$
Exact	0.3750	-0.31875
Desai & Abel (25 nodes, 16 elements)	0.3679	-0.3123
Present code (65 nodes, 16 elements)	0.3750	-0.3186



(a) Cylindrical Triaxial Specimen



(b) Truly Triaxial Specimen

Figure 8.3 Simulation of Triaxial Test Specimens

triaxial specimen, Figure (8.3b), is simulated by using the three-dimensional code. Figure (8.3) shows the finite element meshes containing only one element, and the boundary conditions.

The following properties are used.

$$K = K_0 + K_1 \epsilon_V + K_2 \epsilon_V^2 \quad (7.2a)$$

$$G = G_0 + \gamma_1 p + \gamma_2 \sqrt{J_{2D}} \quad (7.2b)$$

$$E_0 = 1200 \text{ psi (8268.0 kN/m}^2\text{)}$$

$$\nu_0 = 0.30$$

$$K_0 = 1000 \text{ psi (6890.0 kN/m}^2\text{)}$$

$$G_0 = 462 \text{ psi (3183.2 kN/m}^2\text{)}$$

$$K_1 = -10^5 \text{ psi } (-6.89 \times 10^5 \text{ kN/m}^2\text{)}$$

$$K_2 = 4 \times 10^6 \text{ psi (27.56} \times 10^6 \text{ kN/m}^2\text{)}$$

$$\gamma_1 = 60.0$$

$$\gamma_2 = -133.0$$

Conventional triaxial compression (CTC) stress paths are simulated for two confining pressures. One iteration per increment is used in the analysis. Finite element predictions are compared with closed-form results in Figure (8.4). Predictions from both the two- and three-dimensional codes compare very well with the closed-form solution given by Nelson and Baron [60], Equations (4.9) and (4.11).

8.4. Drucker-Prager Model: Two- and Three-Dimensional Analysis

In order to verify the computer codes, a block under plane strain conditions subjected to a uniaxial load is analyzed. This problem is simulated in the three-dimensional code by constraining the nodal

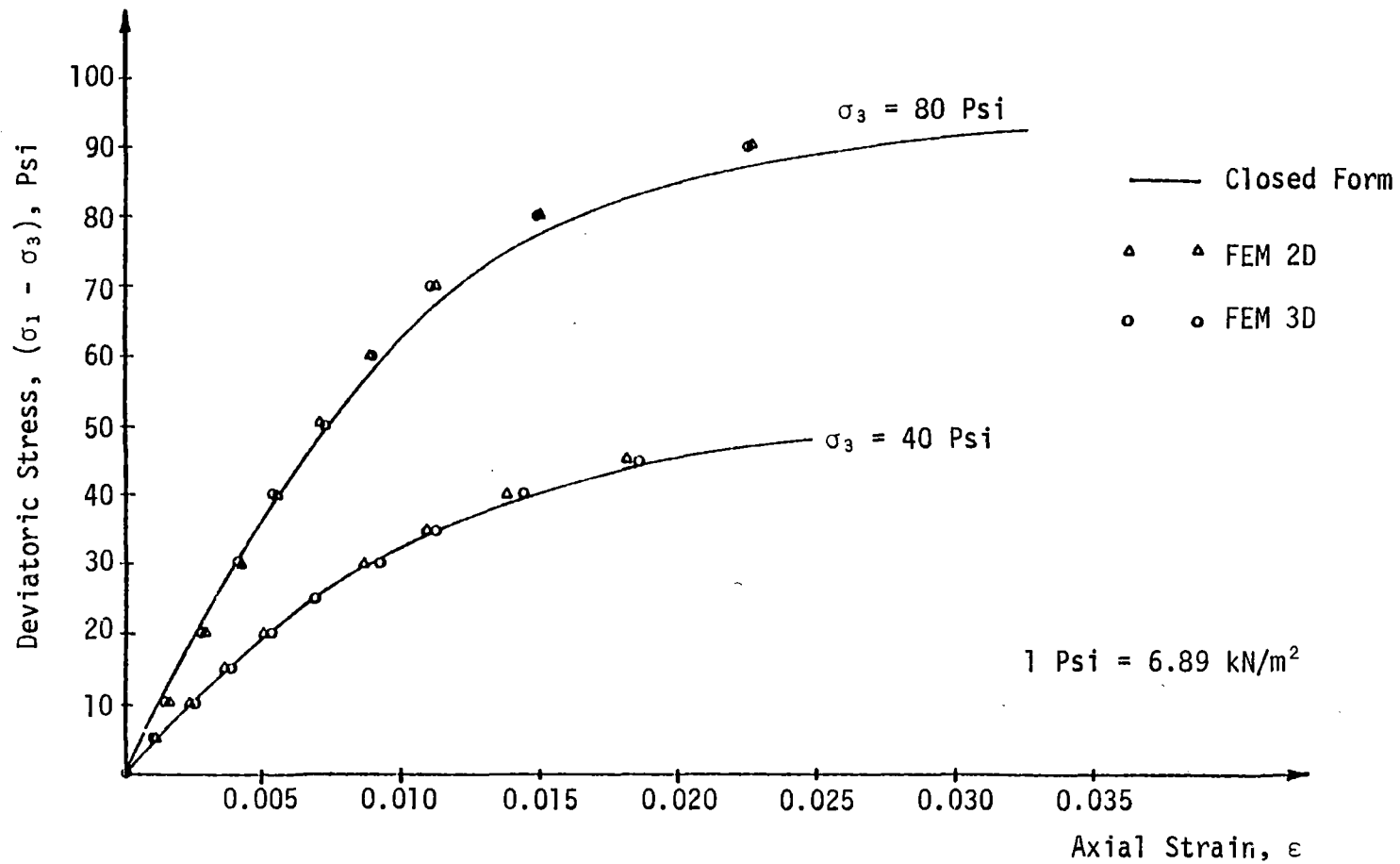


Figure 8.4 Verification of Variable Moduli Model Predictions

displacements in the y-direction as shown in Figure (8.5). The lateral boundary is allowed to deform freely in the x-direction. This problem has been solved by Davidson and Chen [9] by using a two-dimensional procedure which uses constant strain triangles. Here, 8-node plane elements in two-dimensional case, and 8-node brick elements in three-dimensional case are used. Following properties are used for the Drucker-Prager type material model:

$$E = 500,000 \text{ psf (23,950 kN/m}^2\text{)}$$

$$\nu = 0.0$$

$$C = 500.0 \text{ psf (23.95 kN/m}^2\text{)}$$

$$\phi = 30 \text{ degrees}$$

where C is the cohesion, and ϕ is the angle of internal friction. A description of computational algorithms used in the present analysis, and that used by Davidson and Chen [9] is given in Chapter 5. Finite element predictions are compared in Figure (8.5) with the results given in reference [9].

The material behaves elastically up to about 1000 psf (47.9 kN/m²) before the initial yield is detected. Since the Poisson's ratio is taken as zero, out of plane stresses and lateral displacements are zero during elastic deformations. After the initial yield, the material carries additional stresses while moving along the yield surface. This causes changes in out-of-plane stresses and lateral movement. In the present analysis, the material could not sustain an equilibrium state when the load is increased from 1700 psf (81.43 kN/m²) to 1800 psf (86.22 kN/m²), thereby indicating an ultimate state at 1700 psf

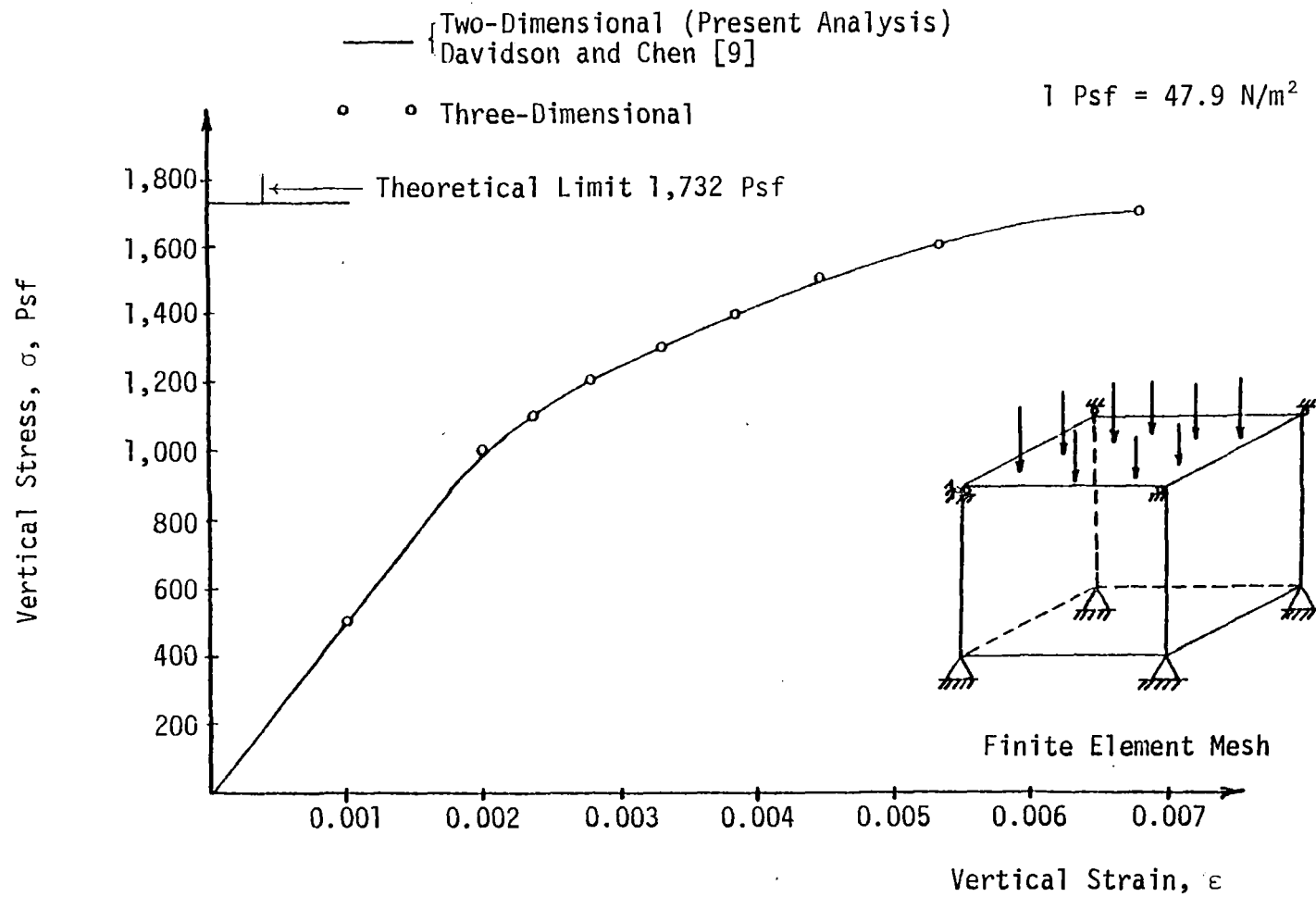


Figure 8.5 Plane Strain Behavior of a Drucker-Prager Material

(81.43 kN/m²). The maximum ultimate state predicted by Davidson and Chen [9] is 1725.0 psf (82.62 kN/m²). The stress-strain curve during the loading history predicted in the current analysis seems to compare very well with that given in reference [9]. If smaller load increments were used in the current analysis, ultimate conditions may have been predicted close to that given in Davidson et al. [9]. The ultimate stress predicted by Mohr-Coulomb criterion with above material properties is 1732.0 psf (82.96 kN/m²). The comparison is considered excellent.

8.5. Critical State Model: Two- and Three-Dimensional Analysis

Since there is a lack of observed or previously solved data from two- and three-dimensional analysis with critical state model, the accuracy has to be verified by solving rather simple problems. In this section, behavior of a conventional triaxial specimen is analyzed by using both two- and three-dimensional codes similar to the verification 8.3. The finite element meshes are shown in Figure (8.3). This problem has also been analyzed by Zienkiewicz and Naylor [91] by using a two-dimensional procedure which uses the initial stress method.

The following properties are used for this model, Equation (4.27) and (4.30).

$$\sigma_a = \sigma_r = 100.0 \text{ kN/m}^2$$

$$M = 1.0$$

$$\lambda_c = 0.14$$

$$\kappa = 0.026$$

$$\nu = 0.30$$

$$E_0 = 9900.0 \text{ kN/m}^2$$

$$e_0 = 1.08$$

$$p_0 = 114 \text{ kN/m}^2$$

The load is applied in increments of 15 kN/m^2 each, and one iteration is performed for each increment. The predictions from the present analysis are compared in Figure (8.6) with those given by Zienkiewicz et al. [91]. The comparison is considered to be excellent. In the present analysis, both two- and three-dimensional procedures gave similar results. However, at higher loads, behavior predicted by Zienkiewicz et al. [91] seems to be slightly stiffer. Furthermore, they appear to have not carried out the analysis until the material reaches a critical state. The initial stress approach employed by them, may require a larger number of iterations where plastic strains are much larger than elastic components. Perhaps, this may be the reason for the stiffer response, and for not having continued the analysis up to the critical state.

8.6. Marching and Iterative Algorithms for Critical State Model

Two potential computational schemes for modelling hardening behavior in the critical state model are described in Chapter 5. They are the iterative scheme, and marching scheme by using subincrements of strain, Section 5.3. Although in the current research, the marching scheme is used, a comparison is made between these two schemes by using the two-dimensional procedure. The problem described in Section 8.5, is solved by using these two schemes. Comparison of results is given in Table 8.2, and plotted in Figure (8.7). Iterative scheme seems

Table 8.2
Comparison of Marching and Iterative Schemes
for Critical State Model

Axial Stress (kN/m ²)	Marching Scheme (Axial Strain %)	Iterative Scheme (Axial Strain %)
100	0.0	0.0
115	0.163	0.163
130	0.748	0.533
145	1.72	1.50
160	3.07	2.88
175	4.84	4.70
190	7.14	7.02
205	10.13	9.97
220	14.19	13.85
235	20.24	19.40
250	31.35	29.10

Load increment size = 15 kN/m²

Number of iterations per step = 1

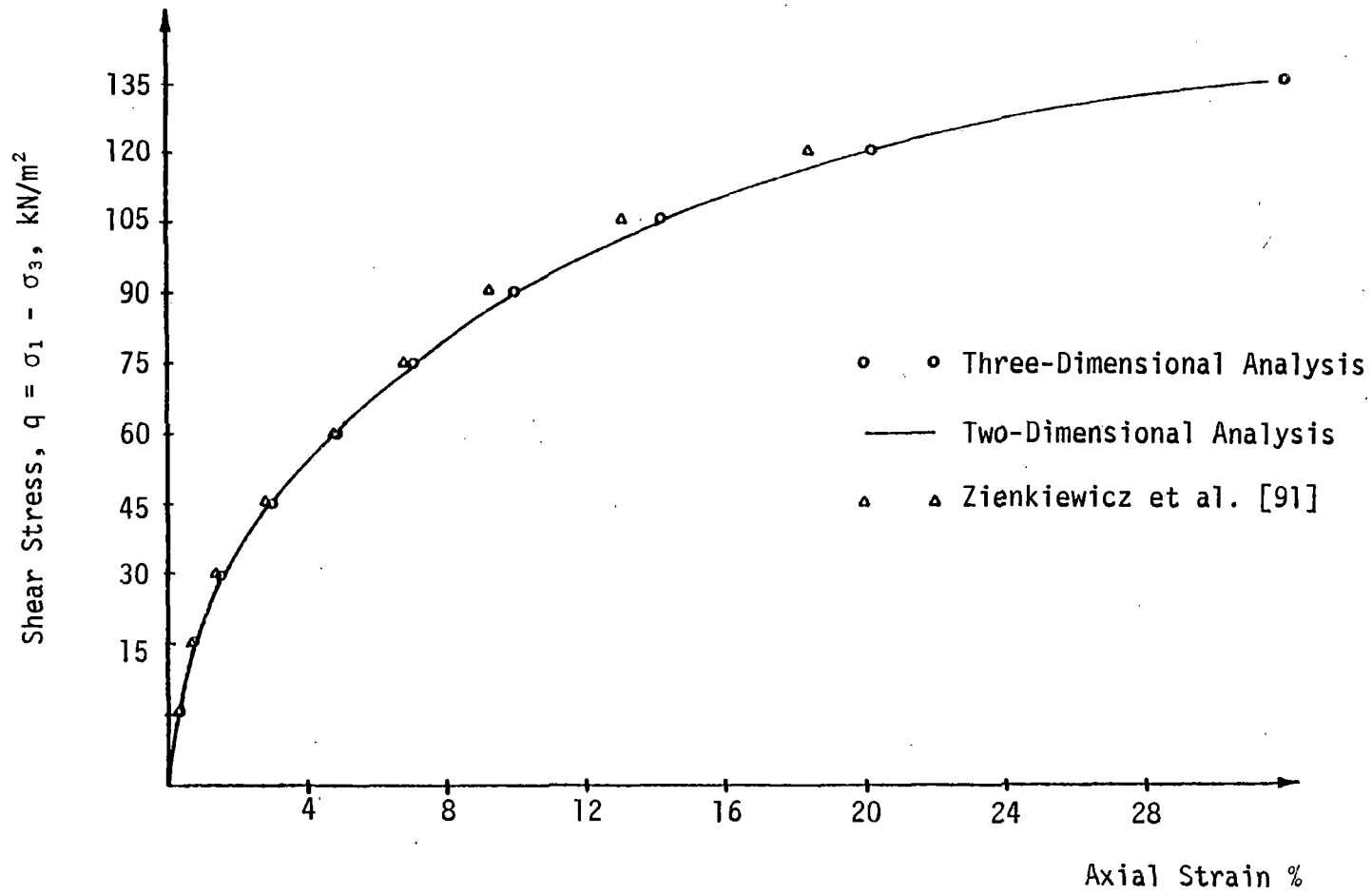


Figure 8.6 Triaxial Test Behavior of Critical State Model

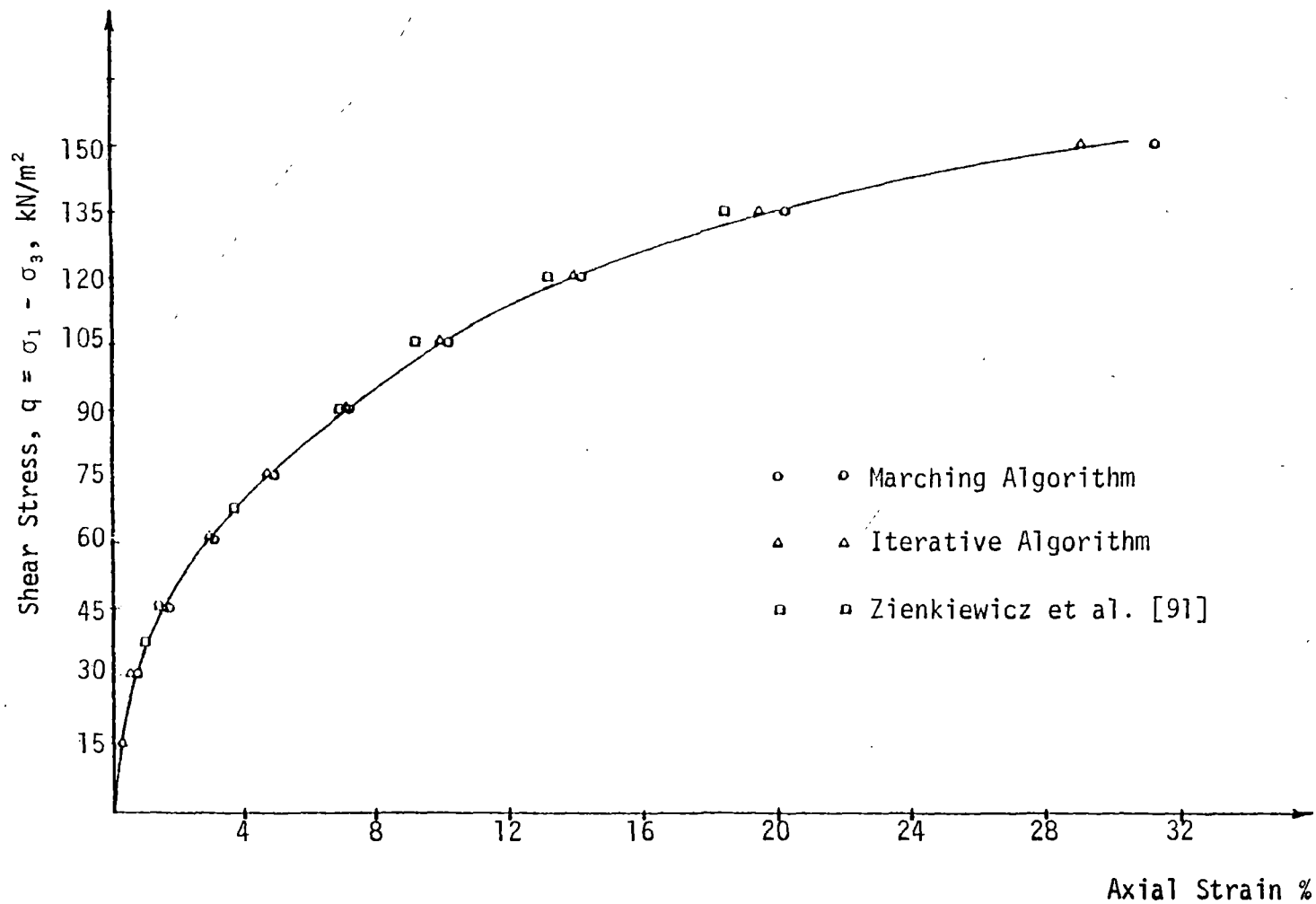


Figure 8.7 Comparison of Two Numerical Schemes for Hardening Models

to give a slightly stiffer response, although the differences are not significant, Figure (8.6). Iterative scheme seems to give results which fall between those obtained by marching scheme and the results of Zienkiewicz et al. [91]. However, the differences are not very significant for this problem. Computer time on IBM 3032 taken by the two schemes for the above problem with one element mesh are given below.

Marching scheme:	Compilation time	9.91 seconds
	Total time	99.88 seconds
Iterative scheme:	Compilation time	10.01 seconds
	Total time	93.49 seconds

This also shows that the iterative scheme has a good potential for future use. Its merit has to be further investigated with respect to several boundary value problems before arriving at a final conclusion.

8.7. Footing Test with Critical State Model

The deformation behavior of a strip footing is analyzed by using the critical state model, Chapter 4, in conjunction with the two-dimensional procedure developed herein. This problem has also been solved by Naylor and Zienkiewicz [57] and the material properties for this analysis were obtained from this reference.

In situ stresses are first calculated using the load vector due to body forces; initial elastic properties are used for this analysis. Since the void ratio and the maximum past pressure, p_0 , varied with depth, the total depth is divided into five element layers, Figure (8.8a), and different properties for void ratio, and p_0 are assigned for each layer.

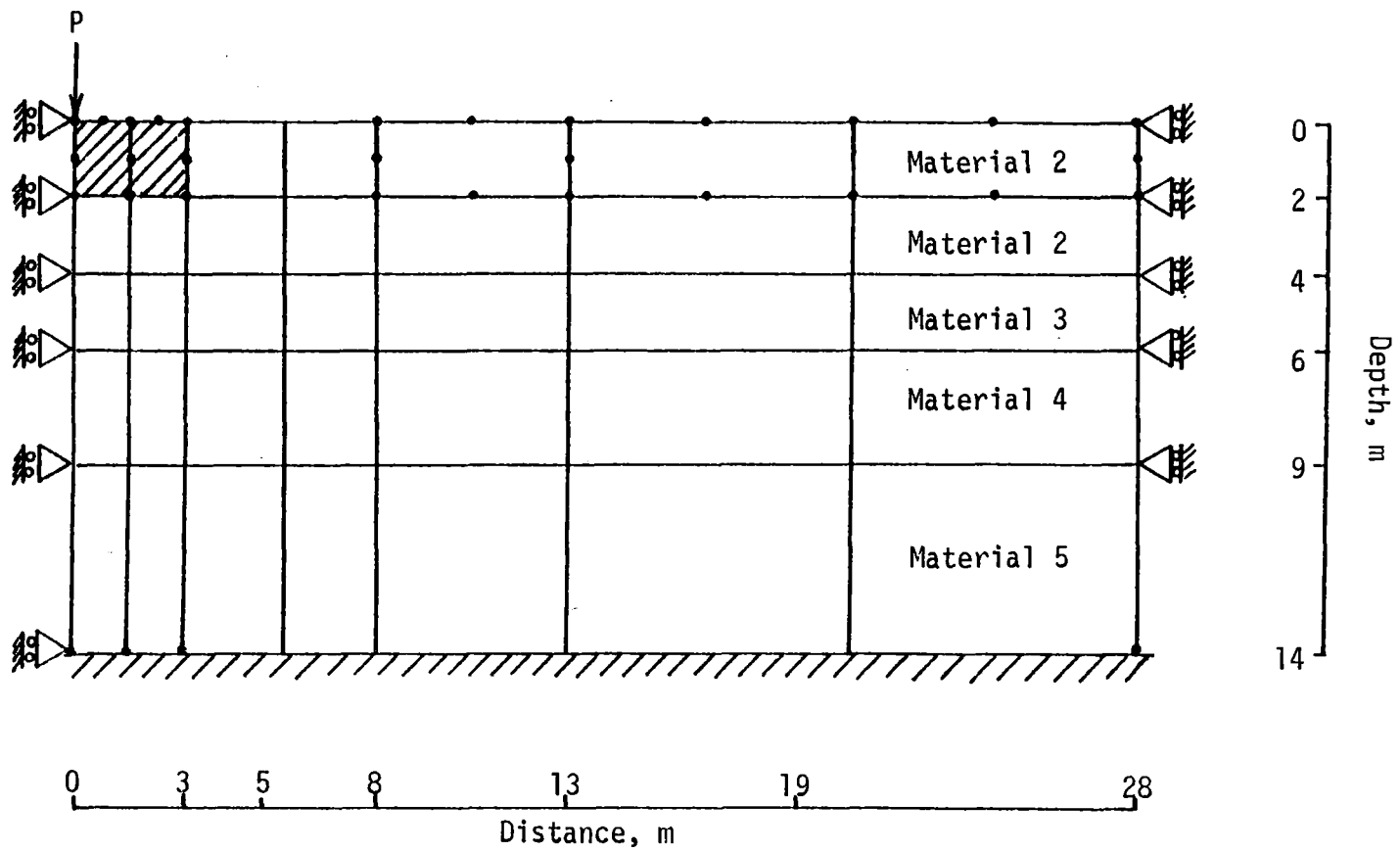


Figure 8.8a Finite Element Mesh for Strip Footing Analysis with Critical State Model

The following material properties are used [57].

Soil:

$$\gamma = 12.5 \text{ kN/m}^3$$

$$M = 1.0$$

$$\lambda_c = 0.174$$

$$\kappa = 0.026$$

$$K_0 = 1.0$$

$$E_0 = 10000.0 \text{ kN/m}^2$$

The following additional properties are used for each layer

<u>Layer</u>	<u>Void Ratio</u>	<u>p_0 (kN/m²)</u>
1	1.15	70.0
2	1.15	70.0
3	1.12	100.0
4	1.08	125.0
5	1.00	175.0

Structure:

$$E = 200,000.00 \text{ kN/m}^2$$

$$\nu = 0.3$$

$$\gamma = 12.5 \text{ kN/m}^2$$

where γ is the unit weight, K_0 is the coefficient of earth pressure, and E_0 is the initial value of Young's modulus used for insitu stress calculation. Since the material deforms elasto-plastically, the calculation of stresses normal to the plane may require the use of $[C^{ep}]$, Equation (4.55), as shown below.

$$\begin{Bmatrix} d\sigma_{xx} \\ d\sigma_{yy} \\ d\tau_{xy} \\ d\sigma_{zz} \end{Bmatrix} = [C^{ep}] \begin{Bmatrix} d\varepsilon_{xx} \\ d\varepsilon_{yy} \\ d\gamma_{xy} \\ 0.0 \end{Bmatrix} \quad (8.3)$$

However, under elastic states, $d\sigma_{zz}$ can be calculated from:

$$d\sigma_{zz} = \nu(d\sigma_{xx} + d\sigma_{yy}) \quad (8.4)$$

The above problem is solved by using both procedures described in Equations (8.3) and (8.4), and results are shown in Figure (8.8b). Both the rigorous, Equation (8.4), and simplified, Equation (8.4), procedures for calculating σ_{zz} seems to give similar results. Comparison with the results given by Naylor et al. [57] is very good. A typical pattern of displacement vectors is given in Figure (8.9) at a footing load of 300 kN. Further comments on these two procedures, Equations (8.3) and (8.4), are given in Chapter 9.

8.8 Beam-Bending, Three-Dimensional Analysis

A problem of cantilever beam subjected to end loads is analyzed by using the three-dimensional procedure with elastic properties. Since bending effects need to be simulated with regular solid elements, a 20-node brick elements with three integration points are used herein. The finite element mesh used is shown in Figure (8.10a). A uniform load is applied at the end of the beam, and it is distributed to the nodes as shown in Figure (8.10b).

The following material properties are used

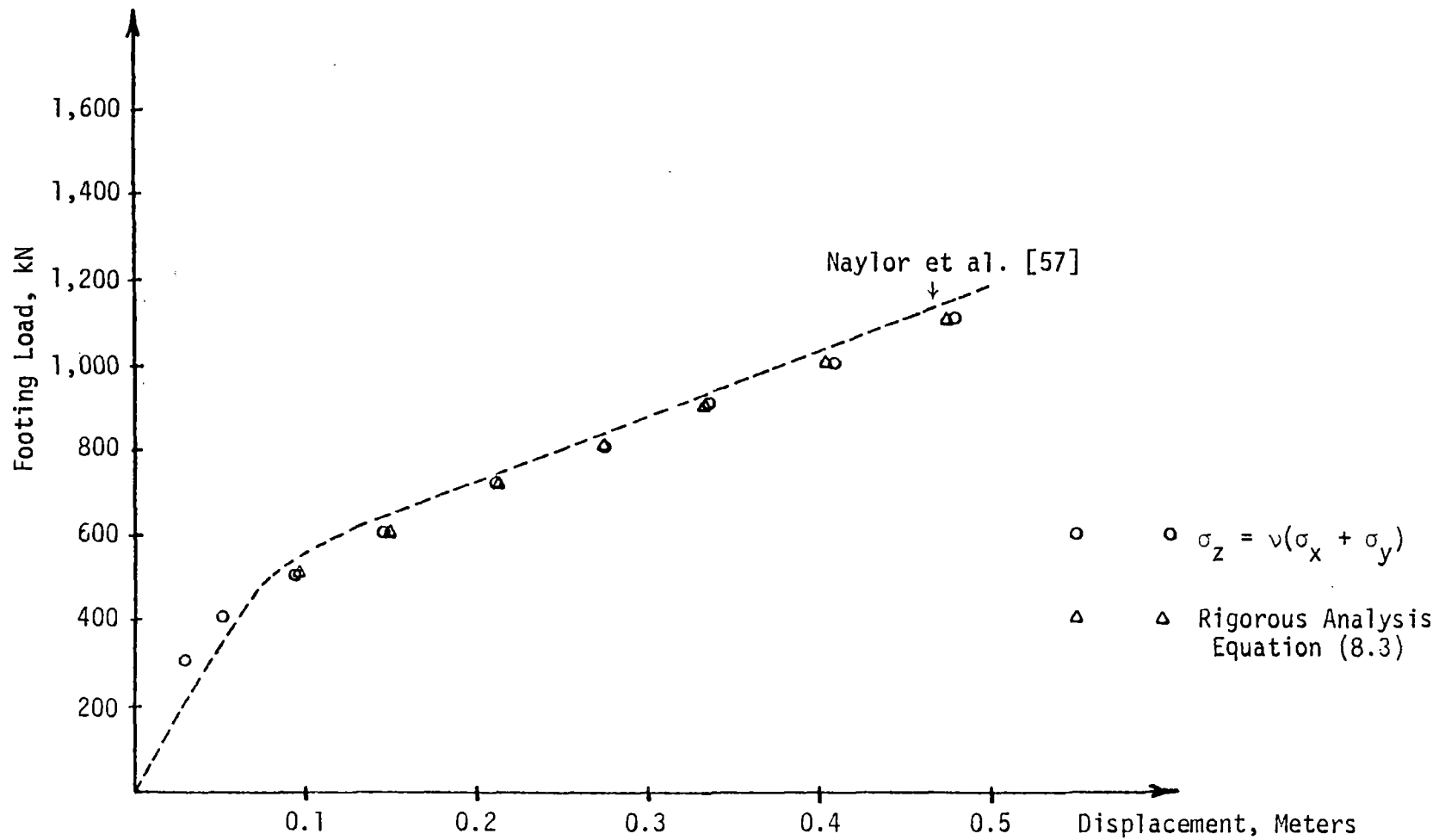


Figure 8.8b Prediction of Footing Displacements with Critical State Model

At $P = 300 \text{ kN}$

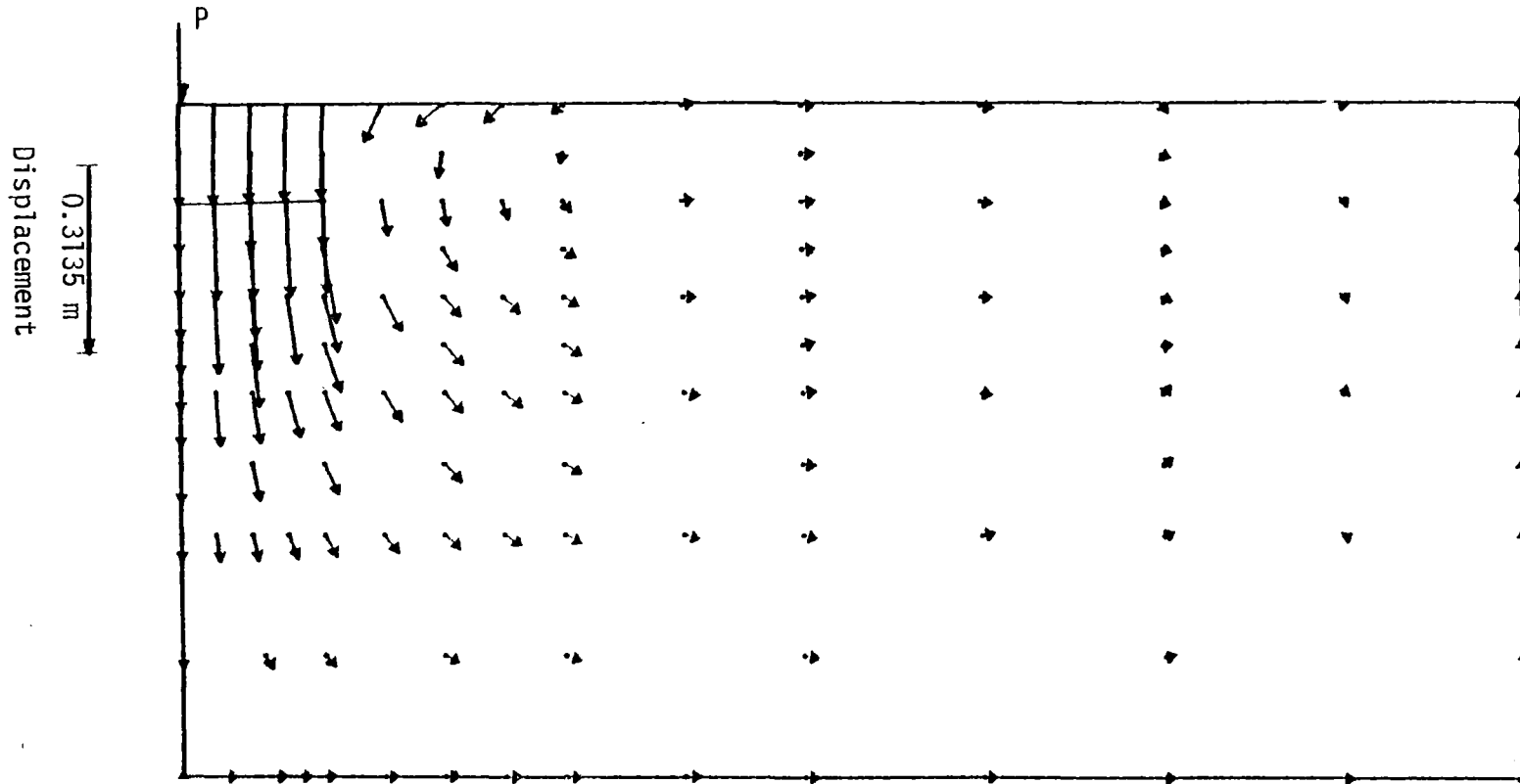
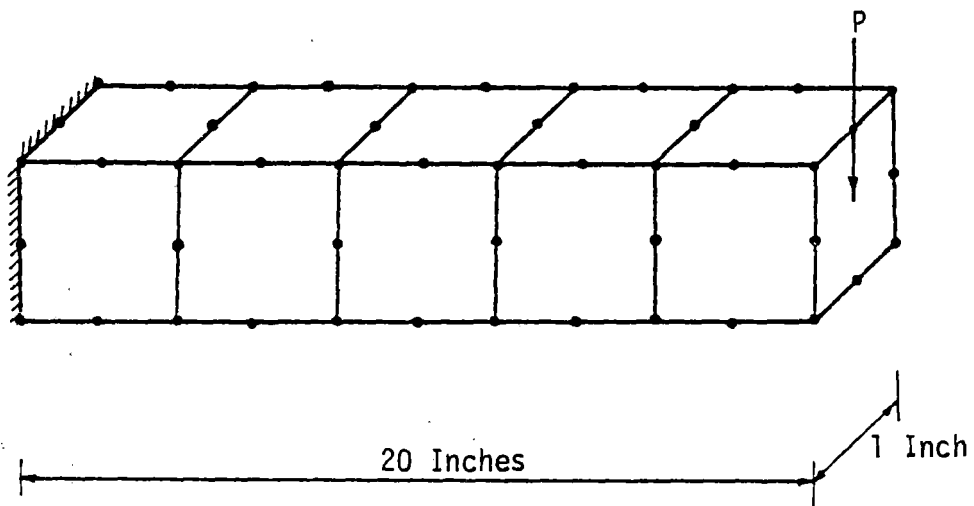
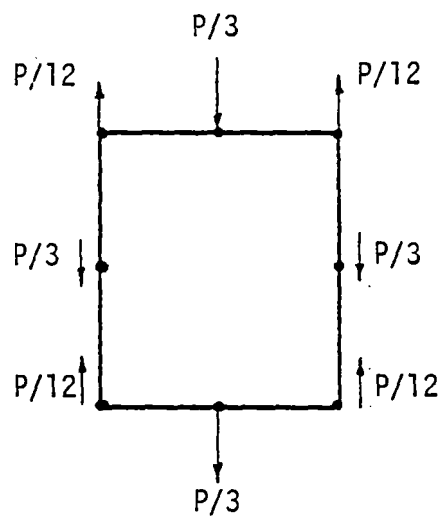


Figure 8.9 Displacement Field from a Strip Footing Analysis



(a) Finite Element Mesh for Beam Bending Analysis

1 Inch = 2.54 cm



(b) Equivalent Loading System

Figure 8.10 Three-Dimensional Analysis of Beam Bending

$$E = 20 \times 10^5 \text{ psi } (13.78 \times 10^6 \text{ kN/m}^2)$$

$$\nu = 0.30$$

The finite element predictions are compared in Figure (8.11) with the closed-form solution given by Timoshenko and Goodier [84] for pure bending under plane stress conditions. Finite element predictions for the shear stress distribution appear to be close to the exact values; they give satisfactory distribution across the section. The closed-form solution for displacements is given in reference [84] as

$$v = \frac{Px^3}{6EI} - \frac{P\ell^2x}{2EI} + \frac{P\ell^2}{EI} \quad (8.5)$$

Here v is the vertical displacement, ℓ is the length of the beam, EI is the flexural rigidity, and x is the distance measured from the free end. Predictions of normal stress and displacements seem to compare very well with the closed-form solution.

8.9 Cap Model: Two- and Three-Dimensional Analysis

Since there is a general lack of previously solved problems in two- and three-dimensional analysis with the cap model, the accuracy is verified with respect to the analysis of a test specimen which is subjected to a triaxial state (conventional) of stress. The finite element meshes with one element used in the analysis are shown in Figure (8.3).

The following properties are relevant to an artificial soil reported in references [20,64] are used in the analysis:

$$\alpha = 5.6 \text{ psi } (38.58 \text{ kN/m}^2)$$

$$\beta = 5.6 \text{ psi } (38.58 \text{ kN/m}^2)$$

$$\gamma = 0.062$$

$$R = 2.0$$

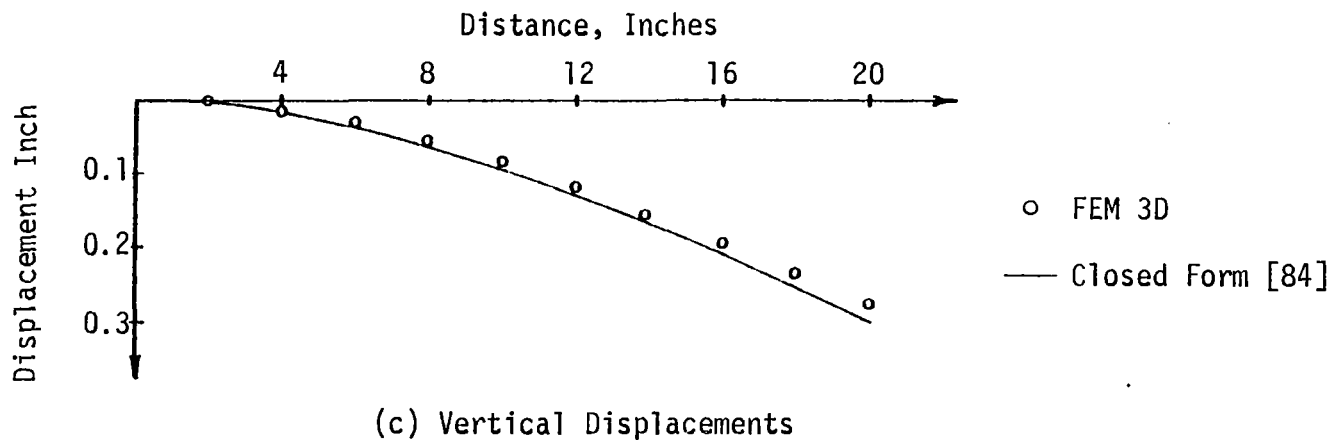
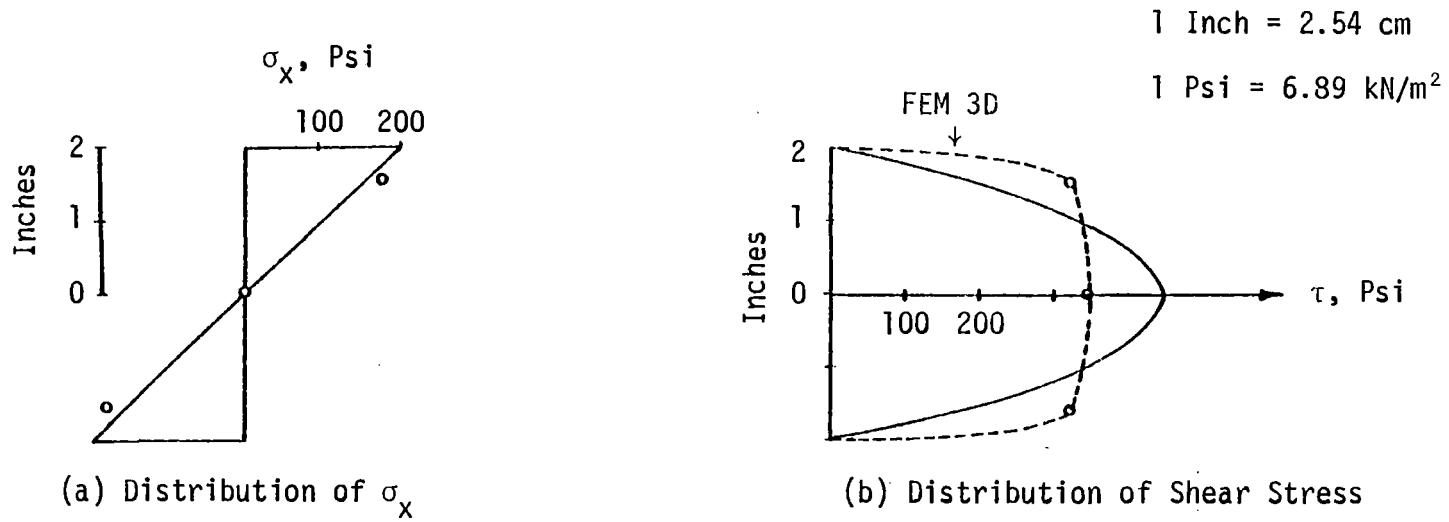


Figure 8.11 Beam Bending Analysis with Three-Dimensional Program

$$D = 0.05 \text{ psi}^{-1} [0.00725 \text{ (kN/m}^2\text{)}^{-1}]$$

$$W = 0.18$$

$$E = 4000.0 \text{ psi (27,560.0 kN/m}^2\text{)}$$

$$\nu = 0.35$$

$$p_0 = 10 \text{ psi (68.90 kN/m}^2\text{)}$$

The analysis is carried out by using increments of 1.0 psi (6.89 kN/m²) with one iteration per increment. Predicted stress-strain curve is shown in Figure (8.12b). Comparison of results from two-dimensional axisymmetric, and three-dimensional analysis, is considered to be very good. The theoretical ultimate strength along the used CTC stress path, Chapter 7, is obtained as shown in Figure (8.12a). The ultimate value of $\sqrt{J_{2D}}$ is 5.1 psi (35.14 kN/m²), Figure (8.12a). This value seems to compare very well with the finite element predictions of ultimate states as shown in Figure (8.12b).

8.10 Interface Behavior

In order to study the interface behavior, a simple plane strain problem is solved. Two elements with an interface in between is loaded with a nonuniform load as shown in Figure (8.13).

The following properties are used in the analysis.

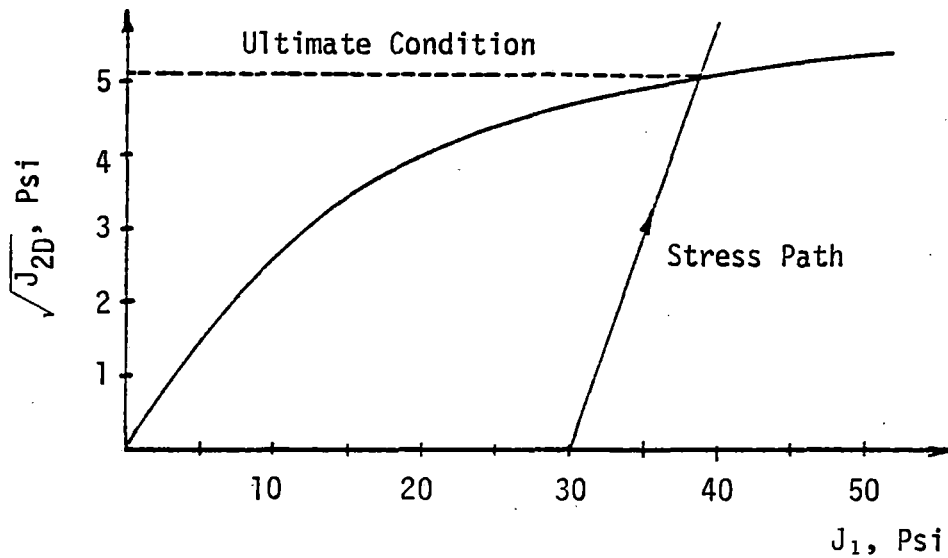
Interface:

$$\text{Thickness of interface} = 0.1 \text{ inch (0.254 cm)}$$

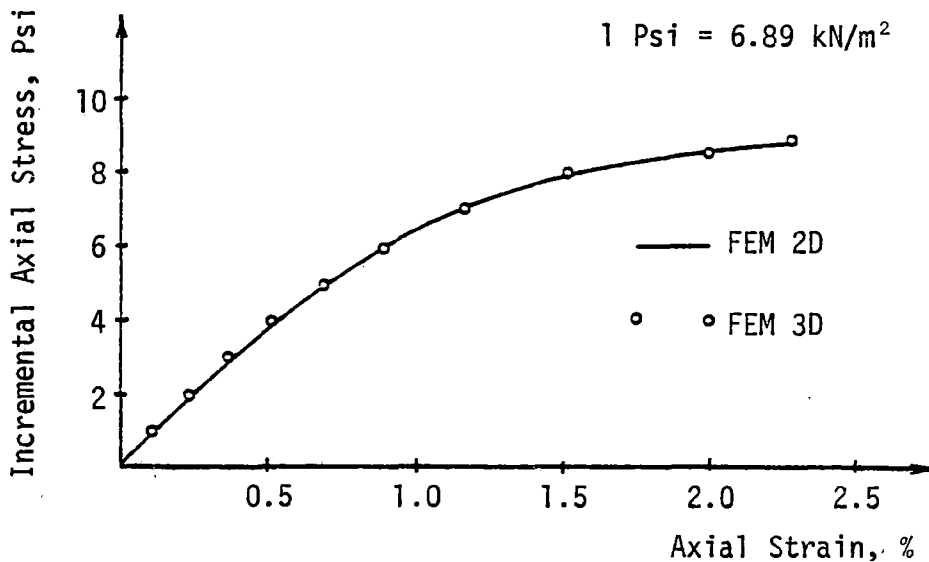
$$E_{\text{int}} = 10000. \text{ psi (68.9} \times 10^3 \text{ kN/m}^2\text{)}$$

$$\nu_{\text{int}} = 0.30$$

$$G_{\text{int}} = 20 \text{ psi (137.8 kN/m}^2\text{)}$$



(a) Experimental Results and Stress Path Followed in CTC Test



(b) Stress-Strain Behavior

Figure 8.12 Triaxial Test Behavior of Cap Model

1 Inch = 2.54 cm

1 Psi = 6.89 kN/m²

Thickness of Interface = 0.1 Inch

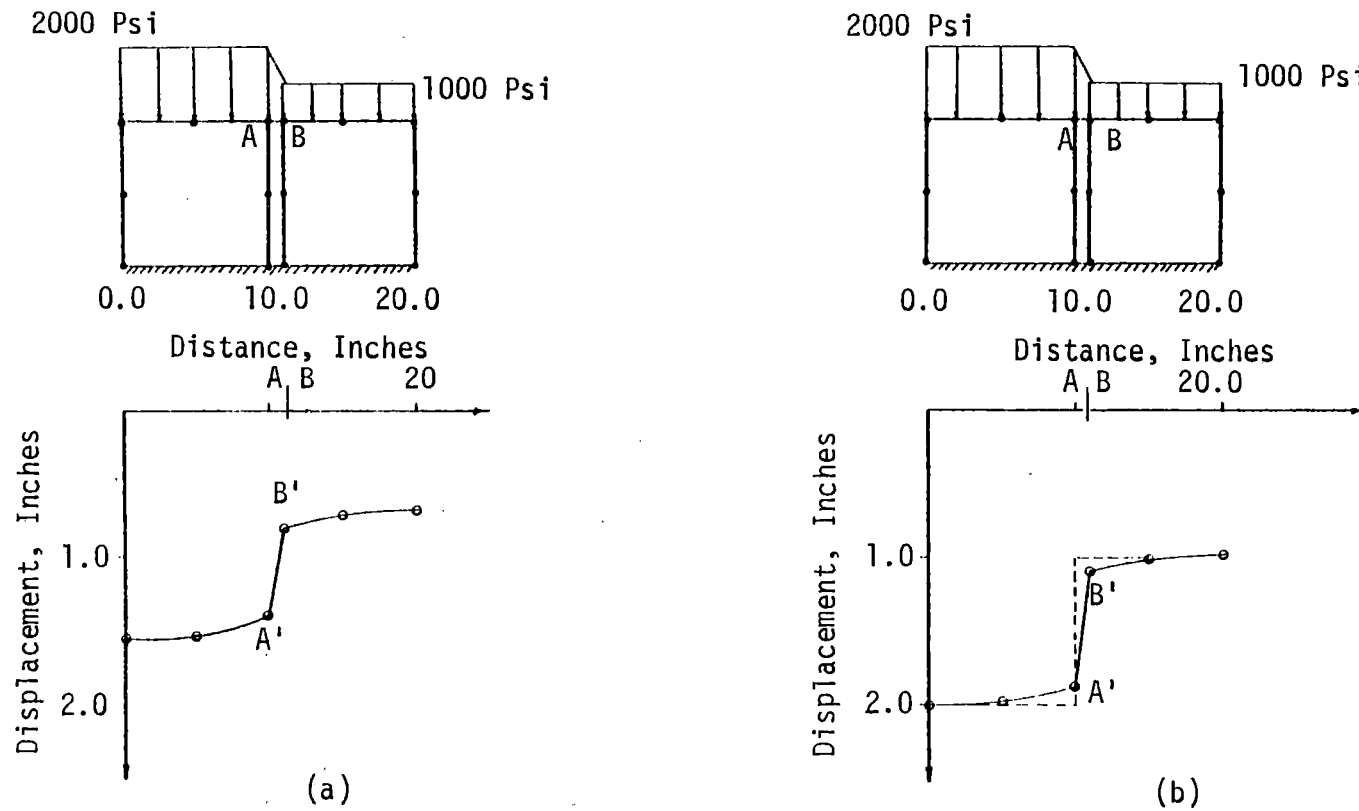


Figure 8.13 Deformation Behavior at an Interface in Plane-Strain Conditions

Solid:

$$E = 10000. \text{ psi } (68.9 \times 10^3 \text{ kN/m}^2)$$

$$\nu = 0.03 \text{ for example (a)}$$

$$\nu = 0.0 \text{ for example (b)}$$

Details of loading are shown in Figure (8.13). Since, the loading intensity on the two solid elements is different, a relative displacement can be expected. Presence of interface element allows relative displacements as shown in Figure (8.13a) and (8.13b). A closed-form solution can be obtained for the case when $\nu = 0.0$, Figure (8.13b). For this case, the finite element predictions of relative displacements seem to be in good agreement with the theoretical values, Figure (8.13b).

The improvement of relative displacements obtained by using the interface element is demonstrated in Figure (8.14). In this figure, A and B are two points across the interface before deformations. With the interface, points A and B move to A' and B', respectively. Without the interface, A and B move to A'' and B'', respectively. The performance of this element appears to be satisfactory. Effect of normal interface stiffness on the deformation behavior is studied by varying the elastic modulus, E, of the interface element. Figure (8.15) shows that the normal stiffness has negligible effects on the relative displacement between the solid elements.

A three-dimensional problem is analyzed, Figure (8.16), by using the same properties used for two-dimensional cases. As could be seen in Figure (8.16), the interface element permits relative displacements between the solid elements. Here the points A and B, move to A' and B',

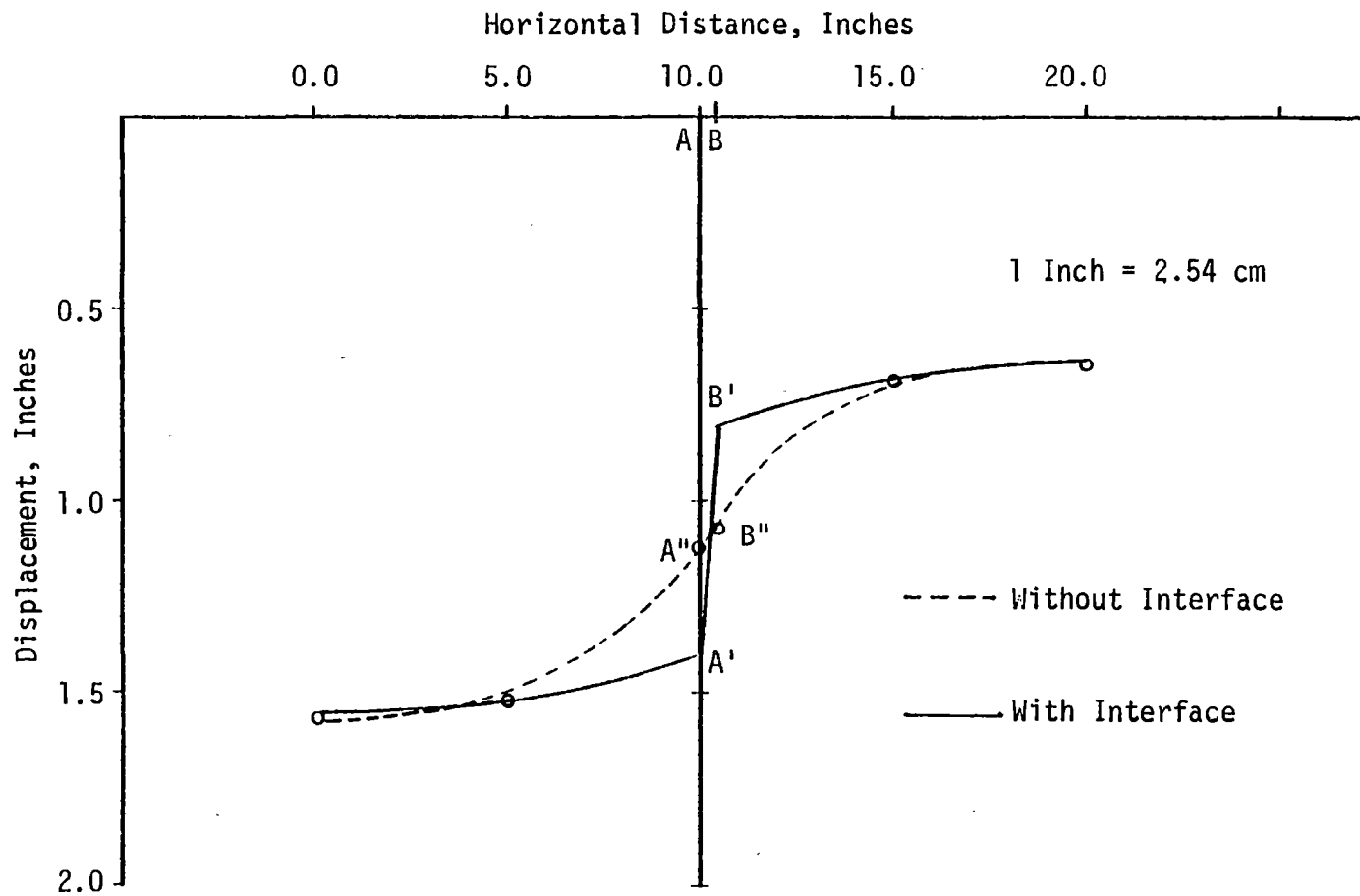


Figure 8.14 Relative Displacements Across an Interface Element

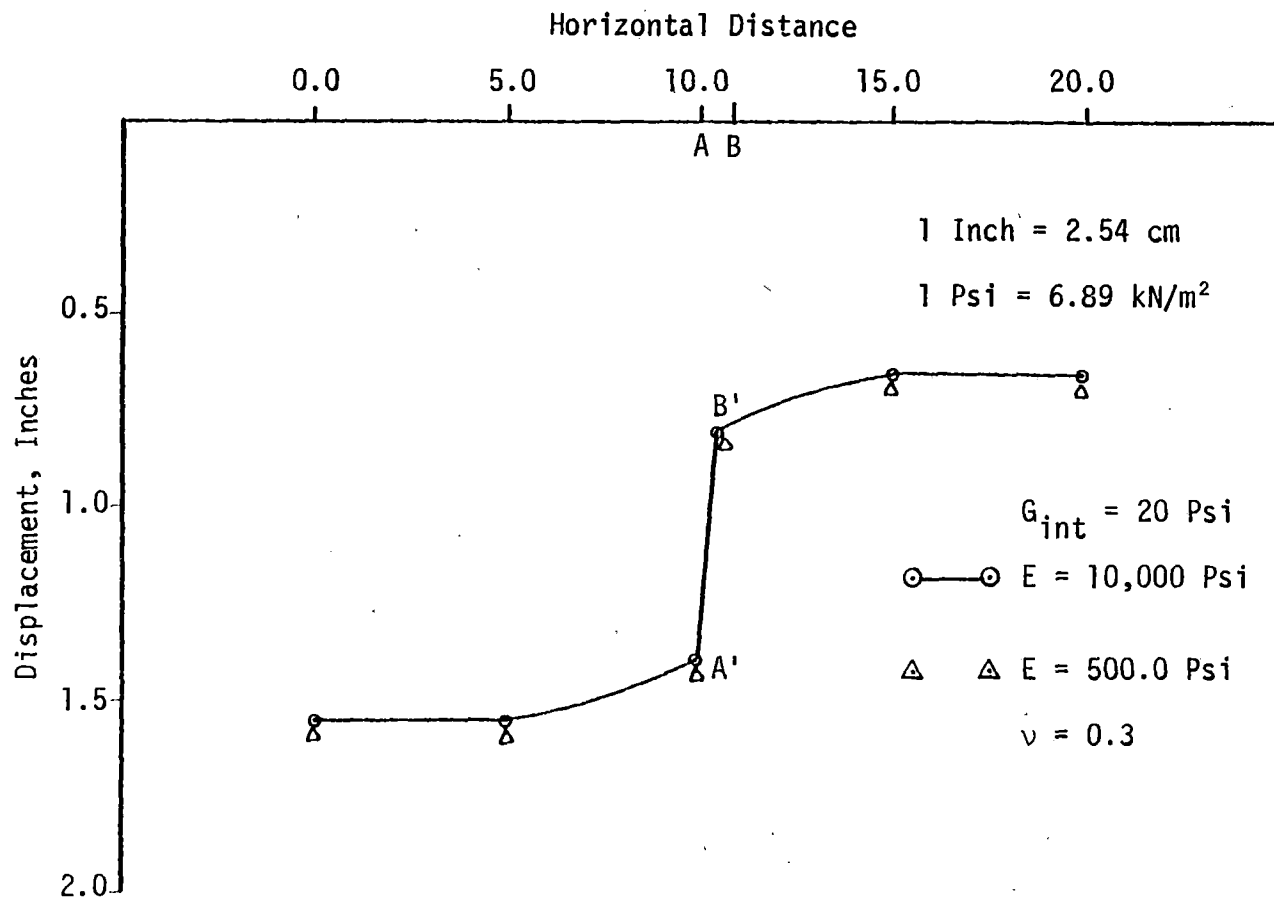


Figure 8.15 Effect of Interface Normal Stiffness on the Deformation Behavior

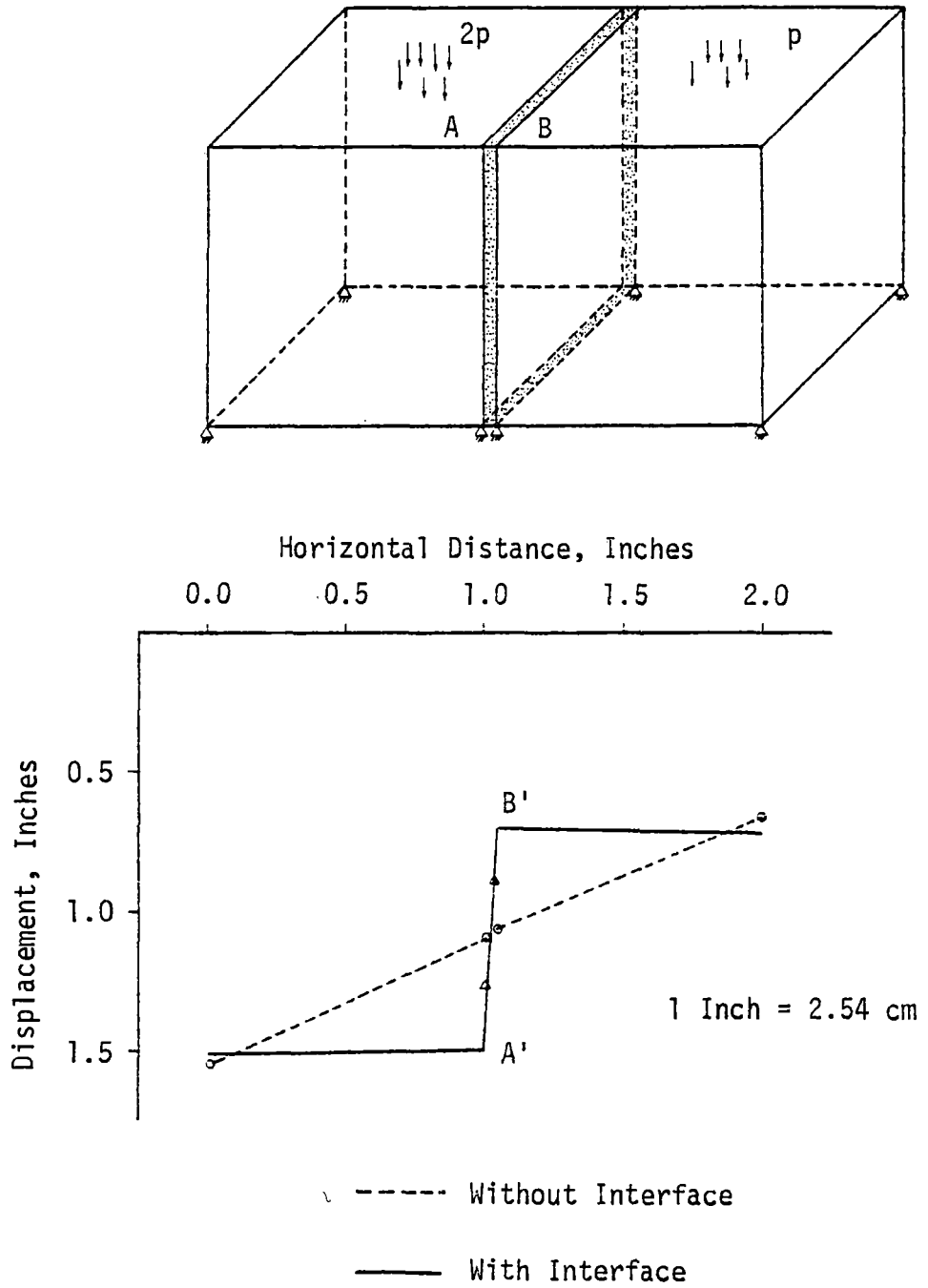


Figure 8.16 Performance of the Three-Dimensional Interface Element

during deformations, respectively. Effects of normal interface stiffness is seen to have negligible effects on relative displacements similar to the two-dimensional case. However, the interface shear stiffness, G_{int} , seems to have a significant effect on the relative displacements as shown in Figure (8.17).

Effect of interface Poisson ratio is studied by varying this value between 0.00 and 0.5, as shown in Figure (8.17). This seems to have a negligible effect on the relative displacements between the solid elements.

The above study reveals that the element used in the current research can perform satisfactorily both in the two- and three-dimensional analysis.

Three-Dimensional Interface Element

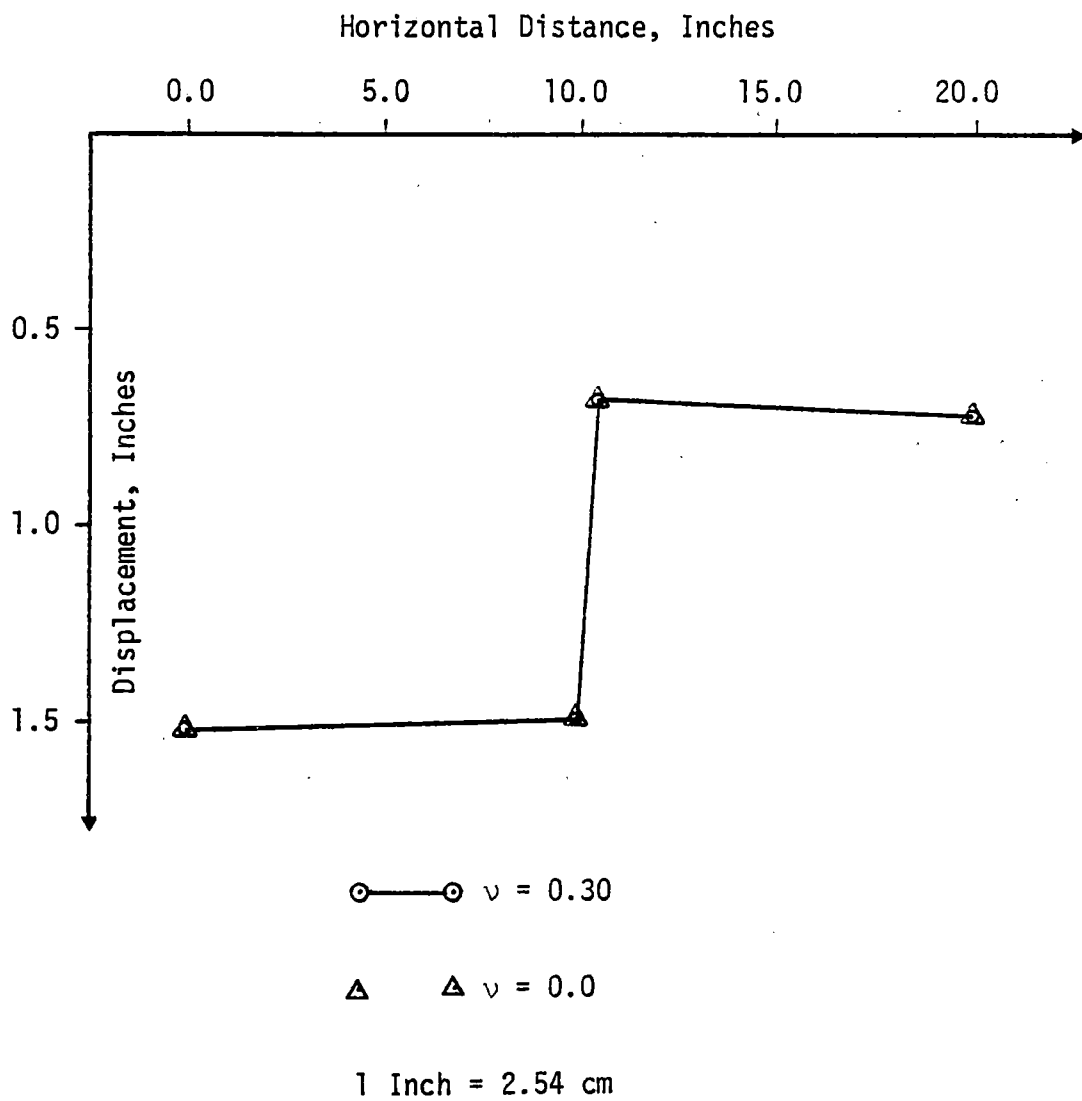


Figure 8.17 Effect of Poisson's Ratio on the Deformations at the Interface

APPLICATIONS TO SOIL-STRUCTURE INTERACTION PROBLEMS

As discussed previously, the purpose of this research is to develop computational procedures for studying nonlinear soil-structure interaction problems. Underlying theoretical foundation is given in the previous chapters. The three computer codes developed in this study are verified with respect to a few problems in Chapter 8. In this chapter, three additional problems are studied to show the applications of the procedures developed. Analysis of one of the problems is verified with respect to experimental data available.

9.1. Analysis of a Footing-Soil System

As an application of the procedures developed herein, nonlinear behavior of a strip footing is studied. A plane strain analysis is carried out by using the two-dimensional code, Chapter 3, with different constitutive models such as linear elastic, variable moduli, Drucker-Prager, critical state and cap models, Chapter 4. Soil-structure interaction behavior is studied by using the interface element described in Chapter 6.

Selection of the Finite Element Mesh

Unlike linear problems, the nonlinear finite element analysis usually includes incremental and iterative techniques. Here, the nonlinear problem is solved by considering a series of piecewise linear problems. Therefore, the computational effort involved in a nonlinear analysis depends on the number of times the linear problem is solved. Most of the computational effort is involved in the solution

of equilibrium equations. However, a considerable amount of effort is also involved in the computation of global stiffness matrix. Hence, the number of degrees of freedom, and the number of elements have to be minimized in view of the computational effort involved in a nonlinear analysis.

Two finite element grids are investigated with respect to accuracy in linear analysis. Corresponding dimensions for the coarse and finer meshes are shown in Figures (9.1) and (9.2), respectively. Following material properties are used.

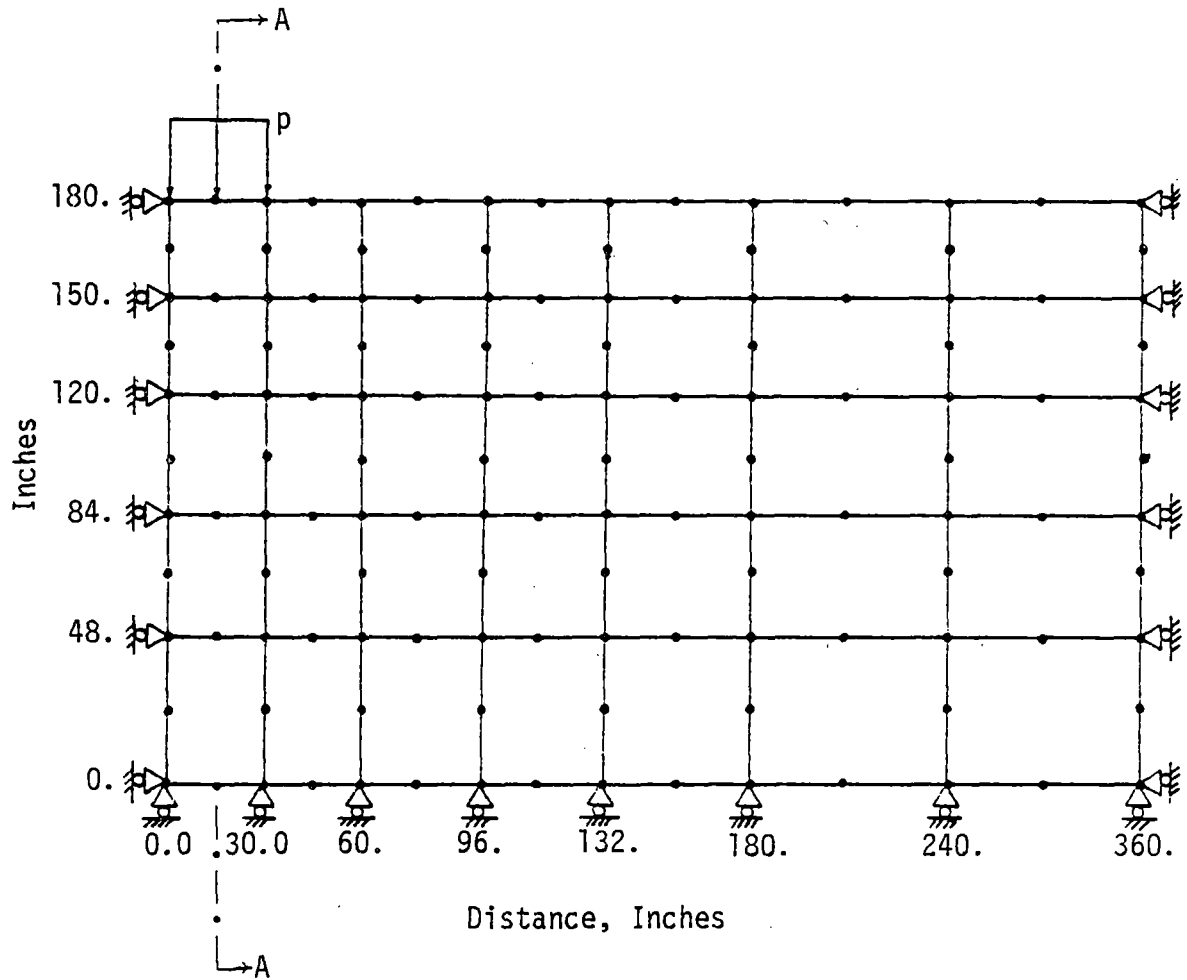
$$E = 10,000 \text{ psi } (69.0 \times 10^3 \text{ kN/M}^2)$$

$$\nu = 0.30$$

A footing load of 40.0 psi (276.0 kN/M²) is applied over a semi-width of 30 inches (76.2 cm), and the displacements obtained by using the coarse and finer meshes are compared in Table 9.1. A comparison of stress distribution is shown in Figure (9.3). These results reveal that the use of coarse mesh in Figure (9.1) is acceptable for purposes of further studies of the behavior.

Constrained Three-Dimensional Analysis

In the foregoing section, a truly two-dimensional finite element procedure is employed to model the plane strain behavior. However, it is also possible to simulate plane strain conditions in a truly three-dimensional analysis by constraining the deformations to one plane. A simulated plane strain (constrained three-dimensional) section, and the finite element mesh is shown in Figure (9.4) Here, constrained



1 Inch = 2.54 cm

Figure 9.1 Finite Element Mesh Used for Analysis of Footing Problem

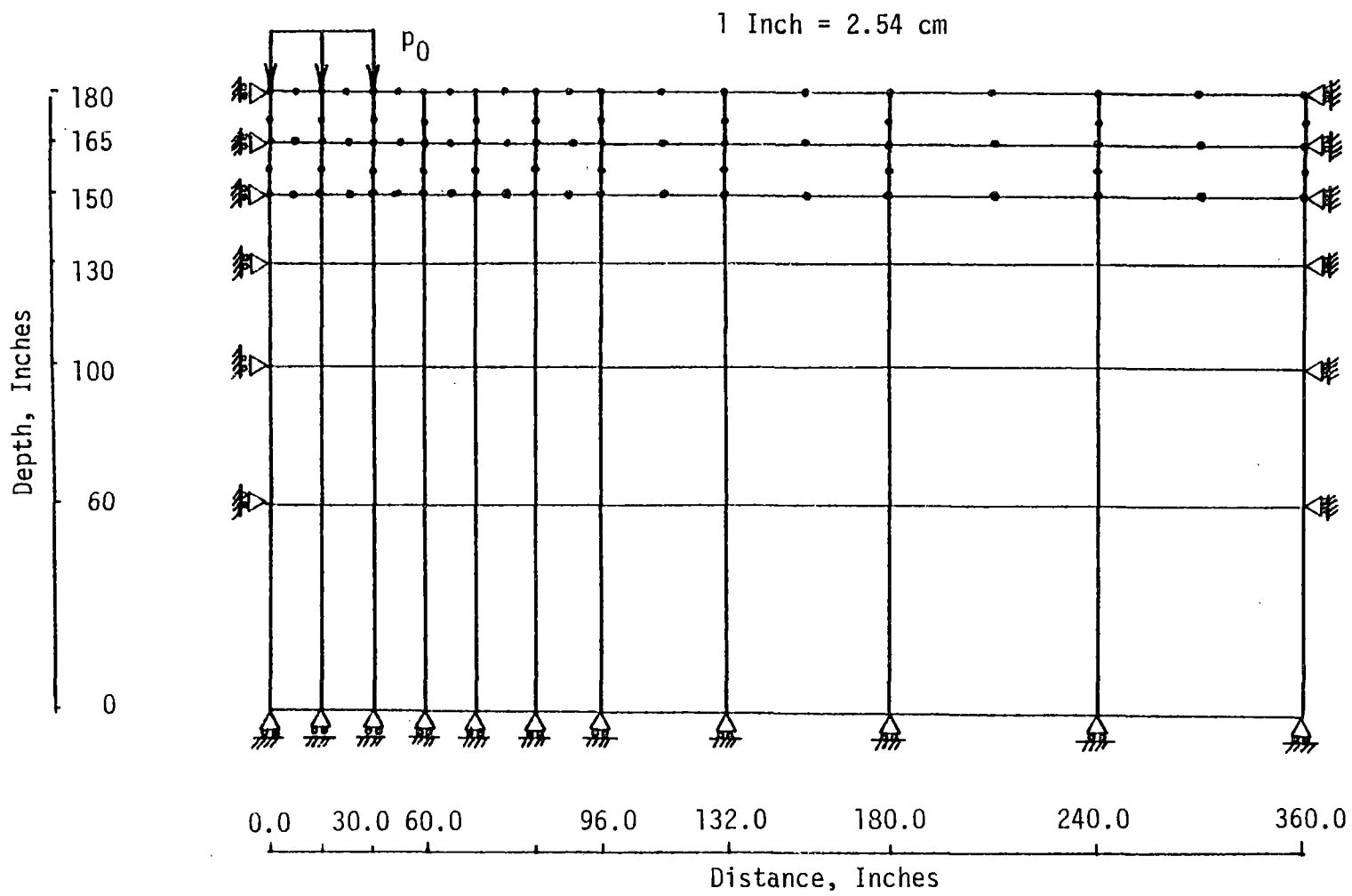


Figure 9.2 Finer Finite Element Used in the Strip Footing Analysis

Table 9.1
 Comparison of Coarse and Finer Meshes
 with Respect to Surface Displacements

Distance from Center Line (Inches)	Vertical Displacement Finer Mesh (Inches)($\times 10^{-1}$)	Vertical Displacement Coarse Mesh (Inches)($\times 10^{-1}$)
0.0	-4.6625	-4.6548
30.0	-4.339	-4.3277
60.0	-2.8822	-2.8835
96.0	-1.1436	-1.1576
132.0	-0.4323	-0.4373
180.0	-0.0386	-0.0391

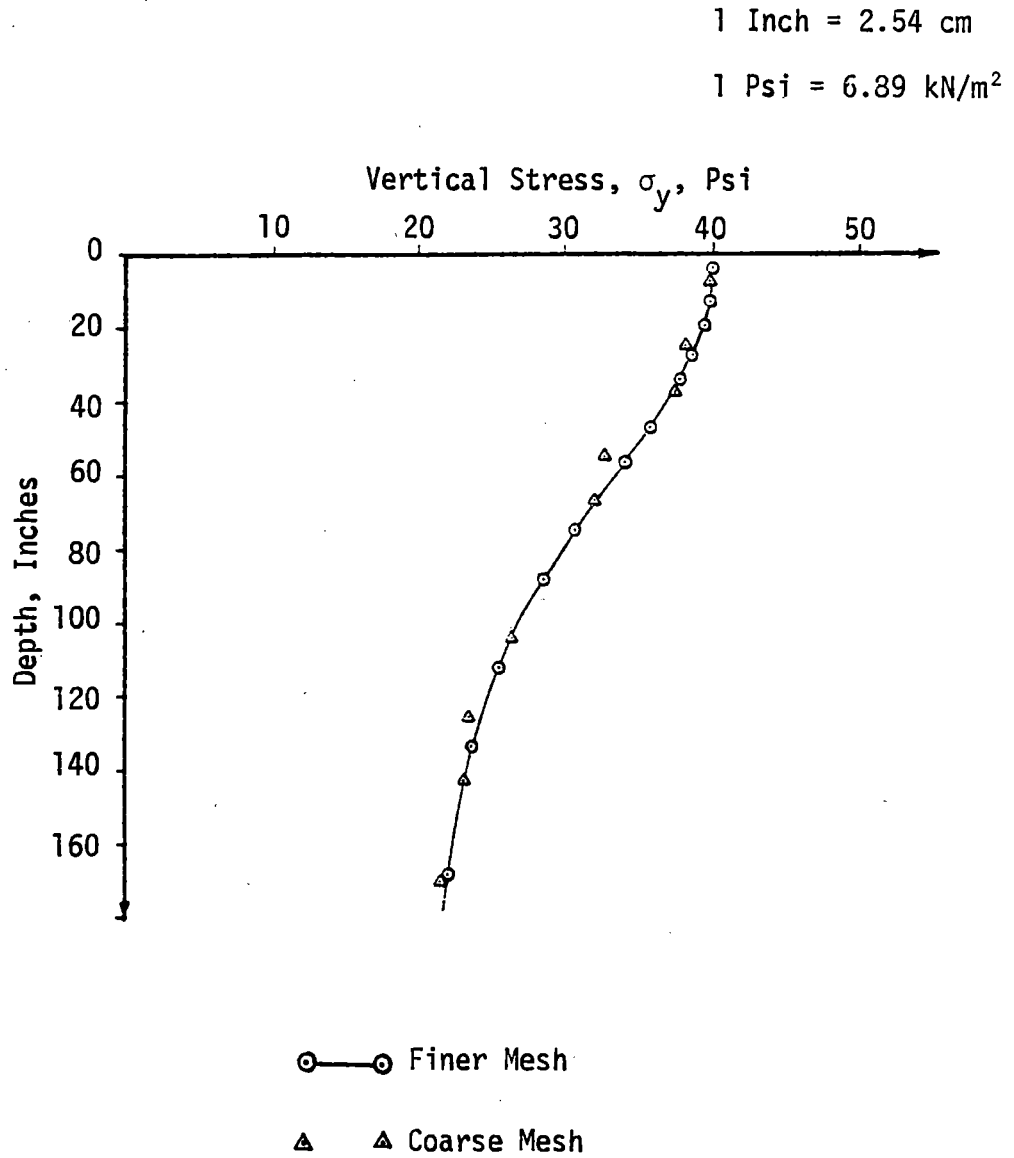


Figure 9.3 Comparison of Predicted Stress Distributions from Finer and Coarse Finite Element Meshes

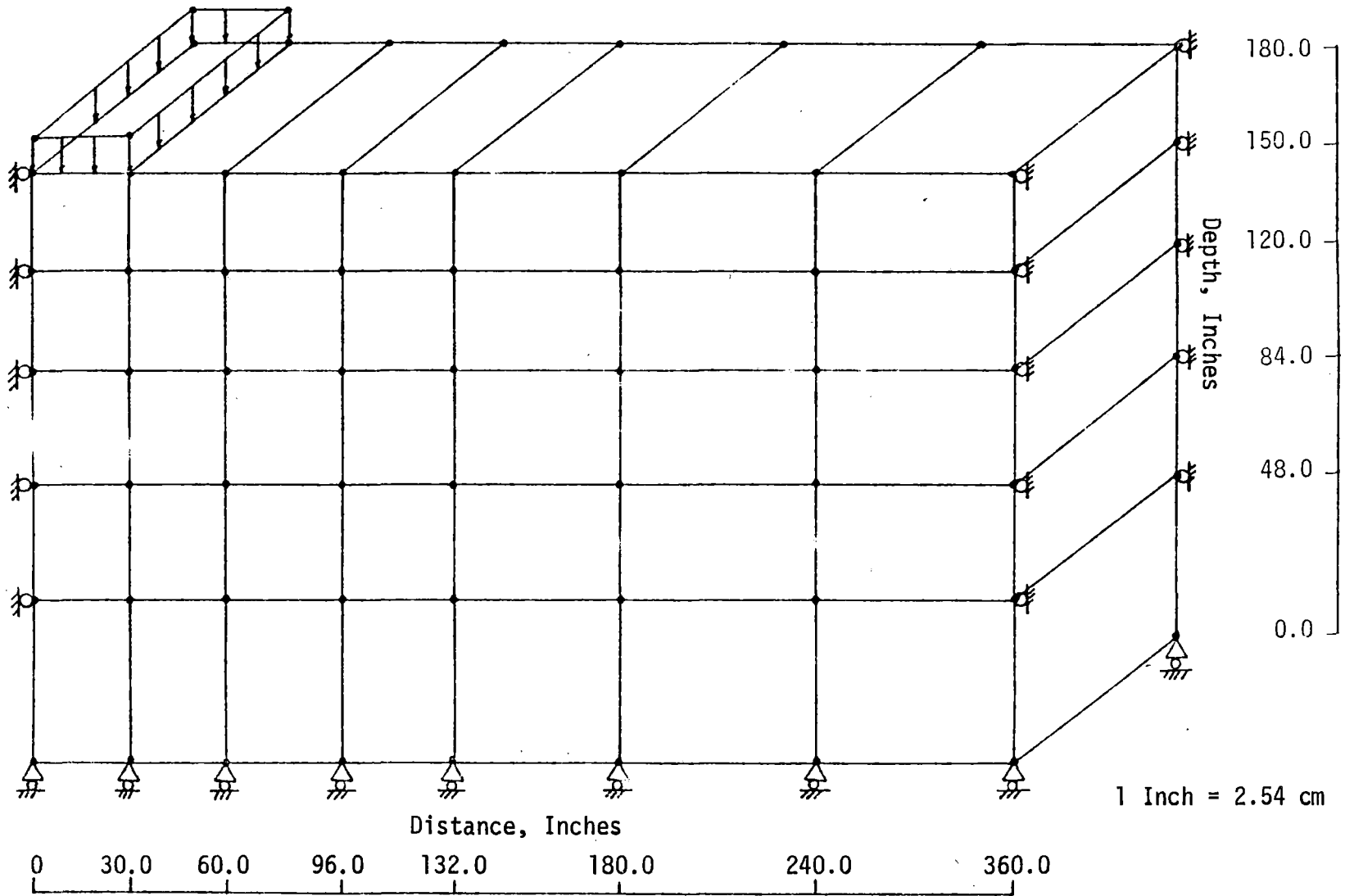


Figure 9.4 Plane Strain Analysis Using a Three-Dimensional Procedure (Simulated Plane Strain)

three-dimensional analysis is carried out by using 8-node brick and 16-node brick elements; this gives the same degrees-of-freedom in the plane of deformation. In the constrained analysis, 8-node bricks simulate 4-node plane elements, while the 16-node bricks simulate 8-node plane elements. The cross section of this three-dimensional finite element mesh in the x-y plane is analogous to the truly two-dimensional mesh shown in Figure (9.1). The idea of having the same geometry is to compare the predictions from truly two-dimensional, and the simulated two-dimensional analysis.

A plane strain flexible footing problems is analyzed using two- and three-dimensional procedures by using the following material properties for the soil.

$$E = 10,000 \text{ psi } (69.0 \times 10^3 \text{ kN/M}^2)$$

$$\nu = 0.3$$

A comparison of displacements and stresses from the above analysis is given in Table (9.2). This shows that the three-dimensional procedure with 8-node bricks predicts a somewhat stiffer response. Stresses predicted by using 8-node bricks seem to be different by about 12.0% in the element just below the loading.

It can be thought that a nonlinear analysis of this problem with 8-node brick elements can predict significantly different deformations since the behavior is highly stress dependent. In order to study these factors, a nonlinear analysis is carried out.

Nonlinear Analysis of Strip Footing

Nonlinear problem of strip footing is studied by using several

Table 9.2
Comparison of Plane-Strain and Constrained
Three-Dimensional Analysis

<u>(a) Displacements</u>			
Depth Along the Center Line(Inches)	<u>Plane Strain</u>	<u>Constrained Three-Dimensional</u>	
	8-Node Element	8-Node Brick	16-Node Brick
0.0	0.3258	0.3235	0.3256
30.0	0.3569	0.2347	0.2457
60.0	0.1696	0.1639	0.1694
96.0	0.1060	0.1030	0.1058
132.0	0.0566	0.0552	0.0565
180.0			
<u>(b) Vertical Stresses</u>			
Average Depth Along A-A (Inches)	<u>Plane Strain</u>	<u>Constrained Three-Dimensional</u>	
	8-Node Element	8-Node Brick	16-Node Brick
165.0	33.82	29.73	33.80
135.0	23.91	21.96	23.90
102.0	17.54	16.46	17.53
66.0	13.80	13.21	13.80
24.0	12.01	11.61	12.00

constitutive models, Chapter 4, and the comparison of results obtained from two-, and three-dimensional analysis are shown in Figures (9.5) to (9.9).

Figure (9.5) shows the load-deformation curve obtained by using the Variable Moduli model, Equation (4.7). Following properties are used with the Variable Moduli model [60].

$$E = 10,000.0 \text{ psi } (690.0 \times 10^3 \text{ kN/M}^2)$$

$$\nu = 0.3$$

$$K_1 = -8.33 \times 10^5 \text{ psi } (57.48 \times 10^5 \text{ kN/M}^2)$$

$$K_2 = 3.33 \times 10^5 \text{ psi } (57.48 \times 10^5 \text{ kN/M}^2)$$

$$\gamma_1 = 60.0$$

$$\gamma_2 = -133.0$$

$$\text{Initial Pressure, } P_0 = 10.0 \text{ psi } (69.0 \text{ kN/M}^2)$$

Results from a plane strain analysis by using 8-node elements seem to compare well with those obtained by using a constrained three-dimensional procedure with 16-node brick elements. The 8-node bricks in the three-dimensional procedure gives a stiffer response for this problem although the mesh size, number of elements, boundary conditions and the material properties are the same. This is perhaps due to the smaller number degrees-of-freedom available when 8-node bricks are used.

Figure (9.6) shows the results obtained by using the Drucker-Prager model, Equation (4.17). Following results are used with the Drucker-Prager model, Equation (4.17)

$$E = 10,000.0 \text{ psi } (690.0 \times 10^3 \text{ kN/M}^2)$$

$$\nu = 0.3$$

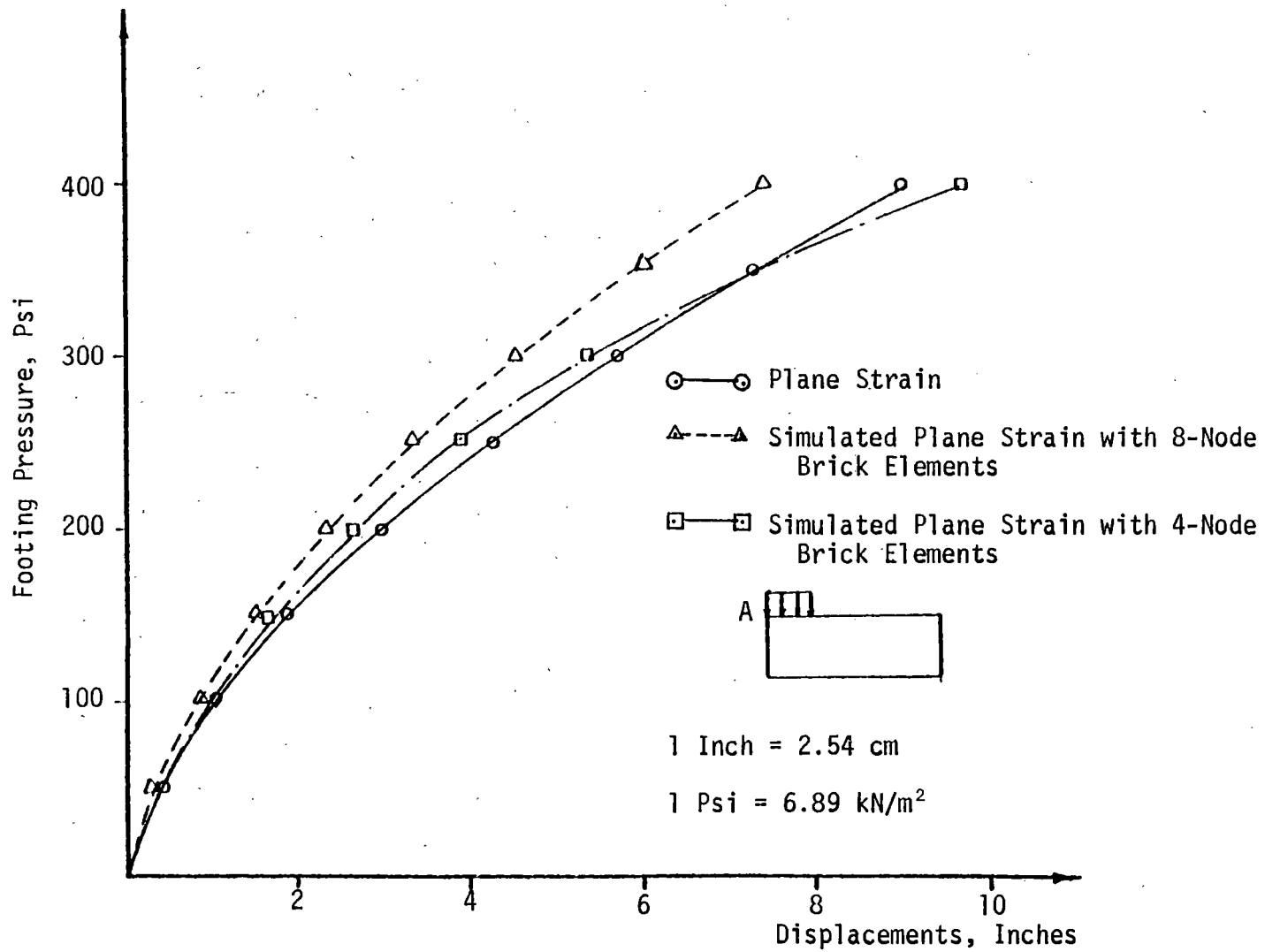


Figure 9.5 Deformation Analysis of a Strip Footing with Variable Moduli Model

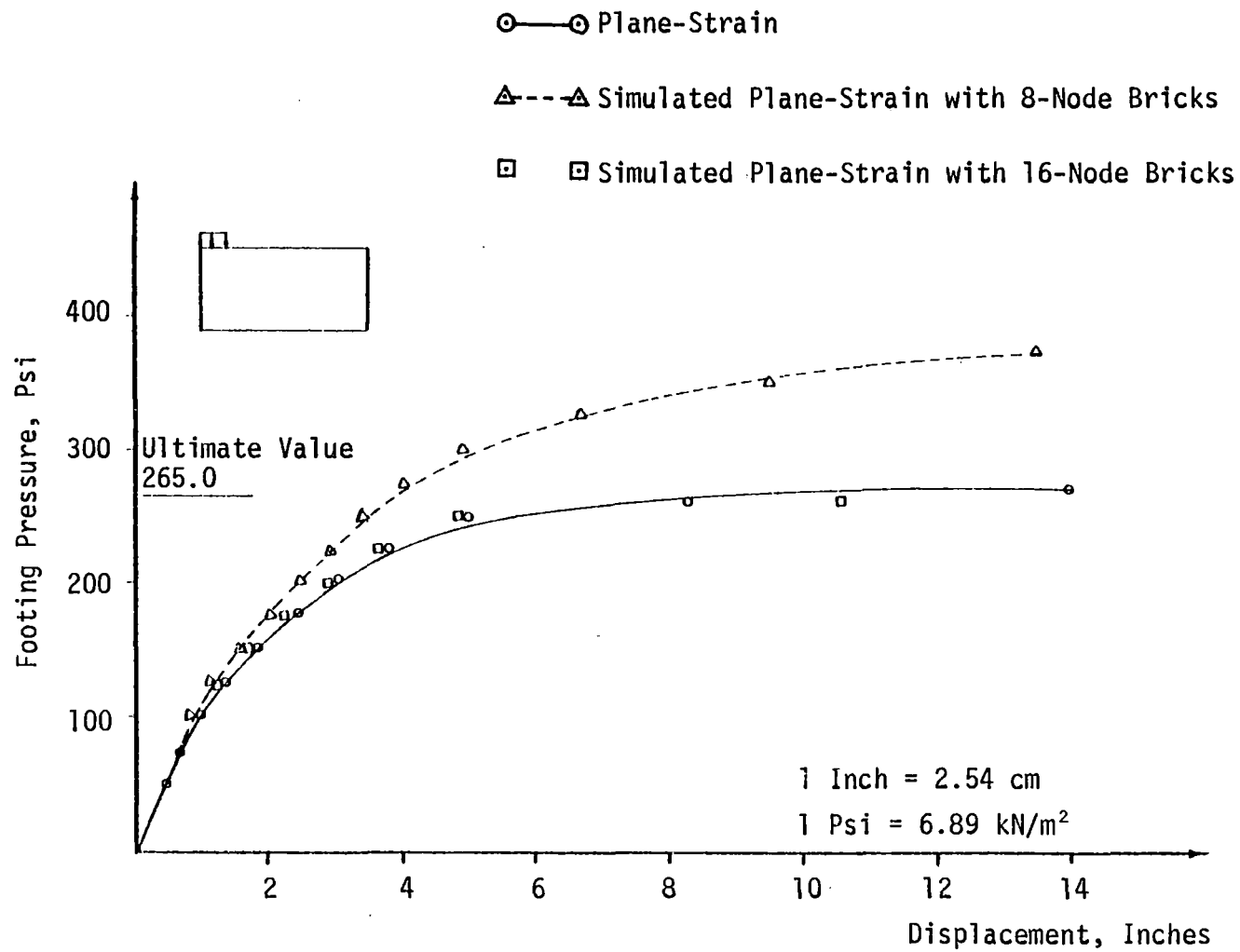


Figure 9.6 Deformation Analysis of a Strip Footing with Drucker-Prager Model

$$C = 15.0 \text{ psi (103.5 kN/M}^2\text{)}$$

$$\phi = 20.0 \text{ degrees}$$

Results obtained by using 8-node quadrilateral elements, seem to compare well with those obtained with 16-node constrained three-dimensional elements. This can be expected since the number of degrees-of-freedom in the plane of deformation is the same for both analyses. Use of 8-node constrained three-dimensional elements seems to give a stiffer response and a higher ultimate value. The ultimate values predicted by using 8-node plane, and 16-node constrained three-dimensional elements, compare well with that obtained from Terzaghi's [83] bearing capacity formula, Figure (9.6); bearing capacity is 265.0 psi (1828.5 kN/m²).

Comparison with Previous Work

Christian et al. [7] have reported that their finite element analysis with Mohr-Coulomb criterion overpredicted the bearing capacity by larger amounts. Furthermore, they have shown that the stiffer response was not due to the coarse finite element mesh used; this was done by using several meshes. They indicated that the overprediction was due to other reasons. Since Drucker-Prager model is a generalization of Mohr-Coulomb criterion, Equation (4.16), one can expect to get similar response for the Drucker-Prager model.

Figure (9.7) shows the results for a strip footing, obtained by using the finite element mesh in Figure (9.1) and the following properties for the Drucker-Prager model; these properties are the same as those used by Christian et al. [7]:

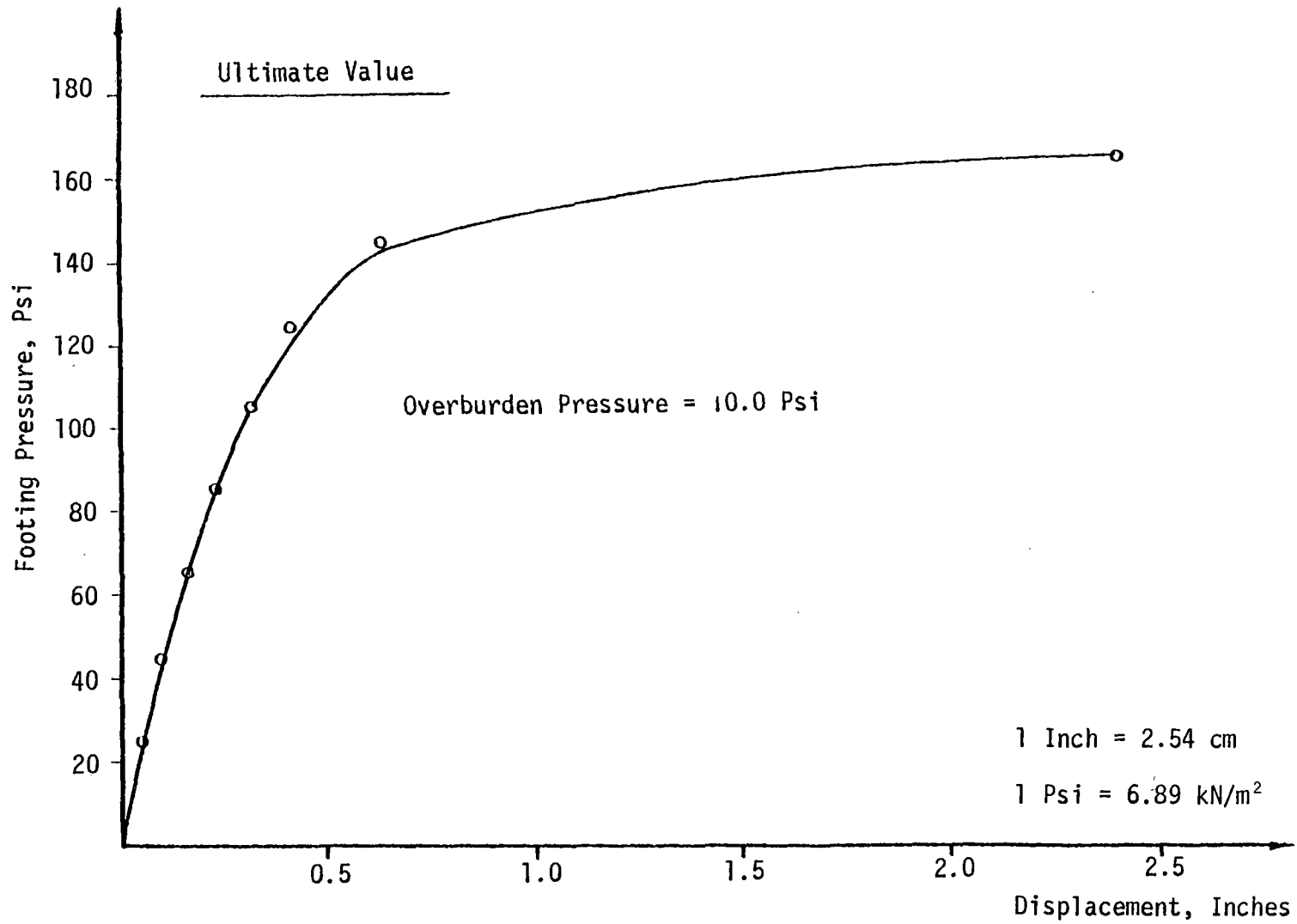


Figure 9.7 Behavior of a Strip Footing at Ultimate Conditions with a Drucker-Prager Model

$$E = 43,350 \text{ psi } (299.1 \times 10^3 \text{ kN/M}^2)$$

$$\nu = 0.30$$

$$\phi = 30 \text{ degrees}$$

$$C = 0.0$$

The present analysis gives an ultimate value close to that predicted by the Terzaghi's formula [83], 178.0 psi (1228. kN/M²). Numerical procedure used in the present study seems to predict a well defined ultimate state.

Figure (9.8) shows the results obtained by using the critical state model, Equation (4.30). Material properties used for this model are given below.

$$E = 5,000.0 \text{ psi } (34.5 \text{ kN/M}^2)$$

$$\nu = 0.3$$

$$M = 1.0$$

$$\lambda_C = 0.14$$

$$\kappa = 0.05$$

$$P_0 = 12.0 \text{ psi } (82.8 \text{ kN/M}^2)$$

$$\text{Initial pressure} = 10.0 \text{ psi } (69 \text{ kN/M}^2)$$

Results obtained by using 8-node plane strain elements, seem to compare well with those obtained with 16-node constrained three-dimensional elements. Use of 8-node constrained three-dimensional elements seems to give a stiffer response beyond a footing pressure of 40 psi (276 kN/M²); below this value the differences are smaller.

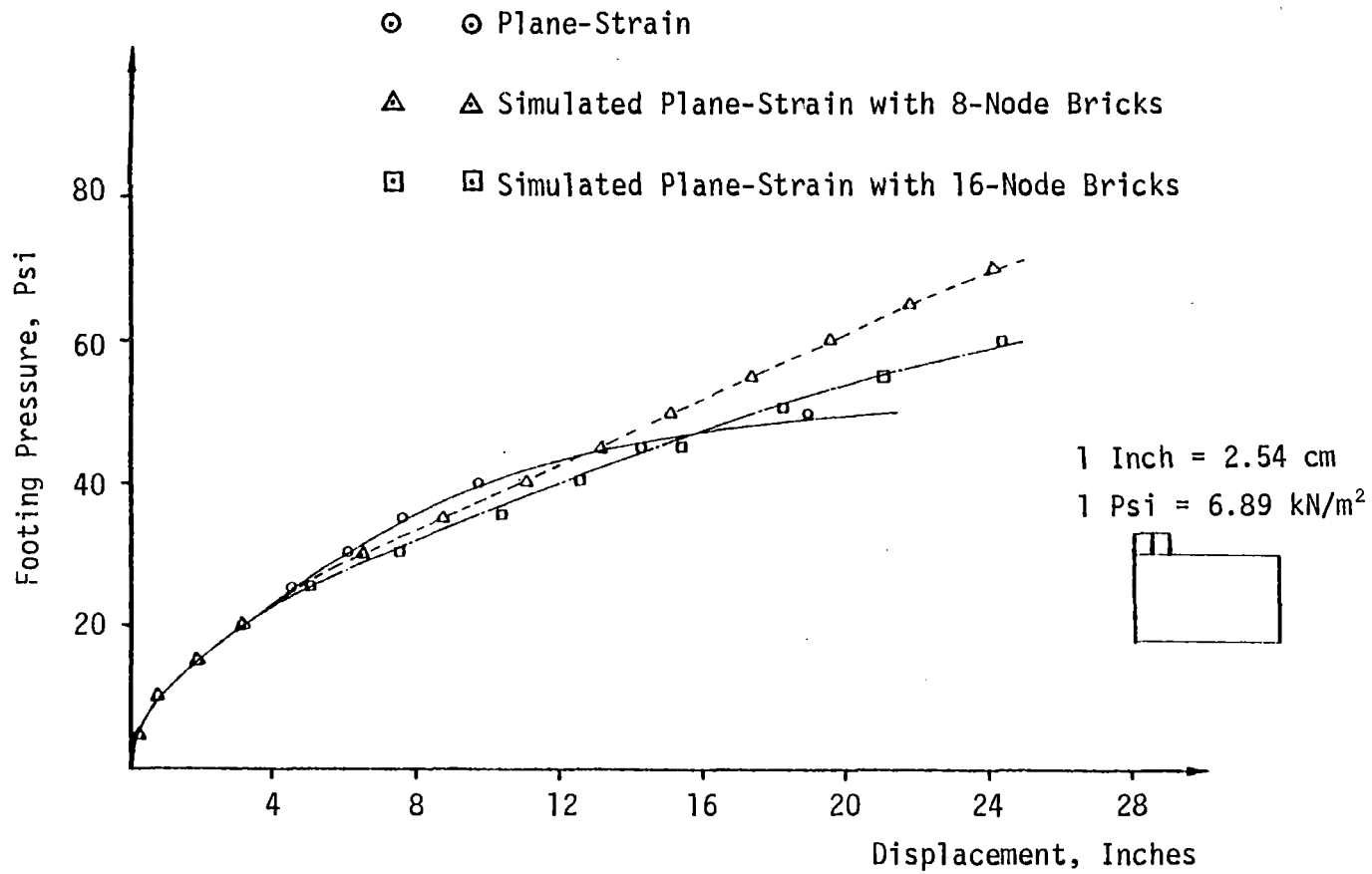


Figure 9.8 Deformation Analysis of a Strip Footing with Critical State Model

Figure (9.9) shows the results obtained by using the cap model, Equation (4.33), for the analysis of a strip footing, shown in Figure (9.1). Following properties [2] are used for the cap model.

$$\alpha = 250.0 \text{ psi (1,725 kN/M}^2\text{)}$$

$$\beta = 6.7 \times 10^{-4} \text{ psi (46.23} \times 10^{-4} \text{ kN/M}^2\text{)}$$

$$\gamma = 180.0 \text{ psi (1,242.0 kN/M}^2\text{)}$$

$$E = 100,000 \text{ psi (690} \times 10^3 \text{ kN/M}^2\text{)}$$

$$\nu = 0.25$$

$$R = 2.5$$

$$W = 0.066$$

$$D = 0.00067 \text{ psi}^{-1} (9.7 \times 10^{-5} \text{ (kN/M}^2\text{)}^{-1})$$

Results obtained by using 8-node plane strain elements seems to compare well with 16-node constrained three-dimensional elements. This can be expected since the number of degrees-of-freedom in the plane of deformation is the same for both analysis. Use of 8-node constrained three-dimensional elements gives stiffer response; this tendency increases with the footing pressure.

Stress Computations in Plane-Strain Analysis

The stress, σ_{zz} , in the normal direction to a plane strain section can be computed by using the theory of elasticity [84] as,

$$\sigma_{zz} = \nu(\sigma_{xx} + \sigma_{yy}) \quad (9.1)$$

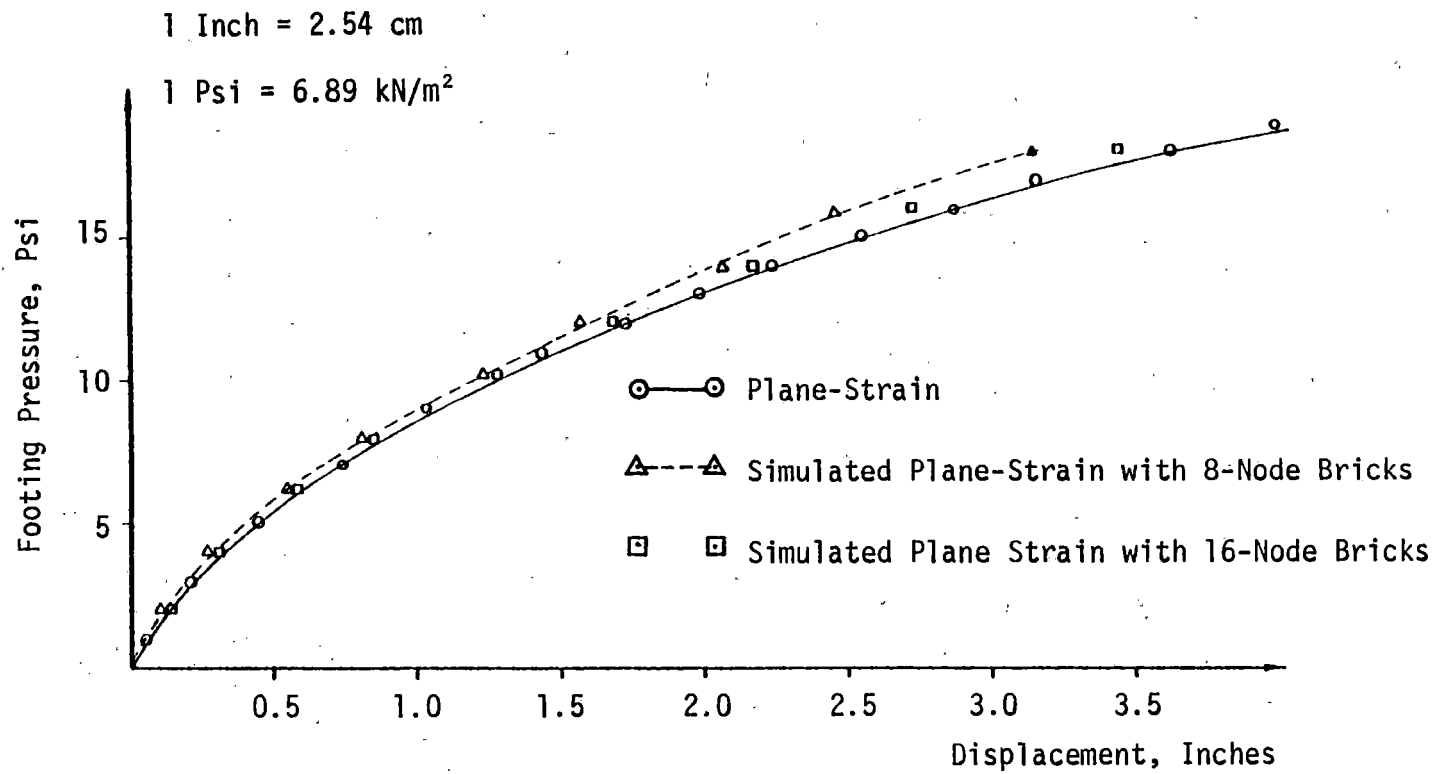


Figure 9.9 Deformation Analysis of a Strip Footing with Cap Model

where σ_{xx} , σ_{yy} are the stresses in the plane. As described in Chapter 8, computation of σ_{zz} in a plastic state becomes difficult since for this purpose elastic strains have to be computed separately. However, in the finite element computations, only total strains (elastic and plastic) are computed explicitly. In this case, the incremental quantities of stresses can be computed by using the current constitutive matrix and the incremental quantities of strains, Equation (8.3). However, this will require additional storage and the computation of a constitutive matrix which is (4×4) . Ordinarily, the constitutive matrix used in plane strain analysis is (3×3) .

An investigation is made to see the effect of using Equation (9.1) to compute the values of σ_{zz} . Since $[C^{ep}]$, Equation (8.3), is dependent on σ_{zz} , the results can be expected to be different if the values of σ_{zz} were different. Figure (9.10) shows a comparison of the above two numerical schemes with respect to a plasticity model based on critical state concepts; material properties given previously in this chapter are used. Both the rigorous method, Equation (8.3), and simplified method, Equation (9.1) give similar results at lower loads. However, the ultimate values predicted by rigorous method are lower than that obtained with the simplified method. Therefore, the use of the simplified method can predict bearing capacities which are higher than the actual values.

Displacement Fields for Different Constitutive Models

Displacement fields for the footing problems considered are obtained by using different constitutive models based on the plasticity theory.

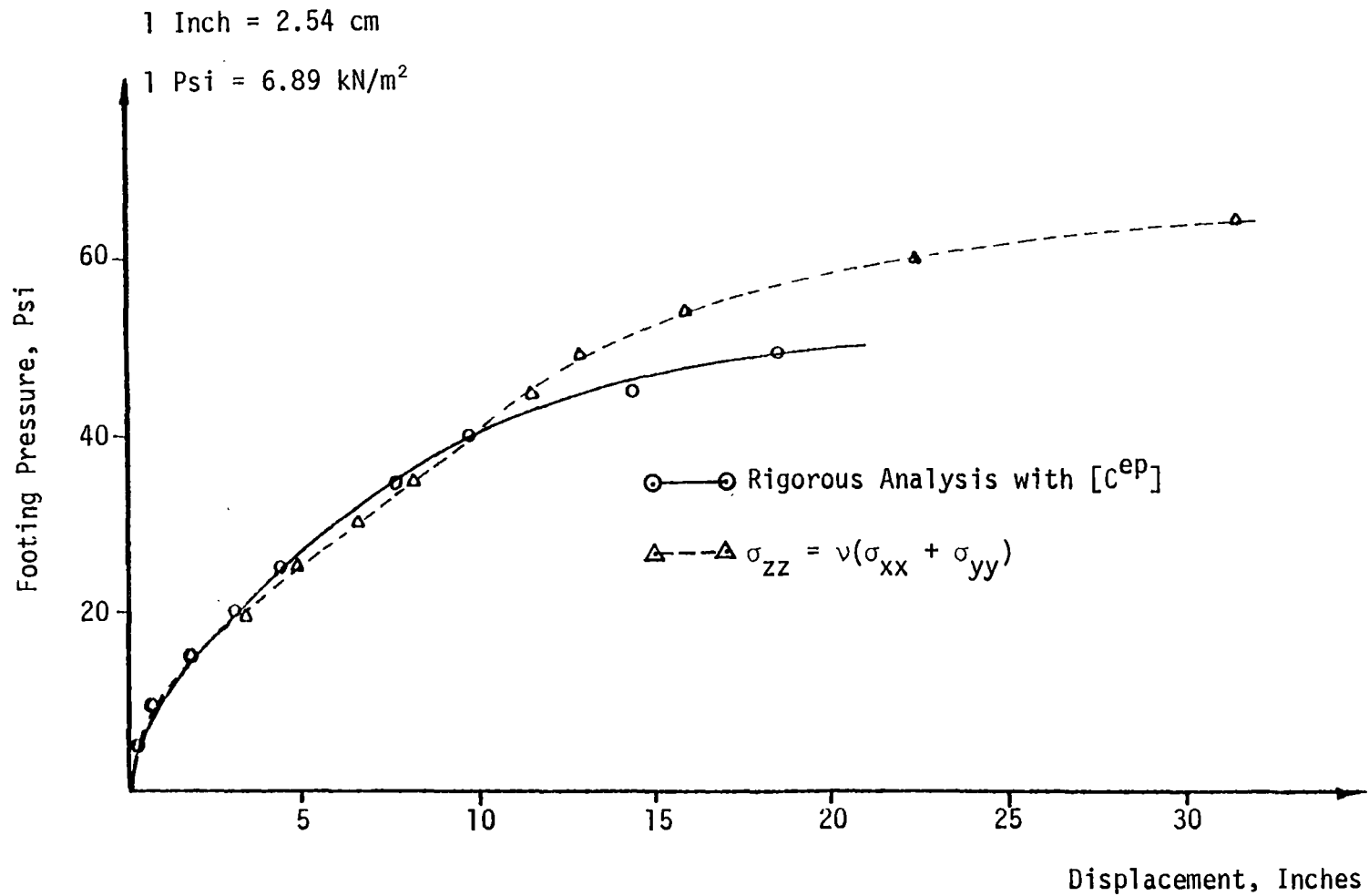


Figure 9.10 Effect of Stresses Normal to the Plane of Deformation on the Behavior of a Elasto-Plastic Material in Plane-Strain Condition

Since, the material parameters used in these analysis do not pertain to one material, only qualitative comparisons are made. Figure (9.11) shows a typical displacement field for a linearly elastic material; this is given for comparison purposes with other models.

Figure (9.12a) shows the displacement field near the ultimate state for the strip footing analysed previously with the Drucker-Prager model. Surface displacements away from the footing indicate volume expansion near failure. In fact, the plastic volumetric expansions predicted by the Drucker-Prager model, Equation (4.22), is one of the characteristics of this model.

Figure (9.12b) shows the displacement field at ultimate state for the same strip footing with critical state model; material properties are given previously in this section, 9.1. Here, the displacements away from the footing are smaller, and surface displacements do not show volume expansion. This displacement field is different from that obtained for the Drucker-Prager model, Figures (9.12a and 9.12b).

Figures (9.13a and 9.13b) show a comparison of displacement fields for Drucker-Prager and cap models. Displacement field for the cap model, Figure (9.13b), seems to be very similar to that of the critical state model, Figure (9.12b). Displacement field is concentrated close to the loading area, and do not show volumetric expansion as observed for Drucker-Prager model. Perhaps, this feature may be a characteristic of the two isotropic hardening models, namely critical state and cap, considered.

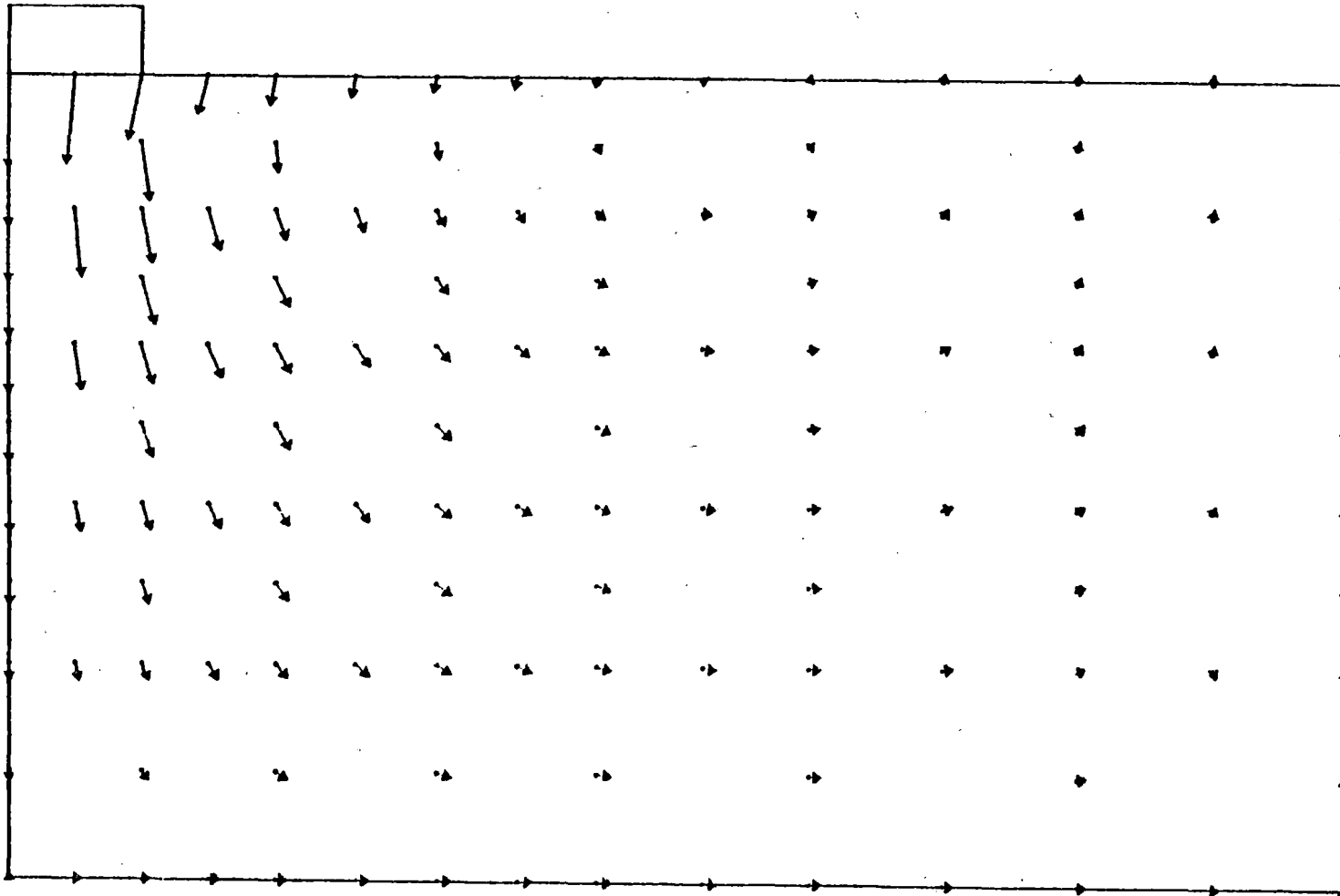
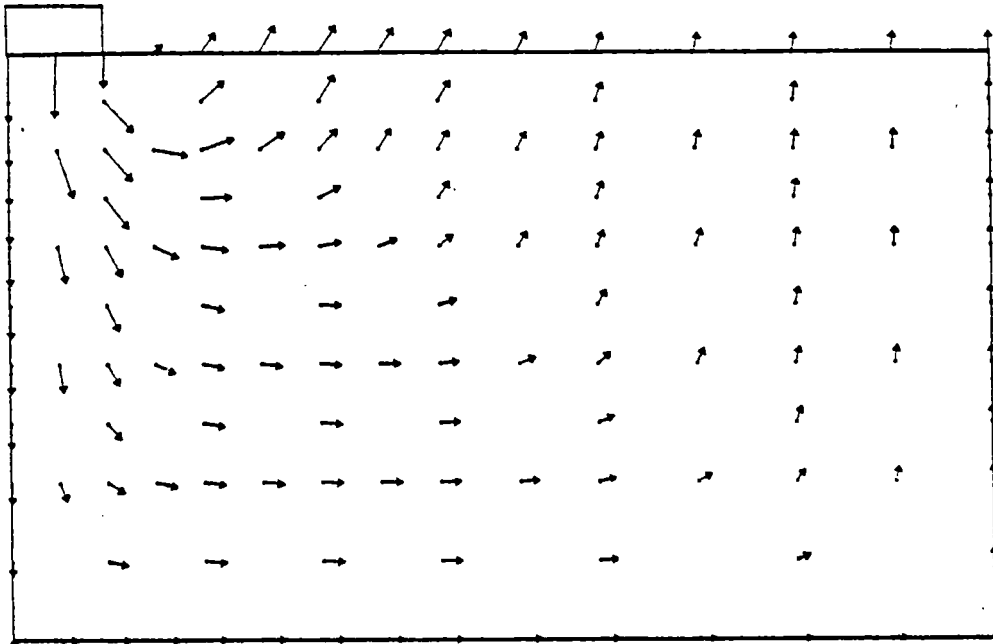
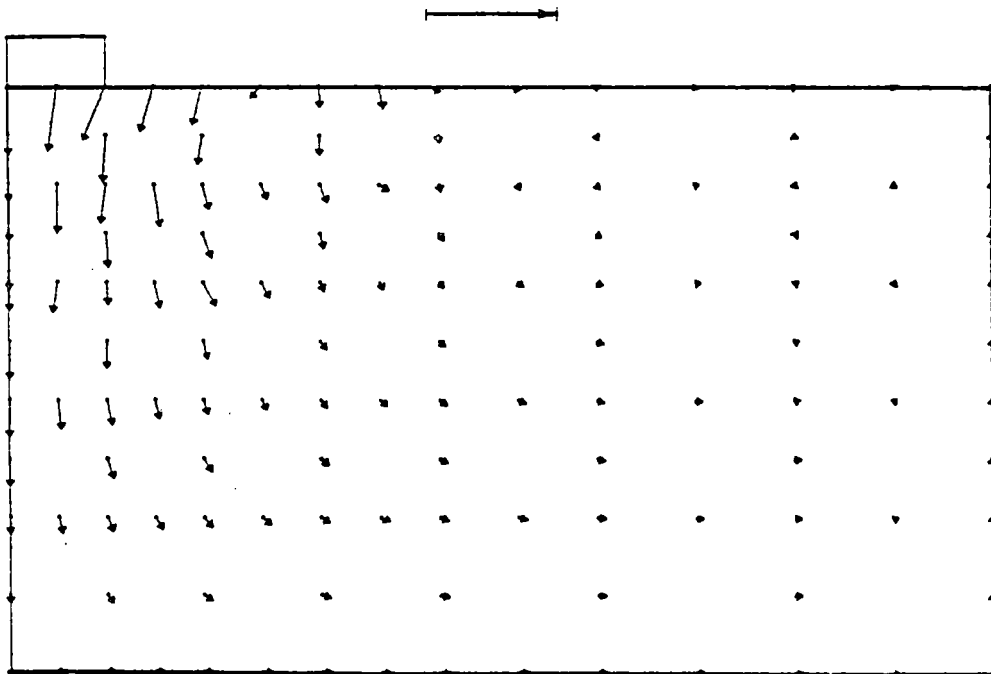


Figure 9.11 Displacement Vector Field for a Strip Footing on a Linear Elastic Material

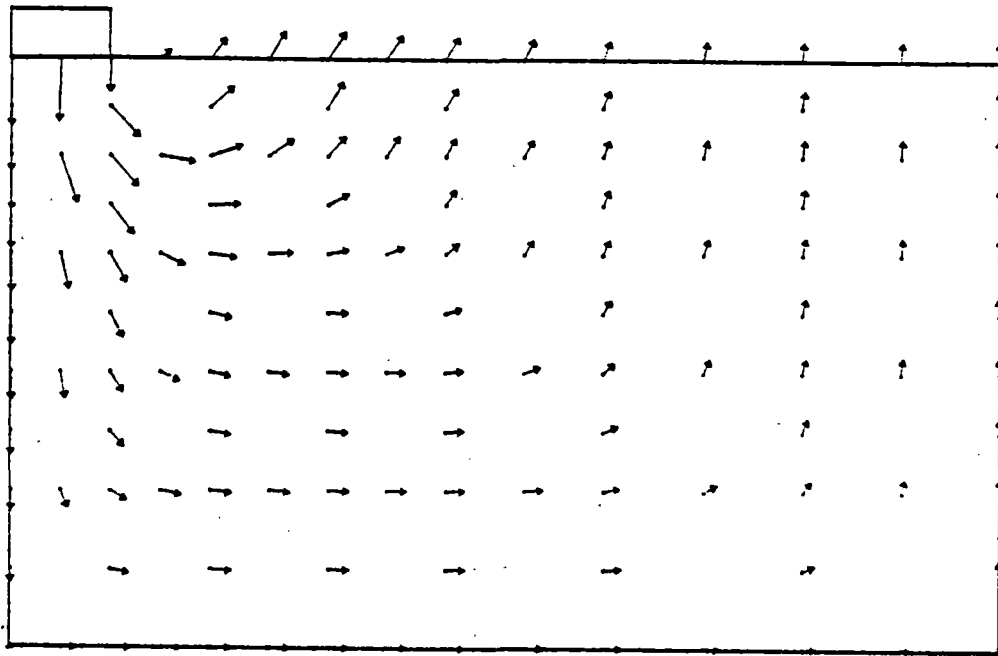


(a) Drucker-Prager Model

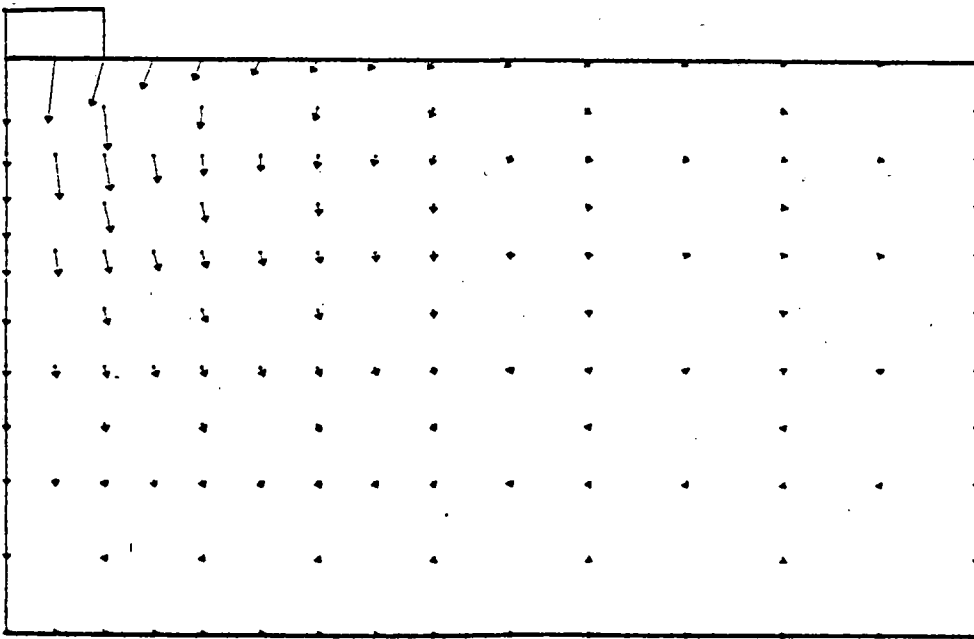


(b) Critical State Model

Figure 9.12 Comparison of Displacement Fields for Drucker-Prager and Critical State Models at Ultimate Conditions



(a) Drucker-Prager Model



(b) Cap Model

Figure 9.13 Comparison of Displacement Fields for Drucker-Prager and Cap Models at Ultimate Conditions

Footing-Soil Interaction with a Lateral Load

In order to study the interaction behavior, a strip footing subjected to both vertical and lateral loads is considered, Figure (9.14). Here, the interface elements described in Chapter 6 are used between the footing and the soil to model the interaction behavior. The depth of the soil layer is taken as 300.0 inches (762.0 cm), and footing width is taken as 40.0 inches (101.6 cm).

First, the interaction is studied by assuming elastic behavior; the following properties are used:

Soil: $E = 10000.0 \text{ psi } (69.0 \times 10^3 \text{ kN/m}^2)$

$\nu = 0.3$

Footing: $E = 100000.0 \text{ psi } (690. \times 10^3 \text{ kN/m}^2)$

$\nu = 0.3$

Interface: $E = 10000.0 \text{ psi } (69.0 \times 10^3 \text{ kN/m}^2)$

$\nu = 0.3$

$G_{int} = 200 \text{ psi } (508.0 \text{ kN/m}^2)$

Thickness = 0.2 inches (0.508 cm)

Figure (9.15) shows the deformed shapes of the footing with and without interfaces. Presence of interface allows relative displacements, Figure (9.15a). Effect of interface on the stress distribution is shown by comparing the average stresses in two typical soil elements just below the footing. That is,

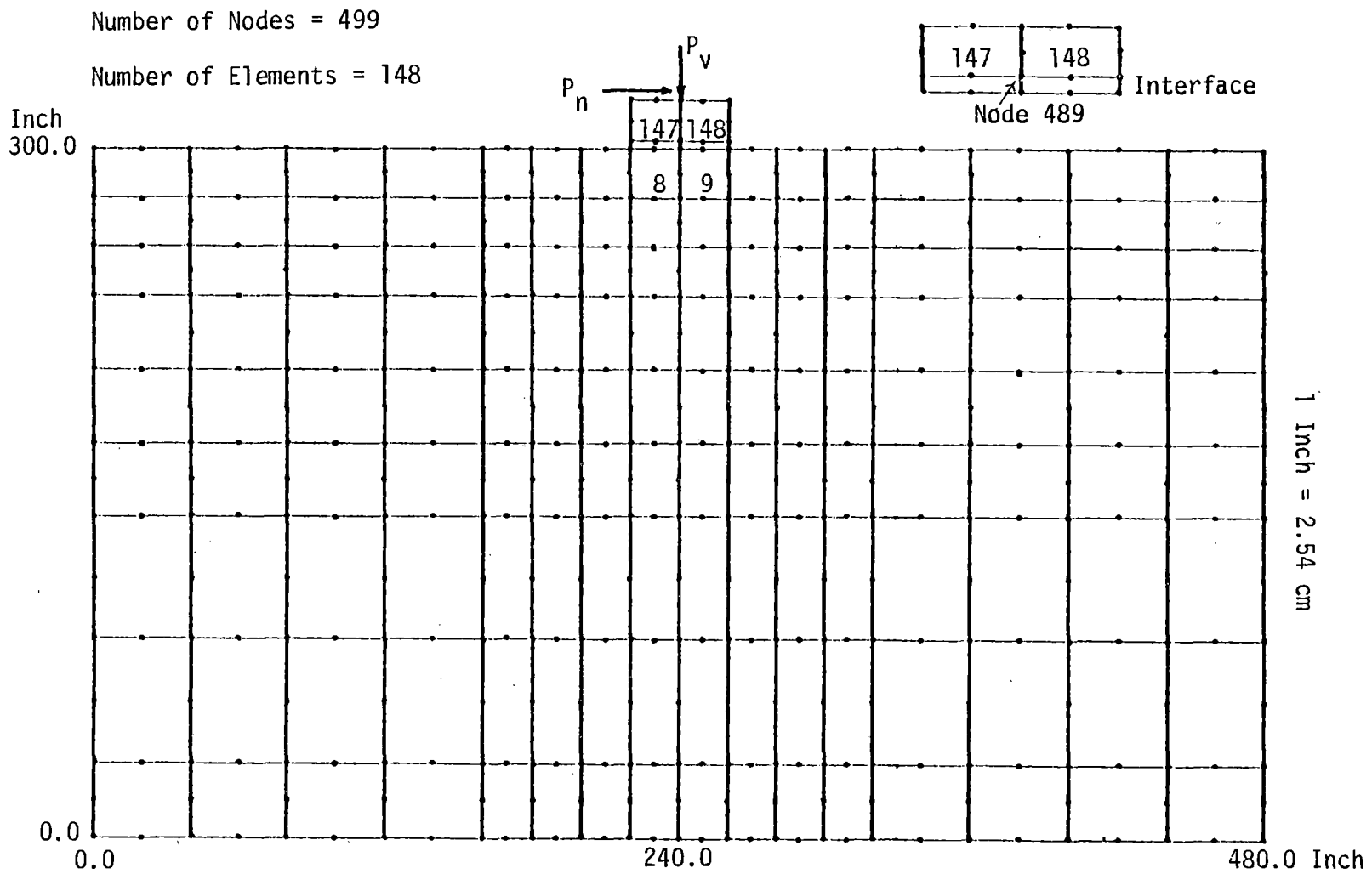
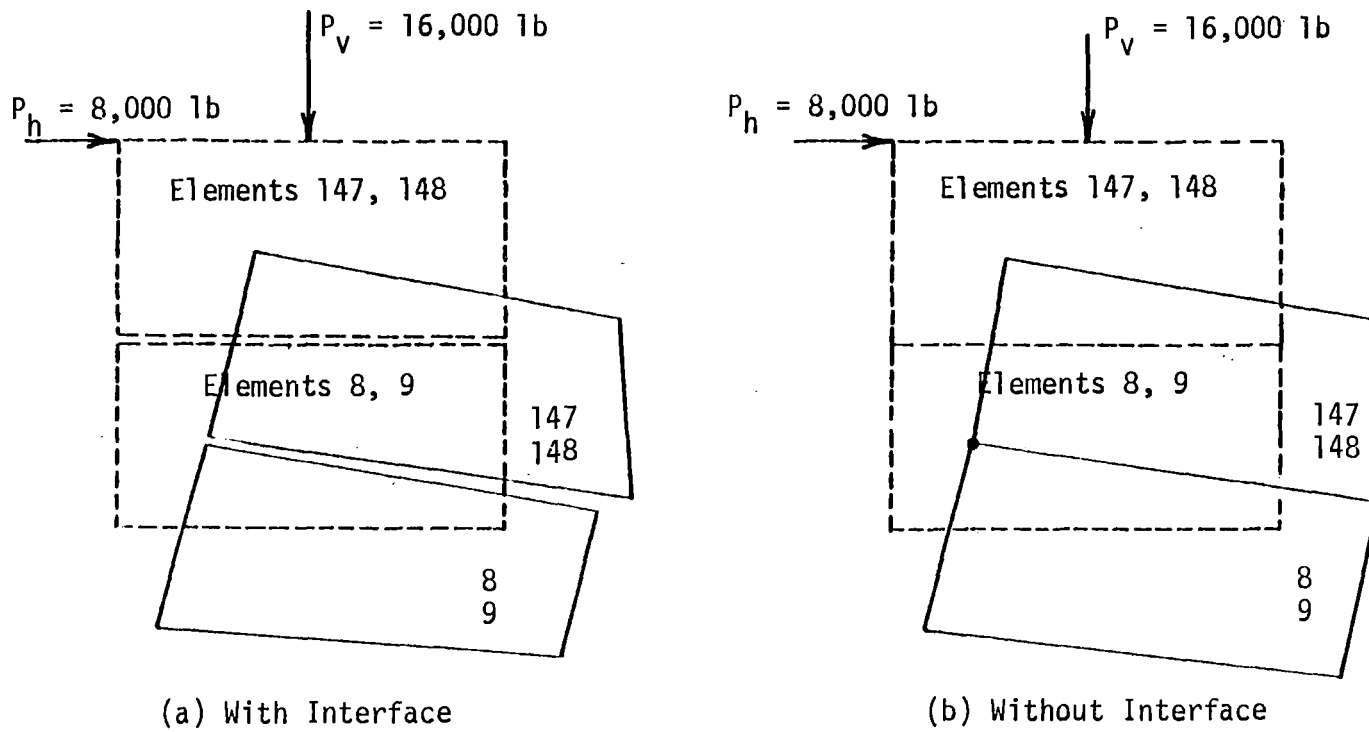


Figure 9.14 Finite Element Mesh for Footing-Soil Interaction with a Lateral Load



Displacement Scale: 1 Inch = 0.20 Inch of Displacement
 Geometry Scale: 1 Inch = 20 Inch
 1 Inch = 2.54 cm
 1 lb = 0.453 kg

Figure 9.15 Interaction Behavior of a Footing with Soil

	Stresses, psi with Interface		Stresses, psi without Interface	
	σ_{xx}	σ_{yy}	σ_{xx}	σ_{yy}
Element 9 (soil)	231.7	440.7	170.2	398.3
Interface	320.9	523.9	—	—
Footing	248.3	513.8	584.8	516.5
Element 8 (soil)	50.25	212.1	32.18	216.0
Interface	- 7.0	277.2	—	—
Footing	-166.0	288.2	-115.2	283.8

Here, σ_{xx} and σ_{yy} represents horizontal and vertical stresses, respectively. Presence of interface element seems to influence the stress distribution in the foundation, and this can have a significant influence on the nonlinear behavior which is stress dependent.

Results from a nonlinear analysis of this interaction problem are shown in Figures (9.16a) and (9.16b); here, the nonlinearity is characterized by a cap model whose material properties are given earlier in this section. Following properties are used for footing and the interfaces.

Footing: $E = 1,000,000$ psi (6900×10^3 kN/m²)

$\nu = 0.25$

Soil: same as given previously

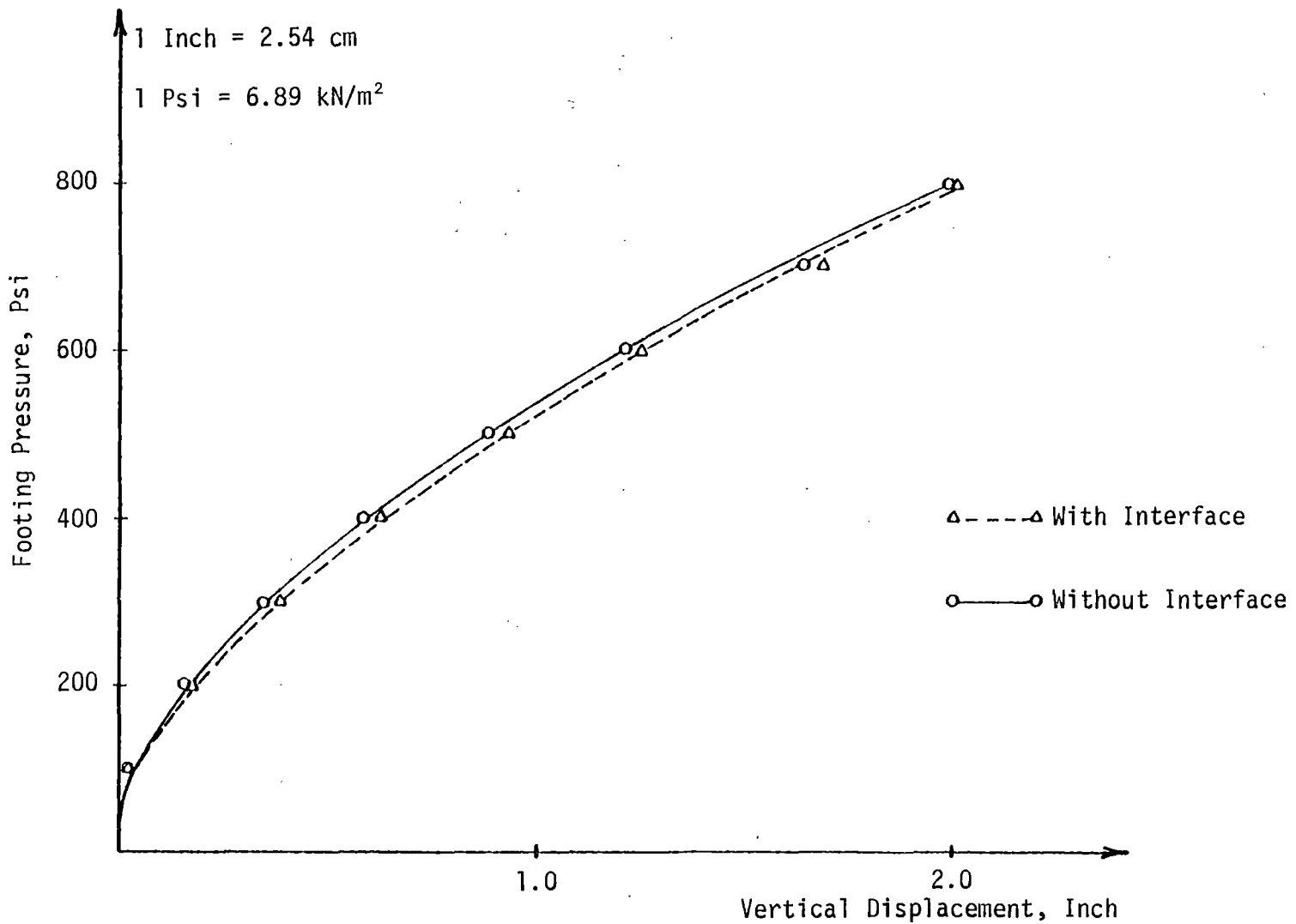


Figure 9.16a Vertical Load-Displacement Relationship for the Strip Footing

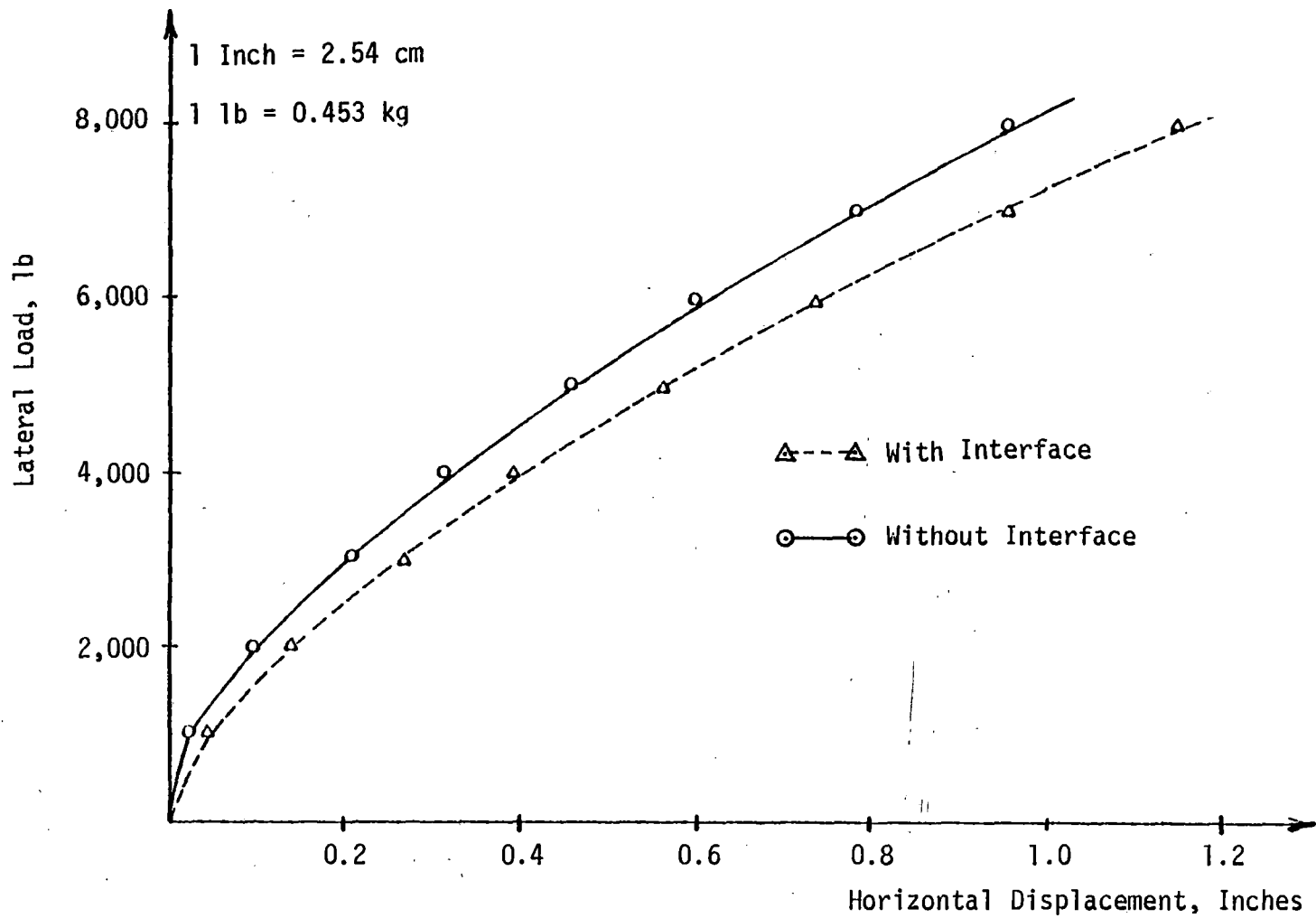


Figure 9.16b Lateral-Load Displacement Relationship for the Strip Footing

Interface: $E = 100,000 \text{ psi}$ ($690 \times 10^3 \text{ kN/m}^2$)

$\nu = 0.25$

$G_{\text{int}} = 200 \text{ psi}$ (1380.0 kN/m^2)

Thickness = 0.2 inch (0.508 cm)

Loading: Vertical pressure = 400 psi (5520.0 kN/m^2)

Horizontal load = 8000 lb (35.6 kN)

Figure (9.16a) shows that the vertical displacements are not significantly affected by the presence of interfaces. However, the horizontal displacements are affected by the presence of interface elements, Figure (9.16b). Effect of interfaces on the stress distribution is shown by comparing the average stresses in two typical soil elements just below the footing. That is,

	Stresses, psi with Interface		Stresses, psi without Interface	
	σ_{xx}	σ_{yy}	σ_{xx}	σ_{yy}
Element 9 (soil)	220.2	324.8	175.1	362.5
Interface	1169.35	505.5	—	—
Footing	372.1	516.0	522.1	526.25
Element 8 (soil)	55.39	220.0	69.9	243.8
Interface	-108.0	315.5	—	—
Footing	- 92.13	304.0	- 58.8	293.3

A typical pattern of displacement vectors for this problem is shown in Figure (9.17).

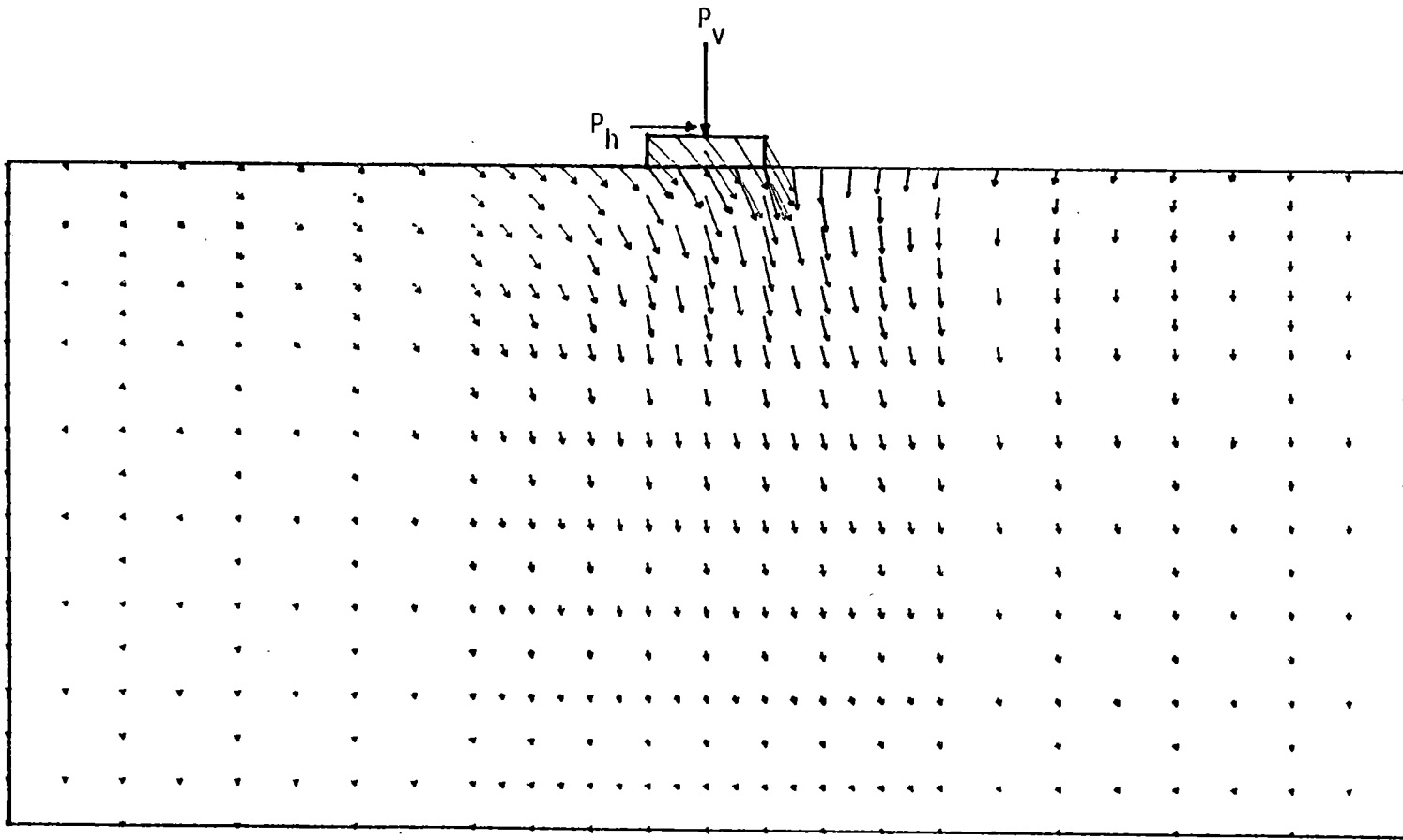


Figure 9.17 Displacement Field for Footing-Soil Interaction with a Lateral Load

9.2 Interaction in a Beam with a Nonlinear Foundation

In this section, interaction behavior of a beam-on-a-deformable foundation is studied by using the one-dimensional finite element procedure described in Chapters 3 and 5. A detailed description of incremental, iterative and stress transfer techniques used in the current study is given in Chapter 5.

Stress Transfer Technique with Linear Behavior

For this analysis a beam of 500 inches (1270 cm) length is considered, and discretized in 25 elements and 26 nodal points. Here, element length is taken as 20 inches (50.8 cm). Both ends of the beam are assumed to be fixed. The foundation is replaced by a series of springs. The following properties are used in the analysis:

$$\text{Beam: } E = 30.0 \times 10^6 \text{ psi } (20.67 \times 10^7 \text{ kN/m}^2)$$

$$I = 94.9 \text{ in}^4 \text{ (3950.0 cm}^4\text{)}$$

$$\text{Foundation spring constant, } k = 390 \times 10^3 \text{ lb/in (683.3 kN/cm)}$$

Here, the spring constant, k , can be determined from the subgrade reaction, k_s , as follows:

$$k = k_s \cdot b \cdot \ell \quad (9.3)$$

where b is the breadth of the beam, and ℓ is the length of an element.

Figure (9.18a) shows the deflected shape of the beam due to a point load. The stress transfer iterations (cycles), Chapter 5, are performed to remove the tensile stress conditions. The deflected shape in the tensile zones is significantly affected by the stress transfer technique; this does not, however, influence significantly the

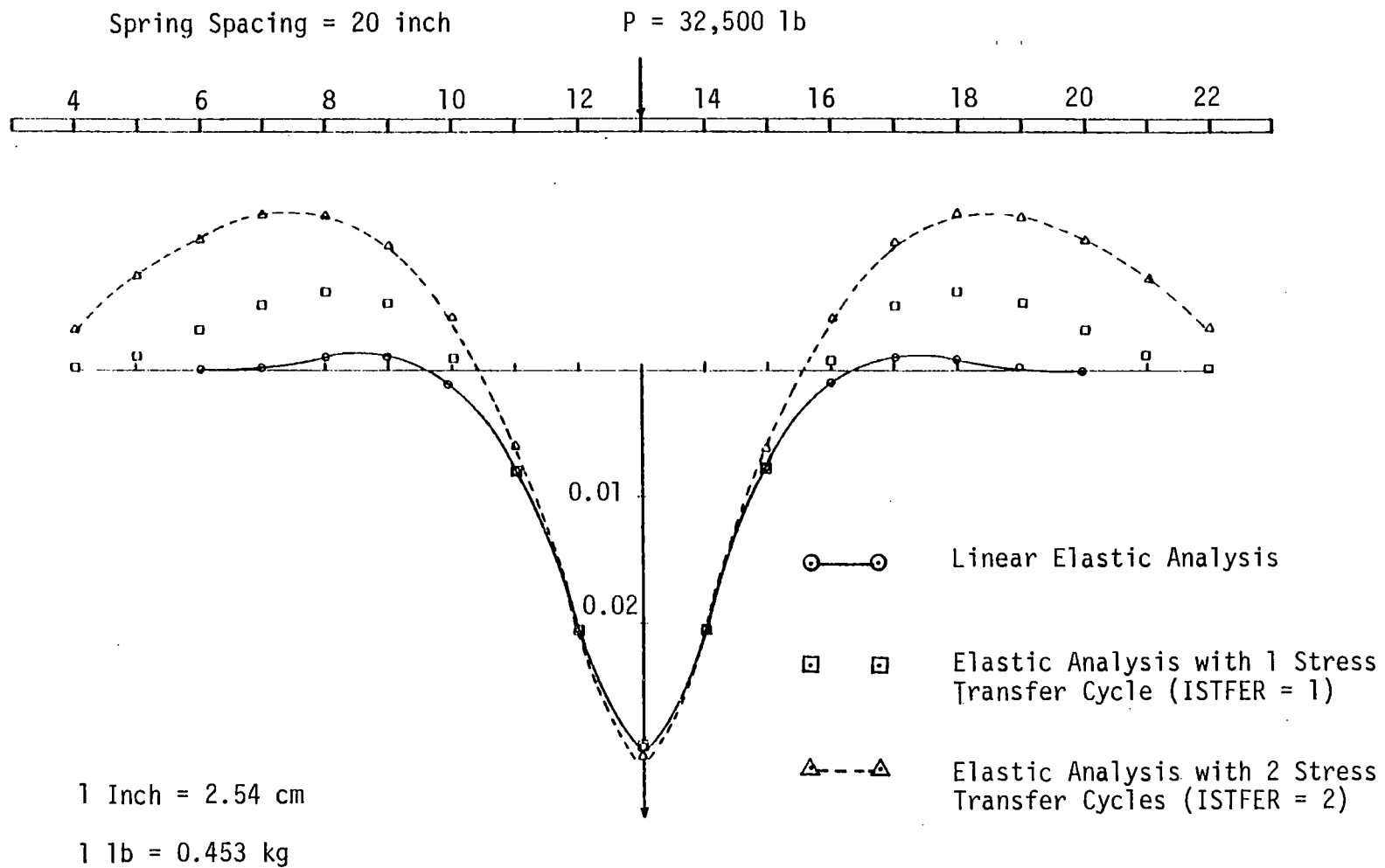


Figure 9.18a Effect of Stress Transfer on Beam Deflections

deflections near the loading. In the first stress transfer cycles (ISTFER = 1), the tensile zones detected after the 'trial solution', Chapter 5, are removed. However, during the process, tension can develop in other zones. This is evident from Figure (9.18a) which shows different deflections for two stress transfer cycles. Figure (9.18b) shows the distribution of support reaction (spring force) along the beam. In this application, the stress transfer does not have significant influence on the compressive reactions; however, it removes tensile reactions along the beam.

In order to study the effect of stress transfer on the equilibrium conditions, two equilibrium iterations, Chapter 5, are performed together with stress transfer cycles. Figures (9.19a) and (9.19b) show the deflected shape, and the reaction distribution along the beam, respectively. The effects of equilibrium iterations seems to be insignificant in this case showing that the equilibrium is maintained during the stress transfer.

Stress Transfer Technique with Nonlinear Behavior

Here, the beam considered has the same dimensions as in the linear case. Nonlinearity is assumed to be in the foundation springs. This is characterized by using the Ramberg-Osgood model, Chapter 5, and the properties used are given below:

$$k_0 = 390.0 \times 10^3 \text{ lb/in (683.3 kN/cm)}$$

$$P_f = 80,000.0 \text{ lb (356.0 kN)}$$

$$K_f = 0.0$$

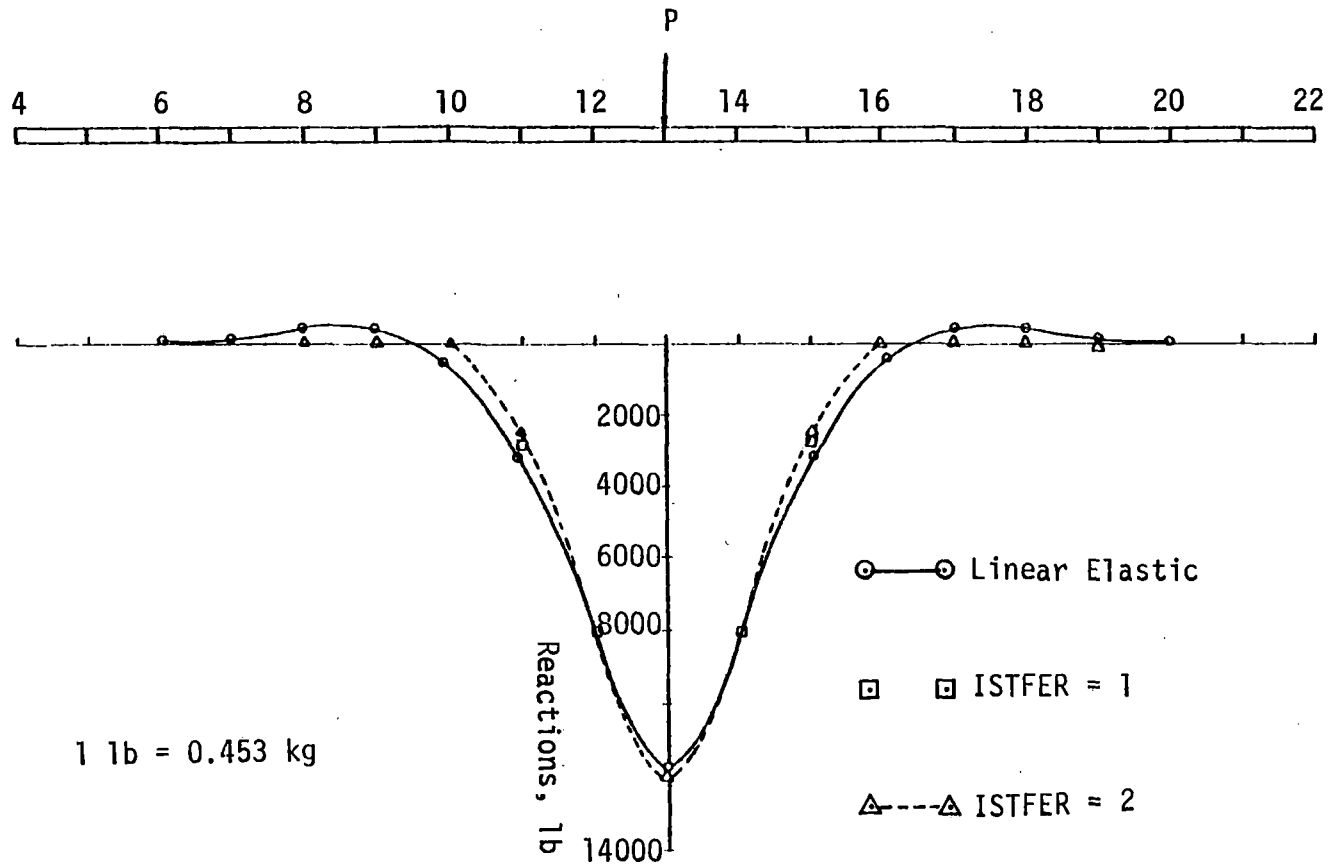


Figure 9.18b Effect of Stress Transfer on Distribution of Reactions

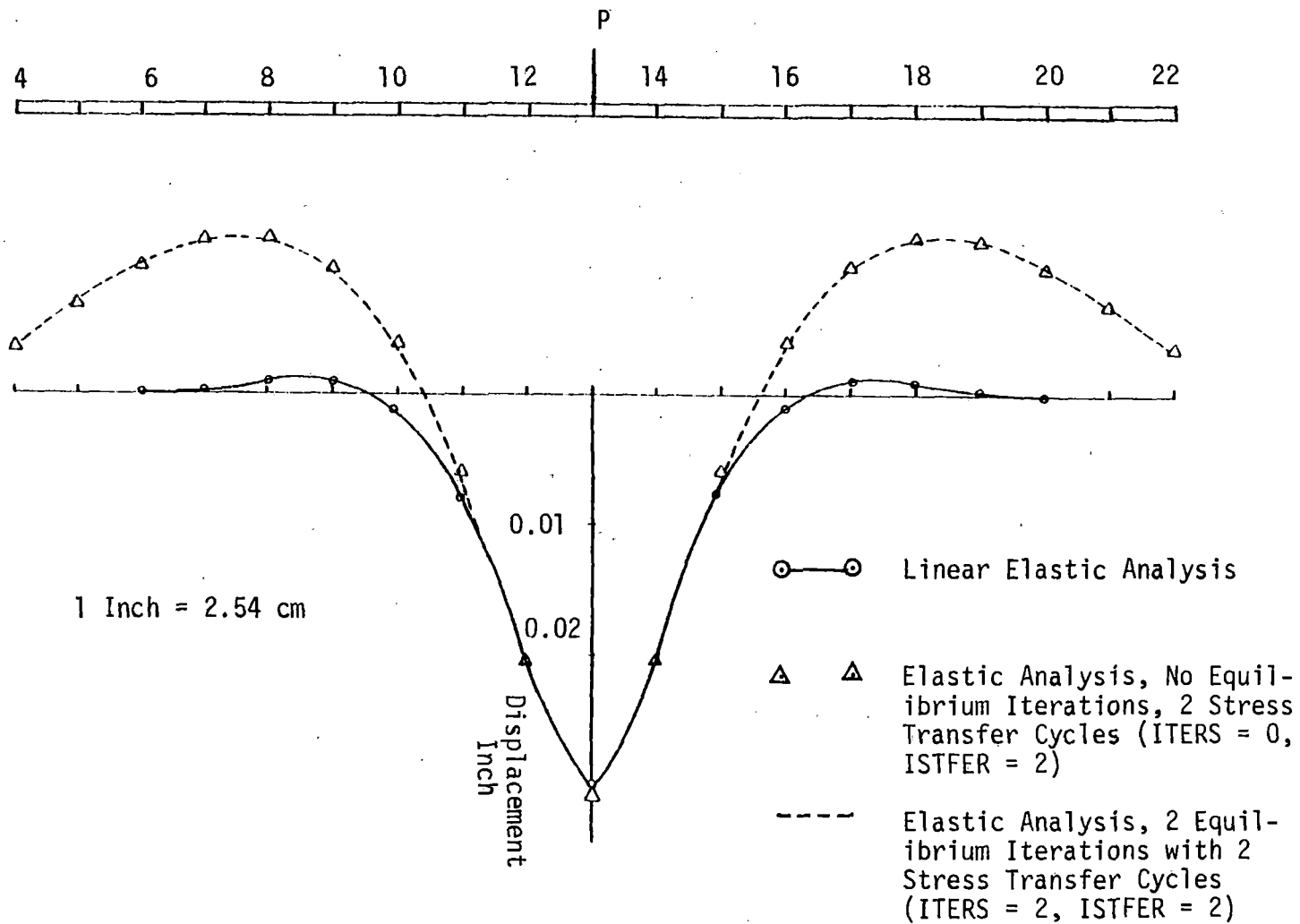


Figure 9.19a Effect of Stress Transfer on Equilibrium Conditions

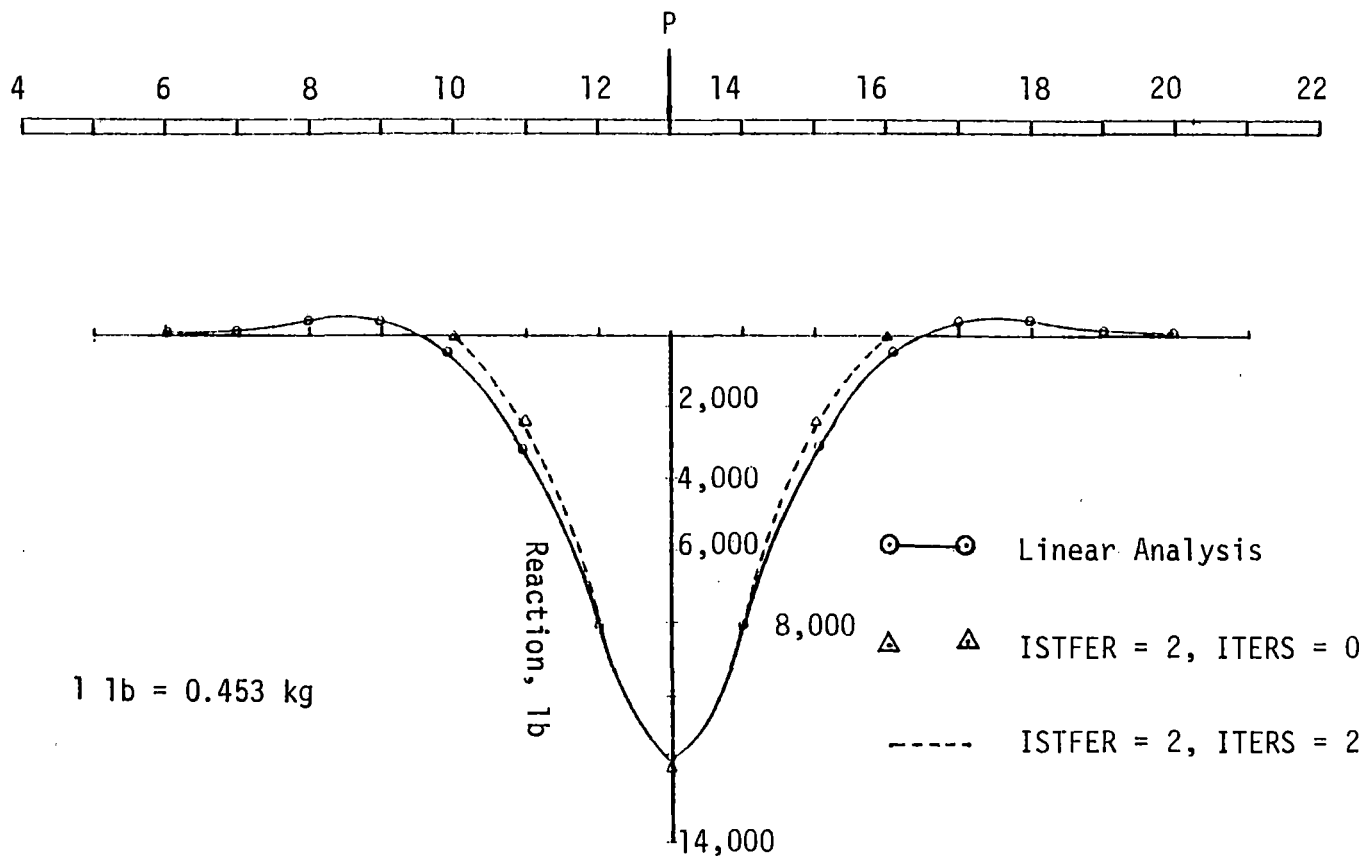


Figure 9.19b Effect of Stress Transfer on Equilibrium Conditions

$$m = 1.0$$

$$k_r = 390.0 \times 10^3 \text{ lb/in (683.3 kN/cm)}$$

where k_r is the spring constant for unloading-reloading states, Chapter 5.

In the linear analysis it is seen that at least two stress transfer iterations are required to remove the tensile zones. Hence, two stress transfer iterations are used in the nonlinear analysis. Figure (9.20a) shows the deflected curve obtained by using two stress transfer cycles. This behavior is very similar to that given in Figure (8.18a) for the linear case. Figure (9.20b) shows the distribution of reaction along the beam. Because of the nonlinearity of spring stiffness, the reactions are different than those computed in the linear analysis. The computed balanced load is only about 95.0% of the external load for this example at zeroth iteration. Hence, equilibrium iterations, Chapter 5, are required to maintain the equilibrium conditions.

Results obtained from a nonlinear analysis with one equilibrium iteration with two cycles of stress transfer are shown in Figures (9.20a) and (9.20b). Displacements close to the point of load application are higher than the linear solution. However, nonlinearity does not seem to affect displacements in the tensile zones. Figure (9.21b) shows the distribution of support reactions. The computed balanced load is 99.7% after one equilibrium iteration. Nonlinear behavior of this problem does not seem to influence the distribution of reactions considerably, Figure (9.21b), although the displacements are affected significantly, Figure (9.21a).

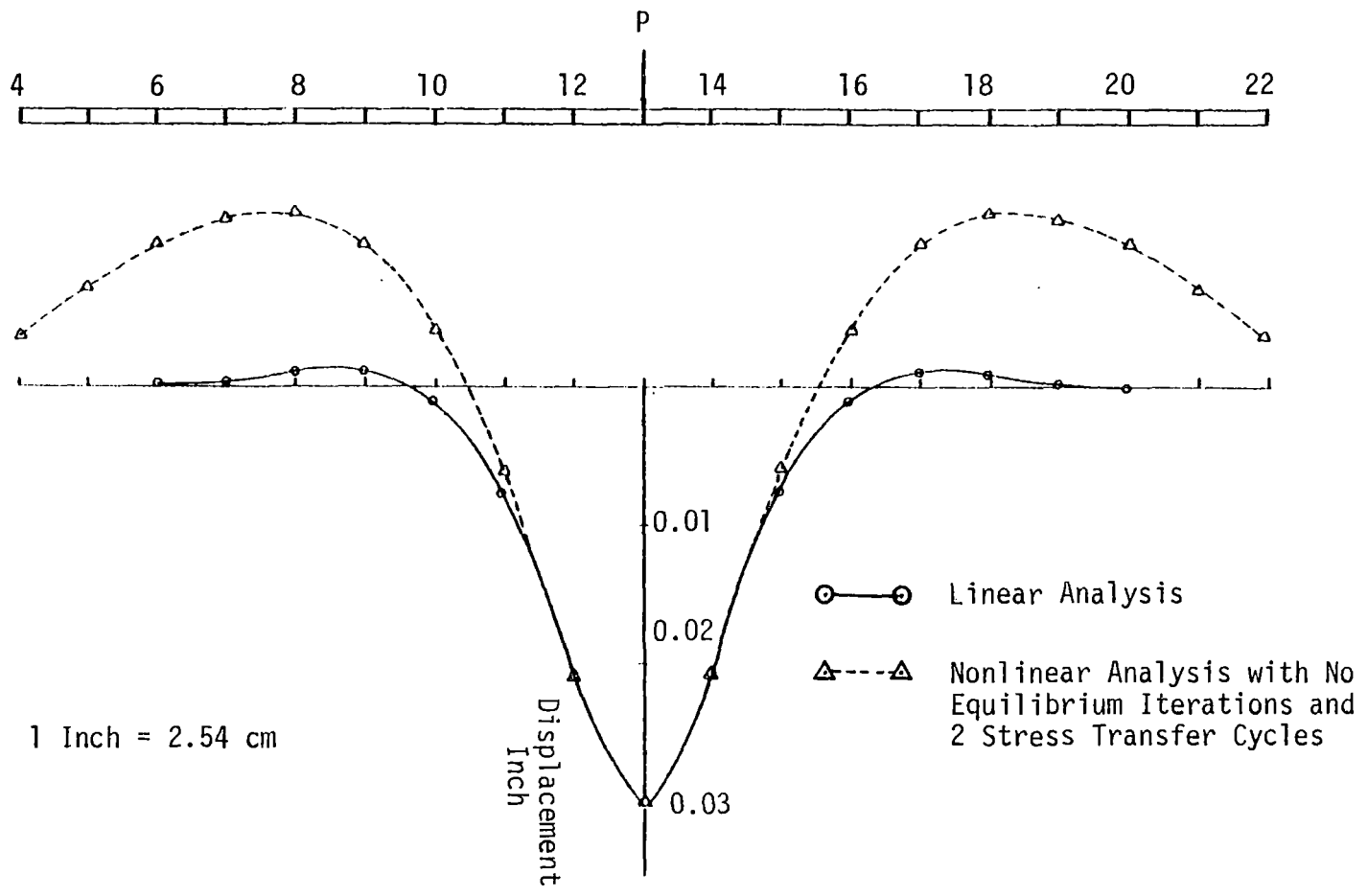


Figure 9.20a Predicted Displacements of Beam-on-Nonlinear-Foundation Without Equilibrium Iterations

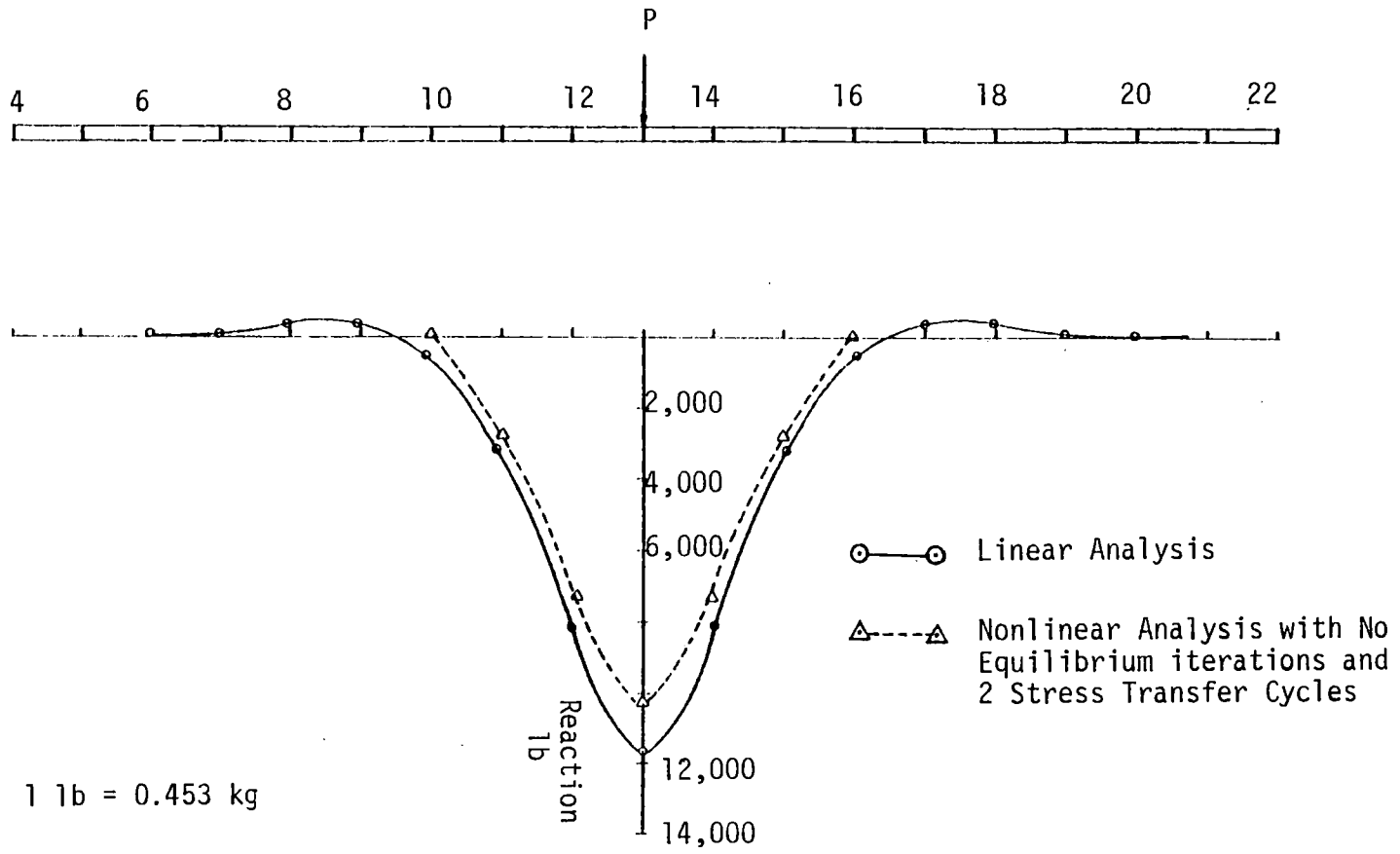


Figure 9.20b Distribution of Reactions from a Nonlinear Analysis Without Equilibrium Iterations

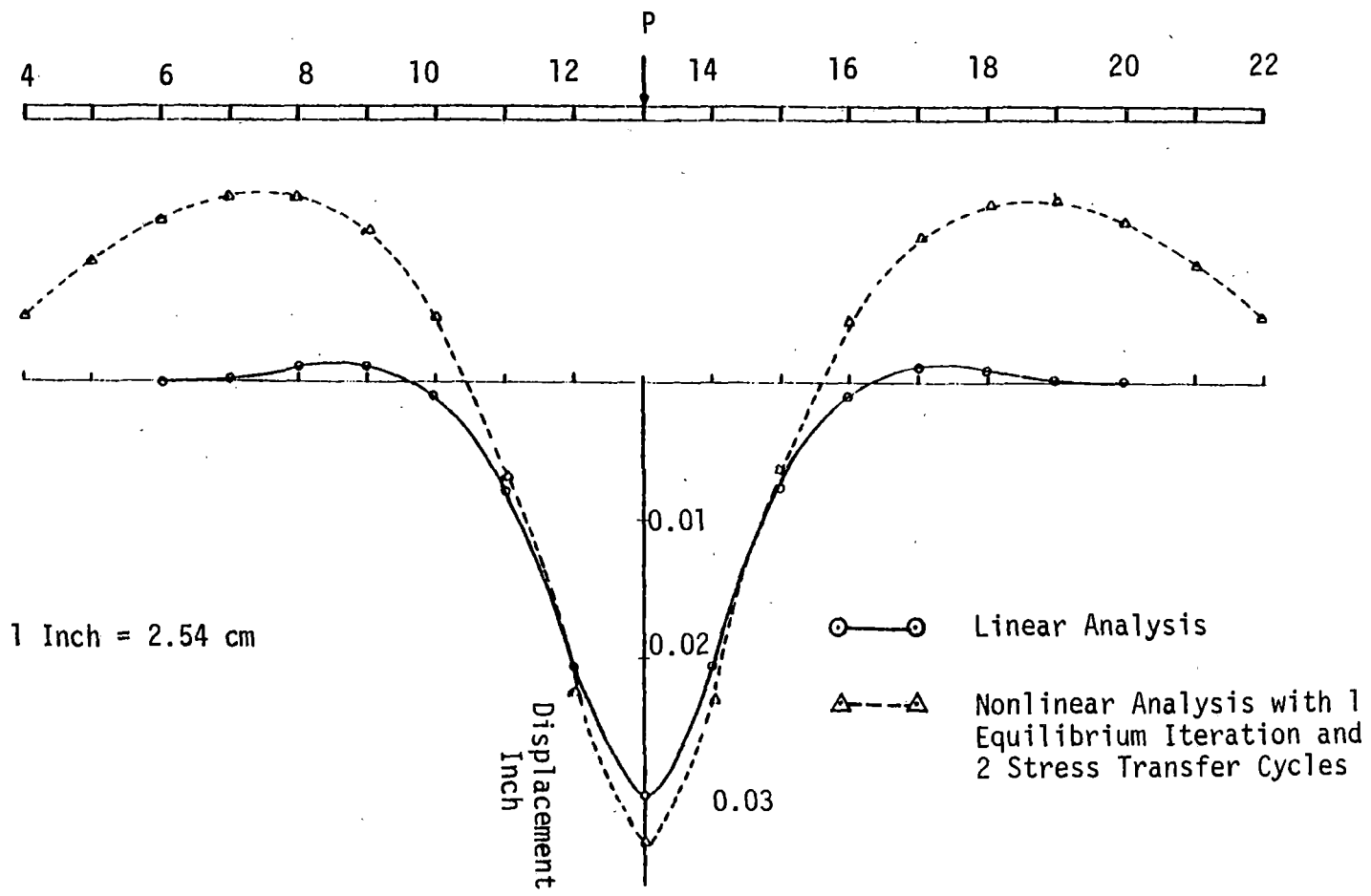


Figure 9.21a Beam Deflections from a Nonlinear Analysis with Equilibrium Iterations

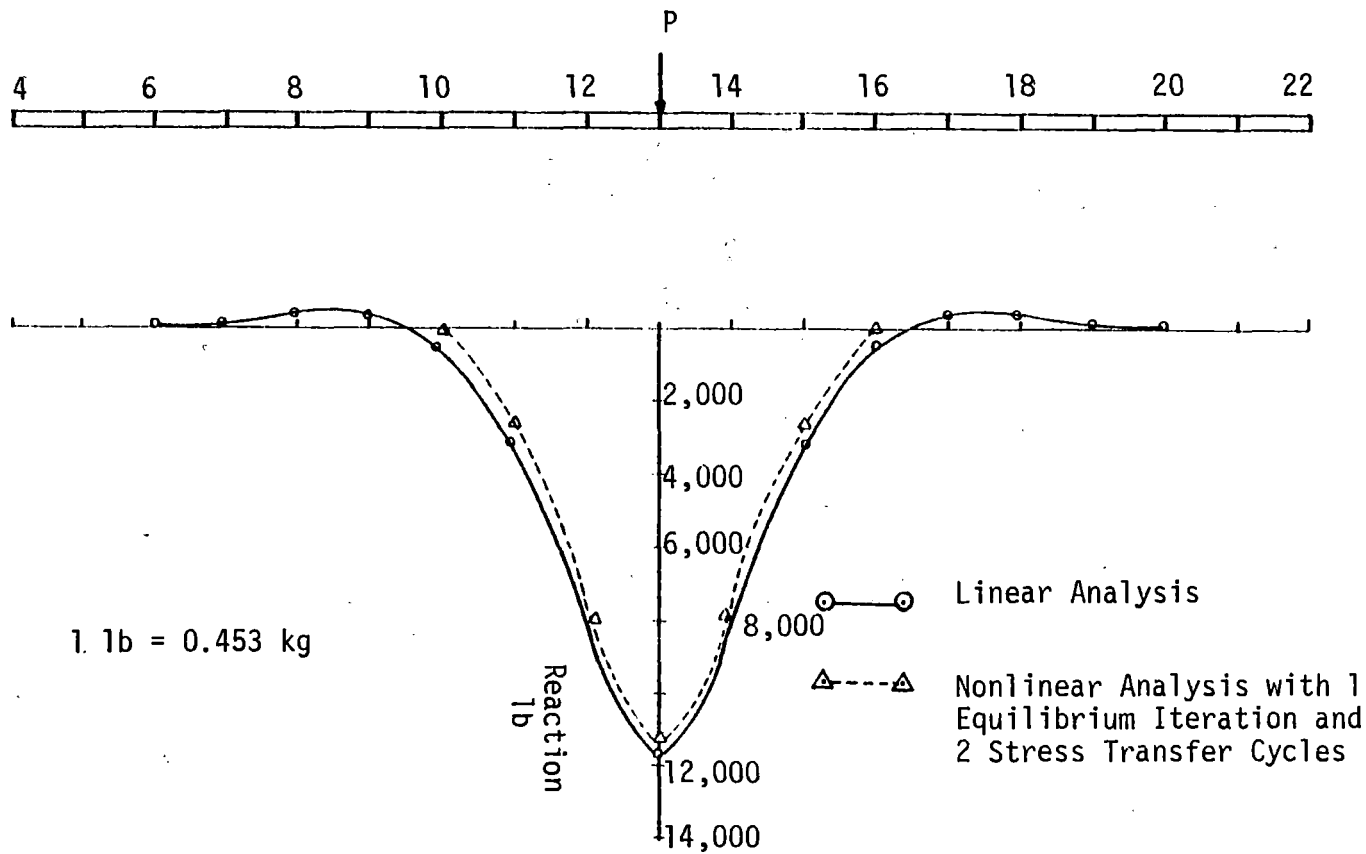


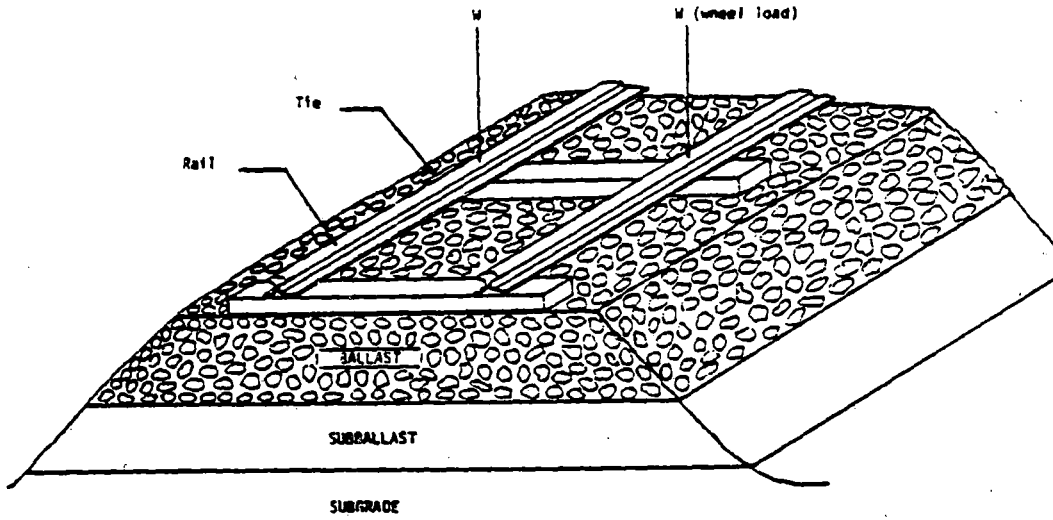
Figure 9.21b Distribution of Reactions from a Nonlinear Analysis
with Equilibrium Iterations

9.3 Interaction in a Multicomponent System such as a Track-Support System

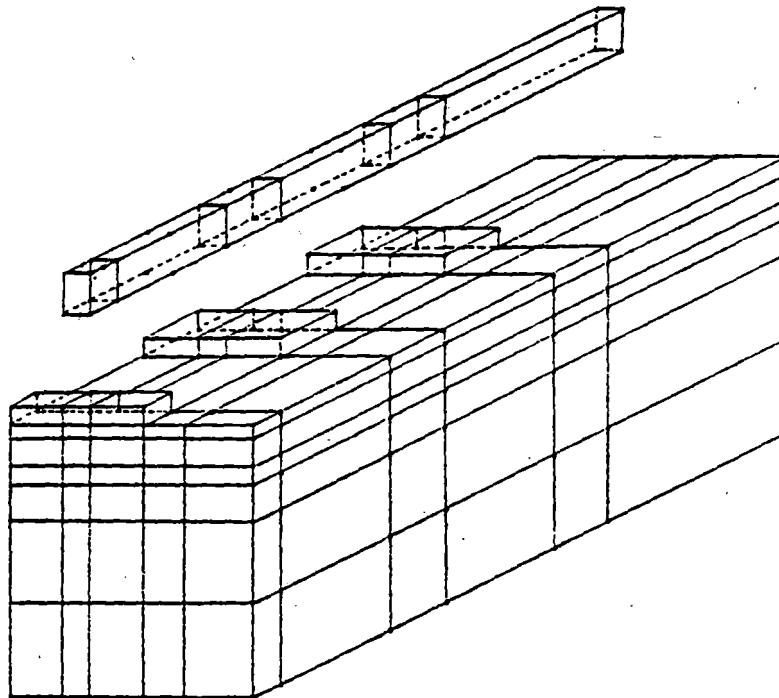
As discussed previously, the purpose of this research is to study the nonlinear interaction behavior in one-, two- and three-dimensional solid media. Variety of sophisticated constitutive relations based on plasticity theory, Chapter 4, are implemented in the finite element computer codes developed herein. An interface element, Chapter 6, is used in the procedure to model the interaction effects.

The problem in this section, Figure (9.22), is selected as one of the applications for the purpose of showing the capability and as a verification of the procedures developed.

This problem, Figure (9.22) is very complex in geometry and the constitutive behavior of its components. A few analytical approaches have been developed for the analysis of track support structures; some of these are ILLITRACK, MULTA and PSA models [39,47,81,82]. The PSA model is based on prismatic solid formulation [39,86], and hence it is applicable only with linear elastic materials. On the other hand MULTA is based on theory of elasticity applied to layered media. ILLITRACK is a two-dimensional finite element procedure developed strictly for the analysis of track support structures. Here, the thickness of the plane strain elements have been varied with the depth on the basis of a stress calculation with elastic properties; this was called a "pseudo plane strain" section. In view of the assumptions involved in ILLITRACK model, the general use is limited [74]. According to recent studies by Selig et al. [74], there is not a single procedure available for



Schematic Representation of Track Support Structure



Three-Dimensional Idealization

Figure 9.22 Finite Element Idealization of a Track Support Structure

nonlinear 3-D analysis of this problem. Furthermore, even for linear elastic behavior, the above models have not been compared with a truly three-dimensional analysis. However, Selig et al. [74] have compared the above three models with respect to predictions of a fully instrumented field experiment done at Pueblo, Colorado. This is referred to as FAST analysis in literature; a complete description of FAST experiment, and the analysis is available in reference [74].

Three-Dimensional Analysis of Previous Problems

A truly three-dimensional stress analysis of the FAST section is carried out by using the three-dimensional procedure. Figure (9.22) shows the finite element mesh used in this analysis. Rail bending effects are modelled by using higher order brick elements. The following material properties used in this analysis are adopted from reference [74]:

Material 1 (subsoil):

$$E = 5,000 \text{ psi } (34.5 \times 10^3 \text{ kN/m}^2)$$

$$\nu = 0.33$$

Material 2 (subballast):

$$E = 20,000 \text{ psi } (138.0 \times 10^3 \text{ kN/m}^2)$$

$$\nu = 0.37$$

Material 3 (ballast):

$$E = 30,000 \text{ psi } (207.0 \times 10^3 \text{ kN/m}^2)$$

$$\nu = 0.37$$

Material 4 (Wood Tie):

$$E = 1.5 \times 10^6 \text{ psi } (10.35 \times 10^6 \text{ kN/m}^2)$$

$$\nu = 0.30$$

Material 5 (Steel Rail):

$$E = 30 \times 10^6 \text{ psi } (207.0 \times 10^6 \text{ kN/m}^2)$$

$$\nu = 0.30$$

In this analysis, Figure (9.23), only a quadrant of the semi-infinite medium is discretized by assuming the problem to be symmetric. Here, only three ties are considered since previous studies have shown that most of the load is distributed to tie under the load and to the adjoining two ties. Furthermore, the computational effort and the required core storage impose a restriction to the size of the finite-element mesh. The bottom boundary of the mesh in Figure (9.23) is assumed to be rough while the boundaries in the x and y directions are assumed to be smooth.

Figures (9.24) and (9.25) show the effects of the extent of discretized longitudinal boundary on the predictions of stresses and displacements. The differences in predictions are insignificant when the longitudinal boundary is changed from 150 inches (381 cm) to 250 inches (635 cm). However, when the longitudinal boundary is selected at 50 inches (127 cm), the displacements, Figure (9.25), increased significantly. One could think that when the boundaries are closer, the system becomes more stiffer, and hence the displacements should be smaller. However, in this case, the smooth boundaries in longitudinal direction brings the situation closer to a plane strain state, and that

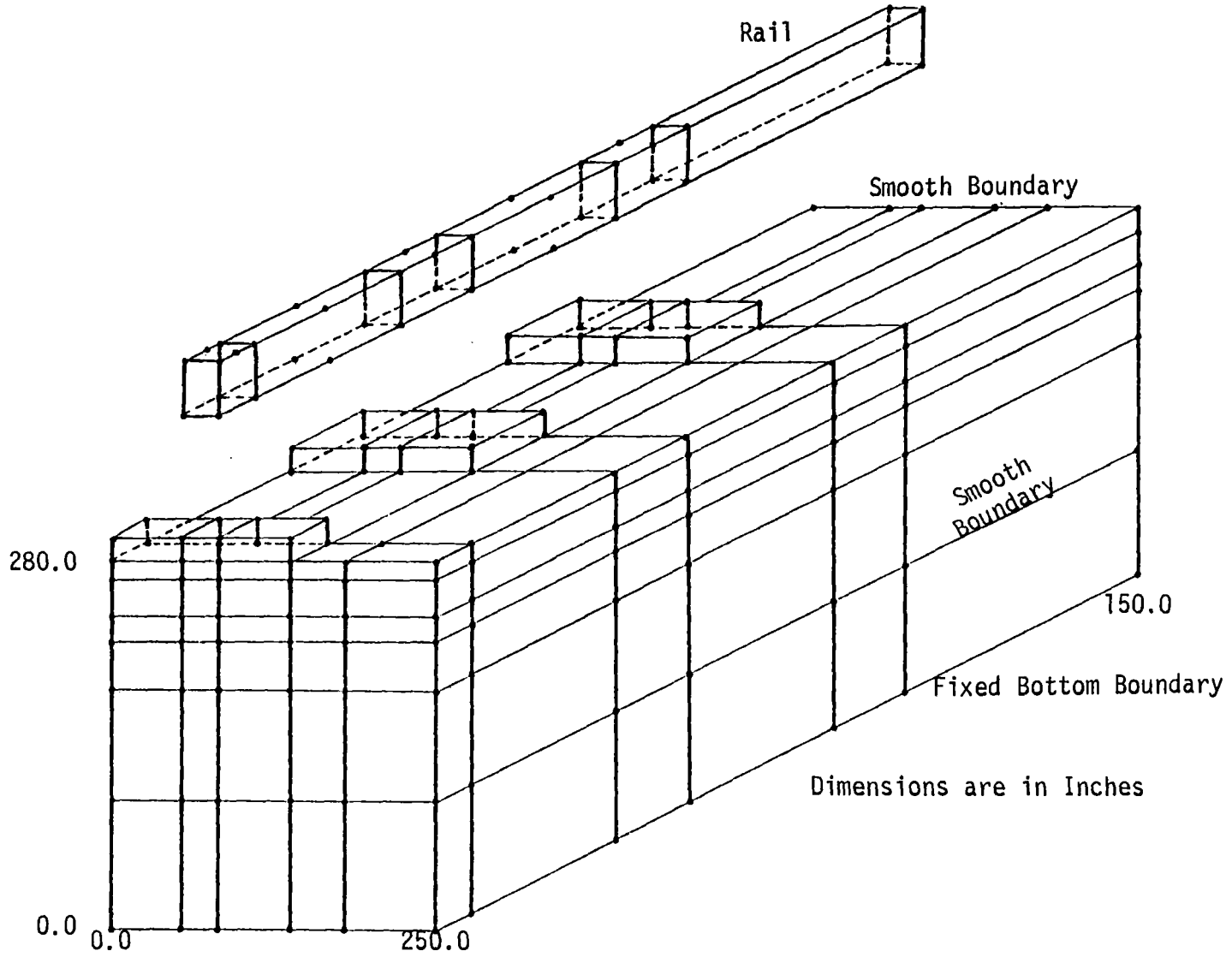


Figure 9.23 Three-Dimensional Finite Element Mesh for Analysis of FAST Section

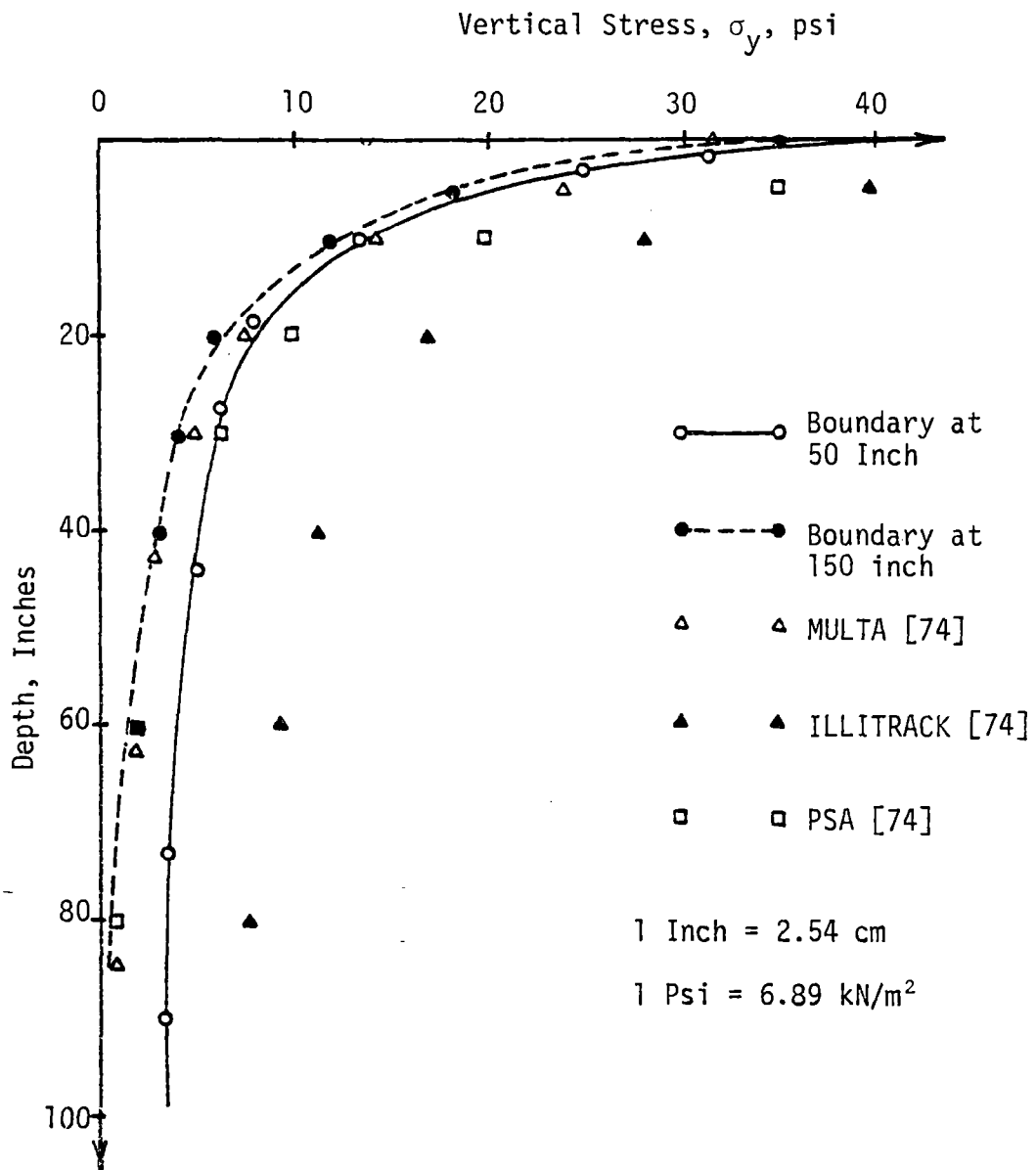


Figure 9.24 Effect of Longitudinal Boundary Distance on the Stress Distribution Below the Wheel Load.

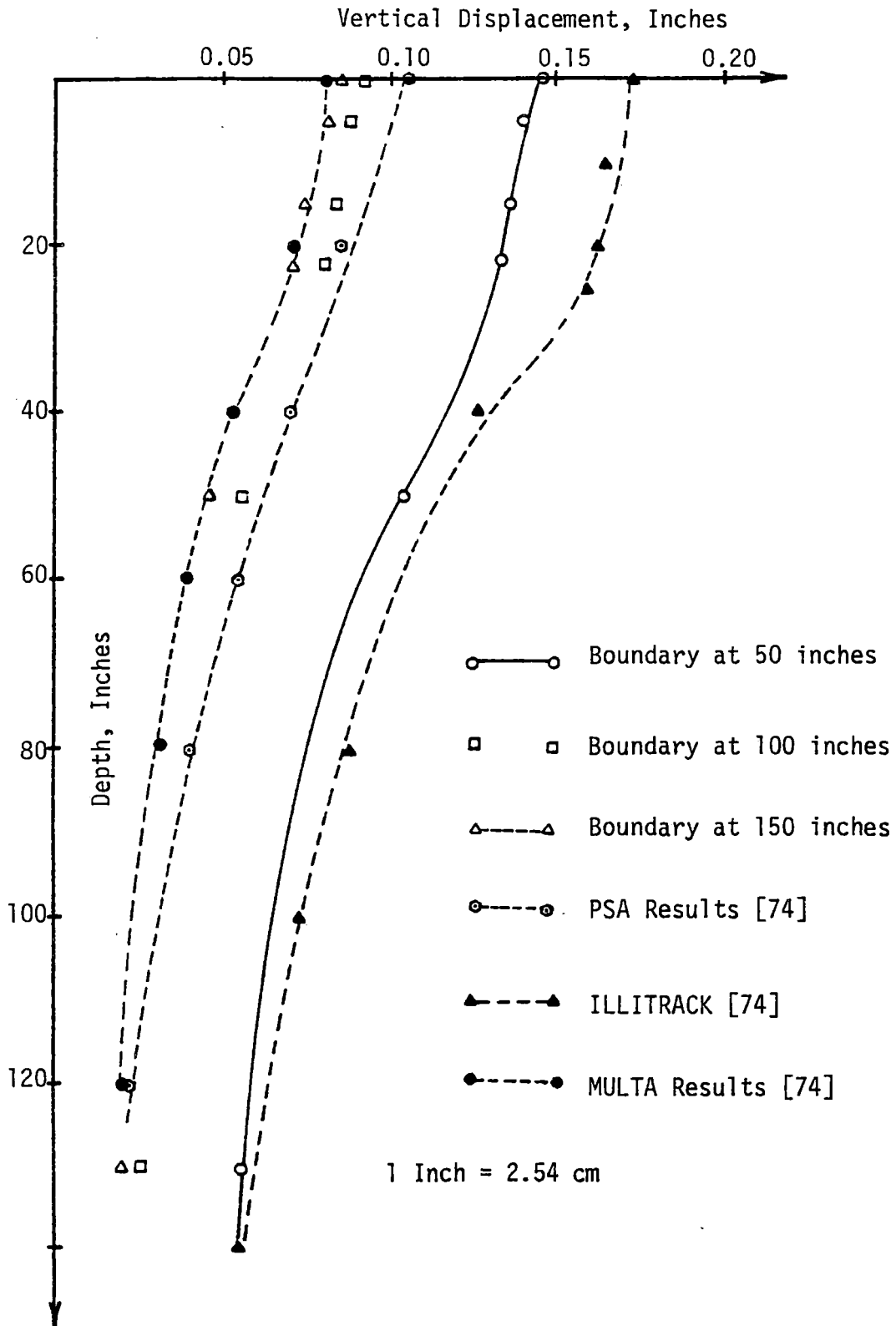


Figure 9.25 Effect of Longitudinal Boundary Distance on the Displacements from a Three-Dimensional Analysis

is why the predicted displacements becomes larger. The smooth boundary acts like a 'reflecting' boundary. This is evident from the fact that the predictions in Figure (9.25) are closer to plane strain predictions from ILLITRACK [82], when the extent of the longitudinal boundary is made smaller.

The stress and displacement distributions predicted by three-dimensional analysis are closer to the predictions from MULTA; this verifies the code since MULTA is based on three-dimensional linear elasticity.

Effect of Tie Stiffness

The effect of tie stiffness of wood tie on the stress and displacement distributions are shown in Figures (9.26) and (9.27). For a stiffer tie, stresses and displacements seem to reduce near the surface.

Load Application

Figure (9.28) shows the surface deformations in the longitudinal directions. Here, two loading cases, A and B, Figure (9.28), are studied. The load case B is based on the information given in reference [74]. Loading case B is based on the assumption that the foundation is linearly elastic. Both the loading cases A and B seem to predict similar deformations for elastic case. Therefore, in the subsequent nonlinear analysis of this problem, loading case A is used.

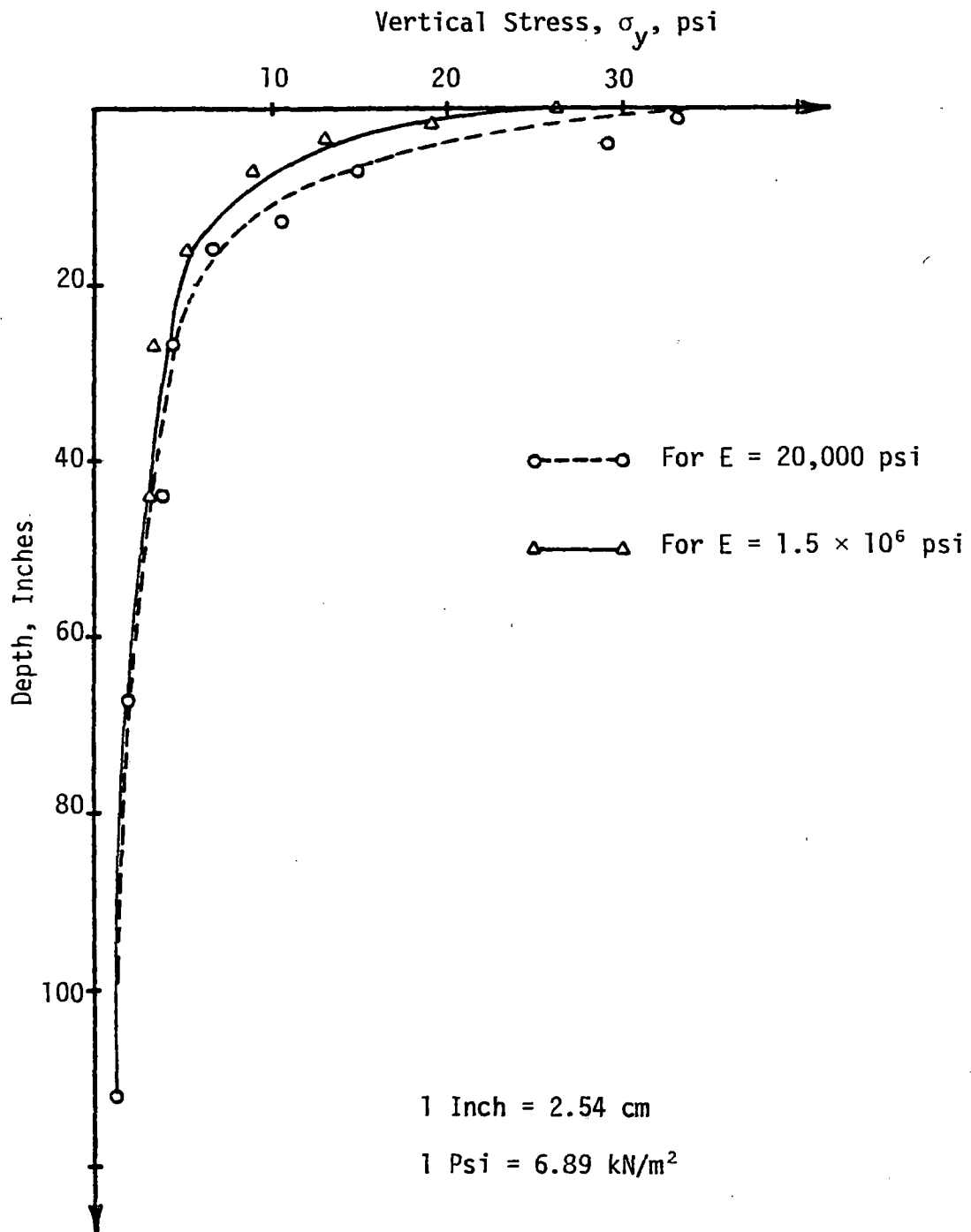


Figure 9.26 Effect of Tie Stiffness on the Stress Distribution Below the Load at FAST Section

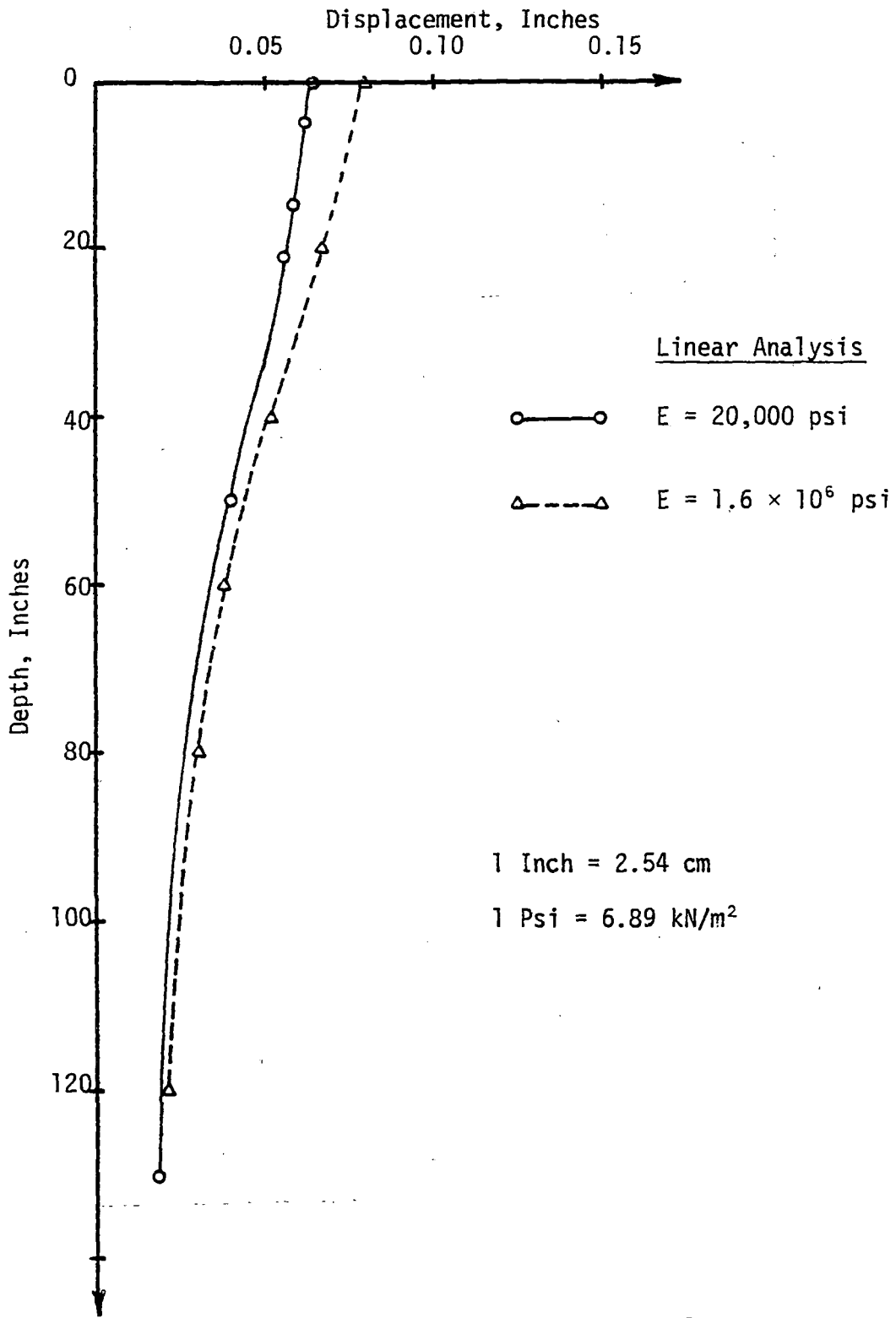


Figure 9.27 Effect of Tie Stiffness on Displacement Distribution

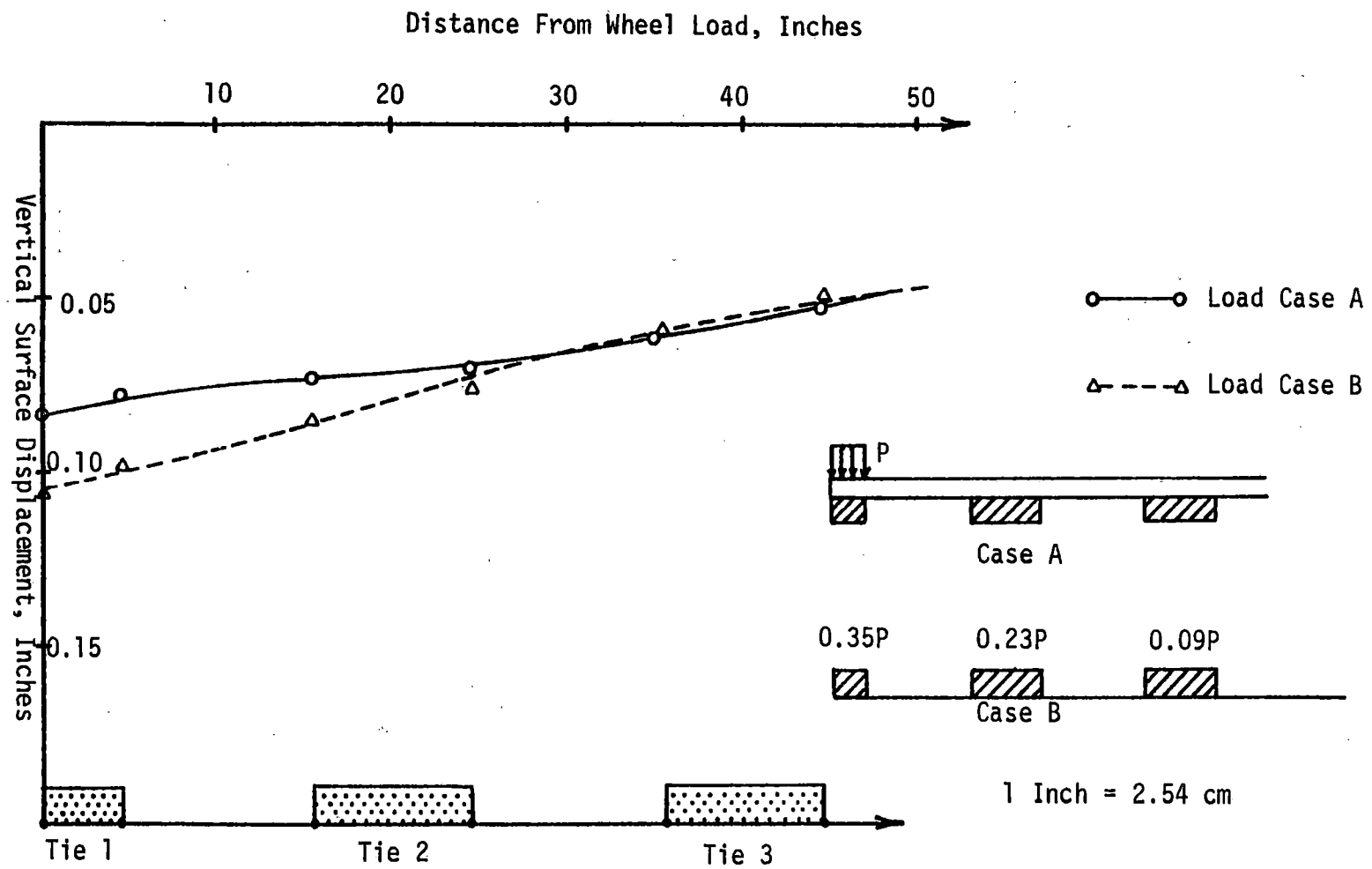


Figure 9.28 Comparison of Two Loading Configurations

Finite Element Analysis

Although, a truly three-dimensional analysis is most appropriate, it can often be expensive. Hence, the possibility of using a two-dimensional plane strain analysis to obtain approximate results was investigated. Figure (9.29) shows the finite element mesh used for the plane strain analysis. Thickness of this section is taken as 20 inches (50 cm); physical significance of this value is that it is the tie spacing used. Since this assumption does not have any theoretical foundation, it does not imply that three-dimensional effects can be reproduced by plane strain idealizations. It is only used to study qualitative behavior.

Figures (9.30) and (9.31) show the results obtained from a linear elastic plane strain analysis. The stress distribution in Figure (9.30) falls between truly three-dimensional analysis performed herein, and the pseudo plane strain analysis carried out in reference [74] by using ILLITRACK model. However, the displacements in Figure (9.31), seem to be fairly higher than the truly three-dimensional analysis. Therefore, plane strain analysis may be used only to get an idea of the stress and displacement distribution in the support structure; three-dimensional analysis may be required for accurate quantitative values.

Analysis of UMTA Test Section

A fully instrumented field experiment has been carried out to study the performance of transit track support systems by Kaman Avidyne Corporation [78]. This study was conducted at a test section, at the facility of Urban Mass Transportation Authority (UMTA), Pueblo,

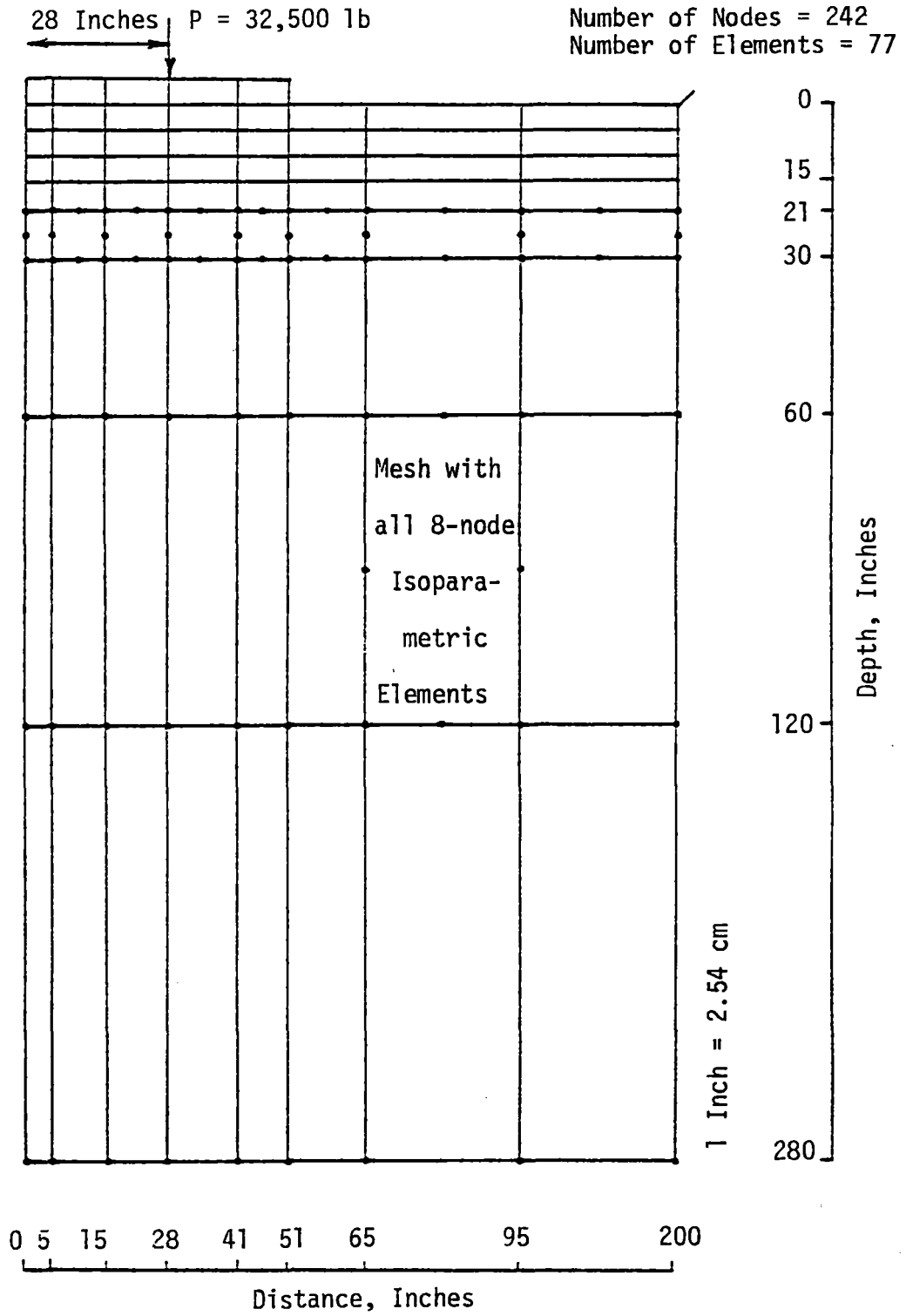


Figure 9.29 Finite Element Mesh for Analysis of FAST Section

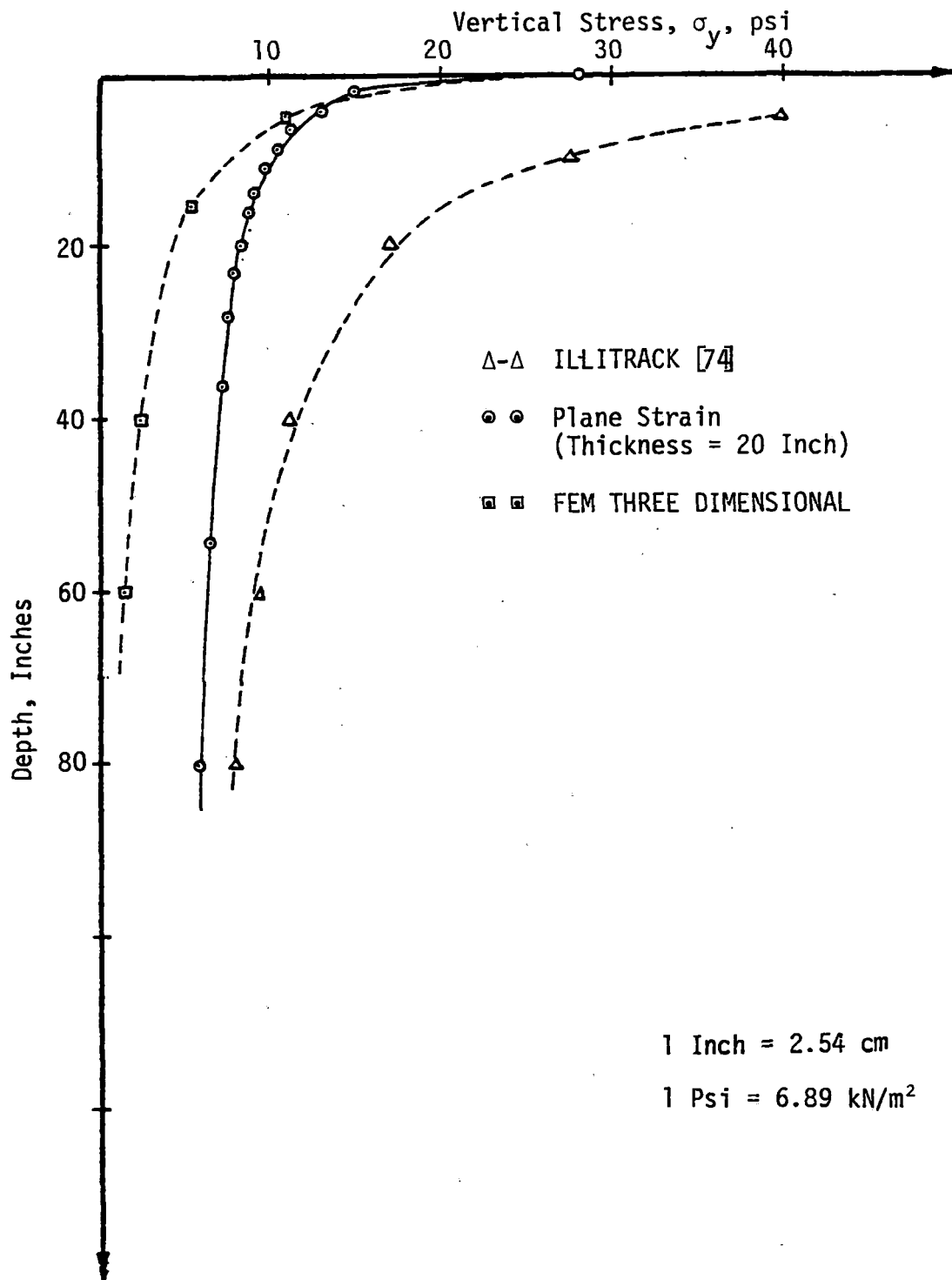


Figure 9.30 Comparison of Plane Strain and Three-Dimensional Stress Distribution

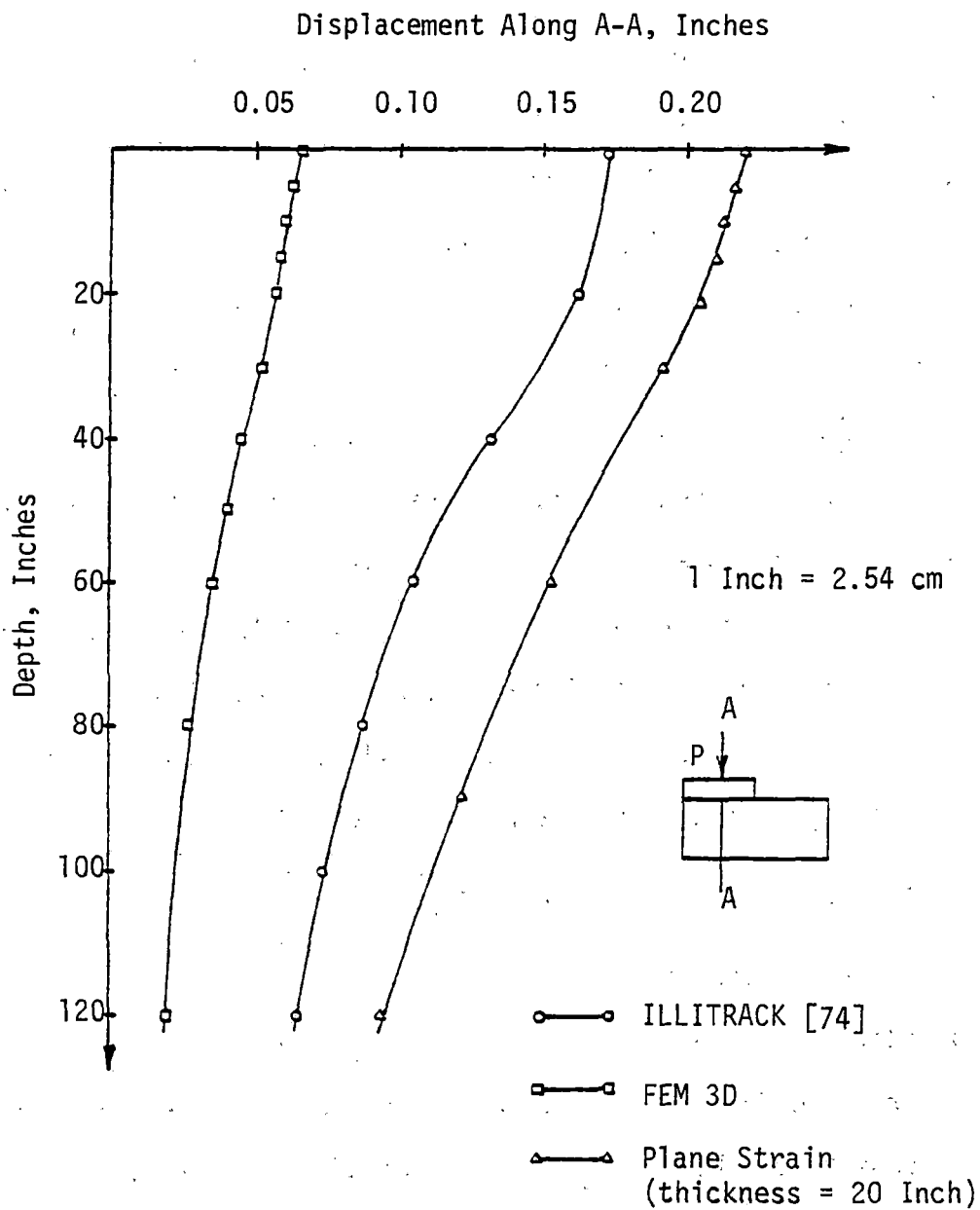


Figure 9.31 Comparison of Plane Strain and Three-Dimensional Displacement Distribution

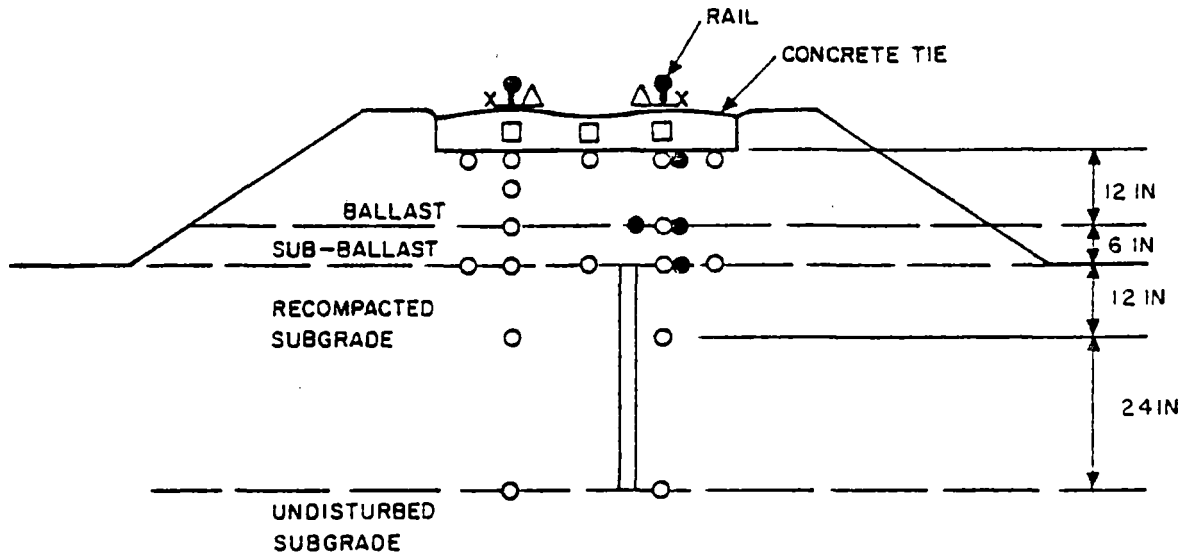
Colorado. A complete description of the test section and other relevant information is available in reference [78].

An analysis of this test section is performed by using the nonlinear one-, two- and three-dimensional finite-element computer programs developed herein. The predictions are then compared with experimental operations made by Kaman AviDyne [78]. The support structure of the test section, Figure (9.32), consists of concrete ties, 12 inch (30.5 cm) thick ballast layer, 6 inch (15 cm) thick subballast layer, and a sand subgrade. The tie spacing is 30 inches (76.2 cm).

As pointed out in previous chapters, one of the important aspects of a nonlinear analysis is the constitutive characterization of materials. A comprehensive test program on the materials obtained from this test site, and the interfaces has been carried out under the research study [23,45]; partial details of the experimental work conducted for the subsoil sand are given in Chapter 7.

Properties Used in Nonlinear Analysis

Field experiments have been carried out at different vehicle speeds, and based on experimental observations a wheel load of 16,000 lb was recommended [78]. Based on laboratory experimental data, different components of the structure are modelled by different constitutive models. For instance, rail and concrete ties are characterized by linear elastic model, Chapter 2, ballast (granular) material by Variable Moduli Model, Equation (4.44), subballast (granular) material by Cap Model, Equation (4.33), and the sandy soil by the Critical State Model,

MEASUREMENT

W/R LOADS
 TIE BENDING STRAINS
 FASTENER STRAINS
 PRESSURES
 SOIL STRAINS
 EXTENSOMETER (STRAIN)

SYMBOL

x
 □
 △
 ○
 ●
 ||

1 Inch = 2.54 cm

Figure 9.32 Instrumentation Locations at UMTA Test Station [78]

Equation (4.30). The corresponding properties of these materials used in the finite element analysis are reported in references [45,78].

Material Properties for Linear Analysis of UMTA Section [78]

Rail:

$$E = 30 \times 10^6 \text{ psi } (207.0 \times 10^6 \text{ kN/m}^2)$$

$$\nu = 0.35$$

Tie:

$$E = 5.0 \times 10^6 \text{ psi } (34.5 \times 10^6 \text{ kN/m}^2)$$

$$\nu = 0.2$$

Ballast:

$$E = 30,000.0 \text{ psi } (207.0 \times 10^6 \text{ kN/m}^2)$$

$$\nu = 0.40$$

Subballast:

$$E = 20,000.0 \text{ psi } (138.0 \times 10^3 \text{ kN/m}^2)$$

$$\nu = 0.35$$

Subgrade:

$$E = 5,000.0 \text{ psi } (34.5 \times 10^3 \text{ kN/m}^2)$$

$$\nu = 0.45$$

Material Properties for Nonlinear UMTA Section [23,45]

Rail (steel):

$$E = 30 \times 10^6 \text{ psi } (207.0 \times 10^6 \text{ kN/m}^2)$$

$$\nu = 0.3$$

$$I = 71.4 \text{ in}^4 \text{ (2971.9 cm}^4\text{)}$$

$$A = 11.65 \text{ in}^2 \text{ (75.16 cm}^2\text{)}$$

Tie (concrete):

$$E = 4.2 \times 10^6 \text{ psi } (28.98 \times 10^6 \text{ kN/m}^2)$$

$$\nu = 0.2$$

Subballast: Cap Model

$$E = 20,000 \text{ psi } (138 \times 10^3 \text{ kN/m}^2)$$

$$D = 0.308 \times 10^{-4} \text{ psi}^{-1} [0.446 \times 10^{-4} (\text{kN/m})^{-1}]$$

$$\nu = 0.40$$

$$\alpha = 26.0 \text{ psi } (179.4 \text{ kN/m}^2)$$

$$\rho = 0.0833 \text{ lb/in}^3$$

$$\gamma = 21.5 \text{ psi } (148.35 \text{ kN/m}^2)$$

$$R = 1.24$$

$$\beta = 0.02$$

$$W = 0.035$$

Ballast: Stress-Strain Variable Moduli Model

$$K_0 = 4 \times 10^3 \text{ psi } (27.6 \text{ kN/m}^2)$$

$$G_0 = 1.7414 \times 10^3 \text{ psi } (11.83 \text{ kN/m}^2)$$

$$K_1 = 5.4917 \times 10^5 \text{ psi } (37.89 \times 10^5 \text{ kN/m}^2)$$

$$\gamma_1 = 2.5593$$

$$K_2 = 2.536 \times 10^7 \text{ psi } (17.50 \times 10^7 \text{ kN/m}^2)$$

$$\gamma_2 = -60.1722$$

$$\rho = 0.0613 \text{ lb/in}^3$$

Subgrade (Sand): Critical State Model

$$M = 1.24$$

$$E_0 = 12,000 \text{ psi } (82.8 \times 10^3 \text{ kN/m}^2)$$

$$\lambda_c = 0.014$$

$$\nu = 0.28$$

$$\kappa = 0.0024$$

$$\rho = 0.081 \text{ lb/in}^3$$

$$e_0 = .270$$

Interfaces:

$$E = 30,000 \text{ psi (208.50 kN/m}^2\text{)}$$

$$\nu = 0.30$$

$$G_{\text{int}} = 225.0 \text{ psi (1552.5 kN/m}^2\text{)}$$

The analysis of this problem can be performed by using different levels of sophistication. These include:

- (1) Analysis of surface deformations using nonlinear one-dimensional beam column idealization
- (2) Approximate analysis by using the nonlinear two-dimensional finite element procedure, or
- (3) Truly three-dimensional analysis using the three-dimensional finite element procedure.

One-Dimensional Analysis

The loads that are transferred through the rail to the supporting ties can be determined by using the procedure developed in Chapters 3 and 5 for the analysis of beam columns on nonlinear supports. One of the important and difficult aspects of this analysis is the determination of support conditions (subgrade reaction) which can be nonlinear in general. This can be determined by using experimental procedures. For the linear situation, the material behavior does not depend on the stress history nor the current state of stress. Therefore, the subgrade reaction determined from a single load can be used to study the response under any number of loads. However, in nonlinear analysis, this

procedure may not be valid. Since the material behavior is governed by state of stress and the stress history, the response of a medium at one location will depend on the loading and its history at other locations. Furthermore, the principle of superposition is not valid in nonlinear mechanics. Therefore, representation of a continuous nonlinear solid medium by a series of discrete nonlinear springs, in general becomes theoretically unsound.

From the above discussion, it is evident that a truly nonlinear analysis of a beam on a nonlinear foundation, from the mechanics point of view, becomes theoretically difficult. However, for certain special cases if the beam supports are far away from each other, then it may be possible to assume that the response at each support is independent of loadings at other supports. Within the scope of this research, this aspect has not been fully studied.

Figure (9.33) shows the displacements and tie load distribution obtained from a one-dimensional analysis with the stress transfer procedure. About 50.0 percent of the load is transferred to the first support while about 25.0 percent of the load is transferred to the second support. These values are consistent with those reported in reference [78]. This load distribution is then used to carry out the approximate two-dimensional analysis.

Two- and Three-Dimensional Procedures

Figures (9.34) and (9.35) show the three- and two-dimensional finite element meshes used for the interaction analysis. The thickness of the plane strain section is assumed as 30 inches (76.2 cm), which is

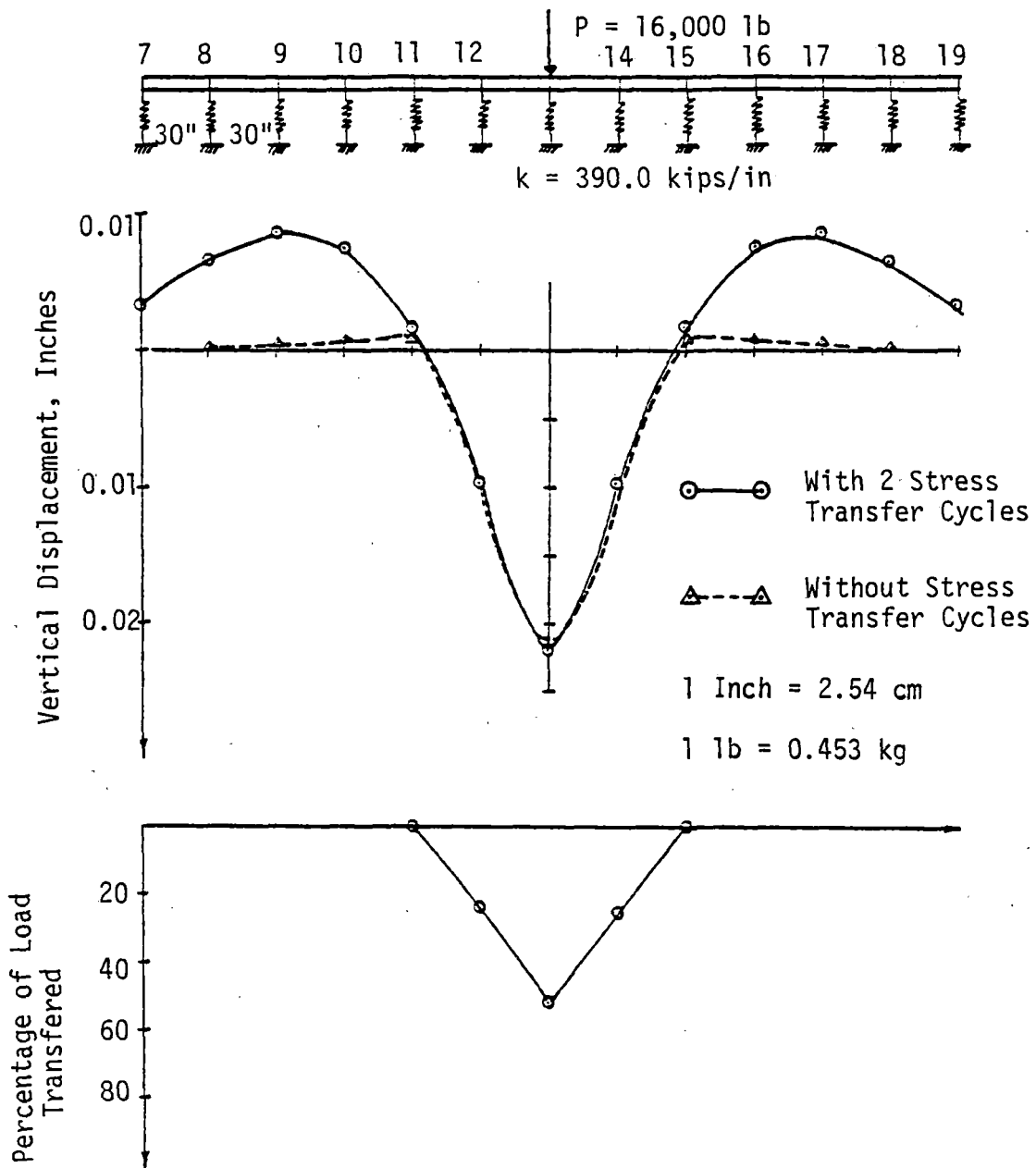


Figure 9.33 One-Dimensional Analysis of UMTA Test Section

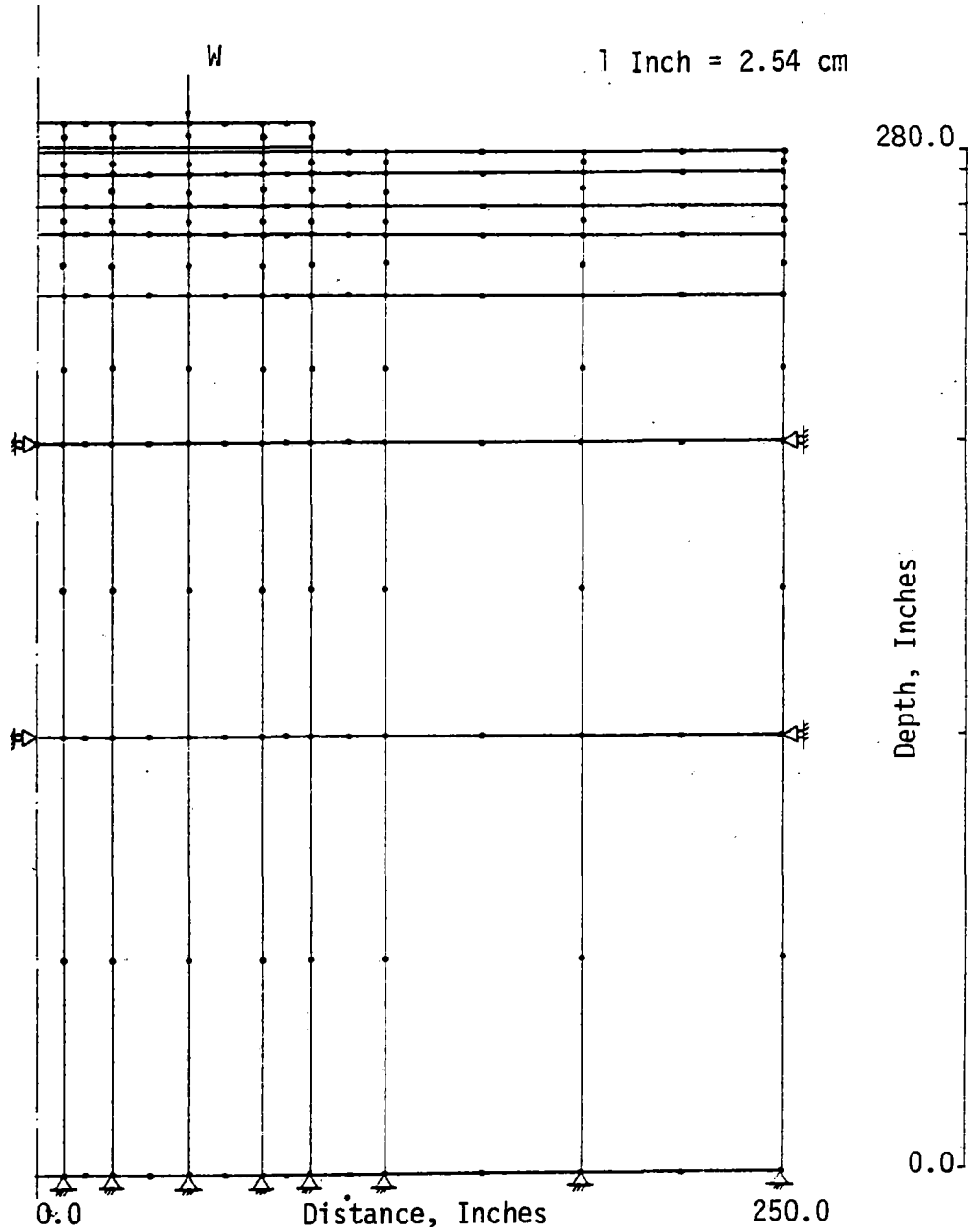


Figure 9.34 Finite Element Mesh for Plane Strain Analysis of UMTA Test Section

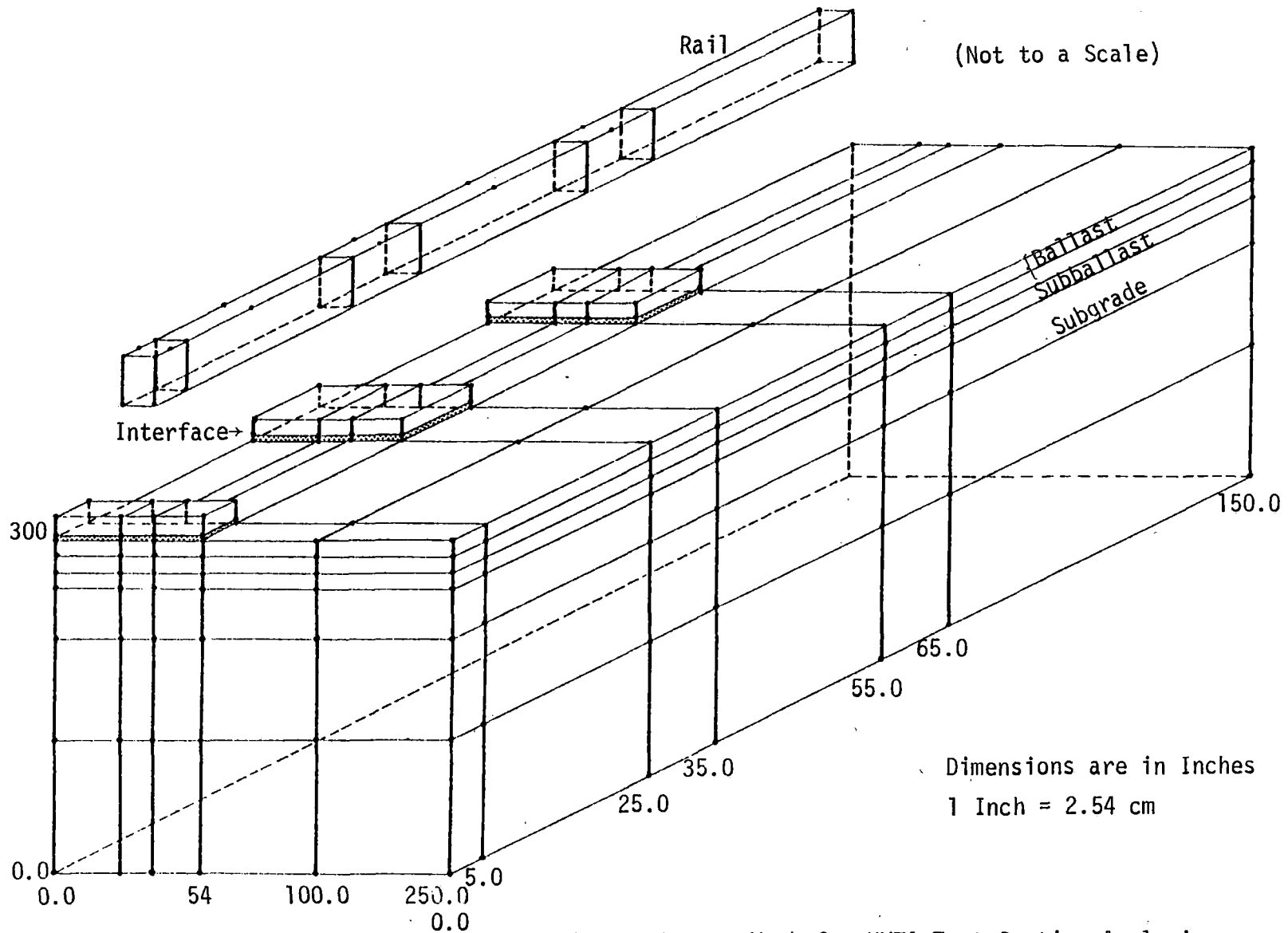


Figure 9.35 Three-Dimensional Finite Element Mesh for UMTA Test Section Analysis

equal to the tie spacing at the test section. Interface elements are used to model interaction between ties and the ballast.

Figure (9.36) shows a comparison of predicted from a linear analysis and measured values of vertical pressure. The measured vertical stresses under inner and outer rail, Figure (9.36), are quite different although they can be expected to be of the same order. The measured stress distribution under the outer rail does not indicate rapid decay that is expected in a three-dimensional situation. Hence, the measured values under the outer rail is questionable. Three-dimensional finite element predictions seems to fall between the measurements [78] made at inner and outer ties; it is closer to the stresses under inner rail. Figure (9.37) shows the stress distribution obtained from nonlinear analysis. Since the constitutive behavior is dependent on initial stresses, and insitu stress analysis is performed, prior to application of external load. In this case three-dimensional predictions seem to be closer to the measurements made at the inner tie.

Comparison of displacements are shown in Table 9.3. Predicted values at the point of load application are much smaller than the measured values; it has been observed [78] that there are unresolved inconsistencies in measured magnitudes of displacements.

Displacement Patterns

The kinematics patterns obtained from nonlinear two- and three-dimensional analysis are shown in Figures (9.38) and (9.39). It seems that the interaction effects are predominant for about 20.0 inches directly below the ties.

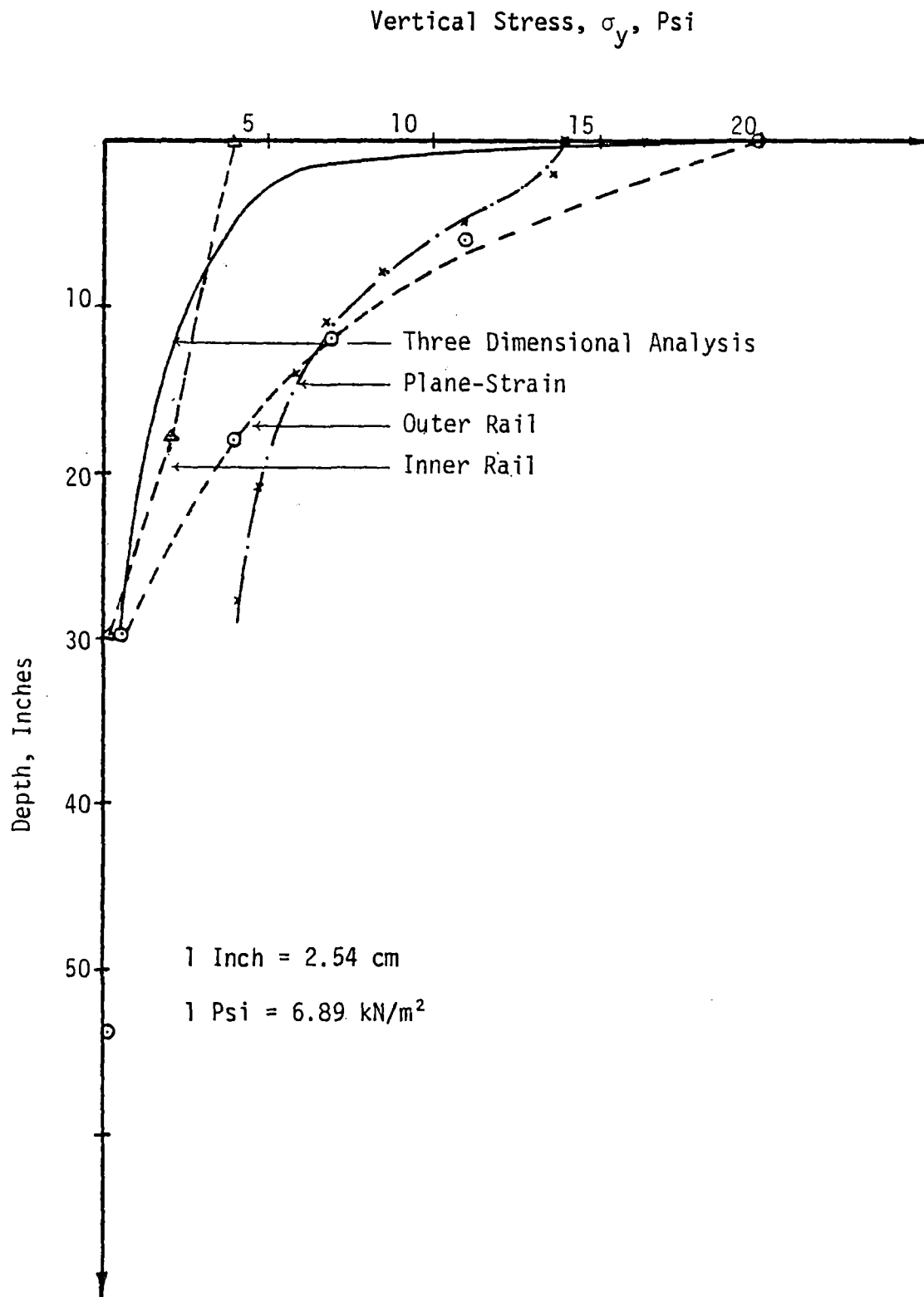


Figure 9.36 Stress Distribution at UMTA Section from a Linear Analysis

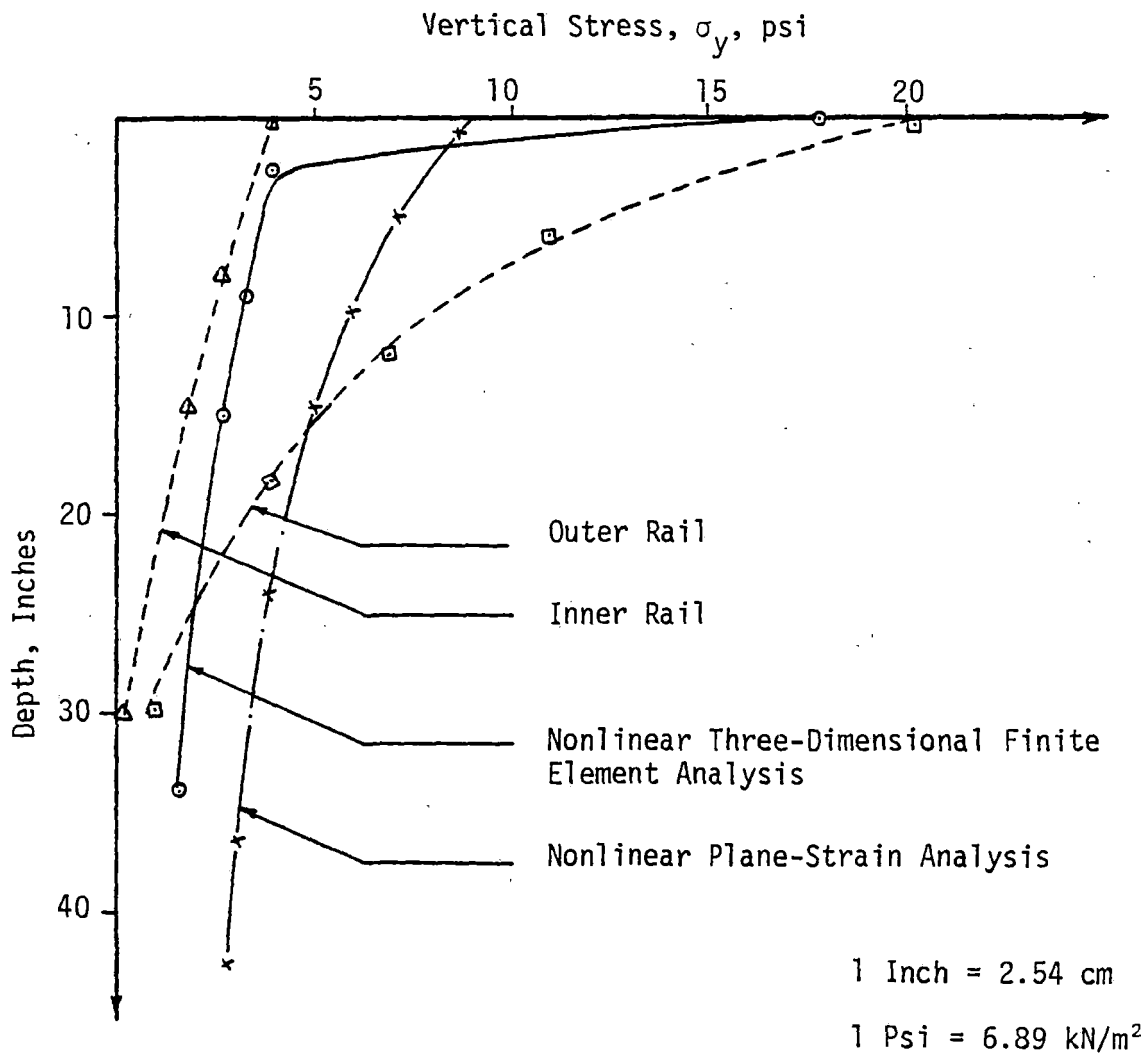


Figure 9.37 Stress-Distribution from a Nonlinear Three-Dimensional Analysis of UMTA Test Section

Table 9.3

Deflections at Point of Load Application at UMTA Test Section

Model	Measured* Values (Inches)	Predictions (Inches)
3-D Linear	0.18	0.023
2-D Linear	0.18	0.081
3-D Nonlinear	0.18	0.029
2-D Nonlinear	0.18	0.202

* Obtained from reference [78]. It has been mentioned in this reference that there are unresolved inconsistencies in measured magnitudes of this data.

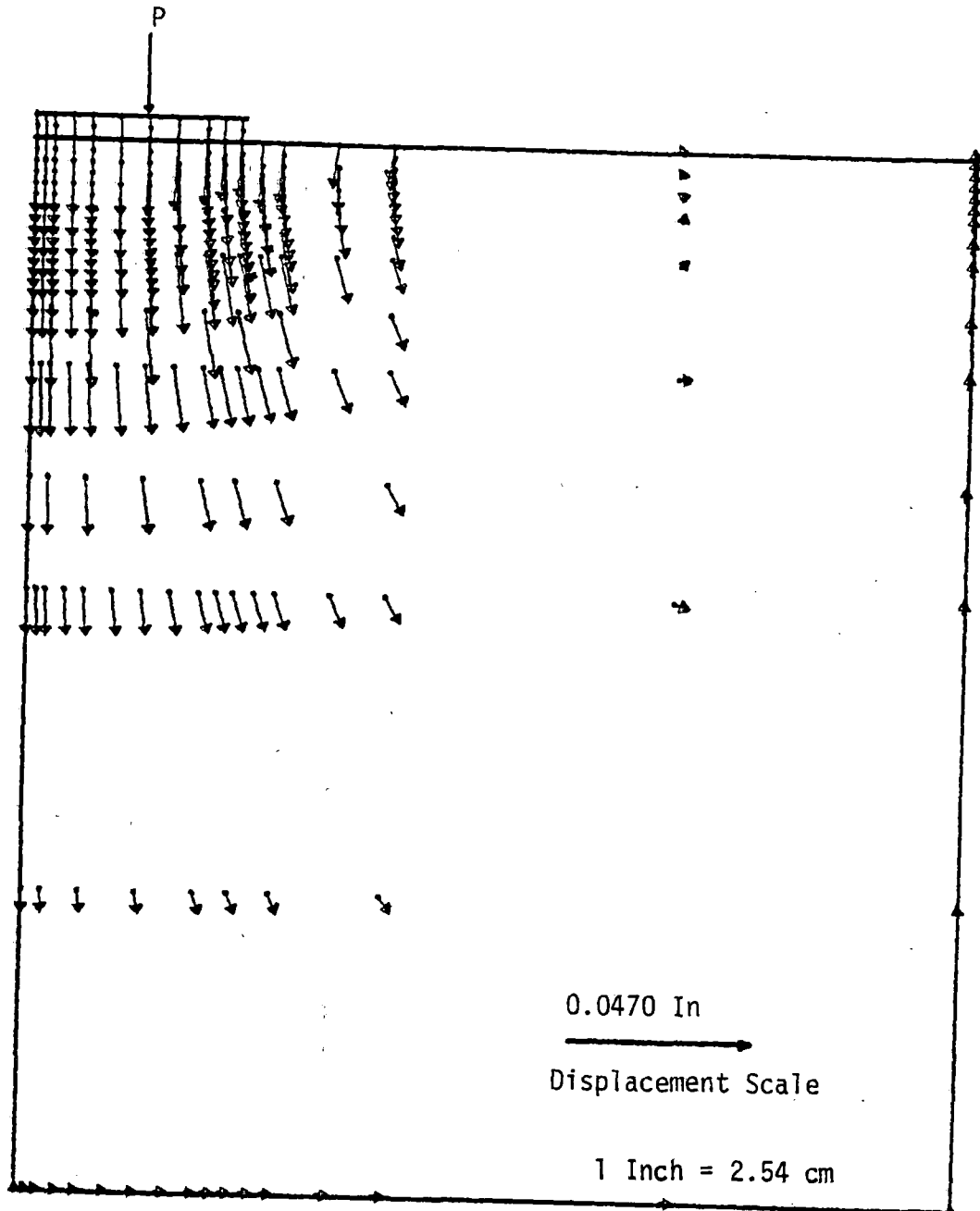
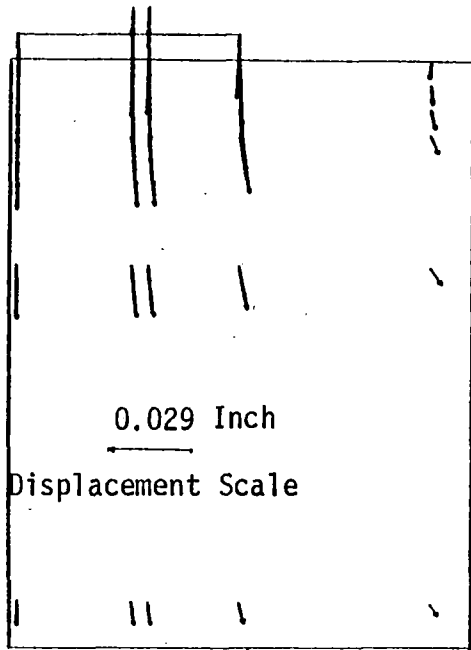
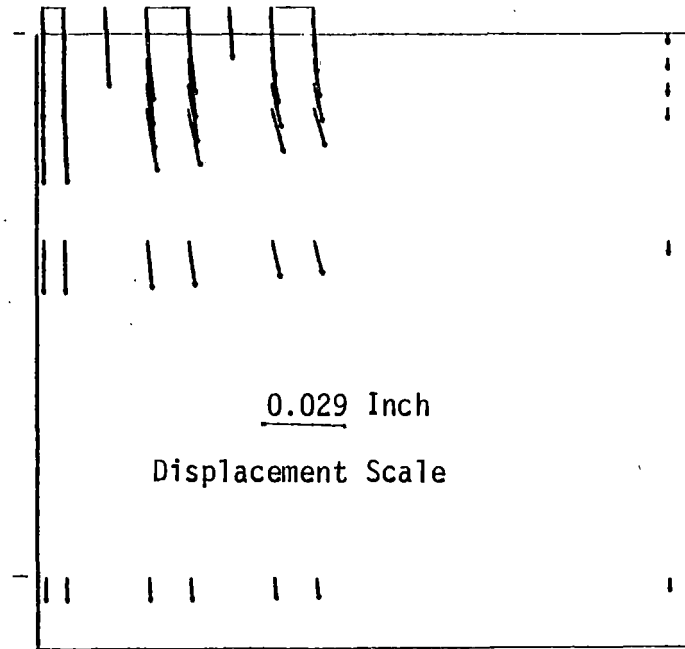


Figure 9.38 Displacement Field for UMTA Test Section from a Two-Dimensional Analysis



(a) Transverse Section



(b) Longitudinal Section

Figure 9.39 Displacement Field from a Three-Dimensional Analysis of UMTA Section

Comment

Analytical results show that the deformation behavior of the system is fairly linear up to the actual load applied in the field experiment. In order to study the nonlinear behavior of the support structure, a load which is five times the 'wheel load' is applied, and a three-dimensional analysis is carried out in ten increments with one iteration per step. The load-displacement curve is shown in Figure (9.40). The response is seen to be fairly linear up to about $2P$, where P is the wheel load. Nonlinearity is seen at very high loads showing that support system is very strong. The allowable displacement at the surface is given as 0.25 inch (0.64 cm) [78]. This indicates that the section is probably overdesigned.

Effects of Interface Elements on Predictions

Figure (9.41) shows the distributions of stress obtained by using nonlinear two- and three-dimensional programs with and without interfaces. It is evident that the effects of interfaces on vertical stress distribution are not significant. Interaction due to lateral and longitudinal loads are recommended for future studies.

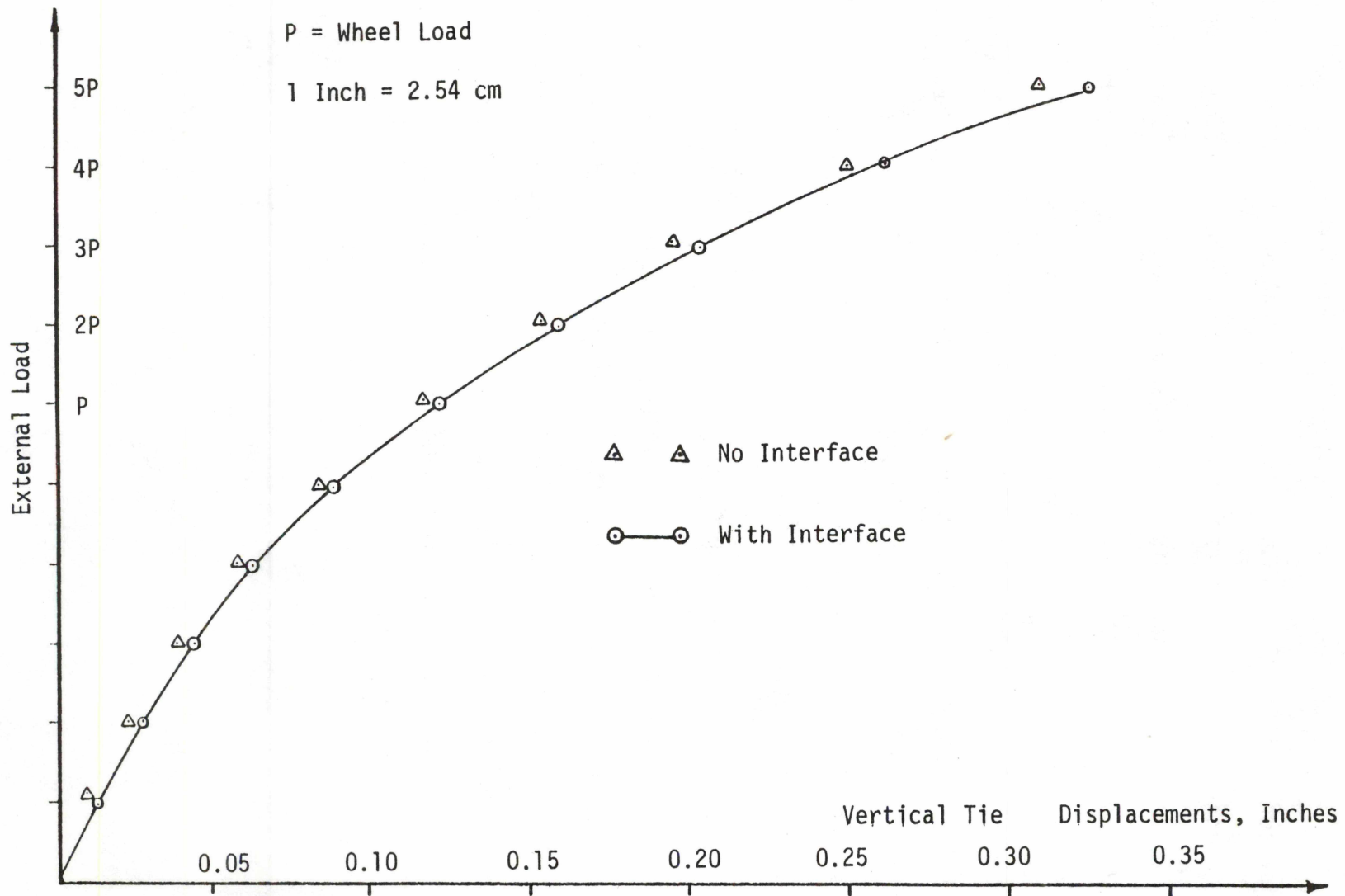
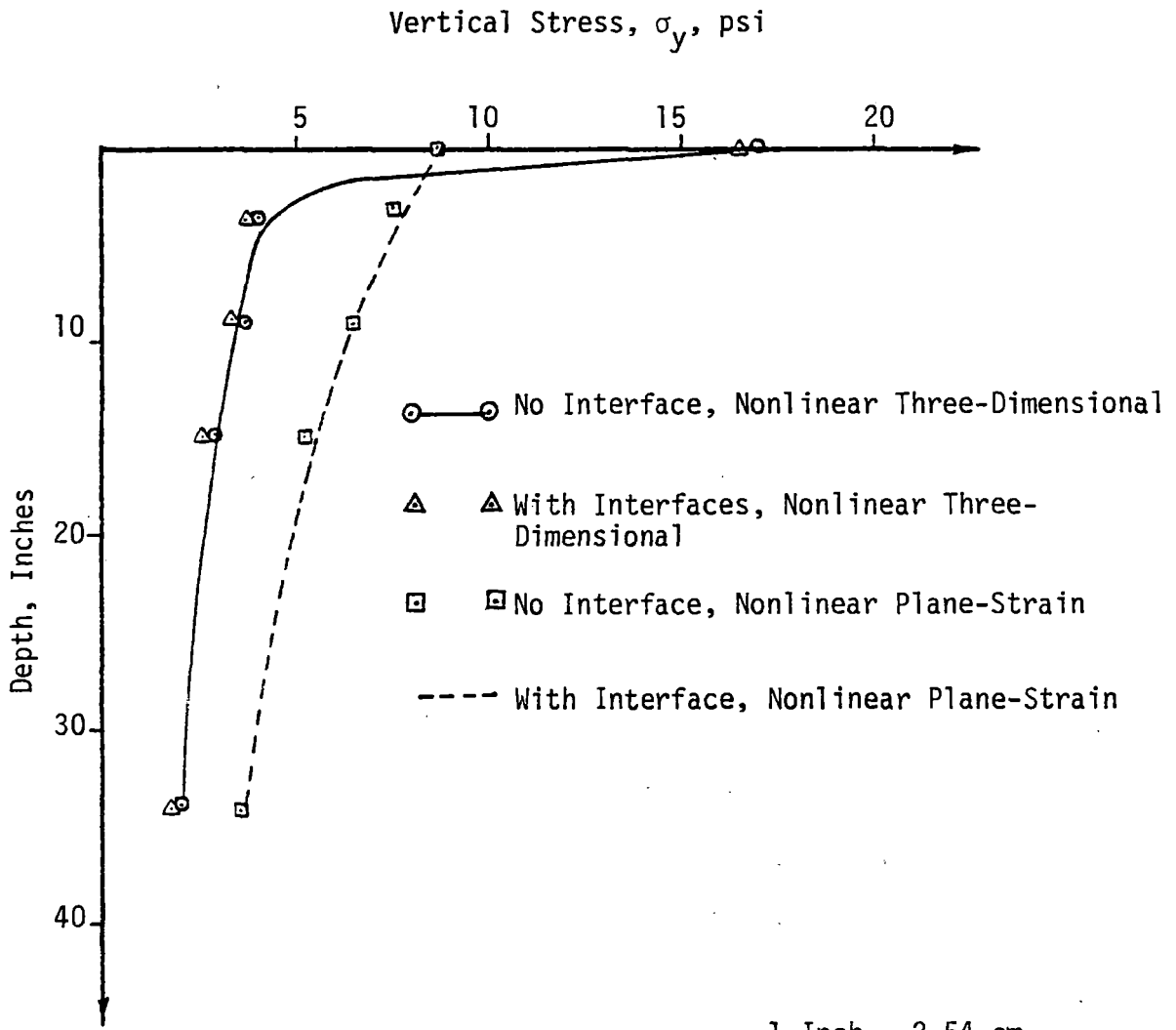


Figure 9.40 Nonlinear Three-Dimensional Interaction Analysis of UMTA Section at Higher Loads



1 Inch = 2.54 cm

1 Psi = 6.89 kN/m²

Figure 9.41 Effect of Interface Elements on the Vertical Stress Distribution

SUMMARY AND CONCLUSIONS

A number of previous studies involving two- and three-dimensional finite element procedures have considered nonlinear elastic and plasticity models. However, particularly in the context of three-dimensional analysis with advanced constitutive laws, hardly any consistent algorithms that can provide reliable results over the entire range of load-deformations history appear to have been reported. Since the main objective of this dissertation was to develop generalized procedures including material and interface nonlinearities, it became necessary to evolve a viable algorithm that can provide convergent solutions, particularly in the zones of the plastic behavior. One of the contributions of this study lies in the development and application of such a procedure in both two- and three-dimensional analysis.

Behavior of geologic media is highly complex, and no single constitutive law has yet been developed for all geologic media. Various laws are suitable only for a limited class of media, and most previous studies have included only one constitutive law. In order to overcome this shortcoming, a number of different and advanced laws, Linear Elastic, Variable-Moduli, Drucker-Prager, Critical State and Cap Models, were defined and introduced in the two- and three-dimensional procedures; this provision allows for using an appropriate law for a given material in a soil-structure interaction problem. Furthermore, detailed derivations of constitutive equations were made for all the

models in the context of three-dimensional analysis; they were then specialized for use in the two-dimensional analysis also.

One-dimensional procedure developed herein can be used to study interaction behavior of beams-on-deformable foundations, including capability to account for separation or closure of gaps between beam and soil. This can be performed by using the stress transfer procedure which uses a rather novel algorithm developed herein. Foundations nonlinearities were characterized by using a Ramberg-Osgood model. Deformation behavior of the beam in the tensile zones was significantly different when the stress transfer cycles were used; the distribution of reaction was not affected significantly, however. This procedure can be used to study interaction problems such as laterally loaded piles, retaining walls, and (long) rails in track support structures.

The two- and three-dimensional procedures have been verified with respect to several problems. A plane strain footing problem was analyzed by using the two-dimensional procedure, and by using the three-dimensional procedure with appropriate constraints. It was concluded that both procedures give similar results when the number of degrees-of-freedom was the same in the plane of deformation. The predicted ultimate strength was seen to be affected by the number of degrees-of-freedom in the finite element mesh used. Therefore, a parametric study with the degrees-of-freedom may be appropriate in selecting a finite element mesh for a nonlinear analysis of a new problem.

The interaction behavior was studied by using a special interface element. Some numerical studies of this element have shown that its performance is satisfactory.

In the plane strain analysis of elasto-plastic problems, the stresses in the direction normal to the plane have to be properly computed. Use of Poisson's ratio to compute these stresses can give acceptable results at low stress levels; however, the ultimate stresses predicted by this procedure was seen to be higher than the values computed by using an alternative and rigorous method based on the incremental elastic-plastic constitutive relation.

Displacement vector field obtained from the above analysis shows that the isotropic hardening models did not predict volume expansions, whereas the Drucker-Prager model predicted large volumetric expansions. The usual experience appears to be more consistent with the former.

Although, procedures for finding constitutive parameters for conventional models such as von-Mises, Mohr-Coulomb, and Drucker-Prager are available, the question of how to find appropriate parameters for advanced laws such as cap and critical state is difficult indeed. Often, in the past, simplified approaches based on conventional testing devices such as cylindrical triaxial configurations have been used. However, for general three-dimensional characterization, this approach is not adequate. Hence, another important contribution of this dissertation has been a rational approach for determination of parameters to define the advanced laws. Here significant attention was given to identification of the parameters and their determination from a sophisticated truly triaxial testing device that permits simulation of various initial densities, confinement and stress paths.

Parameters for a subgrade sand obtained from a test section in Pueblo, Colorado were determined from a detailed laboratory experimental

program. These properties, together with the other parameters available from the testing program for other media conducted under the research program [22,45] were then utilized in analyzing a rather complex problem of nonlinear interaction in a track support structure. The predictions from the finite element procedures developed herein compared well with field measurements.

Preliminary investigations were performed toward a new procedure called resistance-reponse approach, by combining the three finite element formulations developed. Future research and verifications will be needed in order to assess the applicability of the procedure.

In summary, the major contributions of this thesis can be stated as follows.

- (1) Development of rather new computational procedures with special attention to derivation and implementation of advanced constitutive models that can be used in characterizing materials encountered in soil-structure interaction problems.
- (2) Development of general purpose finite element computer codes for a wider class of nonlinear soil-structure interaction problems with one-, two-, and three-dimensional idealizations.
- (4) Identification and development of constitutive models for geologic media by using sophisticated experimental procedures.
- (4) Verifications of the procedures by solving a number of simple and complex problems in soil-structure interactions.

References

1. Banerjee, P. K. and Stipho, A. S., "Associated and Non-Associated Constitutive Relations for Undrained Behavior of Isotropic Soft Clays," Int. J. Num. Analy. Method Geomech., Vol. 2, No. 2, 1978.
2. Baron, M. L., Nelson, I. and Sandler, I. S., "Influence of Constitutive Models on Ground Motion Predictions," J. of Engg. Mech. Div., EM6, December 1973.
3. Bathe, K. J., "ADINA-Static and Dynamic Geometric and Material Nonlinear Analysis," Report 82448-2, M.I.T., Cambridge, MA, 1976.
4. Bathe, K. J., and Wilson, E. L., Numerical Methods in Finite Element Analysis, Prentice-Hall, Englewood Cliffs, NJ, 1976.
5. Bathe, K. J., Wilson, E. L., and Iding, R. H.: "NONSAP: A Structural Analysis Program for Static and Dynamic Response of Nonlinear Systems," Report UCSESM 74-3, Department of Civil Engineering, University of California, Berkley, CA, 1974.
6. Christian, J. T., "Two-Dimensional Analysis of Stress and Strain in Soils, Report 3: Plane-Strain Deformation Analysis of Soil," U.S. Army Engineering Waterways Experiment Station, Contract Report No. 3-129, December 1966.
7. Christian, J. T., Hagmann, A. J. and Marr, A. W., "Incremental Plasticity Analysis of Frictional Soils," Int. J. Num. and Analy. Meth. in Geomechas, Vol. 1, No. 2, 1977.
8. Chung, T. J., and Lee, J. K., "Incremental Plasticity Theory Applied to Boundary Value Problems in Soils," Proc. Symp. Appl.

- Finite Element Method in Geotech. Engg., Ed. Desai, C. S., USAE Waterways Expt. Sta., Vicksburg, MI, 1972.
9. Davidson, H. L. and Chen, W. F. "Elastic-Plastic Large Deformation Response of Clay to Footing Loads," Report No. 355-18, Department of Civil Engineering, Lehigh University, Bethlehem, PA, 1974.
 10. Desai, C. S., "Soil-Structure Interaction and Simulation Problems," Chapter 7, Finite Elements in Geomechanics, Ed. Gudehus, John Wiley, NY, 1977.
 11. Desai, C. S., Elementary Finite Element Method, Prentice-Hall, Inc., Englewood Cliffs, NJ, 1979.
 12. Desai, C. S., "Some Aspects of Constitutive Models for Geologic Media," Proc. 3rd Int. Conf. Num. Meth. in Geomechanics, Aachen, W. Germany, 1979.
 13. Desai, C. S., Personal Communication.
 14. Desai, C. S., "Stress-Strain Behavior of Interfaces between Structures and Geologic Media," Proc. Int. Conf. on Geotech. Earthquake Eng. and Soil Dynamics, St. Louis, MO, 1981.
 15. Desai, C. S. and Abel, J., Introduction to the Finite Element Method, Van Nostrand Reinhold Co., 1972.
 16. Desai, C. S., and Appel, G. C., "3-Dimensional Analysis of Laterally Loaded Structures," Proc. 2nd Int. Conf. Numer. Methods in Geomech., ASCE, NY, 1976.
 17. Desai, C. S., and Christian, J. T., Numerical Methods in Geotechnical Engineering, McGraw-Hill, NY, 1977.
 18. Desai, C. S., and Kuppusamy, T., "User's Manual and Background for a Computer Code for Axially and Laterally Loaded Piles and

- Retaining Walls, SSTIN-IDFE, (CANDICE) 78-2," Department of Civil Engineering, VPI&SU, Blacksburg, VA, 1978.
19. Desai, C. S., Kuppusamy, T., Siriwardane, H. J., and Sture, S., "Interaction and Load Transfer Through Track Guideway Systems," Report 1, submitted to the U.S. Department of Transportation, Washington, DC, under publication by D.O.T., 1979.
 20. Desai, C. S. and Phan, H. V., Perumpral, J. V., "Mechanics of Three-Dimensional Soil-Structure Interaction: Theory and Verifications," submitted to the J. of Engg. Mech. Div., ASCE.
 21. Desai, C. S. and Siriwardane, H. J., Constitutive Laws for Engineering Media, to be published by Prentice-Hall, Inc., Englewood, NJ.
 22. Desai, C. S., Siriwardane, H. J., and Janardanam, R., "Interaction and Load Transfer in Track Guide Systems," Second Year Report, submitted to the U.S. Department of Transportation, Washington, DC, under publication by D.O.T., 1980.
 23. Desai, C. S., Siriwardane, H. J., and Janardanam, R., "Computational Procedures, Constitutive Laws and Verifications," Final Report for Interaction and Load Transfer Through Track Guideway Systems, U.S. Department of Transportation, Washington, DC, 1980-81.
 24. DiMaggio, F. L., and Sandler, I. S., "Material Model for Granular Soils," J. of E.M. Division, ASCE, Vol. 97, No. 3, 1971.
 25. Drucker, D. C., "Some Implications of work hardening and ideal plasticity," Quart. Appl. Math., Vol. 7, pp. 411-418, 1950.
 26. Drucker, D. C., "A More Fundamental Approach to Plastic Stress-Strain Relations," Proc. First U.S. Nat. Congress on Appl. Mech., pp. 487-491, 1951.

27. Drucker, D. C., "On Uniqueness in the Theory of Plasticity," Quart. Appl. Math., Vol. 14, pp. 35, 1956.
28. Drucker, D. C., "A Definition of Stable Inelastic Material," ASME Transactions, pp. 101-106, Vol. 81, 1959.
29. Drucker, D. C., Gibson, R. E. and Hankel, D. J., "Soil Mechanics and Work-Hardening Theories of Plasticity," Proceedings, ASCE, Vol. 81, paper 798, September 1955.
30. Drucker, D. C., and Prager, W., "Soil Mechanics and Plastic Analysis of Limit Design," Quart. Appl. Math., Vol. 10, No. 2, July 1952.
31. Eringen, A. C., "Constitutive Equations for Simple Materials - General Theory," Continuum Physics, Vol. II., Ed. A. C. Eringen, Academic Press, NY, 1975.
32. Fox, L., An Introduction to Numerical Linear Algebra, Oxford University Press, NY, 1965.
33. Frederick, D. and Chang, T. S., Continuum Mechanics, Scientific Publishers, Inc., Boston, MA, 1972.
34. Fung, Y. C., Foundations of Solid Mechanics, Prentice-Hall, Inc., Englewood Cliffs, NY, 1965.
35. Gallagher, R. H., Finite Element Analysis Fundamentals, Prentice-Hall, Englewood Cliffs, NY, 1975.
36. Ghaboussi, J., Wilson, E. L. and Isenberg, J., "Finite Element for Rock Joints and Interfaces," J. of Soil Mech. and Found. Engg., SM 10, ASCE, October 1973.

37. Goodman, R. E., and Christopher, J., "Finite Element Analysis for Discontinuous Rocks," Numerical Methods in Geotechnical Engineering, Desai, C. S. and Christian, J. T., eds., McGraw Hill, NY, 1977.
38. Goodman, R. E., Taylor, R. L., and Brekke, T. L., "A Model for Mechanics of Jointed Rock," J. of Soil Mechanics and Foundations Division, ASCE, Vol. 94, No. SM 5, 1968.
39. Herrman, L. R., "Three-Dimensional Elasticity Analysis of Periodically Loaded Prismatic Solids," Report, University of California at Davis, CA, November, 1968.
40. Herrman, L. R., "Finite Element Analysis of Contact Problems," J. of E.M. Division, ASCE, Vol. 104, No. EM 5, 1978.
41. Hetenyi, M., Beams on Elastic Foundation, University of Michigan Press, 1946.
42. Hill, R., The Mathematical Theory of Plasticity, Oxford University Press, 1950.
43. Hinton, E., and Owen, D. R. J., Finite Element Programming, Academic Press, London, 1977.
44. Irons, B. M., "Frontal Solution Program for Finite Element Analysis," Int. J. Num. Meth. in Engineering, Vol. 2, 1970.
45. Janardhanam, R., "Constitutive Modelling for Various Engineering Media," Ph.D. Dissertation, Department of Civil Engineering, VPI&SU, Blacksburg, VA, 1980-81.
46. Katona, M. G., Smith, J. M., Odello, R. S. and Algood, J. R., "CANDE, A Modern Approach for Structural Design and Analysis of Buried Culverts," Rep. FHWA-RD-77 Prepared for Federal Highway Administration, Washington, DC, 1976.

47. Kennedy, J. C., and Prause, R. H., "Development of a Multilayer Analysis Model for Tie-Ballast Track Structure," Presented at the 57th Annual Meeting of the Transportation Research Board, January 1978.
48. Kikuchi, N., and Oden, J. T., Contact Problems in Elasticity, TICOM Report 79-8, University of Texas, Austin, TX, 1979.
49. Lightner, J. G., Personal Communication.
50. Lightner, J. G., and Desai, C. S., "Improved Numerical Procedures for Soil-Structure Interaction Including Simulation of Construction Sequences," Report VPI-E-79.32, Department of Civil Engineering, VPI&SU, Blacksburg, VA, September, 1979.
51. Livesley, R. K., Matrix Methods of Structural Analysis, Second Edition, Pergamon Press, NY, 1975.
52. Mahtab, M. A. and Goodman, R. E., "Three-Dimensional Finite Element Analysis of Jointed Rock Slopes," Proc. of Second Congress of Int. Soc. of Rock Mech., Belgrade, Yugoslavia, 1970.
53. Marcal, P. V., and King, I. P., "Elastic-Plastic Analysis of Two-Dimensional Stress Systems by the Finite Element Method," Int. J. Mech. Science, Vol. 9, 1967.
54. Mendelson, A., Plasticity: Theory and Applications, The Macmillan Company, NY, 1968.
55. Mould, J. C., and Sture, S., "Constitutive Characterization of Granular Materials at Low Effective Stress Levels," Report No. VPI-E-79.39, Department of Civil Engineering, VPI&SU, Blacksburg, VA, December 1979.

56. Nayak, G. C., and Zienkiewicz, O. C. "Elasto-Plastic Stress Analysis - A Generalization of Various Constitutive Relations Including Strain Softening," Int. J. of Num. Meth. Engng., Vol. 5, pp. 113-135, 1972.
57. Naylor, D. J., and Zienkiewicz, O. C., "Settlement Analysis of a Strip Footing Using a Critical State Model in Conjunction with Finite Elements," Proc. Symp. on Interaction of Structures and Foundations, Birmingham, 1972.
58. Nelson, I., "Investigation of Ground Shock Effects in Nonlinear Hysteretic Media; Modeling the Behavior of a Real Soil," Report 2, Weidlinger Associates, NY, 1970.
59. Nelson, I., and Baron, M. L., "Investigation of Ground Shock Effects in Nonlinear Hysteretic Media," Contract Report S-68-1, Paul Weidlinger Consulting Engineer, NY, 1968.
60. Nelson, I., and Baron, M. L., "Application of Variable Moduli Models to Soil Behavior," Int. J. Solids Structures, Vol. 7, pp. 399-417, 1971.
61. Ngo, D., and Scordelis, A. C., "Finite Element Analysis of Reinforced Concrete Beams," J. of the American Concrete Institute, Vol. 64, No. 3, March 1967.
62. Oden, J. T., "Finite Elements of Elastic Bodies," Finite Elements of Nonlinear Continua, McGraw-Hill, NY, 1972.
63. Pande, G. N., and Sharma, K. G., "On Joint/Interface Elements and Associated Problems of Numerical Ill-Conditioning," short communication, Int. J. Num. and Analy. Meth. in Geomechanics, Vol. 3, 1979.

64. Phan, H. V., "Geometric and Material Nonlinear Analysis of Three-Dimensional Soil-Structure Interaction," Ph.D Dissertation, VPI&SU, Blacksburg, VA, December 1979.
65. Prager, W., "Recent Developments in the Mathematical Theory of Plasticity," J. of Appl. Physics, Vol. 20, No. 3, pp. 235-241, March 1949.
66. Prevost, J. H., "Soil Stress-Strain-Strength Models Based on Plasticity Theory," Ph.D. Dissertation, Stanford University, CA, 1974.
67. Reyes, S. F., and Deere, D. U., "Elasto-Plastic Analysis of Underground Openings by the Finite Element Method," Proc. 1st Int. Cong. Rock Mechanics, Vol. 11, pp. 477-486, Lisbon, 1966.
68. Roscoe, K. H. and Burland, J. B., "On the Generalized Stress-Strain Behavior of 'Wet' Clays," Engineering Plasticity, Heyman, J., and Leckie, F. A., eds., Cambridge University Press, 1968.
69. Roscoe, K. H., Schofield, A. N., and Wroth, C. P., "On the Yielding of Soils," Geotechnique, Vol. 8, No. 1, March 1958.
70. Sandhu, R. S., "Stresses, Deformations and Progressive Failure of Non-Homogeneous Fissured Rock," Semi-Annual Technical Report to U.S. Bureau of Mines, Contract No. HO. 210017, 1971.
71. Sandler, I. S., DiMaggio, F. L., and Baladi, G. Y., "Generalized Cap Model for Geologic Materials," J. of the Geotech. Engg. Div., ASCE, GT 7, July 1976.

72. Sandler, I. S., and Rubin, D., "An Algorithm and a Modular Sub-routine for the Cap Model," Int. J. for Num. and Analy. Methods in Geomechanics, Vol. 3, 1979.
73. Schofield, A. N., and Wroth, C. P., Critical State Soil Mechanics, McGraw-Hill, NY 1968.
74. Selig, E. T., Chang, C. S., Adegoke, C. W., Alva-Hurtado, J. E., "A Theory for Track Maintenance Life Predictions," Report submitted to D.O.T., Washington, DC, 1978.
75. Simpson, B., "Finite Elements Applied to Problems of Plane Strain Deformation in Soils," Ph.D. Dissertation, submitted to the Cambridge University Press, 1973.
76. Siriwardane, H. J., and Desai, C. S., "User's Manuals and Background for Computer Codes for Nonlinear Soil-Structure Interaction in One-, Two-, and Three-Dimensional Problems," Report, Department of Civil Engineering, VPI&SU, Blacksburg, VA, 1980.
77. Siriwardane, H. J., and Desai, C. S., "Two Numerical Schemes for Nonlinear Consolidation," Accepted for Int. J. of Num. Meth. in Engg., 1980.
78. Stagliano, T. R., Mente, L. J., Garden, E. C. Jr., Baxter, B. W., Hale, W. K., Maccabe, R. W., Jr., "Pilot Study for Definition of Track Component Load Environments," Report prepared by Kaman Avidyne for D.O.T., July 1980.
79. Sture, S., "Development of a Multiaxial Cubical Test Device with Pore Pressure Monitoring Facilities," Rep. No. VPI-E-79.18, Prepared for National Science Foundation, VPI&SU, Blacksburg, VA, 1979.

80. Sture, S., and Desai, C. S., "A Fluid Cushion Truly Triaxial or Multiaxial Testing Device," Geotechnical Testing Journal, ASTM, March 1979.
81. Svec, O. J., and Raymond, G. P., "Nonlinear Analysis of Rail Track and Support," Proc. 2nd Int. Conf. on Num. Meth. in Geomechanics, Ed. Desai, C. S., ASCE, NY, 1976.
82. Tayabji, S. D., and Thompson, M. R., "Considerations in the Analysis of Conventional Railway Track Support System," Transportation Engineering Journal, ASCE, TE 2, 1977.
83. Terzaghi, K., and Peck, R. B., Soil Mechanics in Engineering Practice, 2nd Edition, John Wiley and Sons, Inc., NY, 1967.
84. Timoshenko, S. P., and Goodier, J. N., Theory of Elasticity, McGraw-Hill, 1970.
85. Wilson, E. L., "Finite Elements for Foundations, Joints and Fluids," Finite Elements in Geomechanics, Ed. by Gudehus, G., John Wiley & Sons, NY, 1977.
86. Wilson, E. L., and Pretovius, P. C., "A Computer Program for the Analysis of Prismatic Solids," Report, Department of Civil Engineering, University of California, Berkley, CA, September 1970.
87. Wittke, W., Editor, "Proc. 3rd Int. Conf. Num. Meth. in Geomechanics," Aachen, W. Germany, Published by A. A. Balkema, Rotterdam, 1979.
88. Yamada, Y., Yishimura, N., and Sakurai, T., "Plastic Stress-Strain Matrix and its Application for the Solution of Elastic-Plastic Problems by the Finite Element Method," Int. J. Mech. Science, Vol. 10, 1968.

89. Zienkiewicz, O. C., The Finite Element Method in Engineering Science, McGraw Hill, London, 1971.
90. Zienkiewicz, O. C., Irons, B. M., Ergatoudis, J. G., Ahmed, S., and Scott, F. C., "Isoparametric and Associated Element Families for Two-, and Three-Dimensional Analysis," Proc. Course on Finite Element Method in Stress Analysis, Ed. Holand, I., and Bell, K., Trondheim Tech. University, 1969.
91. Zienkiewicz, O. C., and Naylor, D. J., "The Adaptation of Critical State Soil Mechanics Theory for Use in Finite Elements," Proc. Roscoe Memorial Symp. Stress-Strain Behavior of Soils, 1972.
92. Zienkiewicz, O. C., Valliappan, S., Dullage, C., and Stagg, K. G., "Analysis of Nonlinear Problems in Rock Mechanics with Particular Reference to Jointed Rock Systems," Proceedings of Second Congress of Int. Society for Rock Mechanics, Belgrade, Yugoslavia, 1970.
93. Zienkiewicz, O. C., Valliappan, S., King, I. P., "Stress Analysis of Rock as a No-Tension Material," Geotechnique, Vol. 18, No. 1, 1968.
94. Zienkiewicz, O. C., Valliappan, S., and King, I. P., "Elasto-Plastic Solutions of Engineering Problems, Initial-Stress Finite Element Approach," Int. J. for Num. Meth. in Engg., Vol. 1, pp. 75-100, 1969.

Appendix A

Derivation of the Incremental Constitutive Law for Drucker-Prager Model

Details of steps in deriving the incremental law for the Drucker-Prager model are given below.

The failure criterion for Drucker-Prager model is

$$f = \sqrt{J_{2D}} - \alpha J_1 - k \quad (A.1)$$

when the stress point is on the yield surface, Equation (A.1) is always satisfied, and hence the variation of f will be zero. That is,

$$df = 0 \quad (A.2)$$

Using Equation (A.2)

$$df = \frac{\partial f}{\partial \sigma_{ij}} d\sigma_{ij} \quad (A.3)$$

By substituting Equation (A.1) into Equation (A.3) it is possible to get

$$df = \left(\frac{S_{ij}}{2\sqrt{J_{2D}}} - \alpha \delta_{ij} \right) d\sigma_{ij} = 0 \quad (A.4)$$

where S_{ij} is the deviatoric stress tensor, and the other quantities are the same as those defined in previous chapters of the dissertation. Assuming that the total strain can be separated into elastic and plastic components, one can write

$$d\epsilon_{ij}^e = d\epsilon_{ij} - d\epsilon_{ij}^p \quad (A.5)$$

Here, the superscripts 'e' and 'p' denotes elastic and plastic components

separately. However, the incremental plastic strains can be expressed using the flow rule given in Equation (2.17). Therefore,

$$d\varepsilon_{ij}^e = d\varepsilon_{ij} - \lambda \frac{\partial f}{\partial \sigma_{ij}} \quad (\text{A.6})$$

Therefore,

$$d\varepsilon_{ij}^e = d\varepsilon_{ij} - \lambda \left(\frac{S_{ij}}{2\sqrt{J_{2D}}} - \alpha \delta_{ij} \right) \quad (\text{A.7})$$

The elastic stress-strain relationship can be written as,

$$d\sigma_{ij} = K d\varepsilon_{mm}^e \delta_{ij} + 2G \left(d\varepsilon_{ij}^e - \frac{d\varepsilon_{mm}^e}{3} \delta_{ij} \right) \quad (\text{A.8})$$

From Equation (A.7), the incremental volumetric strain can be expressed as,

$$d\varepsilon_{mm}^e = d\varepsilon_{mm} + 3\lambda\alpha \quad (\text{A.9})$$

Substituting this in Equation (A.8) leads to

$$\begin{aligned} d\sigma_{ij} = & K [d\varepsilon_{mm} + 3\lambda\alpha] \delta_{ij} + 2G \left[d\varepsilon_{ij} - \frac{\lambda S_{ij}}{2\sqrt{J_{2D}}} \right. \\ & \left. + \lambda\alpha\delta_{ij} - \frac{d\varepsilon_{mm}}{3} \delta_{ij} - \lambda\alpha\delta_{ij} \right] \end{aligned} \quad (\text{A.10a})$$

Hence,

$$d\sigma_{ij} = K (d\varepsilon_{mm} + 3\lambda\alpha) \delta_{ij} + 2G \left[d\varepsilon_{ij} - \frac{\lambda \delta_{ij}}{2\sqrt{J_{2D}}} - \frac{d\varepsilon_{mm}}{3} \delta_{ij} \right] \quad (\text{A.10b})$$

Substitute Equation (A.10b) into Equation (A.4) to yield

$$\left(\frac{S_{ij}}{2\sqrt{J_{2D}}} - \alpha\delta_{ij}\right)(d\epsilon_{mm} + 3\lambda\alpha)K\delta_{ij} + 2G\left(\frac{S_{ij}}{2\sqrt{J_{2D}}} - \alpha\delta_{ij}\right) \cdot \left(d\epsilon_{ij} - \frac{\lambda S_{ij}}{2\sqrt{J_{2D}}} - \frac{d\epsilon_{mm}}{3}\delta_{ij}\right) = 0 \quad (\text{A.11})$$

By noting that $S_{ij} \cdot \delta_{ij} = S_{ii}$, $\delta_{ij} \cdot \delta_{ij} = 3$ and $S_{ii} = 0$, Equation (A.11) leads to

$$-3\alpha(d\epsilon_{mm} + 3\lambda\alpha)K + \frac{GS_{ij}d\epsilon_{ij}}{\sqrt{J_{2D}}} - \lambda G = 0 \quad (\text{A.12})$$

Collecting terms, it is possible to get,

$$\lambda(9\alpha^2K + G) = \frac{GS_{ij}d\epsilon_{ij}}{\sqrt{J_{2D}}} - 3K\alpha d\epsilon_{mm} \quad (\text{A.13})$$

Substituting $S_{ij} = \sigma_{ij} - \frac{J_1}{3}\delta_{ij}$ in Equation (A.13), we get,

$$\lambda = \frac{\sigma_{ij}d\epsilon_{ij} - d\epsilon_{mm}\left(\frac{J_1}{3} + \frac{3K\alpha\sqrt{J_{2D}}}{G}\right)}{\sqrt{J_{2D}}(1 + 9\alpha^2K/G)} \quad (\text{A.14})$$

Now let

$$p = \frac{\sqrt{J_{2D}}}{k}(1 + 9\alpha^2K/G) \quad (\text{A.15})$$

where p is a nondimensional quantity. From the failure criterion Equation (A.1),

$$J_1 = \frac{\sqrt{J_{2D}} - k}{\alpha} \quad (\text{A.16})$$

Let us consider the factor $\left(\frac{J_1}{3} + \frac{3K\alpha\sqrt{J_{2D}}}{G}\right)$ in Equation (A.14). Using Equation (A.16), we can write

$$\frac{J_1}{3} + \frac{3K\alpha\sqrt{J_{2D}}}{G} = \frac{\sqrt{J_{2D}} - k}{3\alpha} + \frac{3K\alpha\sqrt{J_{2D}}}{G} \quad (\text{A.17})$$

Simplifying the above equation, one gets

$$\frac{J_1}{3} + \frac{3K\alpha\sqrt{J_{2D}}}{G} = \frac{1}{3\alpha} \left[\sqrt{J_{2D}} \left(1 + \frac{9K\alpha^2}{G} \right) - k \right] \quad (\text{A.18})$$

Substituting the value of p from Equation (A.15) into Equation (A.18), it is possible to show that

$$\frac{J_1}{3} + \frac{3K\alpha\sqrt{J_{2D}}}{G} = \frac{k}{3\alpha} (p - 1) \quad (\text{A.19})$$

Substituting (A.19) into Equation (A.14), we get

$$\lambda = \frac{\sigma_{ij} d\epsilon_{ij} - \frac{k}{3\alpha} d\epsilon_{mm} (p - 1)}{pk} \quad (\text{A.20})$$

Now consider Equation (A.10b) and substitute in it the value of λ from Equation (A.20),

$$d\sigma_{ij} = d\epsilon_{mm} \left(K - \frac{2G}{3} \right) \delta_{ij} + 2G d\epsilon_{ij} + \left[\frac{\sigma_{mn} d\epsilon_{mn} - \frac{k}{3\alpha} (p - 1) d\epsilon_{mm}}{pk} \right] \cdot \left[3\alpha K \delta_{ij} - \frac{GS_{ij}}{\sqrt{J_{2D}}} \right] \quad (\text{A.21})$$

Simplifying Equation (A.21) we get

$$d\sigma_{ij} = d\epsilon_{mm} \left(K - \frac{2G}{3} \right) \delta_{ij} + 2G d\epsilon_{ij} + \frac{3\alpha K}{pk} \sigma_{mn} d\epsilon_{mn} \delta_{ij} - \frac{G\sigma_{mn} d\epsilon_{mn}}{pk\sqrt{J_{2D}}} S_{ij} - \frac{K}{p} d\epsilon_{mm} (p - 1) \delta_{ij} + \frac{Gd\epsilon_{mm} (p - 1) S_{ij}}{3\alpha p \sqrt{J_{2D}}} \quad (\text{A.22})$$

Because $S_{ij} = \sigma_{ij} - \frac{J_1}{3} \delta_{ij}$, Equation (A.22) becomes:

$$\begin{aligned}
d\sigma_{ij} = & d\epsilon_{mn} \left(K - \frac{2G}{3} \right) \delta_{ij} + 2Gd\epsilon_{ij} + \frac{3\alpha K}{pk} \sigma_{mn} d\epsilon_{mn} \delta_{ij} - \frac{G\sigma_{mn} d\epsilon_{mn}}{pk\sqrt{J_{2D}}} \sigma_{ij} \\
& + \frac{G\sigma_{mn} d\epsilon_{mn} J_1 \delta_{ij}}{3pk\sqrt{J_{2D}}} - \frac{K(p-1)}{p} d\epsilon_{mn} \delta_{ij} + \frac{Gd\epsilon_{mn}(p-1)}{3\alpha p\sqrt{J_{2D}}} \sigma_{ij} \\
& - \frac{Gd\epsilon_{mn}(p-1)J_1 \delta_{ij}}{9\alpha p\sqrt{J_{2D}}} \tag{A.23}
\end{aligned}$$

Collecting terms in Equation (A.23),

$$\begin{aligned}
d\sigma_{ij} = & 2Gd\epsilon_{ij} - \left[\frac{2G}{3} \left(1 - \frac{3K}{2G} \right) + \frac{K(p-1)}{p} + \frac{G(p-1)J_1}{9\alpha p\sqrt{J_{2D}}} \right] d\epsilon_{mn} \delta_{mn} \delta_{ij} \\
& + \left[\frac{3\alpha K}{pk} + \frac{GJ_1}{3pk\sqrt{J_{2D}}} \right] \sigma_{mn} d\epsilon_{mn} \delta_{ij} + \left[\frac{G(p-1)}{3\alpha p\sqrt{J_{2D}}} \right] \delta_{mn} d\epsilon_{mn} \sigma_{ij} \\
& - \frac{G\sigma_{mn} d\epsilon_{mn} \sigma_{ij}}{pk\sqrt{J_{2D}}} \tag{A.24}
\end{aligned}$$

Hence,

$$\begin{aligned}
d\sigma_{ij} = & 2Gd\epsilon_{ij} - 2G \left[\frac{1}{3} \left(1 - \frac{3K}{2G} \right) + \frac{K}{2Gp} (p-1) + \frac{(p-1)J_1}{18p\sqrt{J_{2D}} \cdot \alpha} \right] d\epsilon_{mn} \delta_{mn} \delta_{ij} \\
& + \frac{2G}{pk} \left[\frac{3\alpha K}{2G} + \frac{J_1}{6\sqrt{J_{2D}}} \right] \sigma_{mn} d\epsilon_{mn} \delta_{ij} + \frac{2G(p-1)}{6\alpha p\sqrt{J_{2D}}} \delta_{mn} d\epsilon_{mn} \sigma_{ij} \\
& - \frac{2G\sigma_{mn} d\epsilon_{mn} \sigma_{ij}}{3pk\sqrt{J_{2D}}} \tag{A.25}
\end{aligned}$$

Let us define a nondimensional quantity, h , as

$$h = - \left(\frac{3\alpha K}{2G} + \frac{J_1}{6\sqrt{J_{2D}}} \right) \tag{A.26}$$

It was seen in Equation (A.19) that,

$$\frac{k}{3\alpha} (p - 1) = \frac{J_1}{3} + \frac{3K\alpha\sqrt{J_{2D}}}{G}$$

Hence, the value of h in Equation (A.26) can be expressed as

$$h = - \frac{k(p - 1)}{6\alpha\sqrt{J_{2D}}} \quad (\text{A.27})$$

Substituting Equation (A.27) into Equation (A.25), we get

$$\begin{aligned} d\sigma_{ij} = 2Gd\epsilon_{ij} - 2G \left[\frac{1}{3} \left(1 - \frac{3K}{2G} \right) + \frac{K}{2Gp} (p - 1) + \frac{(p - 1)J_1}{18\alpha\sqrt{J_{2D}} p} \right] d\epsilon_{mn} \delta_{mn} \delta_{ij} \\ - \frac{2Gh}{pk} (\sigma_{mn} \delta_{ij} + \sigma_{ij} \delta_{mn}) d\epsilon_{mn} - \frac{2G\sigma_{mn} \sigma_{ij} d\epsilon_{mn}}{2pk\sqrt{J_{2D}}} \end{aligned} \quad (\text{A.28})$$

Hence Equation (A.28) can be written as

$$d\sigma_{ij} = 2Gd\epsilon_{ij} - 2G[A(\sigma_{mn} \delta_{ij} + \sigma_{ij} \delta_{mn}) + B\delta_{mn} \delta_{ij} + C\sigma_{mn} \sigma_{ij}] d\epsilon_{mn} \quad (\text{A.29})$$

where

$$A = \frac{h}{pk} \quad (\text{A.30a})$$

$$p = \frac{\sqrt{J_{2D}}}{k} (1 + 9\alpha^2 K/G) \quad (\text{A.30b})$$

$$h = - \frac{k(p - 1)}{6\alpha\sqrt{J_{2D}}} = - \left(\frac{3\alpha K}{2G} + \frac{J_1}{6\alpha\sqrt{J_{2D}}} \right) \quad (\text{A.30c})$$

$$B = \frac{2h^2\sqrt{J_{2D}}}{pk} - \frac{3\nu K}{E} = \frac{2h^2}{(1 + 9\alpha^2 K/G)} - \frac{3\nu K}{E} \quad (\text{A.30d})$$

and

$$C = \frac{1}{2kp\sqrt{J_{2D}}} \quad (\text{A.30e})$$

The matrix form of Equation (A.29) can be written as

$$\{\mathit{d}\sigma\} = [\mathit{C}^{\text{ep}}]\{\mathit{d}\epsilon\}$$

(A.31)

Appendix B

Elasto-Plastic Stress-Strain Matrix for Critical State Model

As shown in Equation (4.30), the yield criterion based on the critical state model is

$$F_c = q^2 - M^2 p_0 p + M^2 p^2 \quad (\text{B.1})$$

where p_0 is the hardening parameter, and other quantities are the same as those defined in Chapter 4. The quantity A_{ij} in Equation (4.51), can be evaluated as follows

$$A_{ij} = \frac{\partial F_c}{\partial \sigma_{ij}} = \frac{\partial F_c}{\partial q} \cdot \frac{\partial q}{\partial \sigma_{ij}} + \frac{\partial F_c}{\partial p} \cdot \frac{\partial p}{\partial \sigma_{ij}} \quad (\text{B.2})$$

Differentiating F_c with respect to q and p , it is possible to show

$$\frac{\partial F_c}{\partial q} = 2q \quad (\text{B.3})$$

and

$$\frac{\partial F_c}{\partial p} = M^2(2p - p_0) \quad (\text{B.4})$$

In the classical critical state soil mechanics literature [69], the quantities q and p are expressed with respect to cylindrical triaxial device. However, for application in plane strain, axisymmetric and three-dimensional stress analysis, it is required to define these quantities with respect to a general state of stress. The quantity, q , can be expressed as

$$q = \frac{3\tau_{\text{oct}}}{\sqrt{2}} = \sqrt{3J_{2D}} \quad (\text{B.5})$$

$$= \frac{1}{\sqrt{2}} [(\sigma_{11} - \sigma_{22})^2 + (\sigma_{22} - \sigma_{33})^2 + (\sigma_{11} - \sigma_{33})^2 + 6(\sigma_{12}^2 + \sigma_{23}^2 + \sigma_{13}^2)]^{1/2} \quad (\text{B.6})$$

The quantity, p , can be expressed as

$$p = (\sigma_{11} + \sigma_{22} + \sigma_{33})/3.0 = J_1/3. \quad (\text{B.7})$$

Now by differentiation,

$$\frac{dp}{\sigma_{ij}} = \frac{1}{3} \delta_{ij} \quad (\text{B.8})$$

$$\frac{dq}{\sigma_{ij}} = \frac{3}{2q} (\sigma_{ij} - p\delta_{ij}) \quad (\text{B.9})$$

By substituting Equations (B.3), (B.4), (B.8), and (B.9) into Equation (B.2), A_{ij} can be evaluated. Since A_{ij} is symmetric, it is easier to express its quantities in a vectorial form.

The incremental plastic strain vector is defined as

$$\{d\epsilon^p\}^T = [d\epsilon_{11}^p, d\epsilon_{22}^p, d\epsilon_{33}^p, d\epsilon_{12}^p + d\epsilon_{21}^p, d\epsilon_{23}^p + d\epsilon_{32}^p, d\epsilon_{13}^p + d\epsilon_{31}^p] \quad (\text{B.10})$$

Hence, A_{ij} can be expressed in the vectorial form as,

$$\{A\}^T = \left[\frac{\partial F_c}{\partial \sigma_{11}}, \frac{\partial F_c}{\partial \sigma_{22}}, \frac{\partial F_c}{\partial \sigma_{33}}, \frac{\partial F_c}{\partial \sigma_{12}} + \frac{\partial F_c}{\partial \sigma_{21}}, \frac{\partial F_c}{\partial \sigma_{23}} + \frac{\partial F_c}{\partial \sigma_{32}}, \frac{\partial F_c}{\partial \sigma_{13}} + \frac{\partial F_c}{\partial \sigma_{31}} \right] \quad (\text{B.11})$$

Appendix C
[C^{ep}] for Cap Model

Elasto-Plastic Stress-Strain Matrix for Hardening Cap

In this section the relationship described in Equation (4.50) is determined with regard to the cap model. The quantity A_{ij} in Equation (4.50) can be evaluated as follows

$$A_{ij} = \frac{\partial F_c}{\partial \sigma_{ij}} = \frac{\partial F_c}{\partial \sqrt{J_{2D}}} \cdot \frac{\partial \sqrt{J_{2D}}}{\partial \sigma_{ij}} + \frac{\partial F_c}{\partial J_1} \cdot \frac{\partial J_1}{\partial \sigma_{ij}} \quad (C.1)$$

Substituting Equation (4.36b) into Equation (C.1), it is possible to obtain,

$$A_{ij} = R^2 S_{ij} + 2(J_1 - L)\delta_{ij} \quad (C.2)$$

This can be expressed in the vectorial form as described in Appendix B for the critical state model.

The quantity $\frac{\partial F_c}{\partial I_1^p}$ in Equation (4.50a), can be evaluated as follows

$$\frac{\partial F_c}{\partial I_1^p} = \frac{\partial F_c}{\partial \epsilon_v^p} = \frac{\partial F_c}{\partial L} \cdot \frac{\partial L}{\partial \epsilon_v^p} \quad (C.3)$$

By differentiating Equations (4.36) and (4.38), and combining them, the following relationship can be obtained

$$\frac{\partial L}{\partial \epsilon_v^p} = \frac{1}{[1 + \theta R + \gamma \beta R e^{-\beta L}]} \left[\frac{1}{D w e^{-Dx}} \right] \quad (C.4)$$

Substituting Equation (4.35) into Equation (4.36b), and differentiating with respect to L, the value of $\frac{\partial F_c}{\partial L}$ can be evaluated, and hence, $\frac{\partial F_c}{\partial I_1^p}$ in

Equation (C.3) can be computed. Now, $[C^{ep}]$ for the cap model can be computed by substituting $\{A\}$, $\frac{\partial F}{\partial I_1^p}$ and $[C^e]$ in Equation (4.55).

Resistance-Response Approach [19,22,23]

Because the three-dimensional approximation can be expensive and complex, a rather new approach is proposed for this problem, and is called R-R (Resistance-Response) approach. This approach is based on a combination of the one-, two- and three-dimensional models, with minimum use of the three-dimensional aspect. A description of R-R approach is given below.

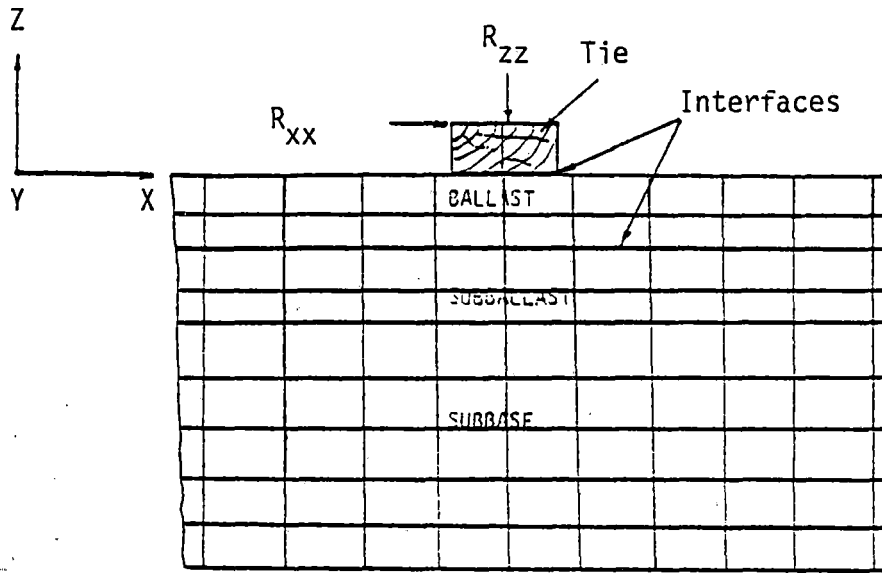
The problem of load transfer behavior in certain classes of problems such as laterally loaded piles, long retaining walls, dams, and track-support structures, etc., may be solved approximately by using the Resistance-Response approach. Here, the procedure is described with respect to the analysis of a track-support structure. In this model, the three-dimensional effects are accounted for in an indirect manner. Basically, there are three steps in this approach. In step 1 of the procedure, the foundation including interface behavior is analyzed by using the three-dimensional finite element model, and a set of Resistance-Response functions are derived. These relationships are obtained as generalized response functions corresponding to various modes of loadings. In general matrix notation, the resistance-response (displacement = δ) relations are expressed as:

$$\{R\} = [k_r]\{\delta\} \quad (9.4a)$$

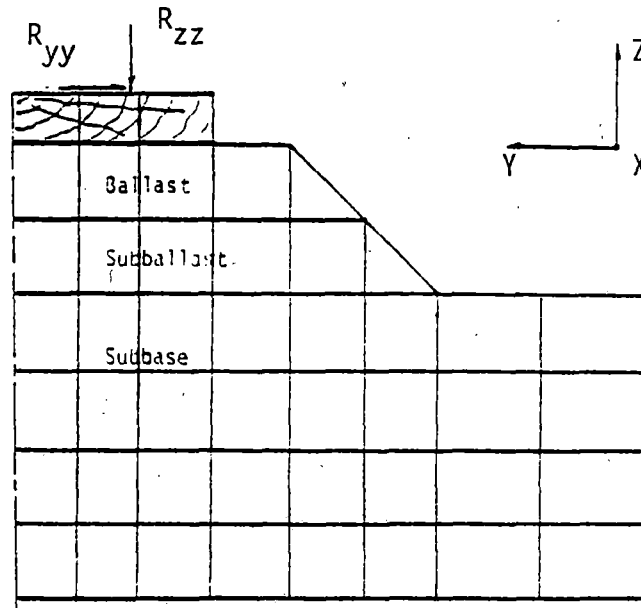
where

$$\{R\}^T = [R_{xx} \ R_{yy} \ R_{zz} \ R_{xy} \ R_{yz} \ R_{zx}],$$

$$\{\delta\}^T = [\delta_{xx} \ \delta_{yy} \ \delta_{zz} \ \delta_{xy} \ \delta_{yz} \ \delta_{zx}].$$



Logitudinal Section in Three-Dimensional Mesh



Transverse Section in Three-Dimensional Mesh

Figure D.1 Determination of RR Curves from Three-Dimensional Analysis

Symbolic curves for the R - δ relations are shown in Figure (D.2a). Use of the three-dimensional nonlinear finite element procedure will involve, essentially one finite element mesh, Figure (D.2a), to derive the response parameters in $[k_f]$. These response parameters need to be computed and stored only once. They provide the simulation of the three-dimensional medium for the next two steps.

Step 2: One-Dimensional Idealization of (Longitudinal) Structure, Figure (D.2b)

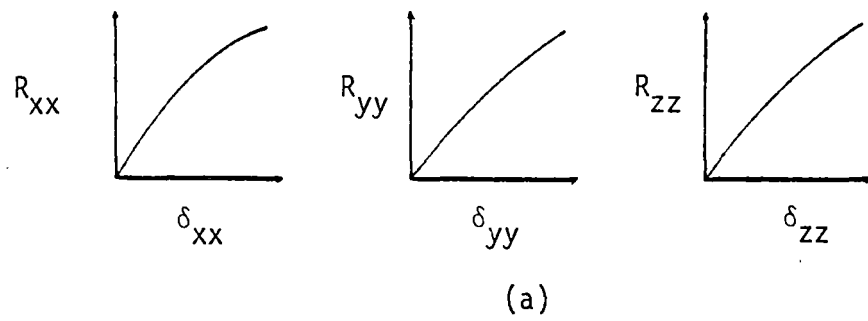
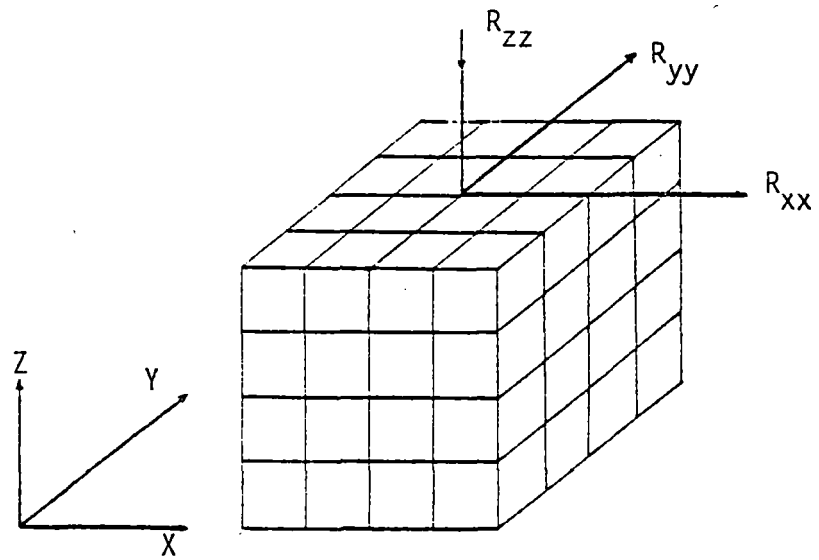
A general finite element procedure for the one-dimensional idealization of the longitudinal behavior of the rail (structure) as a beam-column is used in this step. The loads p_i ($i = 1, 2, \dots, N$) are applied at appropriate locations along the structure included in the analysis; here N = number of ties (supports) included. The stress-strain parameters for the supports that simulate the three-dimensional medium will be those in $[k_f]$ determined in Step 1. Because of the one-dimensional nature of this approximation, considerable length of the rail (structure) can be analyzed at a small cost.

The results from this step are in terms of the resistance and response (generalized displacements) developed in the support "springs" during an incremental loading. These quantities act as input for the next step.

Step 3: Analysis of Transverse Sections

The reactions R_i ($i = 1, 2, \dots, N$) are now applied to the corresponding transverse sections, Figure (D.2c). Each of these sections is now analyzed as a two-dimensional (plane-strain) body by

Step 1



Step 2

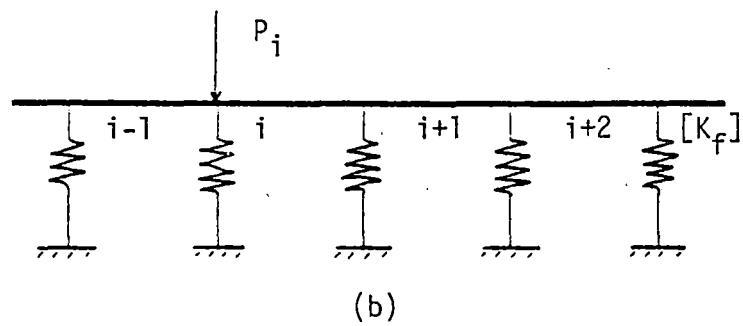


Figure D.2 Representation of Proposed Resistance-Response Procedure (RR)

Step 3

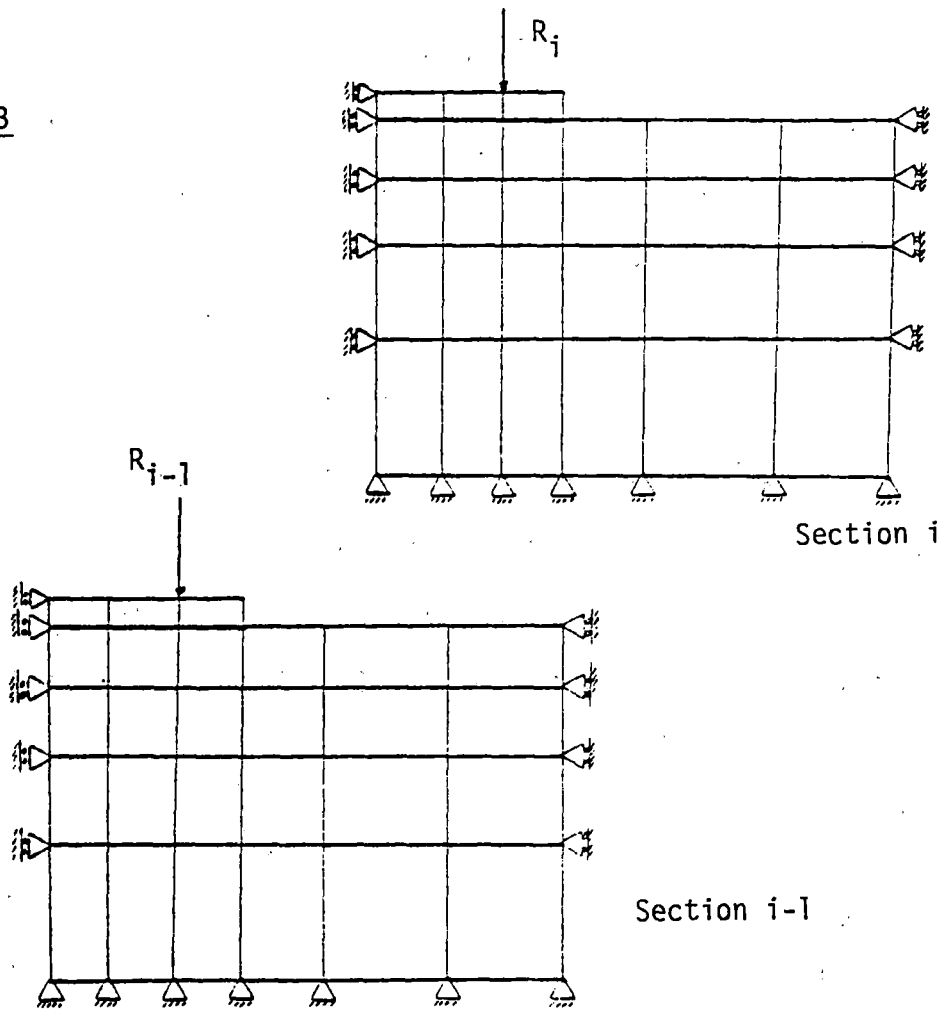


Figure D.2. (Continued)

using the finite element procedure with nonlinear properties for the components and interfaces.

Step 4: Compatibility

The displacements computed at the points in the transverse sections common with the points of load applications in Step 2 will be compared with those computed at those points (Step 3). If they differ by amounts greater than a small acceptable value, Step 2 and Step 3 will be repeated. Here, the displacements just computed in Step 4 will be used to revise the values of response function $[k_f]$ by using the R-R relations found in Step 1. These revised values will be used in the new calculations for Step 2.

Analysis

Within the scope of this study, preliminary work has been done on the resistance-response approach by using the finite element procedures developed. Two major factors involved in this approach are the (1) thickness of the plane strain section, and (2) the area and shape of contact between tie and ballast.

Effect of Contact Area

Effect of contact area on the fraction of load transferred to a tie is studied by varying it from 25.5 in x 9.0 in (64 cm x 24 cm) to 25.5 in x 5 in (64 cm x 12.5 cm). The following properties are used in the three-dimensional analysis, Figure (D.3), in the study of effect of contact area.

$$E = 9,600.0 \text{ N/cm}^2$$

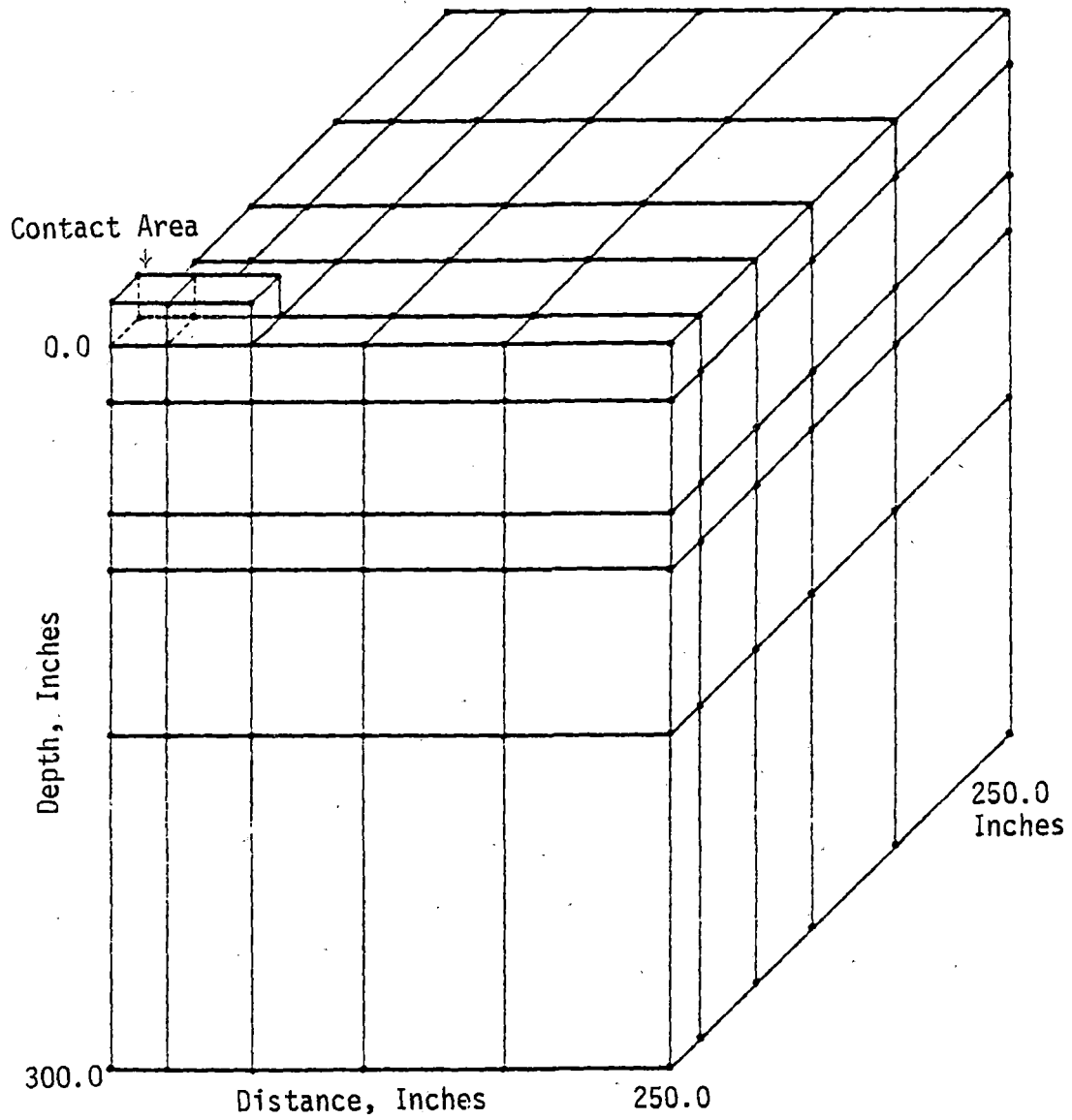


Figure D.3 Three-Dimensional Finite Element Mesh for Determining Resistance-Response Curves

$$\nu = 0.30$$

For this study, the whole section is assumed to be homogeneous. The effect of contact area on the response parameter is shown below.

<u>Contact Area (cm²)</u>	<u>k_{zz} (kN/cm)</u>
64 × 24	723.0
64 × 20	709.0
64 × 17.75	667.0
64 × 12.5	629.0

Here k_{zz} is defined as the ratio of the applied load to the average vertical displacement over the loading area; the applied load is equal to the wheel load, 32500 lb (144.6 kN) which is uniformly distributed.

One-Dimensional Analysis

Rail deflections due to a wheel load are studied by using beam-column idealization with the stiffness values, k_{zz} , computed in the foregoing section. A length of 500.0 inches (1270 cm) of rail is used in the idealization, Figure (8.1); tie spacing is taken as 20.0 in (50.8 cm). Following rail properties are used.

$$E = 30 \times 10^6 \text{ psi } (20.67 \times 10^7 \text{ kN/m}^2)$$

$$I = 94.9 \text{ in}^4 \text{ (3950.0 cm}^4\text{)}$$

The vertical force induced in the spring i , Figure (D.2), caused by the external point load equal to the wheel load of 32,500 lb (144.6 kN) is given below.

<u>Area (cm²)</u>	<u>k_{zz} (kN/cm)</u>	<u>Spring Load, % of the Wheel Load</u>
64 × 20	723.0	36.0
64 × 20	709.0	35.9
64 × 17.75	667.0	35.5
64 × 12.5	629.0	35.0

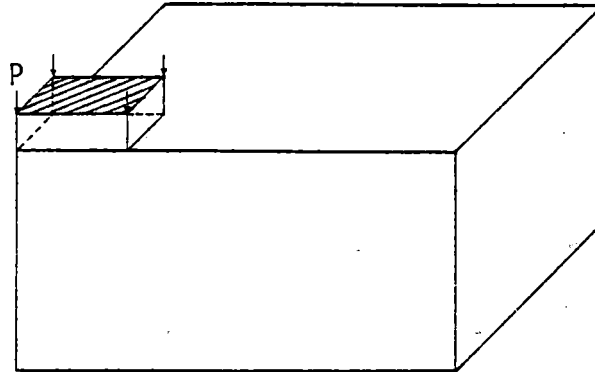
The above results show that the contact area does not have a significant effect on the fraction of load transferred to the tie.

Thickness of Plane Strain Section

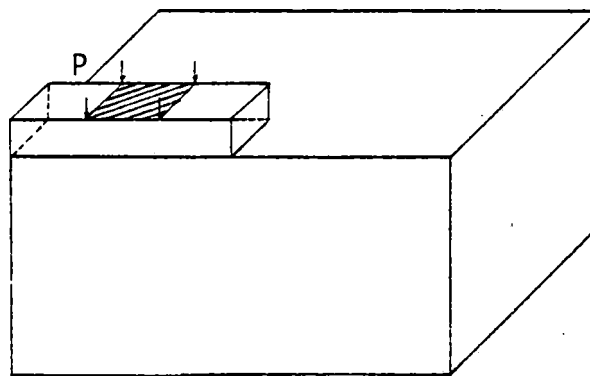
In order to obtain approximate three-dimensional results from a plane strain analysis, it is required to assume an effective thickness of a plane strain section. Based on the results from parametric studies in the present and a previous work [22], thickness of the plane strain section is assumed to be equal to the tie spacing.

Resistance-Response Function

In this section, the behavior of a track support structure is predicted by using the Resistance-Response approach. Here, FAST analysis described in Chapter 9 is considered as an example. The first step in this approach is the establishment of response functions. This is done by using the truly three-dimensional finite element procedure, Figure (D.3). Properties for various components of the track for the FAST analysis described previously in Chapter 9 are used here. Since the geometry is complicated and no prior experience is available with Resistance-Response approach, two possibilities, Figure (D.4), are



(a) Load Case 1



(b) Load Case 6

Figure D.4 Two Loading Cases for Resistance-Response Analysis

considered in establishing Resistance-Response function; here, only the vertical mode is considered.

In the analysis, the total loaded area is assumed to be 4.0×9.0 in² (10.0×22.9 cm²), which is the contact between the rail and the tie. The following Resistance-Response function for the vertical mode is obtained from a truly three-dimensional analysis.

<u>Case</u>	<u>k_{zz} (lb/in)</u>
1	$252. \times 10^3$ (441.5×10^3 N/cm)
2	$268. \times 10^3$ (469.5×10^3 N/cm)

Wheel load = 32500. lb (144.6 kN)

Based on these values, a one-dimensional analysis is carried out to study the load transfer behavior. The following results show how the load is transmitted to the supporting ties, Figure (D.5).

		<u>Load Transferred (%)</u>		
	<u>R-R (lb/in)</u>	<u>Tie 1</u>	<u>Tie 2</u>	<u>Tie 3</u>
Case 1	$252. \times 10^3$ (441.5 kN/cm)	31.0	23.0	11.0
Case 2	$268. \times 10^3$ (469.5 kN/cm)	31.0	23.0	11.0

Results in the foregoing section show that the predictions of load transfer behavior is not affected to the first decimal place by the loading case used for Resistance-Response determination. Therefore, load case 1, Figure (D.4), can be used since its geometry is simpler than Case 2.

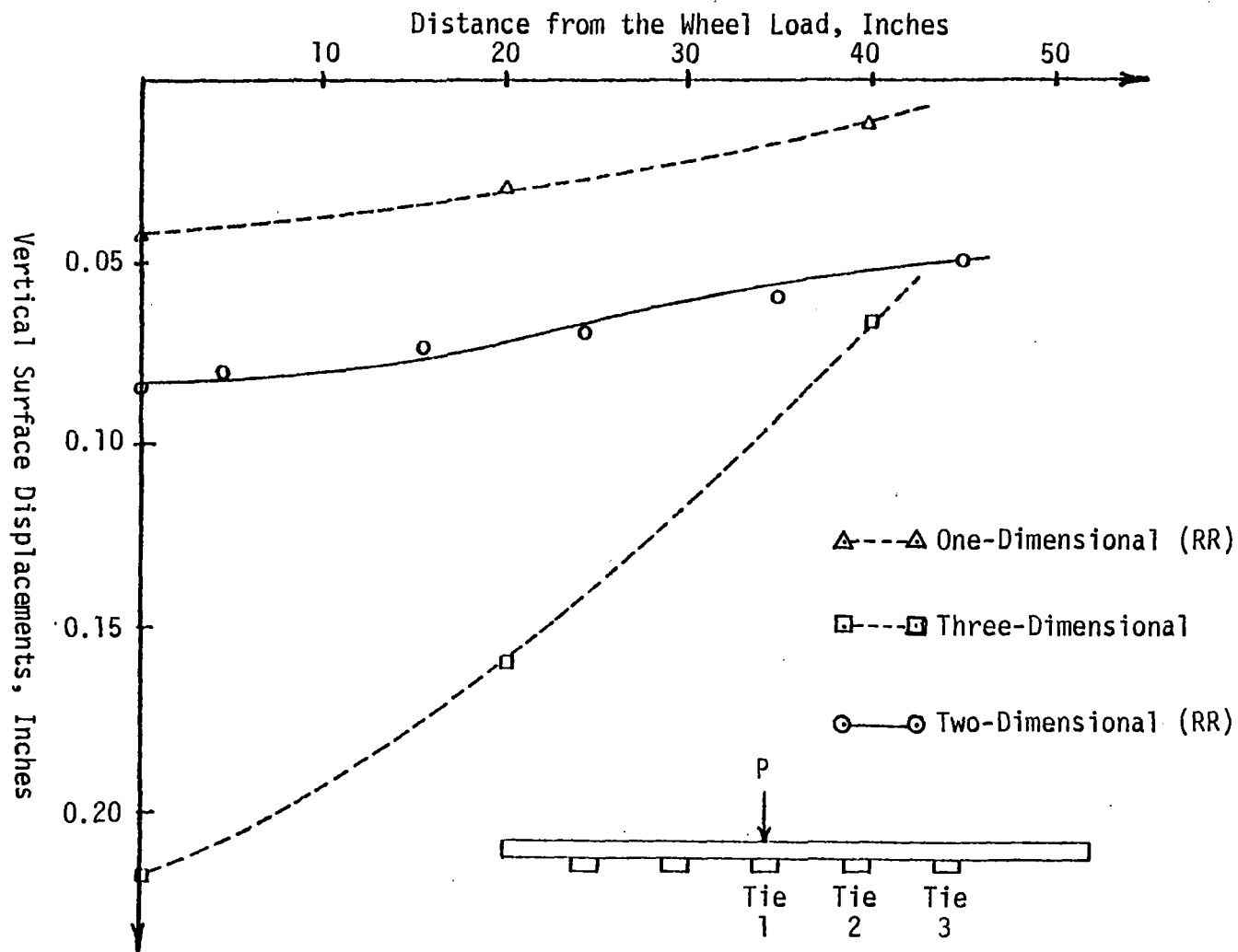


Figure D.5 Displacement Predictions from Resistance-Response Analysis

Figure (D.5) shows the results obtained from the Resistance-Response approach. Using the R-R relationship for the vertical mode, behavior of a rail due to a vertical load of 32,500 lb (144.6 kN) is analyzed by using the one-dimensional procedure. The deformed shape of the beam is shown in Figure (D.5). Then, the reactions at each support (tie) are computed, and these are applied to a series of plane strain sections with thickness equal to 20 inch (50.8 cm). Computed deformations are shown in the above figure. Deformations computed from a truly three-dimensional analysis are plotted on the same figure; the three-dimensional results fall between those obtained by one- and two-dimensional procedures.

Comment

Only first three steps of the R-R approach are presented above. The fourth step involving compatibility will have to be performed and investigated before any final conclusions can be made, and this work is expected to continue under the current DOT research. It would involve examination of a number of factors concerning development of R-R functions, and effect of coupling of loads on these functions, and verifications with respect to boundary value problems.

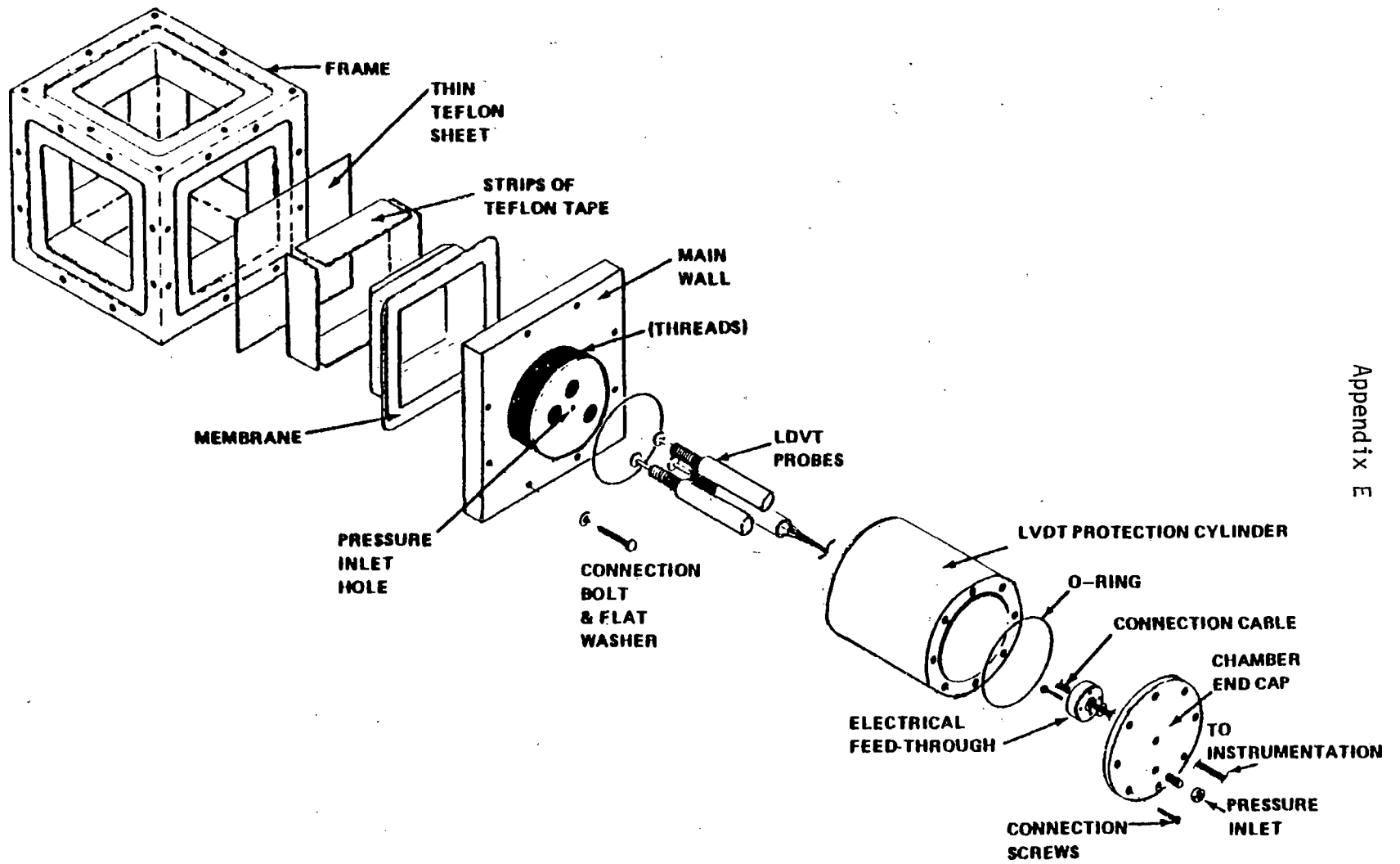


Figure E.1 Exploded View Showing One Face Assembly of Multi-axial Cubical Test Apparatus [80]

REQUEST FOR FEEDBACK TO The DOT Program Of University Research

This booklet is intended to serve as a reference source for transportation analysts, planners and operators. Your comments will be reviewed by the persons responsible for writing and publishing this material. Feedback is extremely important in improving the quality of research results, the transfer of research information, and the communication link between the researcher and the user.

- | YES | NO | |
|--------------------------|--------------------------|--|
| <input type="checkbox"/> | <input type="checkbox"/> | Did you find the report useful for your particular needs?
If so, how? |
| <input type="checkbox"/> | <input type="checkbox"/> | Did you find the research to be of high quality? |
| <input type="checkbox"/> | <input type="checkbox"/> | Were the results of the research communicated effectively
by this report? |
| <input type="checkbox"/> | <input type="checkbox"/> | Do you think this report will be valuable to workers in the
field of transportation represented by the subject area of
the research? |
| <input type="checkbox"/> | <input type="checkbox"/> | Are there one or more areas of the report which need
strengthening? Which areas? |
| <input type="checkbox"/> | <input type="checkbox"/> | Would you be interested in receiving further reports in this
area of research? If so, fill out form on other side. |

Please furnish in the space below any comments you may have concerning the report. We are particularly interested in further elaboration of the above questions.

COMMENTS

Thank you for your cooperation. No postage necessary if mailed in the U.S.A.

RESEARCH INTEREST

PLEASE CHECK YOUR AREAS OF INTEREST. YOU WILL BE NOTIFIED AS NEW REPORTS ARE PUBLISHED.

TRANSPORTATION

- Air
- Highway
- Maritime & Ports
- Mass Transit
- Pipeline
- Rail

ECONOMIC REGULATION

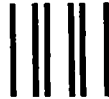
- Air Carrier
- Motor Carrier
- Railroads

TRANSPORTATION STUDIES IN SPECIAL AREAS

- Advanced Technology
- Energy
- Environment
- Facilities & Terminals
- Hazardous Materials
- Safety
- Tunnelling
- Construction, Rehabilitation & Maintenance
- Efficiency, Productivity & Innovation
- Elderly, Handicapped & Disadvantaged
- Freight, Goods Movement & Commodity Flow
- Modeling - Demand, Supply & Traffic
- Rural Development, Planning & Policy
- Urban Development, Planning & Policy

OTHER (PLEASE LIST) _____

U.S. DEPARTMENT OF TRANSPORTATION
 Research and Special Programs Administration
 Washington, D.C. 20590



NO POSTAGE
 NECESSARY
 IF MAILED
 IN THE
 UNITED STATES

BUSINESS REPLY MAIL
 FIRST CLASS PERMIT NO. G-126

POSTAGE WILL BE PAID BY ADDRESSEE



Dr. Lloyd J. Money, DMA-50
 Director, Office of University Research
 U. S. Department of Transportation
 400 7th Street, S. W.
 Washington, D. C. 20590

PLEASE LIST YOUR NAME AND ADDRESS.

NAME _____

TITLE _____

ORGANIZATION _____

STREET _____

CITY, STATE, ZIP CODE _____

U.S. Department
of Transportation

**Research and
Special Programs
Administration**

400 Seventh St., S.W.
Washington, D.C. 20590

Official Business
Penalty for Private Use \$300

Postage and Fees Paid
Research and Special
Programs
Administration
DOT 513



UNIVERSITY RESEARCH RESULTS